

**MAGNETIC PROPERTIES MEASUREMENT OF NEW
MAGNETIC MATERIAL: SOMALOY 700 (5P)**

Ashraf Rohanim Binti Asari

Faculty of Engineering and Information Technology

University of Technology Sydney

This dissertation is submitted for the degree of

Doctor of Philosophy

April 2018

CERTIFICATE OF ORIGINAL AUTHORSHIP

I, Ashraf Rohanim Asari declare that this thesis, is submitted in fulfilment of the requirements for the award of Doctor of Philosophy, in the Faculty of Engineering and Information Technology at the University of Technology Sydney

This thesis is wholly my own work unless otherwise reference or acknowledged. In addition, I certify that all information source and literature used are indicated in the thesis.

This thesis is the result of a research candidature conducted with another University as part of a collaborative Doctoral degree.

This document has not been submitted for qualifications at any other academic institution. This research is supported by the Australian Government Research Training Program.

Production Note:
Signature removed
prior to publication.

Ashraf Rohanim Asari

8 April 2018

ABSTRACT

The everyday lives of people have been dramatically changed due to the evolution of technology. The invention of electrical machines has enabled human to do their chores with easier and more comfortable way. Presently, electromagnetic technology is improving day by day and most of the current electrical machines require the magnetic cores to operate at higher frequency to meet the demand of high-speed performance in catching up the aggressive technological evolution. On top of that, the researchers and engineers are aiming for the lower loss magnetic material in order to obtain the high efficiency of the electrical machines. Magnetic properties of soft magnetic material have been actively studied under 1-D and 2-D magnetic flux excitations to estimate the total core loss produced by the material during the magnetisation of electrical machine. In the past years, soft magnetic composite (SMC) materials were used in designing flexible electromagnetic devices due to their unique properties such as magnetic isotropy that consists of small insulated iron particles with low eddy current. SMC materials are suitable for these applications because of their properties like high electrical resistivity which leads to the low eddy current loss, and 3-D magnetic isotropy which provides great design flexibility of various electromagnetic devices. In this project, the magnetic properties of a new SMC material, SOMALOY 700 (5P) from Hoganas has been studied since it offers low core loss during magnetisation. The magnetic properties should be properly measured as there are some variations of vector flux density in the rotating machine. 1-D and 2-D magnetic measurements are conducted by controlling magnetic flux densities to be in various shapes by using LabVIEW software. The x-, y- and z-axes of magnetic flux densities were generated by using the 3-D magnetic property testing system. The results of the measurement are analysed by using the Mathcad software before being compared to other materials. The performances of this material at wide range of frequency are exhibited by plotting the loss curves in the same graph. The finding indicates that the magnetisation at 1000 Hz contributes higher core loss for all types of magnetic flux excitation. At high frequency, the total core losses are dominated by hysteresis loss. The core loss curves with clockwise and anti-clockwise directions presented the similar rotational core loss. Besides that, the elliptical core loss with B_x and B_y as the major axes are similar in magnitude. All types of core losses are analysed and verified by comparing them with the calculation theory. The accuracy of the core loss has been obtained by considering Mean Absolute Percentage Error (MAPE) to compute the percentage error of the measurement. The details of SOMALOY 700 (5P) material provide good information to engineers in designing electrical machine at different variation of frequencies.

ACKNOWLEDGEMENTS

Firstly, I would like to express my sincere gratitude to my supervisor Associate Professor Youguang Guo for the continuous support of my Ph.D study and related research, for his patience, motivation, and immense knowledge. His guidance helped me in all the time of research and writing of this thesis. I could not have imagined to have a better supervisor and mentor for my Ph.D study.

Besides my supervisor, I would like to thank the co-supervisors of my Ph.D project, Prof. Jianguo Zhu, and Dr. Fatimah Sham Ismail for their insightful comments and encouragement, but also for the hard questions which triggered me to widen my research from various perspectives.

I am also grateful to the following university staff, Jan Szymanski and Russell Nicholson for their unfailing support and assistance during my Ph.D lab works in the CEMPE Lab. Without their support, I could not have imagined that I can finish my lab works smoothly and successfully.

A very special gratitude goes out to my sponsorship Majlis Amanah Rakyat (MARA) Malaysia and Universiti Kuala Lumpur (UNIKL) for helping and providing the funding of my Ph.D study and four years allowance for me and my family members during my stay in Sydney, Australia.

I am grateful to my parents and siblings, who have provided me through moral and emotional support in my life. I am also grateful to my other family members and friends who have supported me along the way from my home country, Malaysia.

And most of all for my loving, supportive, encouraging, and patient husband Azlan Zawawi whose faithful support from the beginning until the final stages of this Ph.D. is so appreciated. With a special mention to my sweet daughter, Fathanah Aisya Azlan, thank you for being a nice girl and always understanding my busy life. I owe you the precious quality time from the start of your existence in this world. I promise that I will compensate the missed moment after my submission of thesis.

Last but not the least, I would like to thank my colleagues for supporting me spiritually throughout the writing of this thesis. Thanks for all your encouragement!

ABBREVIATION

Abbreviation	Full Term
SMC	Soft Magnetic Composite
HR	High Resistivity
SE	Steinmetz Equation
DC	Direct Current
AC	Alternating Current
iGSE	Improved Generalized Steinmetz Equation
GSE	Generalized Steinmetz Equation
SPG	Steinmetz Pre-Magnetisation Graph
EMF	Electromotive Force
FEA	Finite Element Analysis
UTS	University of Technology Sydney
NI	National Instrument
DAQ	Data Acquisition Card
3-D	Three-dimensional
2-D	Two-dimensional
1-D	One-dimensional
A/D	Analog to Digital
D/A	Digital to Analog
ES&S	Enokizono, Soda and Shimoji Model
FEM	Finite Element Method

NOMENCLATURE

Symbol	Physical Quantity
H	magnetic flux density strength
B	magnetic flux density
H_c	coercivity
χ_m	susceptibility
μ	permeability
f	frequency
P_t	total power loss or core loss
P_α	alternating core loss
P_r	rotational core loss
$P_e/P_{e\alpha}/P_{er}$	eddy current loss
$P_h/P_{h\alpha}/P_{hr}$	hysteresis loss
$P_a/P_{a\alpha}/P_{ar}$	anomalous loss
k	material parameter
A	material parameter
B	material parameter
$C_h/C_{h\alpha}$	loss coefficient
N	loss coefficient
$C_e/C_{e\alpha}/C_{er}$	loss coefficient
$C_{a\alpha}/C_{ar}$	loss coefficient
B_s	saturation magnetic flux density
μ_0	permeability of vacuum
K_H/K_B	coil coefficient
V_H	terminal voltage of the H sensing coil
V_m	scalar magnetic potential
l_{AB}	distance between points A and B
A_H/A_{sp}	cross-sectional area
n_c	number of turns per unit length of the coil
T	thickness of the plate
R_H	Hall constant

Symbol	Physical Quantity
C	specific heat capacity
ϑ	temperature of the sample
T	time period of magnetisation
M	magnetisation
ρ_m	sample mass density
E_B / E_H	excitation of current
a_r	radius of the bottom circle
b_r	radius of the upper circle
l_0	half length of the air gap
Θ	cone angle with the axis
ε	axis ratio
v_{xr}	magnetic reluctivity coefficient
v_{xi}	magnetic hysteresis coefficient
v	magnetic reluctivity tensor
Φ	inclination angles
N	number of turns
I	current / magnetisation current
\varnothing	magnetic flux
l_m	mean length of magnetic flux path
V	induced electromotive force
d	thickness of the sample

TABLE OF CONTENTS

ABSTRACT	I
ACKNOWLEDGEMENTS	II
ABBREVIATION	III
NOMENCLATURE	IV
LIST OF FIGURES	IX
LIST OF TABLES	XIV
CHAPTER 1: INTRODUCTION	1
1.1 Research background	1
1.2 Research aim and objectives	4
1.3 Thesis structure	5
CHAPTER 2 : LITERATURE REVIEW	8
2.1 Core loss calculation	8
2.1.1 Core loss prediction by empirical equation	8
2.1.1.1 Core loss in magnetic material	8
2.1.1.2 Core loss in rotating electrical machines	15
2.1.2 Core loss prediction by hysteresis loop	17
2.2 Techniques measuring the magnetic flux density and magnetic field strength	18
2.2.1 Magnetisation current method	18
2.2.2 Sensing coil method	18
2.2.2.1 Conventional H coil	18
2.2.2.2 Two H coil arrangement	19
2.2.2.3 The Rogowski-Chattock coil	20
2.2.2.4 B Coil	21
2.2.2.5 Embedded B coil	21
2.2.3 Hall element	22
2.2.4 B- tips	23
2.3 Methods of measuring the rotational core losses	24
2.3.1 Torque-metric method	24
2.3.2 Thermometric method	24
2.3.3 Field-metric method	25
2.3.4 Watt-metric method	25
2.4 Measuring apparatus of core loss	26

2.4.1 Disk and ring samples	26
2.4.2 Cross and strip samples	30
2.4.3 Epstein frame	33
2.4.4 Toroid tester	33
2.4.5 Square samples	34
2.4.6 3-D Magnetic property testing system	40
2.5 Magnetic properties measurement of soft magnetic material by using 3-D magnetic properties system	51
2.6 Summary	83
CHAPTER 3 : PREPARATION FOR MEASUREMENT TESTING SET UP	95
3.1 Introduction	95
3.2 Calibration of sensing coils	96
3.3 Software skills	101
3.3.1 LabVIEW software	103
3.3.2 Mathcad software	105
3.4 Experimental set up	105
3.5 Conclusion	107
CHAPTER 4 : CORE LOSS MEASUREMENT UNDER ALTERNATING MAGNETIC FLUX DENSITY	110
4.1 Introduction	110
4.2 Principle of alternating core loss	111
4.2.1 Hysteresis loop	111
4.2.2 Core loss curve	112
4.3 Experimental results	112
4.3.1 Hysteresis loops of alternating core loss	113
4.3.2 Core loss of alternating magnetic flux density	117
4.3.2.1 Loss coefficient	120
4.3.2.2 Core loss curve	121
4.4 Core loss separation	125
4.5 Conclusion	129
CHAPTER 5 : CORE LOSS MEASUREMENT UNDER CIRCULAR LOCI OF MAGNETIC FLUX DENSITY	132
5.1 Introduction	132
5.2 Principle and production of rotating magnetic flux density	133

5.3 Experimental results	133
5.3.1 B-H loops of rotating core loss	134
5.3.2 Core loss of rotating magnetic flux density	135
5.3.3 Clockwise and anti-clockwise 2-D measurements	140
5.3.4 Core loss under alternating and rotating magnetic flux densities	143
5.4 Core loss separation	146
5.4.1 Hysteresis loss, eddy current loss and anomalous loss	146
5.4.2 Rotational hysteresis loss	151
5.5 Conclusion	155
CHAPTER 6 : CORE LOSS MEASUREMENT UNDER ELLIPTICAL LOCI OF MAGNETIC FLUX DENSITY	158
6.1 Introduction	158
6.2 Rotating elliptical magnetic flux density	159
6.3 Experimental results	160
6.3.1 B-H Loci under elliptical magnetic flux density	160
6.3.2 Core loss curve under rotating magnetic flux density	163
6.3.2.1 Circular and elliptical core loss	166
6.3.2.2 Accuracy of core loss measurement	168
6.4 Conclusion	172
CHAPTER 7 : CONCLUSIONS AND RECOMMENDATIONS	174
7.1 Conclusions	174
7.2 Recommendations for future research	177
APPENDIX A: List of publications	179
APPENDIX B: Procedures applied in Software used	180
APPENDIX C: Figures and apparatus of experiment	183

LIST OF FIGURES

Fig. 2.1 The efficiency and loss percentage in (a) 110 kW permanent magnet high-speed generator (51000 rpm) (b) 11 kW induction machine (1470 rpm) (c) 1 kW slot-less permanent magnet motor (36000 rpm) [2.14]	11
Fig. 2.2 Rotational hysteresis loss of iron and steel obtained by Baily in 1896 [2.20]	13
Fig. 2.3 (a) Alternating hysteresis loss (b) Rotational hysteresis loss [2.24]	14
Fig. 2.4 Comparison between (a) alternating core loss and (b) rotational core loss at wide range of frequency [2.25].....	14
Fig. 2.5 One pole pitch of one stack of a claw pole machine [2.26].....	15
Fig. 2.6 Hysteresis loops of the SMC sample with 5 Hz sinusoidal magnetic flux density on (a) x-and (b) y-axes [2.22].....	17
Fig. 2.7(a) 1-D H coil (b) 2-D H coil (c) position of H coils on the sample surface [2.16]	19
Fig. 2.8 Two H coil arrangement [2.35], [2.36]	19
Fig. 2.9 The Rogowski- Chattock coil [2.39].....	20
Fig.2.10 (a) Wound coil in uniform magnetic field, (b) threaded coil in non-uniform magnetic field [2.39]	21
Fig. 2.11 Structure of B coil and H coil [2.40].....	22
Fig. 2.12 Relationship between magnetic field strength, current and EMF in the Hall Effect [2.41]	22
Fig. 2.13 Principle of measuring one component of B using tips [2.45]	23
Fig. 2.14 Torque magnetometer with the labelled parts [2.21]	27
Fig. 2.15 Layout of the experiment built by Fiorillo and Reitto (1988) [2.58]	28
Fig. 2.16 Rotational core loss versus flux density in three materials: (1) soft iron, (2) grain oriented silicon iron, and (3) non-oriented silicon iron [2.58].....	29
Fig. 2.17 The set up apparatus of rotational power loss measuring system that uses a stack of ring sample built in 1987 [2.50].....	29
Fig. 2.18 The circular diagram of the rotational power loss measuring system by [2.50].....	30
Fig. 2.19 Cross sample used by Moses & Bleddyn Thomas (1973) [2.50]	30
Fig. 2.20 The measuring rotational core loss apparatus where A and B are the fixed ends and C and D are the spring loaded ends [2.59].....	31
Fig. 2.21 Rotational core loss measuring system using cross samples [2.43] (a) Block diagram of the system (b) Arrangement of B and H sensing coils [2.43].....	32
Fig. 2.22 Rotational core loss measuring system using an Epstein strip (a) configuration (b) magnetic flux search coils, and (c) system diagram [2.35], [2.60]	33
Fig. 2.23 Rotational core loss tester using square samples: (a) Arrangement of yoke, sample and sensors, and (b) details of sensor head for one component of H and B [2.21], [2.65].....	34

Fig. 2.24 Rotational core loss measuring system was built by Enokizono and Sievert: (a) Outline of system and B tips, (b) magnetic circuit and B sensing coils, (c) H sensing coils, and (d) setting of H coils [2.44], [2.66]	35
Fig. 2.25 The square specimen tester with complicated auxiliary yokes: (a) position of specimen, B and H coils, (b) dimension of H coils, (c) flux flow parallel to the auxiliary yoke, and (d) flux flow perpendicular to auxiliary yoke [2.70]	36
Fig. 2.26 The structure of square specimen tester developed by Gumaidh et al.: (a) tester, (b) sample and sensor holder [2.71]	37
Fig. 2.27 Rotational core loss tester built by Kedous-Lebouc et al. (1991): (a) tester, (b) B and H search coils [2.72]	37
Fig. 2.28 Schematic diagram of square sample tester [2.16], [2.33]	38
Fig. 2.29 Sandwich arrangement of H sensing coils [2.16], [2.33]	39
Fig. 2.30 (a) 2-D Rogowski-Chattock [2.79]. (b) Position of the sample between the magnetisation poles with attached conventional H coils [2.22]	39
Fig. 2.31 (a) 3-D magnetic property testing system [2.86]. (b) Framework of 3-D Tester [2.82]	41
Fig. 2.32 A cubic sample and its B and H sensing coils [2.82]	41
Fig. 2.33 Calibration of H sensing coils in the long solenoid [2.86]	43
Fig. 2.34 Improved structure of H coils and B coils [2.40]	44
Fig. 2.35 Sample with sensing coils [2.40]	44
Fig. 2.36 Magnetic line of force through the coil [2.40]	44
Fig. 2.37 The EMF signals of B and H sensing coils under three axes excitation current [2.88]	46
Fig. 2.38 Structure of guarding pieces or field core shoes: (a) cubic sensing box with sample, sensing coils and guard pieces [2.83] (b) cubic specimen with homogeneous field core shoes [2.96]	48
Fig. 2.39 Schematic diagram and cross section of the 3-D tester [2.88]	48
Fig. 2.40 Magnetic field distribution of the specimen without (left) and with (right) guarding pieces [2.96]	49
Fig. 2.41 Model of 3-D magnetisation structure with “C-types” cores [2.96]	49
Fig. 2.42 (a) Prototype of laminated “C-type” core and excitation windings [2.96] (b) Schematic frustum structure of the core pole [2.96]	50
Fig. 2.43 Magnetic flux density distribution in the magnetic concentration model by finite element method [2.97]	51
Fig. 2.44 (a) Hysteresis loop at 50 Hz along x-, y- and z-axes (b) B and H loci of grain oriented Hi-B in the XOY-plane [2.82]	52
Fig. 2.45 (a) B loci when magnetic fluxes have been controlled to make B in circle shape (b) the corresponding of H loci [2.98]	52
Fig. 2.46 Misalignment of sensors [2.98]	54
Fig. 2.47 (a) B loci and (b) the corresponding of H loci at operating frequency of 50 Hz [2.83] ..	55
Fig. 2.48 The Hysteresis loop at 50 Hz along x-, y- and z-axes [2.83]	55

Fig. 2.49 Arrangement of B and H sensing coils (left) with consideration of planar structure for H coils (right) [2.85]	56
Fig. 2.50 (a) Circular B loci when the magnetic field has amplitude of 1.3 T at 50 Hz. (b) The corresponding of H loci in 3-D space [2.85].....	56
Fig. 2.51 (a) B loci in spherical shape at 50 Hz lying in three orthogonal planes. (b) The corresponding H loci [2.85]	56
Fig. 2.52 Round B loci in (a) XOY-plane, (b) YOZ-plane, (c) ZOX-plane and the corresponding H loci in (d) XOY-plane, (e) YOZ-plane and (f) ZOX-plane at 50 Hz [2.99].....	58
Fig. 2.53 Power core loss under (a) alternating magnetic fluxes along x-, y- and z-axes (b) rotational magnetic fluxes in three different planes at 50 Hz [2.99]	59
Fig. 2.54 Elliptical B loci with y as a major axis in (a) XOY- (b) YOZ- (c) ZOX-planes and their corresponding H loci in (d) XOY- (e) YOZ- (f) ZOX-planes [2.100].....	60
Fig. 2.55 Ellipse B loci with x as a major axis in the (a) XOY- (b) YOZ- (c) ZOX-planes and their corresponding H loci in (d) XOY- (e) YOZ- (f) ZOX-planes [2.100].....	61
Fig. 2.56 (a) Alternating flux condition. (b) Rotating flux condition [2.101].....	62
Fig. 2.57 Comparison of core losses depending of θ_B for (a) grain oriented and (b) non-oriented electrical steel sheets [2.101]	64
Fig. 2.58 Relationship among maximum magnetic flux density B_m , axis ratio ϵ , and inclination angles φ of the elliptical B locus [2.104].....	66
Fig. 2.59 Magnetic reluctivity tensor of one cycle in the XOY-plane when B is round rotating ($\epsilon = 1$), (a) $B_r = 0.22$ T (b) $B_r = 1.32$ T [2.104].....	67
Fig. 2.60 Magnetic reluctivity tensor against the magnitude of the maximum B when the circle angle $\theta = 45^\circ$. (a) Diagonal elements and (b) Off-diagonal elements [2.104]	68
Fig. 2.61 Magnetic reluctivity tensor against the magnitude of the maximum round rotating B [2.104].....	68
Fig. 2.62 Relation among the instant values of magnetic reluctivity of off-diagonal elements, axis ratio and phase angle $\theta = 45^\circ$ [2.104].....	69
Fig. 2.63 The hysteresis loops of SOMALOY 500 at (a) 5 Hz (b) 20 Hz (c) 500 Hz and (d) 1000 Hz under alternating flux densities [2.93].....	70
Fig. 2.64 Hysteresis loops along the x-, y- and z-axes at 50 Hz [2.93]	71
Fig. 2.65 (a) B loci and (b) the corresponding of H loci at 50 Hz of operating frequency [2.93] ..	71
Fig. 2.66 Loss curve along the y-axis at wide range of frequency up to 1000 Hz [2.93].....	72
Fig. 2.67 3-D magnetic properties of SOMALOY 500 with elliptical rotating magnetic flux density at 200 Hz. (a) x, y and z as major axes for red, blue and green B loci, respectively.(b) The corresponding H loci for major axes x, y and z are represented by red, blue and green lines, respectively. (c) x, y and z as major axes for green, red and blue B loci, respectively and (d) the corresponding H loci for axes x, y and z are represented by green, red and blue lines, respectively [2.93].....	73

Fig. 2.68 The projection of (a) blue B loci with y as a major axis, (b) the corresponding blue H loci for y major axis (c) green B loci with x as a major axis and (d) the corresponding green H loci for x major axis [2.89].....	74
Fig. 2.69 The core losses versus ratio axis of elliptical B loci (0-1) and amplitudes of round B loci [2.89].....	75
Fig. 2.70 (a) Sphere B loci are controlled in 3-D space at 50 Hz of operating frequency (b) the corresponding H loci in 3-D space [2.89]	75
Fig. 2.71 The round B loci and H loci in the XOY-plane at (a) 200 Hz, (b) 500 Hz and (c) 1000 Hz [2.106].....	76
Fig. 2.72 The core loss at 50 Hz, 100 Hz, 200 Hz, 500 Hz and 1000 Hz under (a) alternating magnetic fluxes (b) rotational magnetic fluxes [2.106]	77
Fig. 2.73 B locus in the middle part of SMC stator core with the blue line shows the no load motor, the green line is the B locus for half load motor and the red line represents the full load motor [2.28].....	78
Fig. 2.74 Waveforms of B components from three different situations; no load, half load and full load [2.28]	78
Fig. 2.75 Round B loci and the corresponding H loci at (a) 5 Hz, (b) 20 Hz, (c) 200 Hz and (d) 500 Hz [2.107].....	81
Fig. 2.76 Relationship between alternating and rotational excitations at 0.5 T of magnetic flux density [2.107].....	82
Fig. 2.77 Spherical B loci of magnetic material on three planes [2.96]	83
Fig. 3.1 SOMALOY 700 (5P) cubic sample with sensing coils	96
Fig. 3.2 An acrylic sensing box and guarding pieces hold the sensing coils to locate on the surfaces of the cubic sample	96
Fig. 3.3 Calibration of B and H sensing coils.....	98
Fig. 3.4 Circuit diagram of calibration process	98
Fig. 3.5 Graph of V against I	99
Fig. 3.6 Excitation of magnetic flux density before and during the calibration	100
Fig. 3.7 The induced voltages of B and H coils during the calibration process.....	100
Fig. 3.8 A uniform wire of length L, and cross-sectional area A, [3.4]	101
Fig. 3.9 Block diagram of LabVIEW in recording the induced sensing voltages during calibration process.....	103
Fig. 3.10 Block diagram of LabVIEW in generating and controlling the magnetic flux density and determining the sensing voltages during magnetisation process.....	104
Fig. 3.11 Magnetic properties testing system [3.5]	105
Fig. 3.12 Op-Amp module with 10x, 100x and 1000x amplification gain	106
Fig. 3.13 Measurements of magnetic properties of SOMALOY 700 (5P) material	106
Fig. 4.1 The core loss curve of SOMALOY 500 at 50 Hz along the x-, y- and z-axes [4.5]	112
Fig. 4.2 The hysteresis loops of SOMALOY 700 (5P) and SOMALOY 500 at 50 Hz	114

Fig. 4.3 The hysteresis loops of SOMALLOY 700 (5P) in the x-axis at (a) 50 Hz (b) 100 Hz (c) 500 Hz and (d) 1000 Hz	116
Fig. 4.4 Three reading of alternating core loss with 0.405 of standard deviation	118
Fig. 4.5 Loss curve of SOMALLOY 700 (5P) at 50 Hz for three different axes	119
Fig. 4.6 The alternating core loss at 50 Hz	119
Fig. 4.7 Loss curve of SOMALLOY 700 (5P) material at 50 Hz, 100 Hz, 500 Hz and 1000 Hz ..	120
Fig. 4.8 Comparison between calculated and measured data at (a) 50 Hz (b) 100 Hz (c) 500 Hz and (d) 1000 Hz	122
Fig. 4.9 The core loss curve of measured data and manufacturing data from Hogan as at (a) 50 Hz (b) 100 Hz, (c) 500 Hz and (d) 1000 Hz	124
Fig. 4.10 Core loss components at (a) 50 Hz, (b) 100 Hz, (c) 500 Hz and (d) 1000 Hz	126
Fig. 5.1 Round B loci and corresponding H loci in the XOY-plane at (a) 50 Hz (b) 100 Hz (c) 500 Hz and (d) 1000 Hz	135
Fig. 5.2 Three times of rotational core loss measurements with 0.474 of standard deviation ...	136
Fig. 5.3 The individual core losses and total core loss at 50 Hz in (a) clockwise and (b) anti-clockwise directions.....	137
Fig. 5.4 Loss curve of SOMALLOY 700 (5P) material in the XOY-plane when flux densities are controlled to in round shape at (a) 50 Hz (b) 100 Hz, (c) 500 Hz and (d) 1000 Hz	139
Fig. 5.5 The rotating core losses at low to high frequencies	140
Fig. 5.6 The loss curve of SOMALLOY 700 (5P) material in clockwise and anti-clockwise 2-D measurements at (a) 50 Hz (b) 100 Hz (c) 500 Hz and (d) 1000 Hz	142
Fig. 5.7 The alternating core loss and rotational core loss of SOMALLOY 700 (5P) at (a) 50 Hz, (b) 100 Hz, (c) 500 Hz and (d) 1000 Hz	145
Fig. 5.8 Separation of total core loss which contains P_h , P_e and P_a when B is controlled to be in round shape at (a) 50 Hz, (b) 500 Hz and (c) 1000 Hz.....	149
Fig. 5.9 The measured and calculated rotational core loss at 50 Hz, 100 Hz, 500 Hz and 1000 Hz	151
Fig. 5.10 The components of rotational core loss of SOMALLOY 700 (5P) material in the XOY-plane (a) hysteresis core loss (b) eddy current core loss (c) anomalous loss.....	153
Fig. 5.11 The measured and calculated hysteresis losses per cycle at 50 Hz.....	155
Fig. 6.1 The induction machine (a) The stator and rotor parts (b) the inner part of stator [6.1].	158
Fig. 6.2 B loci at 50 Hz, 100 Hz and 1000 Hz of operating frequency: (a) x- and (b) y-major axes	161
Fig. 6.3 H loci at 50 Hz, 100 Hz and 1000 Hz of operating frequency: (a) x- and (b) y-major axes	162
Fig. 6.4 Elliptical core loss curve of SOMALLOY 700 (5P) material when B loci are elliptical at (a) 50 Hz, (b) 100 Hz and (c) 1000 Hz	164
Fig. 6.5 Elliptical core loss curves of SOMALLOY 700 (5P) material when B loci are elliptical at 50 Hz, 100 Hz and 1000 Hz.....	166

Fig. 6.6 Comparison between elliptical and circular core losses of SOMALLOY 700 (5P) material when B loci are elliptical at (a) 50 Hz, (b) 100 Hz and (c) 1000 Hz168

Fig. 6.7 Comparison between measured and calculated core losses of SOMALLOY 700 (5P) material when B loci are elliptical at (a) 50 Hz, (b) 100 Hz and (c) 1000 Hz170

LIST OF TABLES

Table 2-1 Diagonal coefficients of the B and H sensing coils in unit of m^2 [2.88]	46
Table 2-2 Off- diagonal coefficient of the B and H sensing coils in unit of m^2 [2.88]	46
Table 3-1 Parameters of the wide-range of frequency experiment	107
Table 4-1 The components of alternating core losses at 50 Hz, 100 Hz, 500 Hz and 1000 Hz	128
Table 5-1 The components of rotating core losses at 50 Hz, 100 Hz, 500 Hz and 1000 Hz	147
Table 6-1 The elliptical core loss for x- and y-major axes and their average at 50 Hz, 100 Hz and 1000 Hz.	165
Table 6-2 The absolute percent errors of elliptical core loss measurement at (a) 50 Hz, (b) 100 Hz and (c) 1000 Hz	171
Table 6-3 Criteria of MAPE [6.7]	172

Chapter 1: INTRODUCTION

1.1 Research background

Year by year, magnetic materials have gained a place in the heart of developmental technology. Most electromagnetic devices rely on soft magnetic material or hard magnetic material which depends on the ability of the material to retain the magnetisation. Soft magnetic material is a temporary magnet and it has been used in the devices that are easy to be magnetised and demagnetised like the cores of transformer, generators, motors, dynamos and switching devices. Relative area of hysteresis loop must be small, since this represents the low core loss.

Part of core losses are resulted from electric current that is induced in a material by the changes of magnetic field with time and it can be called as eddy current. Increasing of the electrical resistivity can reduce the core losses in soft magnetic material. Soft magnetic materials have high initial permeability μ , high susceptibility χ_m , and low coercivity H_c . The movement of domain walls is easy as the magnetic field changes magnitude and direction. It leads to the low value of coercivity. Any defects or voids in soft magnetic material tend to restrict the motion of domain wall and thus increase the coercivity. The eddy current loss is small because of high resistivity.

When domain walls are difficult to move, magnetisation of the material occurs in the exertion of high magnetic field. Once magnetised, it is very hard to be demagnetised. This material is called as hard magnetic material which has the ability to retain the magnetism even after the removal of the external magnetic field. It is suitable in making permanent magnets since the movement of domain wall is prevented. Hard magnetic materials have low initial permeability μ , low susceptibility χ_m , and high coercivity, H_c . The presence of impurities contributes to the reduced value of coercivity and thus will increase the strength of hard magnetic materials.

For over a century, soft magnetic materials have been adopted in various scientific and commercial appliances at various operating frequencies by on-going technology growth. By development of powder metallurgy process, the soft magnetic composite (SMC) materials have been introduced to face the low core loss production and make them be isotropic. Powder metallurgy process is started by mixing of powders, forming the mixed powder into a compact and sintering the compact powder to improve the strength bond

formation between the powder particles. The process is continued with secondary operation until the fabrication of finished product.

SMC is the pure iron powder which has been developed to support the needs of advanced electrical motor product with complex structure and three-dimensional (3-D) magnetic flux path design solutions. Due to some improvements in production technology and fabrication process, SMC materials have offered several advantages such as the reduction of weight and size [1.1] which leads to the lighter and smaller electrical machines. These materials also offer high magnetic saturation, relatively high permeability, and low remnant magnetism with high electrical resistivity. The electrical resistivity becomes high due to the insulated iron particles which introduces the lower loss material.

These materials are suitable in fabricating core components of electromagnetic devices due to the low loss feature.

Hoganas provides Somaloy technology with the iron based SMC which has been commercialized after going through some innovation. Somaloy technology is designed by undergone powder metallurgy process to apply in electromagnetic devices which aim for the high efficiency of the mass volume production at low cost and the reduction of losses during the operation. Uni-axial compaction of the powder is applied under immense pressure by using a tool-set mould in a single press.

This kind of SMC material comes with unique 3-D magnetic properties and the net shaping capabilities which would offer the engineers the flexible opportunities to the high performance and cost-effective in a suitable design with tight tolerance. Somaloy material is formed by insulating the surface of the iron particles with thin insulation to decrease the eddy current loss at high frequency operation [1.2].

Somaloy material has gone through a fabrication process of the 3-D net shapes in order to form the desired shapes. There are some grades of Somaloy products developed by Hoganas that suit the customers' need. Somaloy can be divided into some level performances 1P, 3P, 5P and high resistivity (HR) as explained below [1.3]:

- Somaloy 1P (Baseline)
- Somaloy 3P (Mechanical strength, permeability)
- Somaloy 5P (Lowest losses)
- Somaloy HR (Low eddy current losses in large cross-sections)

Previously, the SOMALLOY 500 (1P) was released by Hoganas AB and it is known as one of the SMC materials which have been categorized as base line performance for fast switching actuators. The magnetic properties of SOMALLOY 500 (1P) have been studied and this material has showed about 30% lower direct current (DC) losses compared to the polymer bonded materials [1.4].

A few years ago, Hoganas AB introduced SOMALLOY 700 (5P) material to the market by aiming for the lowest losses during the operation. This material has a larger grain with ultra-thin insulation, a new coating concept by experiencing the high-temperature treatment at 630 - 650 °C under acceptable mechanical strength which is more than 55 MPa [1.5], [1.6]. These highly pure iron particles with surface coating have controlled the electrical resistivity in order to reduce the bulk eddy current losses. It has significantly reduced the core loss and has recorded as the lowest loss material. In parallel to achieve the high efficiency in electromagnetic devices application, SOMALLOY 700 (5P) material has started to be applied in real application. Due to that, the accuracies in predicting of SOMALLOY 700 (5P) core loss have to be critically emphasized.

In high magnetisation frequency of the high speed electrical machine, there is the core loss dissipated which is a main contributor of the power loss with high percentage of loss compared to the other losses like friction loss, mechanical loss and winding loss during the rotating operation [1.7].

Core losses is an energy waste when electrical power dissipates in the form of heat within the core of electrical machines due to the changing of magnetic flux field [1.8]. Therefore, the prediction of core loss is very important for researchers and engineers to design the electrical machines. By predicting the core losses of the magnetic material and element part of electrical machines, the core losses can be reduced in electrical equipment and this makes the machines more reliable and the efficiency of the system also can be increased. The industries always demand for the higher efficiency devices to make the world less polluted and global warming effects can then be reduced significantly.

In a typical rotating electrical machine, the direction of the magnetic flux vector varies with time in the 3-D space of the magnetic materials [1.9] and the estimation of core loss become more complex since there is an involvement of both alternating and rotating magnetic fluxes. The core losses need to be measured by considering both types of fluxes depending on the applications [1.10]. The specific total core loss is summed up by three components; hysteresis losses, eddy current losses and anomalous losses where

the measurement of alternating core loss become standardized and the alternating magnetic property data of magnetic materials are normally provided by the manufacturers. Nevertheless, the rotational core loss of magnetic material still lacks any standardization and it needs more effort in order to predict the core loss accurately [1.11].

Previously, both alternating and rotational core loss of the SMC sample are determined by the measurement of magnetic field strength H , and magnetic flux density B , with a single sheet two-dimensional (2-D) core loss tester and they also can be determined by 3-D tester since both testers have considered the involvement of rotating magnetic field.

The rotational core loss of electrical machine is largely contributed by rotating magnetic field and this amount of rotational core loss may be twice the alternating core loss [1.12]. Because of that, calculation of rotational core loss under different types of rotating magnetic fluxes should be seriously considered for a better design of electrical machines. In order to estimate and predict the core losses in SMC materials, the previous researchers have come up with some measuring techniques, methods, testers and models.

The 3-D magnetic tester is used to measure the magnetic properties of SOMALOY 700 (5P) material. By considering two types of magnetic fluxes penetration on the sample; alternating and rotating magnetic flux, the core loss should be accurately determined in order to provide the useful information to engineers to apply the given data in designing the future parts of rotating electromagnetic devices.

However, there is no study found on investigating and measuring the rotational core of this material, SOMALOY 700 (5P) by the presence of rotating magnetic fluxes. The lack of information about the magnetic properties of this material will complicate and prevent the engineers and researchers to invent and produce the motor system with high efficiency form this material.

1.2 Research aim and objectives

The research aims to measure the magnetic properties of SOMALOY 700 (5P) under variation of magnetic flux excitations, providing guidelines to other researchers and engineers for developing advanced electrical machines in the future. Therefore, in order to achieve the aim of this research, the following objectives are set:

- i. To critically review the suitable tool, method, tester and model in measuring the core loss of SOMALOY 700 (5P) material.
- ii. To measure the alternating core loss of SOMALOY 700 (5P) material.
- iii. To determine the magnetic properties of SOMALOY 700 (5P) material under circular loci of magnetic flux density.
- iv. To determine the magnetic properties of SOMALOY 700 (5P) material under elliptical loci of magnetic flux density.
- v. To compare the characteristics of SOMALOY 700 (5P) material with those of SOMALOY 500 material.

1.3 Thesis structure

Chapter 1 is an overview of the project which briefly explains about the research background, problem statement, research scope, research aim and objectives in this study.

In Chapter 2, previous works are studied by reviewing the types of techniques, methods and testers, which have been used in measuring the magnetic properties of SMC material. The core loss predictions also have been studied in this chapter and followed by analysing the results or data which are determined by previous researchers.

In subsequent chapters, the measurement works are explained in details. Chapter 3 presents the beginning work of fabricating the sensing coils and it also describes the calibration of sensing coils which has been conducted inside a long solenoid. The procedures in setting the components before the experiment are designated. The calibration of the sensing coils is described in order to acquire the box coefficients before the measurements begin. Brief software skill developments in data acquisition system and data analysis are introduced.

Chapter 4 discusses the magnetic properties of SOMALOY 700 (5P) HR under one-dimensional (1-D) alternating magnetic fluxes at 50 Hz, 100 Hz, 500 Hz and 1000 Hz. The measurement is conducted under 2-D vector fluxes excitation, as presented in chapter 5. The circular B loci are formed with up to 1000 Hz of frequency. Then, the magnitude and direction of magnetic fluxes are varied by controlling them to be elliptical shapes in chapter 6. The performance of SOMALOY 700 (5P) material is analysed by comparing the measurement data with the calculation data.

Finally, chapter 7 concludes the thesis and states the limitation in measuring the magnetic properties of SOMALOY 700 (5P) material. This chapter also reviews the significant contributions of the thesis. Recommendations for future research are explained in the last part of this chapter.

Appendix A lists the publications based on the thesis work. Appendix B describes the steps applied in generating the magnetic flux densities and analysing the recorded data. Appendix C gives the apparatus used in calibrating the sensing coils and measuring the magnetic properties of the sample.

References

- [1.1] H. Shokrollahi and K. Janghorban, "Soft Magnetic Composite Materials (SMCs)," *Journal of Materials Processing Technology*, vol. 189, no. 1–3, pp. 1–12, 2007.
- [1.2] Höganäs AB, "*Production of Sintered Components*", vol. 1, 2013.
- [1.3] Hoganas AB, "*Somaloy® Technology for Electric Motors*," p. 2, 2011.
- [1.4] L. Hultman and O. Andersson, "SMC Developments Boost Performance and Strength," *Metal Powder Report*, vol. 65, no. 5, pp. 28–30, 2010.
- [1.5] SGTechology. Soft Magnetic Composite, SMC, Somaloy 500, 130i, 700 3P, 700 5P, [Online]. Available: <https://www.sgtec.com/materials/soft-magnetic-components-smc>. [Accessed 13 March 2014].
- [1.6] Z. Ye, "Modeling and Experimental Analysis of Core Losses of SMC Components", *Advances in Powder Metallurgy and Particulate Materials, Metal Powders Industry Federation*, Princeton, NJ, 2014, pp.1641-1648, 2014
- [1.7] Y. Chung, J. Galayda, and A. P. Source, "Effect of Eddy Current in the Laminations on the Magnet Field," LS Note 200, Argonne Nat. Lab, 1992.
- [1.8] H. Toda, K. Senda, and M. Lshida, "Effect of Material Properties on Motor Iron Loss," *IEEE Transactions on Magnetics*, vol. 41, no. 10, pp. 725–726, 2005.
- [1.9] Y. Guo, J. Zhu, D. Dorrell, H. Lu, and Y. Wang, "Development of a Claw Pole Permanent Magnet Motor with a Molded Low-Density Soft Magnetic Composite Stator Core," *IEEE Energy Conversion Congress and Exposition (ECCE2009)*, San Jose, California, USA, 2009.
- [1.10] Y. Okada and H. Dohmeki, "Examination about the Stator Structure of the Brushless DC Motor Manufactured in the Soft Magnetic Composite," *12th International Conference on Electrical Machines and Systems*, Tokyo, Japan, pp. 1–4, 2009.
- [1.11] G. S. Liew, E. C. Y. Tsang, N. Ertugrul, W. L. Soong, D. Atkinson, and D. B. Gehlert, "Analysis of a Segmented Brushless PM Machine Utilising Soft Magnetic Composites," *IEEE Industrial Electronics Society (IECON)*, pp. 1268–1273, 2007.
- [1.12] Steve Vidal. Electrical Construction and Maintenance, Differentiating between DC and AC Motors, [Online]. Available: <http://www.ecmweb.com/author/steve-vidal>, 2007 [Accessed 20 March 2014].

Chapter 2 : LITERATURE REVIEW

2.1 Core loss calculation

2.1.1 Core loss prediction by empirical equation

2.1.1.1 Core loss in magnetic material

The time varying of the magnetic flux which excites the material has caused the presence of the core loss in magnetic material. Sometimes the core loss can be sensed by the heat within the magnetic material. The variation of magnetic flux density rate has strong influence upon the core loss and it is proportional to some parameters like frequency of the magnetic field variation [2.1]. For designing and analysing the electromagnetic devices, the core loss data are provided by manufacturers in form of tables and curves of total core loss versus flux density or frequency. The loss coefficients in the formula expression of core loss can be extracted from the data provided.

The core loss measurement in inductive components has not been entirely solved and the equation that has been used to characterize the core losses is known as power law equation as expressed by Snelling (1988) [2.2]

$$P_v = kf^\alpha \hat{B}^\beta \quad (2.1)$$

where B is the peak flux density of a sinusoidal excitation with frequency f , P_v is the time-average power loss per unit volume or weight, and k , α , and β are the material parameters. In 1892, Charles P. Steinmetz proposed a similar equation named Steinmetz equation (SE) without the frequency dependence [2.3]. Besides that, the SE is only valid for sinusoidal excitation, but most devices in power electronics applications are exposed to non-sinusoidal magnetic flux waveforms [2.4]. Conventionally, the total core loss P_t , can be divided into two components which are the hysteresis loss P_h , and eddy current loss P_e . Based on the SE, the core losses are measured and identified under sinusoidal magnetic flux density with variation of magnetic flux magnitude and frequency. The model of total core loss with two components is stated as

$$P_t = P_h + P_e = C_h f B^n + C_e f^2 B^2 \quad (2.2)$$

where f is the frequency of external magnetic field, B is the peak value of flux density vector, and C_h , C_e and n are the coefficients. The coefficients depend on the lamination material, thickness, conductivity, and some other factors and they can be determined by experiment.

This formula is limited to about 1 T of magnetic flux density and only for static condition of hysteresis loop. A big discrepancy is resulted on equation (2.2) when the magnetic flux density is set to be over 1 T and when the frequency becomes high.

Some corrections and modifications have been done to the conventional formula by focusing on the core loss dependence such as peak magnetic induction, magnetisation frequency and microstructure of the soft magnetic material. Based on the statistical loss theory [2.5], the total core loss has been justified and it shows that the anomalous loss also contributes to the total core loss. It is described in magnetisation dynamics in terms of a random distribution of magnetic correlation regions that are the groups of interacting domain walls, termed magnetic objects. The anomalous loss has been assumed to be governed by the statistical distribution of the local threshold fields [2.1]. The total core loss can then be expressed as [2.1]

$$P_a = P_{h\alpha} + P_{e\alpha} + P_{a\alpha} = C_{ha}fB^n + C_{ea}(fB)^2 + C_{aa}(fB)^{1.5} \quad (2.3)$$

where $P_{a\alpha}$ is referred to the anomalous loss and C_{aa} is the coefficient of anomalous loss. This coefficient is related to the material thickness, cross-sectional area, conductivity, and the parameters that describe the material microstructure. The values of loss coefficients C_{ha} , n , C_{ea} and C_{aa} can be deduced by fitting the model to the experimental results.

The formula (2.3) is parallel to the other experiment results which give good agreement on that [2.6]. However, it is not sufficiently general since there are still some discrepancies and the value of C_{aa} is not truly a constant.

The constant n in (2.3) will be replaced by the flux density dependent term $(a + bB + cB^2)$, which represents the difference between the static hysteresis loop and the dynamic hysteresis loop. The coefficients a , b and c are changed with frequency [2.7].

The SE model has many benefits. One of these benefits is the simple expression that consists of three components. Also, the SE can be very accurate and precise over a limited range of magnetic flux density and frequency. Multiple set of coefficients can be

used to increase the accuracy over wide range of magnetic flux density and frequency. It is a standard model that has been used in describing the core loss of soft magnetic material [2.8]. However, the SE has also a lot of disadvantages. This model is unable to be extrapolated with a very good accuracy. It is not a 'physical' model and it makes some difficulties when the coefficients need to be applied for physical factors such as size, temperature, DC bias and duty cycle [2.8].

Some approaches are used in order to overcome these drawbacks and the magnetisation can be done under wider variety of waveforms instead of sinusoidal waveform only. An improved generalized Steinmetz equation (iGSE) was proposed in 2002 after the failure was detected on the generalized Steinmetz equation (GSE). The iGSE model is capable of obtaining the losses of any flux waveform without requiring extra characterization of material parameters based on some approaches [2.9], [2.10], [2.11]. The iGSE can be formulated as

$$P_v = \frac{1}{T} \int_0^T k_i \left| \frac{dB}{dt} \right|^\alpha (\Delta B)^{\beta-\alpha} dt \quad (2.4)$$

where ΔB is the peak-to-peak value of flux density and

$$k_i = \frac{k}{(2\pi)^{\alpha-1} \int_0^{2\pi} |\cos\theta|^\alpha 2^{\beta-\alpha} d\theta} \quad (2.5)$$

The material parameters k , α , and β are the parameters that have been used in SE. However, this model has a shortcoming due to ignorance of the fact that core losses vary under dc bias conditions which lead to the change of Steinmetz parameters with the presence of these conditions [2.4].

The calculations of core losses considering the DC bias conditions became possible by introducing the Steinmetz pre-magnetisation graph (SPG) in 2012. The Steinmetz parameters k , α and β are dependent on the DC pre-magnetisation during the core loss measurement of certain materials. Muhlethaler *et al.* have done experiments on four different materials such as molypermalloy powder, silicon steel, nanocrystalline material and ferrite cores [2.4]. The idea of this method has led to the development of the simple material curve-fitting model in analysing the magnetic core loss in inductor. In this model, the alternating current (AC) flux density and DC bias field have been taken into consideration and the core losses are analysed by combining the curve-fitting model and

the finite element method [2.12]. The core loss in electromagnetic devices that is influenced by the type of excitation whether in alternating or rotating excitation of magnetic flux is needed to be considered. The selection of SMC as a core material will help the device to control the eddy current loss. Eddy current loss is significantly low for the SMC materials, and as illustrated by Krings in Fig. 2.1, the iron losses or core losses are non-negligible contributor in in all machine types [2.13].

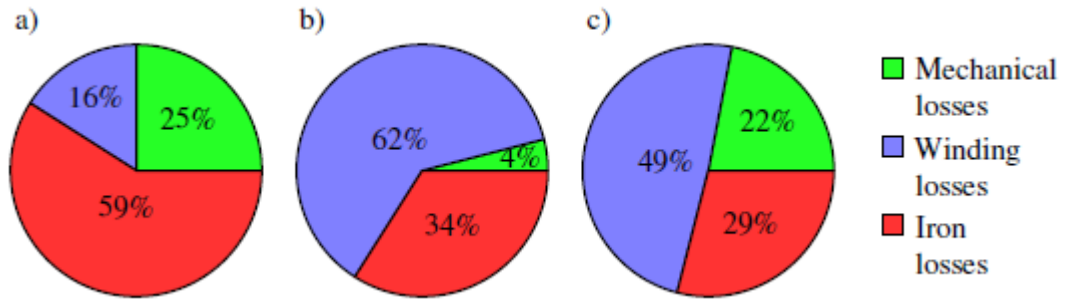


Fig. 2.1 The efficiency and loss percentage in (a) 110 kW permanent magnet high-speed generator (51000 rpm) (b) 11 kW induction machine (1470 rpm) (c) 1 kW slot-less permanent magnet motor (36000 rpm) [2.14]

The alternating hysteresis loss acts differently from rotational hysteresis loss. A standard way for alternating core loss is to separate it into three components; hysteresis, eddy current and anomalous losses as shown below and can be seen in equation (2.3). The techniques of measuring the alternating core loss have been standardized and the magnetic properties under alternating magnetic flux normally can be obtained from the manufacturer.

Likewise, the rotational core losses of the soft magnetic material also can be separated into three components as [2.15]

$$P_r = P_{hr} + C_{er}(fB)^2 + C_{ar}(fB)^{1.5} \quad (2.6)$$

where P_{hr} is the hysteresis rotational loss that acts differently from alternating hysteresis loss P_{ha} and C_{er} and C_{ar} are the eddy current and anomalous loss coefficients, respectively. C_{ar} would reduce to zero [2.16]. The anomalous parts for both losses give the different interpretation since the anomalous coefficient of rotating core loss C_{ar} , is a function of magnetic flux density B , while the anomalous part for alternating core loss is a constant.

In 1990, Fiorillo and Rietto reported that the rotational core loss of 3.2% non-oriented SiFe at different frequencies up to 50 Hz can be separated into rotational hysteresis, classical eddy current and anomalous losses which resemble alternating core loss [2.15], [2.17], [2.18]. This three-term model of SE was supported by [2.6] in the following year with measuring the core loss of an induction motor. In calculating the rotational hysteresis loss with an elliptical rotating magnetic flux, a linear interpolation between purely circular and alternating core losses had been considered. The experimental results showed that the calculated core losses were about 20% lower than the measured ones. In 1991, Zhu *et al.* used this model and finite element method in determining the core loss of a permanent magnet motor by modifying the model with consideration of rotational effects. However, owing to the lack of rotational hysteresis loss data of the material, the alternating hysteresis was calculated [2.19]. The measured results were about 15% higher than calculated ones. The improvement of the rotational hysteresis loss was continued in 1993 and it could reduce the discrepancy to less than 10% [2.20].

Several studies in rotational core losses in magnetic material have been done and early researches dealt more with rotational hysteresis core loss. The dependency of rotational and alternating hysteresis loss was obtained in 1896 by measuring the hard and soft irons using rotational hysteresis measuring apparatus [2.21]. The rotational hysteresis losses of both materials are larger than alternating hysteresis loss for a range of magnetic flux density which is up to 70% of the saturation value. After that value, the rotational hysteresis losses decrease and drop to zero when the flux density is saturated [2.21] as shown in Fig. 2.2. By contrast, the alternating core losses continue to increase.

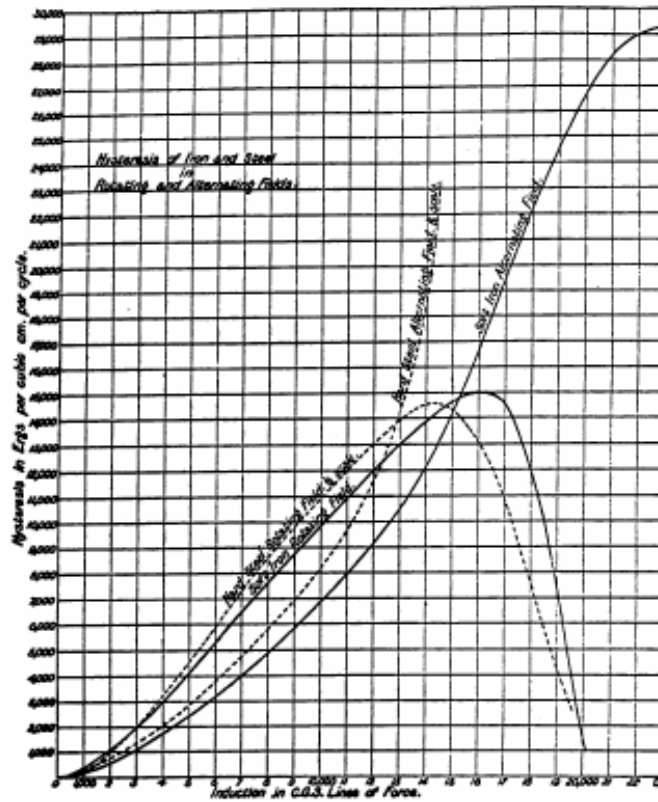


Fig. 2.2 Rotational hysteresis loss of iron and steel obtained by Baily in 1896 [2.20]

The ratio of rotational hysteresis loss to alternating hysteresis loss at low to middle of flux densities varies from 1 to 2 for different material as explained by different researchers [2.22].

A formulation of the rotational hysteresis loss per cycle in an electrical steel sheet and SMC sample has been modelled in 1998 by Zhu *et al.* as below [2.23]

$$\frac{P_{hr}}{f} = \alpha_1 \left[\frac{1/s}{\left(\alpha_2 + \frac{1}{s}\right)^2 + a^3} - \frac{1/(2-s)}{\left(a_2 + \frac{1}{2-s}\right)^2 + a^3} \right] \quad (2.7)$$

This equation can be expressed in terms of four parameters, α_1 (in J/kg), α_2 (non-dimensional), α_3 (non-dimensional) and B_s (in T) which is the saturation magnetic flux density and s can be defined as

$$s = 1 - \frac{B}{B_s} \sqrt{1 - \frac{1}{\frac{a^2}{2} + a^3}} \quad (2.8)$$

The coefficients of the tested SMC specimen are obtained by fitting the formulations to the rotational loss curves in Fig. 2.3.

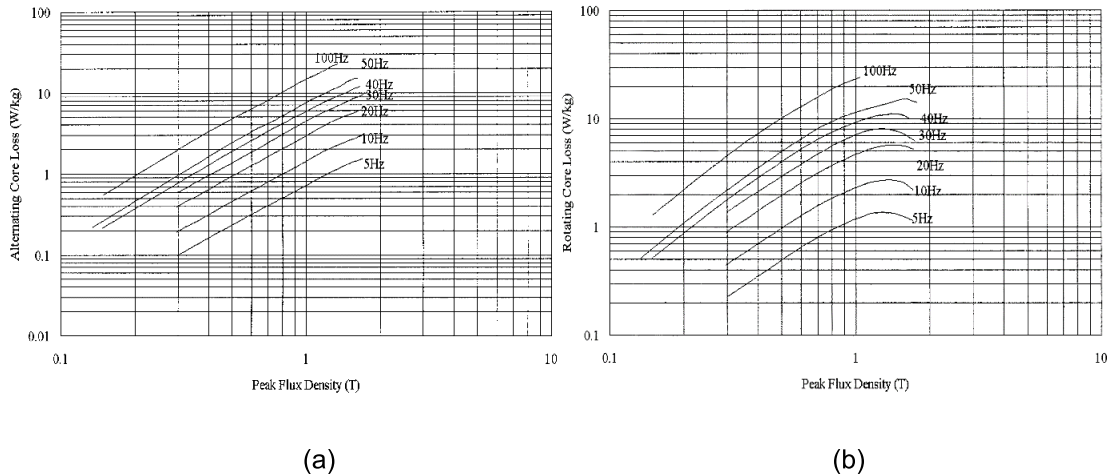


Fig. 2.3 (a) Alternating hysteresis loss (b) Rotational hysteresis loss [2.24]

From Fig. 2.3 and Fig. 2.4, the experimental data show that the core losses of SMC sample are different for both types of hysteresis losses and there is reduction of rotational hysteresis losses when the magnetic flux density B , is at saturation value. It can be seen that the total rotational hysteresis loss is about two times of its alternating counterpart when B is lower than saturation value.

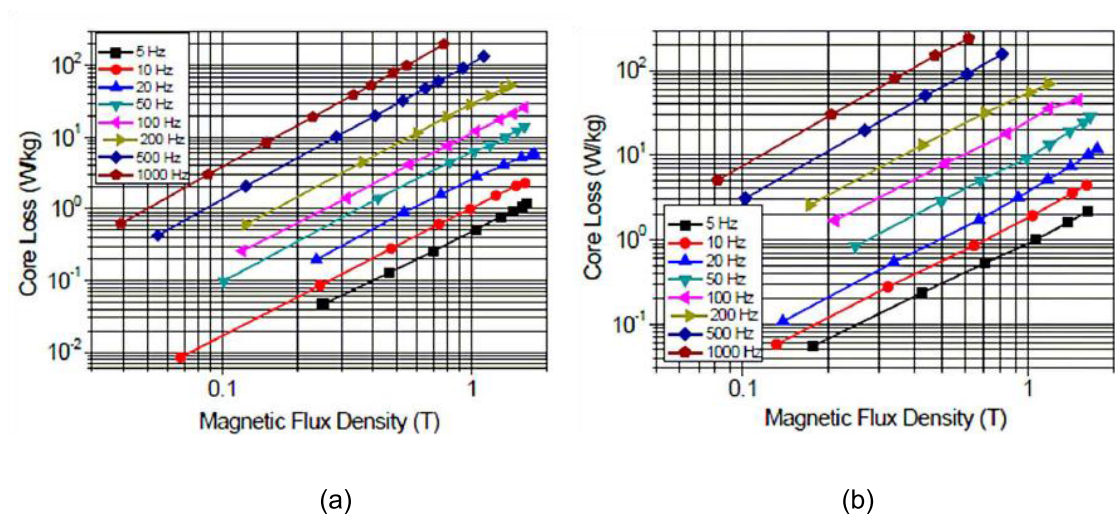


Fig. 2.4 Comparison between (a) alternating core loss and (b) rotational core loss at wide range of frequency [2.25]

The density flux loci in 3-D flux machine can be elliptical, including the special cases of alternating B ($R_B = 0$) and circularly rotating B ($R_B = 1$), where $R_B = B_{min}/B_{maj}$, B_{min} and B_{maj} are the minor axis and major axis of the elliptical B locus, respectively. The elliptical core loss can be determined by the alternating and purely circular formulation as

$$P_t = R_B P_r + (1 - R_B)^2 P_a \quad (2.9)$$

where P_a is the core loss with an alternating B , P_r is the core loss with a circular B and $B_{maj} = B_p$ is the peak value of alternating B .

Model of the core losses and coefficients can be used together with the magnetic field finite element analysis in order to calculate the core loss in electrical machines with SMC cores [2.24].

2.1.1.2 Core loss in rotating electrical machines

Fig. 2.5 displays the complex structure of a high-speed motor that contains permanent magnet, claw pole, rotor core, yoke, winding and coil window parts.

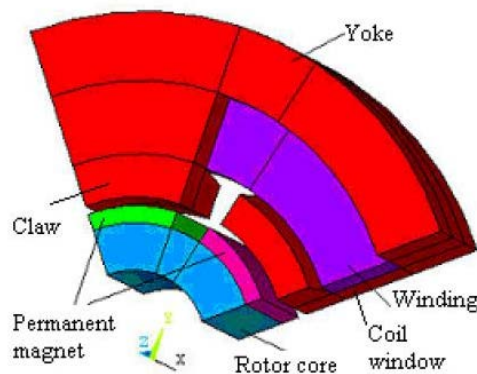


Fig. 2.5 One pole pitch of one stack of a claw pole machine [2.26]

Formulation (2.10) is the rotational hysteresis loss under elliptical rotating flux excitation where $R_B = B_{min}/B_{maj}$ [2.26]. Based on the structure of high speed SMC claw pole motor which contains some parts for one pole pitch of one stack in Fig. 2.5, the total core loss of the high-speed machine can be determined by summing up the core loss of each element [2.26].

$$P_{core} = \sum_{j=1}^{N_e} \sum_{k=0}^{\infty} [R_{Bkj} P_{rotkj} + (1 - R_{Bkj})^2 P_{altkj}] \quad (2.10)$$

where P_{rotkj} and P_{altkj} are the rotational and alternating core losses, respectively, and R_{Bkj} is the axis ratio of the elliptical locus of the k -th harmonic in the j -th element [2.26].

For any B locus in 3-D space, it can be expanded into a Fourier series as

$$\begin{aligned} B_r(t) &= \sum_{k=0}^{\infty} [B_{rsk} \sin(2\pi k ft) + B_{rck} \cos(2\pi k ft)] \\ &= \sum_{k=0}^{\infty} B_{rmk} \sin(2\pi k ft + \phi_{rk}) \end{aligned} \quad (2.11)$$

$$\begin{aligned} B_{\theta}(t) &= \sum_{k=0}^{\infty} [B_{\theta sk} \sin(2\pi k ft) + B_{\theta ck} \cos(2\pi k ft)] \\ &= \sum_{k=0}^{\infty} B_{\theta mk} \sin(2\pi k ft + \phi_{\theta k}) \end{aligned} \quad (2.12)$$

$$\begin{aligned} B_z(t) &= \sum_{k=0}^{\infty} [B_{zsk} \sin(2\pi k ft) + B_{zck} \cos(2\pi k ft)] \\ &= \sum_{k=0}^{\infty} B_{zmk} \sin(2\pi k ft + \phi_{zk}) \end{aligned} \quad (2.13)$$

where

B_r , B_{θ} and B_z are the radial, circumferential, and axial components of the rotating flux density;

B_{rmk} , $B_{\theta mk}$ and B_{zmk} are the magnitudes of the k -th harmonics of B_r , B_{θ} and B_z ;

ϕ_{rk} , $\phi_{\theta k}$ and ϕ_{zk} are the phase angles of these harmonics, respectively.

The two axes B_{msk} and B_{mck} can be calculated by

$$B_{msk} = \sqrt{B_{rsk}^2 + B_{\theta sk}^2 + B_{zsk}^2} \quad (2.14)$$

$$B_{mck} = \sqrt{B_{rck}^2 + B_{\theta ck}^2 + B_{zck}^2} \quad (2.15)$$

The larger of B_{msk} and B_{mck} is taken as B_{kmaj} and the other as the minor axis B_{kmin} of the k -th harmonic of the elliptical flux density vector [2.22], [2.27], [2.28], [2.29].

2.1.2 Core loss prediction by hysteresis loop

A small area of the hysteresis loop for the soft magnetic material is very important since it is related to the magnetic energy loss per unit volume of material. The loop is affected by the existence of insulated layer of each particle which will lead to the distributed air gap and the eddy current losses are significantly low. The reduction of eddy current loss will decrease the total iron losses since the total losses basically include hysteresis, eddy current and anomalous losses. Fig. 2.6 shows the hysteresis loop of SMC material after being excited under sinusoidal excitation of magnetic flux density [2.22].

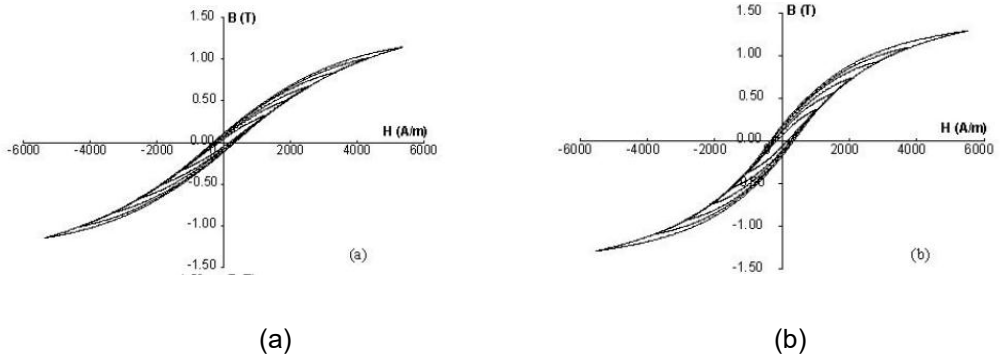


Fig. 2.6 Hysteresis loops of the SMC sample with 5 Hz sinusoidal magnetic flux density on (a) x-and (b) y-axes [2.22]

In alternative way, the hysteresis loop area of magnetic material can also be measured with alternating and rotating fields. Both losses of an SMC sample can be obtained via measurement and calculation of magnetic field intensity H , and magnetic flux density B . By using Poynting's theorem the total core loss P_t , can be measured as explained in equation (2.26).

2.2 Techniques measuring the magnetic flux density and magnetic field strength

The magnetic properties of magnetic materials can be identified by knowing the exact values of magnetic flux density B , and the corresponding magnetic field strength H . These two physical quantities are able to obtain some parameters such as core loss, hysteresis loop, B loci and corresponding H loci. Thus, the appropriate techniques in measuring should be considered in order to get the accurate experimental results. There are four major techniques which have been invented by the researchers such as the magnetisation current method, the sensing coil method, the Hall element method, and the B-tips method.

2.2.1 Magnetisation current method

This measurement method is widely used in annular rings, Epstein tester and single sheet tester for obtaining the alternating core loss, but the rotational core loss is unlikely obtained due to that the magnetic flux paths of sample is 1-D. The magnetic field strength H , can be determined from the magnetisation current I , by considering Ampere's Law

$$H = \frac{NI}{l_m} \quad (2.16)$$

where N , I and l_m are the number of coil turns, magnetisation current and mean length of magnetic flux path, respectively.

2.2.2 Sensing coil method

2.2.2.1 Conventional H coil

By locating the sensing H coils on the sample surface, one is able to acquire the values of the tangential components of magnetic field strength H_x and H_y . Fig. 2.7 illustrates the overview of the conventional coil. When the magnetic flux density B , is parallel with the sample, the magnetic field strength H , can be deduced as

$$H = \frac{1}{\mu_0 K_H} \int V_H dt \quad (2.17)$$

where μ_0 , K_H and V_H are respectively the permeability of vacuum, coil coefficient that can be determined by the calibration in long solenoid, and the terminal voltage of the H sensing coil.

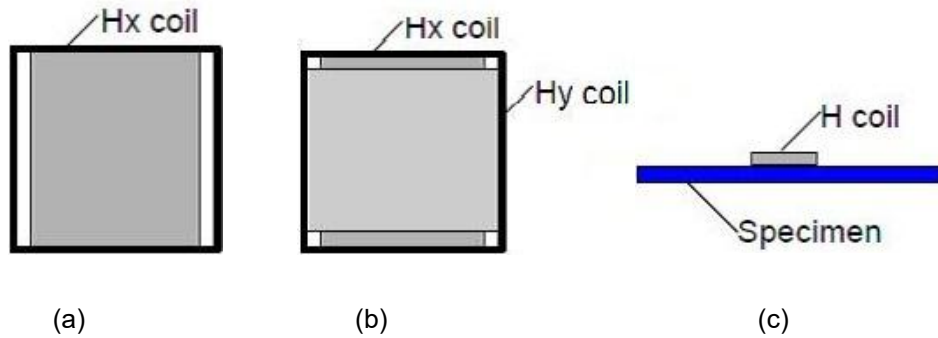


Fig. 2.7(a) 1-D H coil (b) 2-D H coil (c) position of H coils on the sample surface [2.16]

The uniform magnetic flux density on the sample surface can produce accurate results. This method can be applied for both alternating and rotational core loss testers. Nevertheless, in the square sample rotational core loss tester with the horizontal yokes, the magnetic fields vary significantly with the distance between the sample surface and conventional H coils [2.30], [2.31], [2.32], [2.33], [2.34]. Because of that, the sensing coils must be made extremely thin and located as close as possible to the sample surface to avoid the error.

2.2.2.2 Two H coil arrangement

Reflecting to the variation of magnetic field from the previous model, the two H coil arrangement technique is illustrated in Fig. 2.8, is created in order to reduce the error caused by the distance above the specimen surface. The magnetic field strength H , at the sample surface can be calculated by

$$H = \frac{d_2 H_1 - d_1 H_2}{d_2 - d_1} \quad (2.18)$$

where H_1 and H_2 are the magnetic field strength measured by H coil #1 and coil #2, and d_1 and d_2 are the distances of two H coils away from the sample surface.

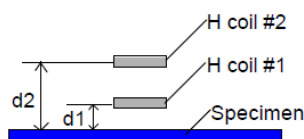


Fig. 2.8 Two H coil arrangement [2.35], [2.36]

When the two H coils are placed not far away from sample surface, the linear extrapolation is a reasonable approximation that has been shown by both numerical analysis [2.30], [2.31], [2.32] experimental measurement [2.33], [2.35].

2.2.2.3 The Rogowski-Chattock coil

This technique also can be known as the magnetic potentiometer [2.34], [2.35], [2.37] [2.38] and the principle of this technique is based on the existence of the scalar magnetic potential V_m , without the presence of the currents.

From Fig. 2.9, the magnetic potential difference between point A and point B can be evaluated by

$$V_{mA} - V_{mB} = \int_{C_1} H \cdot dl = \int_{C_2} H \cdot dl \quad (2.19)$$

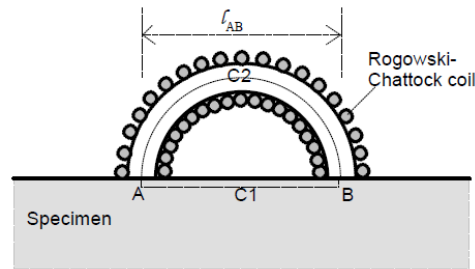


Fig. 2.9 The Rogowski- Chattock coil [2.39]

If the magnetic field is uniform between points A and B, the line integral of H along path C_1 can be calculated as

$$\int_{C_1} H \cdot dl = H l_{AB} \quad (2.20)$$

where l_{AB} is the distance between points A and B.

When there is variation of magnetic field with time, the induced terminal voltage of the coil is

$$V_H = \frac{d\lambda}{dt} = \mu_0 A_H n_c \frac{d}{dt} \int_{C_2} H \cdot dl \quad (2.21)$$

where λ , A_H and n_c are the total flux linkage, the cross-sectional area, and the number of turns per unit length of the coil. The final expression can be formulated as

$$V_H = \mu_0 A_H n_c \frac{d(Hl_{AB})}{dl} = \mu_0 K_H \frac{dH}{dt} \quad (2.22)$$

where the coil coefficient can be expressed as $K_H = A_H n_c l_{AB}$, which can be determined by calibration in a long solenoid. Hence the magnetic field strength H , can be obtained by the time integral of V_H .

High accuracy in detecting the H can be obtained by the installation of both coils which are very close to the sample surface. Besides that, the higher sensitivity can be achieved by a larger coil coefficient K_H , which is proportional to the number of turns per unit length of the coil.

2.2.2.4 B Coil

The magnetic flux density B , in the tester is measured by the sensing coil [2.39]. If the magnetic flux density is uniformly distributed over the cross section of the sample, the sensing coil can be wound around the whole sample as depicted in Fig. 2.10 (a). If the magnetic flux density is non-uniform across the cross section of the sample, the coil can be threaded through the small holes at particular areas with uniform field as illustrated in Fig. 2.10 (b).

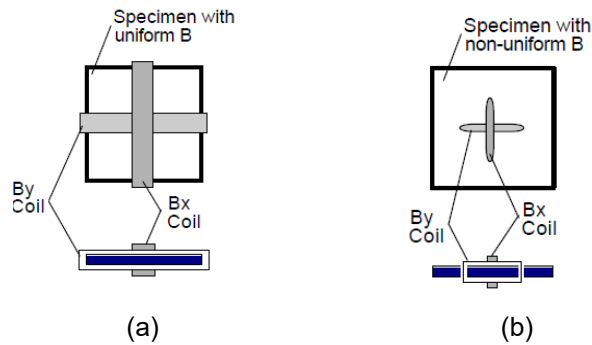


Fig.2.10 (a) Wound coil in uniform magnetic field, (b) threaded coil in non-uniform magnetic field [2.39]

2.2.2.5 Embedded B coil

In order to achieve the high magnitude of magnetic flux density B , with uniform distribution, Li *et al.* (2009) proposed some improvements of the B-H sensing coils considering the epoxy resin structure. Circular B coil is placed in the centre of the epoxy resin and H coil is wound and attached to the surface of epoxy base which is closely

placed on the sample surface. Fig. 2.11 shows the structure of improve B-H sensing coils with details of their dimensions [2.40].

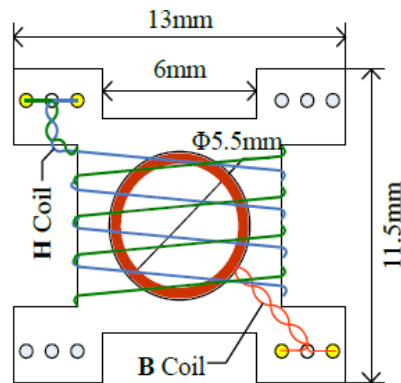


Fig. 2.11 Structure of B coil and H coil [2.40]

2.2.3 Hall element

This technique is based on Hall Effect concept. From Fig. 2.12, it can be seen that the magnetic flux density, current and EMF are really related together in the Hall Effect structure. The electromagnetic force EMF e_H , is developed between points A and B.

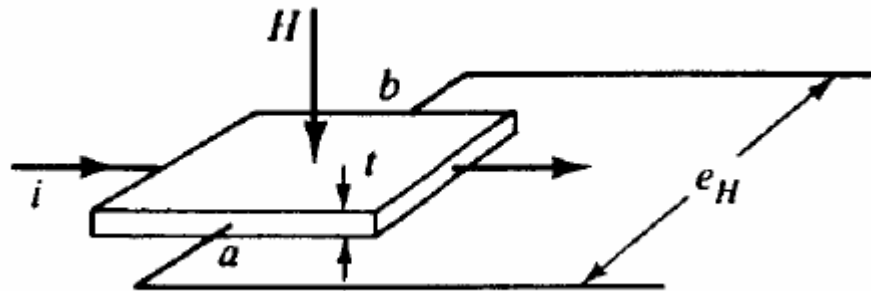


Fig. 2.12 Relationship between magnetic field strength, current and EMF in the Hall Effect [2.41]

The magnitude of the magnetic field strength can be obtained by $H = \frac{e_H t}{R_H i}$ where t is the thickness of the plate and R_H is the Hall constant which is a property of the material. This technique of measurement is not suitable for rotating core loss testers due to the difficulty in the installation except in a rotating disk sample which was developed by Flanders in 1985 [2.41].

2.2.4 B- tips

In 1949, Werner developed the B-tip method which is used in determining the magnetic flux density of the sample. In 1961, Kaplan used it for rotational core measurement [2.42] and followed by Brix in 1982 [2.43], Sievert in 1990 [2.44]. Fig. 2.13 shows that two needle tips are placed at certain distance apart in contact with the sample surface in order to acquire the value of the induced electromotive force V .

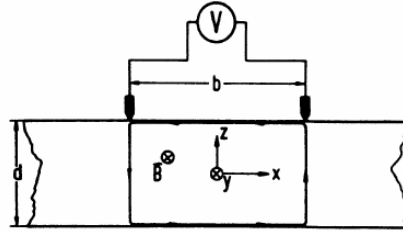


Fig. 2.13 Principle of measuring one component of B using tips [2.45]

If the sample is a thin lamination, the measured voltage can be measured based on the Maxwell's equations and the expression become

$$V = \frac{bd}{2} \frac{d}{dt} B_y \quad (2.23)$$

where d is the thickness of the sample, b is the distance between two tips, and B_y is the magnetic flux density in the y -axis. Thus,

$$B_y = \frac{2}{bd} \int V dt \quad (2.24)$$

The B-tip method is more suitable for batch measurement but it is only applicable for conducting material and high quality of preamplifier is also needed in detecting the weakest signal of voltage. Besides that, there is a difficulty in ignoring the stray fluxes through the air which gives an effect to the small size of sample. This technique is very sensitive compared to the B search coil technique.

2.3 Methods of measuring the rotational core losses

The first quantitative investigation on rotational core loss was studied by Baily in 1896. He investigated the rotational core hysteresis loss by measuring the torque exerted on a cylindrical armature consisting of a stack of iron laminations which is placed between pole pieces of rotational electromagnet. Hysteresis loss was obtained by eliminating the eddy current loss. The success story of Baily has driven more ideas and inventions of measuring techniques and system in determining the rotational core loss in magnetic materials [2.21].

2.3.1 Torque-metric method

Normally, this type of method is used in disk or ring sample apparatus by considering the mechanical torque meter in order to measure the torque due to the rotational core loss in the sample [2.21], [2.46], [2.47]. Besides that, the rotational core loss can also be evaluated by the calculation of the angular speed variation of sample [2.48]. The rotational core loss can be obtained directly from the reading of the torque and it is also able to measure the rotational core loss with the presence of high magnetic flux density. However, the construction of the torque meter is difficult which leads to the complicated mechanics.

2.3.2 Thermometric method

By measuring the temperature of the sample, the rotational core loss can be obtained. The devices that can be used in detecting the temperature in this method are thermocouples, thermistors, or thermo-viewers. The rotational core loss is proportional to the initial rate of the sample temperature rise if no cooling process is involved.

$$P_r = C \frac{d\theta}{dt} \quad (2.25)$$

where P_r , C and θ are the specific rotational core loss in Watt/kg, specific heat capacity of the sample and temperature of the sample, respectively.

This versatile method has been used in apparatus that use various types of sample, such as square [2.49], disc, ring [2.50] and cross [2.51] under various rotating magnetic fields. It can also measure the localized core loss at the T joints of a three-phase transformer

core as reported by Moses and Thomas in 1973 [2.52]. There are some shortcomings of this method such as the difficulties in calibrating and installing the thermosensors in the apparatus, and isolation against the surrounding.

2.3.3 Field-metric method

This method has high accuracy and great versatility during the process of measurement. The rotational core loss is measured by the existence of the magnetic field strength H , at the sample surface, and magnetic flux density B , inside the sample. The instantaneous B and H can give more desirable information such as various loss contributions, B loci and corresponding H loci, and harmonics, etc. Nevertheless, there are difficulties in manufacturing, calibrating and installing the B and H sensor coils. It is also very sensitive with the errors of the preamplifier phase angle.

There are two types of formula in calculating the rotational core loss using this field metric method, Type I and Type II. Type I evaluates the total specific core loss P_r , by using the Poynting's theorem as shown in [2.16], [2.42], [2.53], [2.54] and [2.55]

$$P_t = \frac{1}{T\rho_m} \int_0^T \left(H \cdot \frac{dB}{dt} \right) dt \quad (2.26)$$

where T is the time period of magnetisation, ρ_m is the mass density of sample, \mathbf{H} and \mathbf{B} are the vectors of magnetic field strength and magnetic flux density.

In Type II, the torque per unit volume due to the rotational core loss of the sample is calculated by [2.56]

$$T_r = \mu_0 |\mathbf{H} \times \mathbf{M}| = \mu_0 H M \sin\alpha \quad (2.27)$$

where μ_0 is the magnetic permeability of vacuum, M is the magnetisation, and α is the angle between \mathbf{H} and \mathbf{M} vectors.

2.3.4 Watt-metric method

For this method, the magnetic field strength H , is determined by the magnetisation current. The magnetic field strength H , magnetic flux density B , and core loss are measured by ammeter, voltmeter and wattmeter, respectively. The total specific core

loss can be evaluated using the Poynting's theorem equation. In rotational core loss measurement, this method is only valid to be applied to the vertical yoke single sheet tester due to the absence of the air gaps between the sample and the yoke. In the rotational core loss tester, the magnetic flux paths in the sample and the yoke are not well defined which lead to the excessive systematic error in magnetic field strength measurement. Due to the non-uniform magnetic field in the sample, the wound sensing coils through the small holes or B-tip technique are used to obtain the reading of magnetic field at the centre of the sample. The accuracy of this method depends on the structure of the yoke and the shape of the sample which are used in defining the magnetic flux paths.

2.4 Measuring apparatus of core loss

2.4.1 Disk and ring samples

In 1938, the first apparatus used in core loss measurement was developed by Brailsford [2.21]. The measurement of torque due to the rotational hysteresis is able to obtain the rotational hysteresis loss. The torque magnetometer as depicted in the Fig. 2.14 is used in the torque measurement. In order to ignore the torque caused by the anisotropy effect, a stack of several disks was arranged with the adoption of easy directions uniformly oriented and the sample was rotated in clockwise or anticlockwise directions. The average torque curve of these rotations gives the torque curve due to the rotational hysteresis loss. The friction of the mechanical system should be small in order to gain high accuracy in torque measurement.

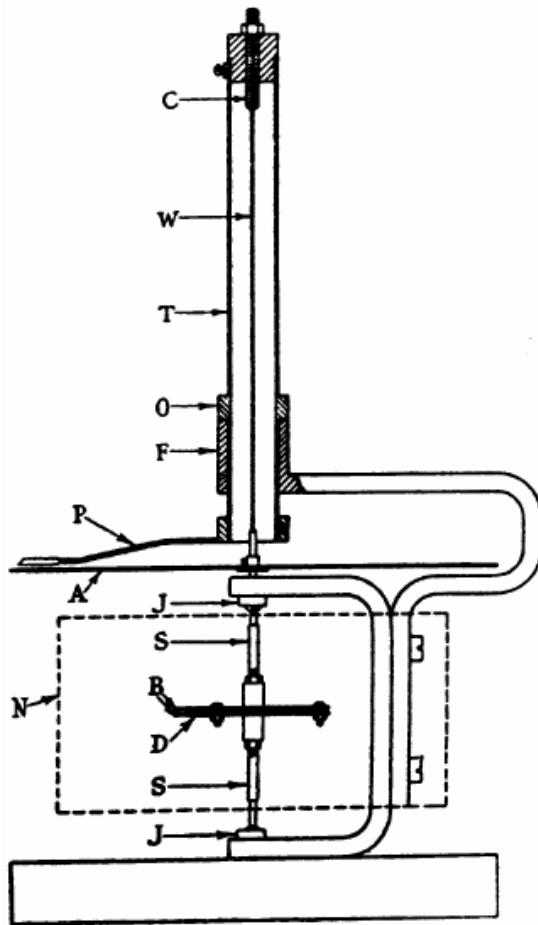


Fig. 2.14 Torque magnetometer with the labelled parts [2.21]

A represents the graduated aluminium disk, B is the brass disks to clamp the sample, D is the sample, N is the pole faces of an electromagnet to generate the applied field, and P is the pointer.

Flanders invented a rotating sample magnetometer in 1967 [2.57], which can be used for multiple purposes of measurement such as magnetic moment, rotational hysteresis, spin flop, and properties related to anisotropic energy. The measurements were performed on the single piece of rotating sample and the sensing coils were used to detect the magnetisation which is perpendicular to the applied magnetic field. In this invention, Type II of field-metric method can be used in evaluating the torque measurement due to the rotational hysteresis. Two sensing coils should be connected in series opposition in order to minimize the pickup error caused by variation of magnetic field or by coil motion relative to H. The effect of mechanical friction was removed in this rotating sample magnetometer and it gives better results compared to the torque

magnetometer. This magnetometer was improved by replacing the sensing coils technique with the new technique called Hall elements in 1985 [2.41].

A fixed disk sample was used by Fiorillo and Reitto in 1988 and 1991 [2.17], [2.58], as illustrated in Fig. 2.15. The equipment used the thermometric method to measure the temperature variation of a sample. The three-phase motor stator will generate the rotating field and rotational core loss that will be estimated by using both the methods: thermometric method and field-metric method Type I. The results for both methods are well explained in Fig. 2.16 when the experiments were conducted at 50 Hz in three different materials: soft iron, grain oriented silicon iron and non-oriented silicon iron.

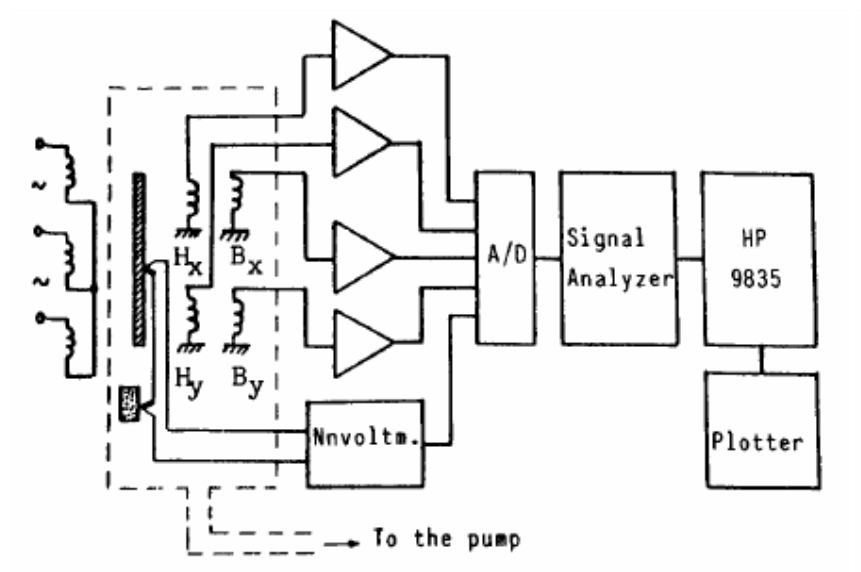


Fig. 2.15 Layout of the experiment built by Fiorillo and Reitto (1988) [2.58]

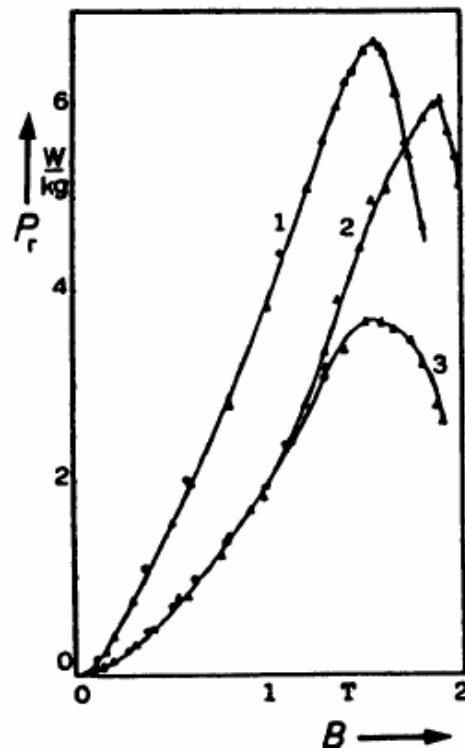


Fig. 2.16 Rotational core loss versus flux density in three materials: (1) soft iron, (2) grain oriented silicon iron, and (3) non-oriented silicon iron [2.58]

Reisinger (1987) created an apparatus using the thermometric and field-metric methods during the operation. This apparatus used a stack of ring samples and it has the same features as the apparatus that uses the disk samples as shown in Fig. 2.17 and Fig. 2.18.

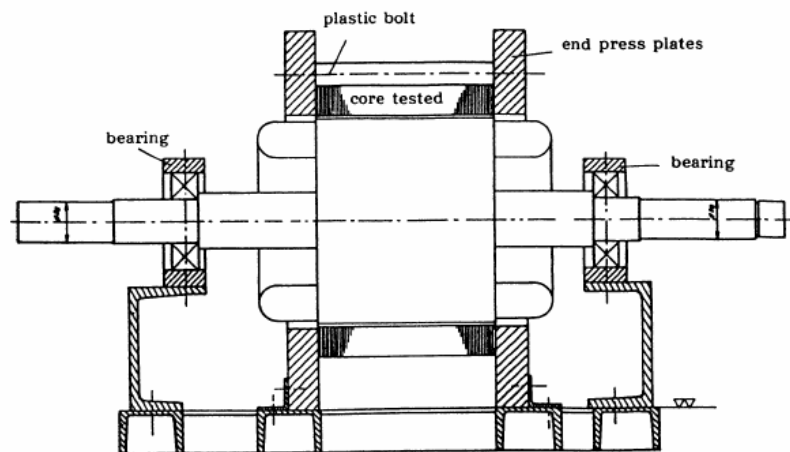


Fig. 2.17 The set up apparatus of rotational power loss measuring system that uses a stack of ring sample built in 1987 [2.50]

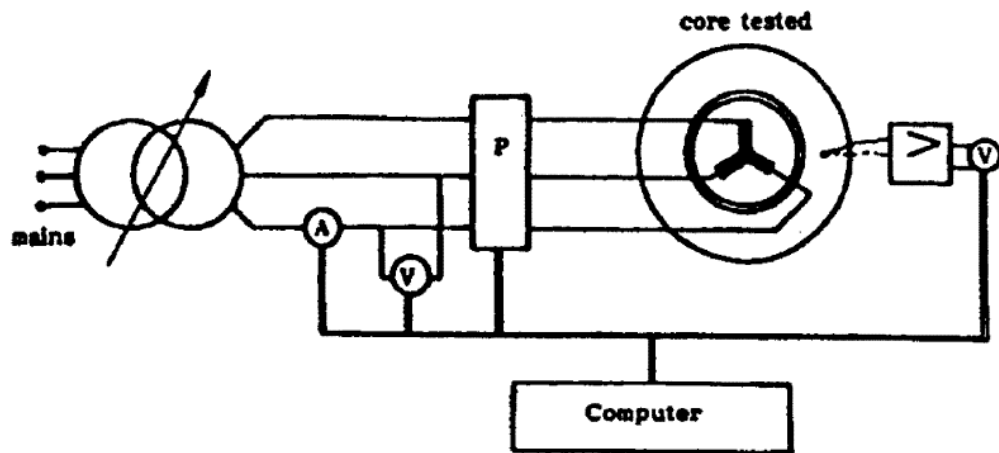


Fig. 2.18 The circular diagram of the rotational power loss measuring system by [2.50]

2.4.2 Cross and strip samples

The measurement of the rotating magnetic flux and rotating core loss in silicon iron lamination was conducted by generation of two-dimensional magnetic field due to the wound excitation windings on the cross sample. As in detail, the rotational core loss was measured by the thermometric method and the magnetic flux density can be determined by the sensing coils or the centre of the cross, while the magnetic field strength was obtained by the magnetisation current. There was no flux density feedback control for this set-up which gives an effect on the grain oriented sample. It will cause the magnitude of the flux density not to be in constant value. Fig. 2.19 shows the cross sample which has been invented in 1973 [2.51].

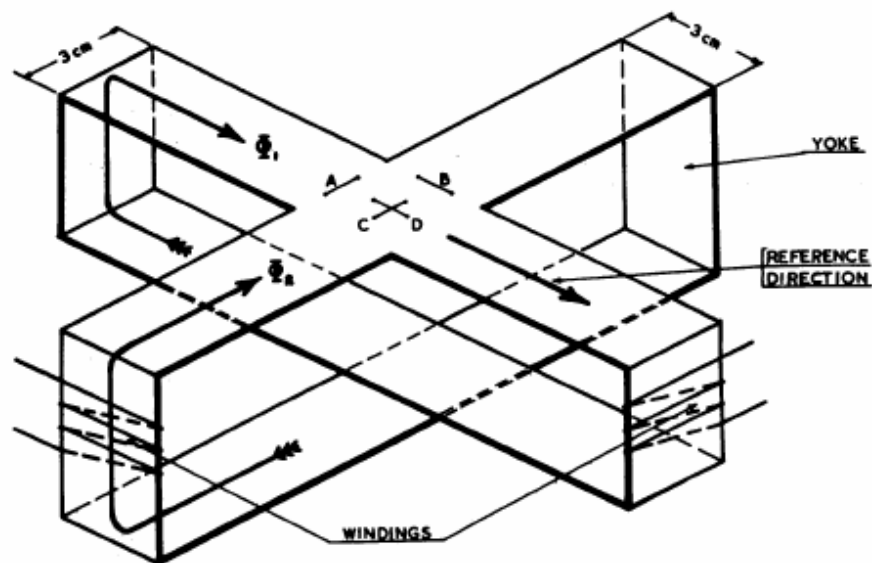


Fig. 2.19 Cross sample used by Moses & Bleddyn Thomas (1973) [2.50]

Basak *et al.* (1978) considered cross samples and flux density feedback to increase the mechanical stress sensitivity of the rotational power loss in silicon iron and Fig. 2.20 explains the overview of this creation.

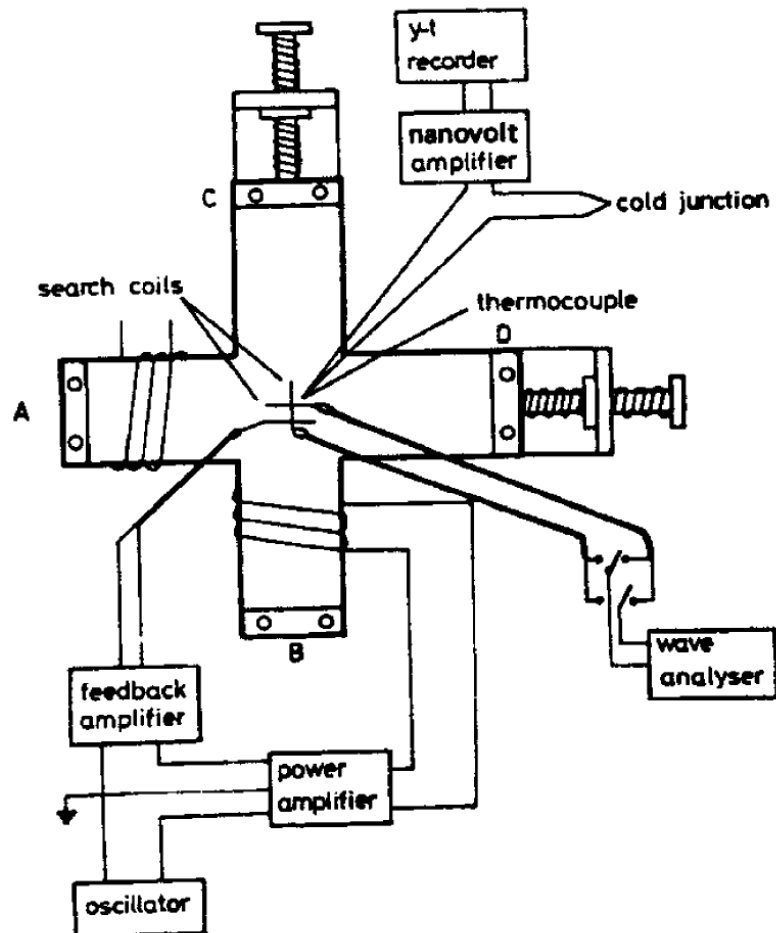


Fig. 2.20 The measuring rotational core loss apparatus where A and B are the fixed ends and C and D are the spring loaded ends [2.59]

A fully computerized control was developed by W. Brix (1982) together with cross sample in measurement system as illustrated in Fig. 2.21. The sensing coils were used to determine the magnetic field strength H , and magnetic flux density B , while the power loss was obtained by the field-metric method Type I.

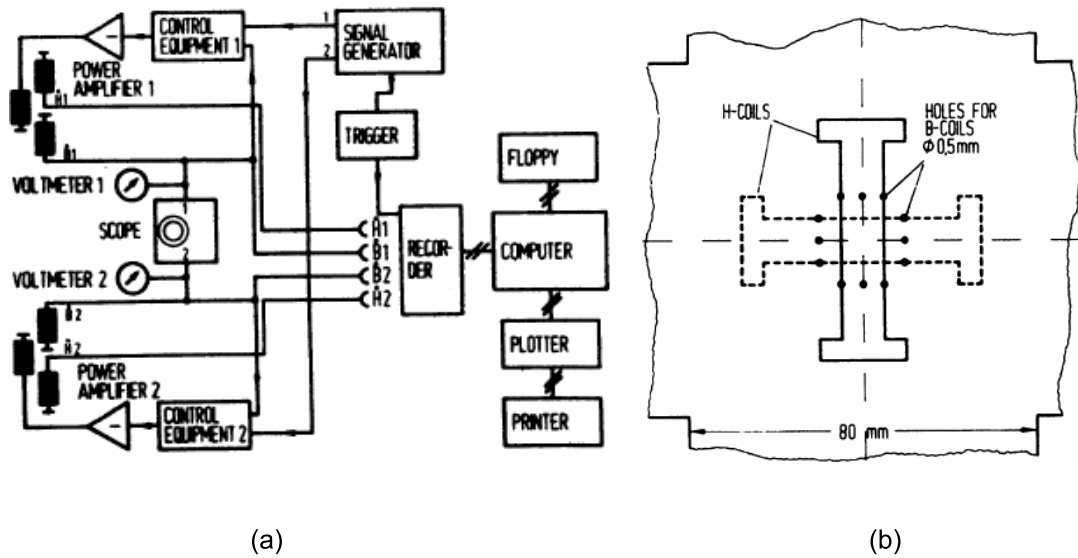
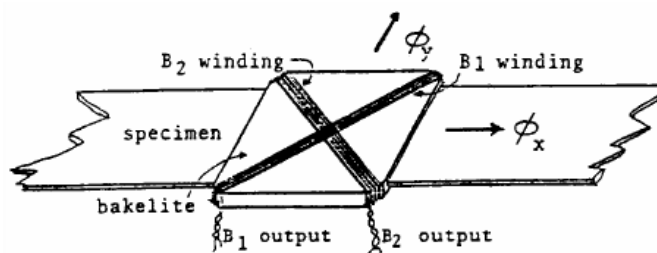
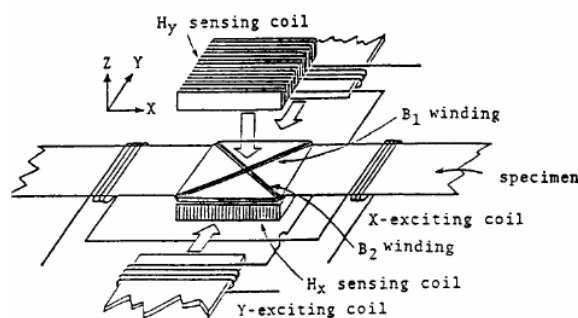


Fig. 2.21 Rotational core loss measuring system using cross samples [2.43] (a) Block diagram of the system (b) Arrangement of B and H sensing coils [2.43]

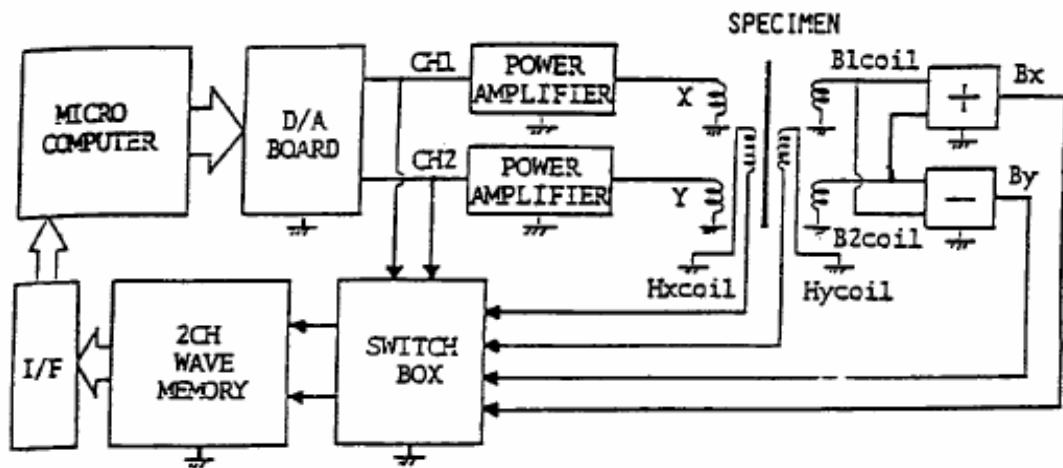
The measuring system with the single Epstein strip was built by T. Tanaka, S. Takada in 1991 and Tadashi Sasaki & Imamura in 1985. In this set-up, the sensing coils were used to measure magnetic field strength H , and magnetic flux density B , while the core loss was obtained by the field-metric method Type I. The overview of the measuring system can be seen in Fig. 2.22.



(a)



(b)



(c)

Fig. 2.22 Rotational core loss measuring system using an Epstein strip (a) configuration (b) magnetic flux search coils, and (c) system diagram [2.35], [2.60]

2.4.3 Epstein frame

The Epstein frame consists of 28 x 28 cm four-sided frame with 700 turns of both primary and secondary windings. Steel samples or strips should be 28 cm (± 2.05 cm) long and 3 cm wide and must be multiples of 4, with a recommended minimum number of 12 strips [2.61]. In order to remove any magnetic structure on the sample during the operation, the steel sample must be demagnetised. The core losses are determined by multiplying the primary current with the induced voltage from secondary windings to produce the instantaneous power waveform. The average value of instantaneous power is defined for the core loss in the sample [2.62]. There are some drawbacks in using the Epstein frame as a tester such as the non-uniformity distribution of flux density [2.63], the requirement of great amount of steel samples, complexity in sample preparation, and the existence of the system errors due to the magnetic flux harmonics.

2.4.4 Toroid tester

It is quite similar with the testing setup of Epstein frame but the specimen sample of this type of tester is a wound toroid. There are primary and secondary windings of toroid while the excitations have been applied to the primary and induced the secondary to give the induced voltage. The toroid tester is good in small motor application compared to the Epstein frames due to the geometry of the toroid which resembles the motor. However,

when there is a small size of toroid tester, the cutting stresses may propagate to the centre of the samples and this will affect the measurement results. Because of that, the stress should be relieved in order to get high accuracy in measurement. Besides that, the operation of the core loss measurement of this tester is similar with the Epstein frames. The major disadvantage of the toroid tester is the complexity in forming the toroid since the toroid must be wound properly and this will take much time to complete [2.64].

2.4.5 Square samples

The square samples were found as the suitable shape in getting more uniform magnetic field [2.21], [2.65]. Because of that, Brix, Hempel and Schulte were developed a tester which used the square samples in 1984. The B-tip technique has been used in detecting the magnetic flux density. Fig. 2.23 shows the tester with the whole arrangement and the installation of the sensors.

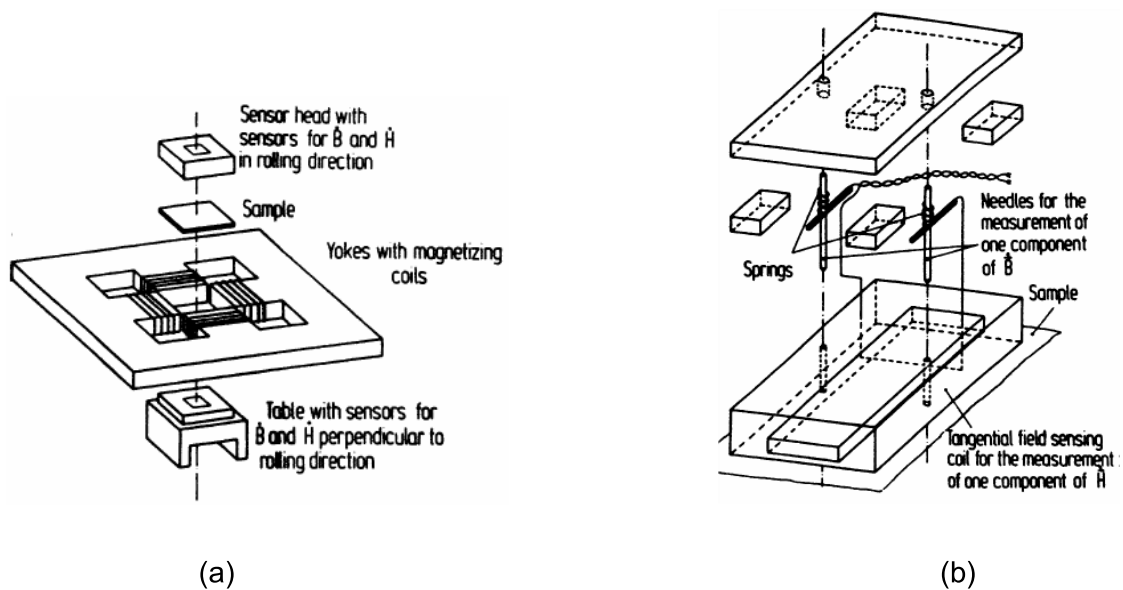


Fig. 2.23 Rotational core loss tester using square samples: (a) Arrangement of yoke, sample and sensors, and (b) details of sensor head for one component of H and B [2.21], [2.65]

In 1989, the system that can examine the behaviour of ferromagnetic material under alternating and rotational magnetic fields was developed by Enokizono and Sievert [2.30], [2.32] [2.45] [2.66], [2.67], [2.68]. This flexible system consists of a horizontal magnetic circuit with a square single sheet sample and adjustable air gap, an analog electronic circuit for flux density feedback control, and a computer which performs function generation and data acquisition in rotational core loss measurement. The

conventional H sensing coils and B sensing coils were used in detecting the magnetic field strength H , and the magnetic flux density B , Enokizono suggested to thread the B sensing coils through small holes and the centre of square sample [2.66], [2.67] while for batch measurement, the B-tip technique is more convenient [2.44]. In order to get the optimum performance in the H measurement, the yoke laminations are arranged vertically and the magnetisation poles are shaped in wedges. Fig. 2.24 gives the overview of the measuring system, which is able to obtain the rotational core loss by considering the variation of techniques in determining the magnetic flux density.

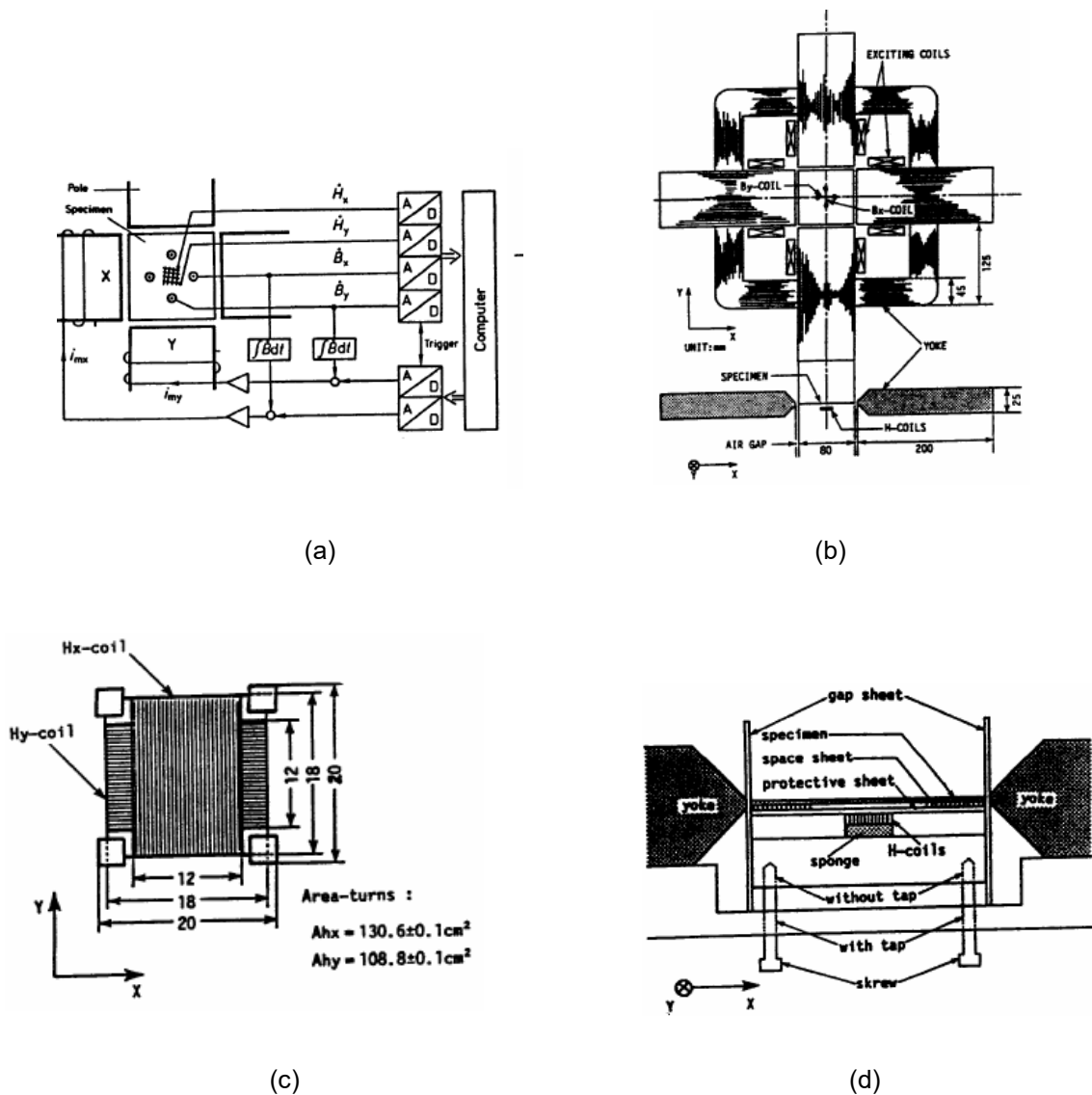


Fig. 2.24 Rotational core loss measuring system was built by Enokizono and Sievert: (a) Outline of system and B tips, (b) magnetic circuit and B sensing coils, (c) H sensing coils, and (d) setting of H coils [2.44], [2.66]

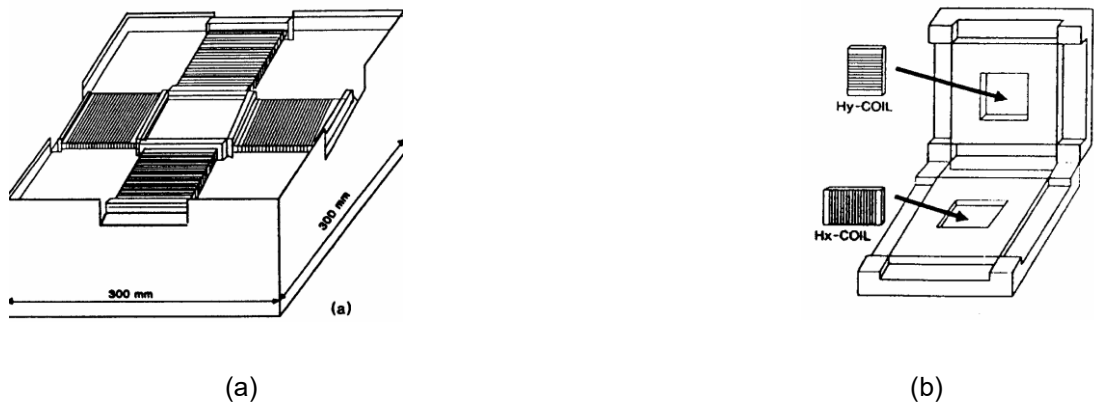


Fig. 2.26 The structure of square specimen tester developed by Gumaidh *et al.*: (a) tester, (b) sample and sensor holder [2.71]

The double vertical yokes were introduced by Kedous-Lebouc *et al.* (1991) and Zouzou *et al.* (1992) [2.72], [2.73]. The performance of the tester is similar with the invention by Enokizono and Sievert. Fig. 2.27 shows the overview of the tester with the structure of B and H search coils.

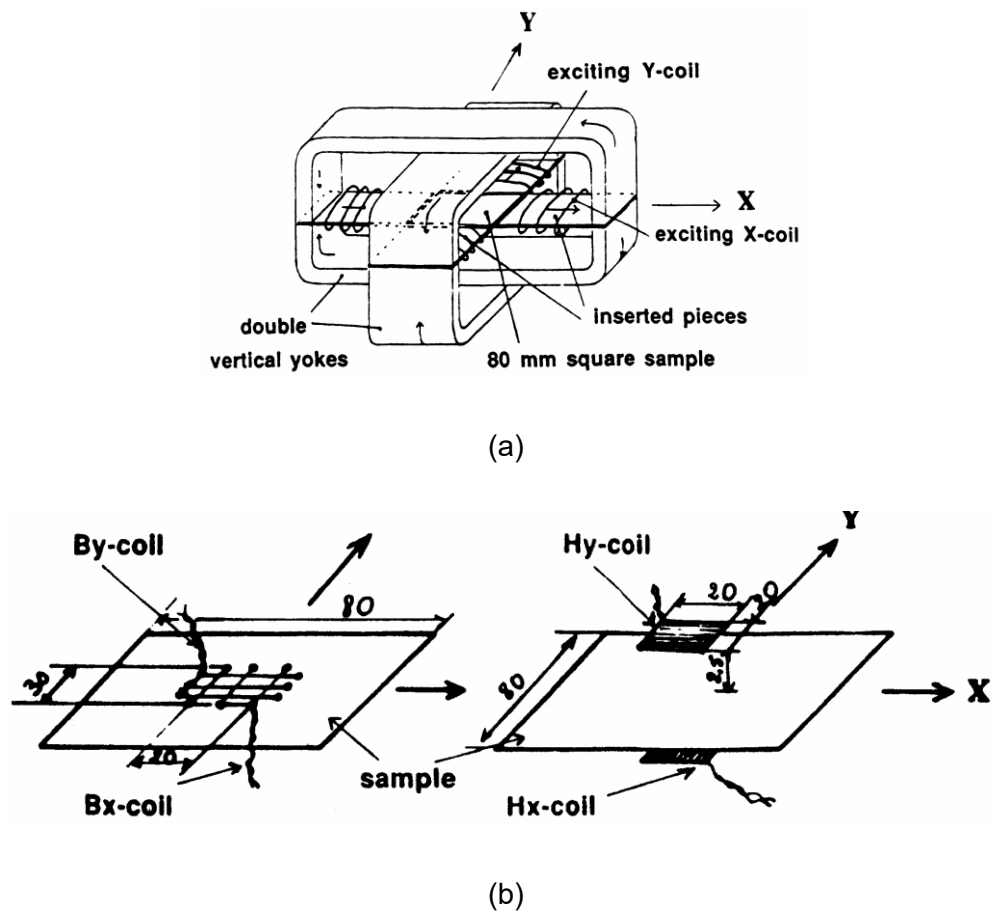


Fig. 2.27 Rotational core loss tester built by Kedous-Lebouc *et al.* (1991): (a) tester, (b) B and H search coils [2.72]

In 1993, Zhu *et al.* developed a square sample tester which contains the horizontal magnetic circuit with a square single sheet, which was designed to be at the centre of the system. B tips method is used for detecting the magnetic flux density. Magnetic properties under alternating and rotating magnetic flux is able to be measured by using this tester [2.16]. Fig. 2.28 shows the schematic diagram of the core loss testing system.

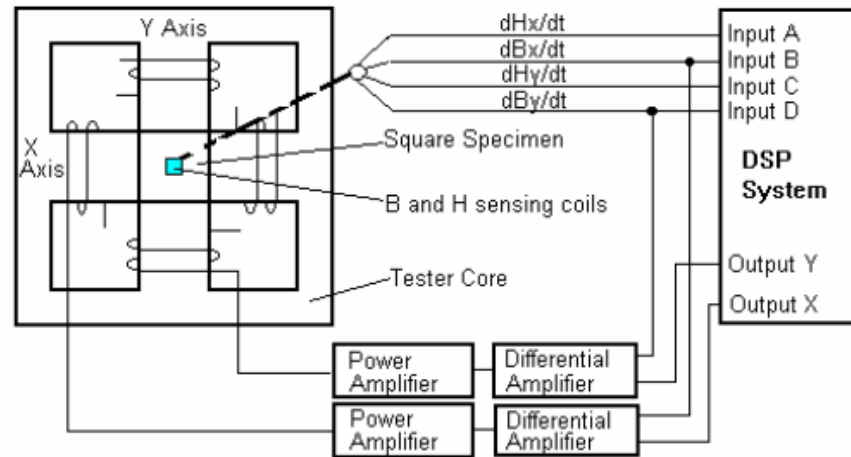


Fig. 2.28 Schematic diagram of square sample tester [2.16], [2.33]

This tester has been used to measure the magnetic properties of SMC material under 2-D excitation magnetic flux density by considering a novel sandwich arrangement of magnetic field sensing coils as illustrated in Fig. 2.29 [2.33].

Two groups of excitation coils in the single sheet tester are arranged on the x- and y-axes, respectively, and these coils generate the 2-D magnetic field in the square sample [2.74]. There are two power amplifiers which supply excitation voltages and excitation currents. Various 1-D and 2-D magnetic flux density vectors will be generated by controlling the waveforms and by changing the magnitudes and phase angle of excitation currents on the x- and y-axes [2.74]. Two identical differential amplifiers are needed to give a feedback control of magnetic flux density on both axes and the data signal processing is used for the specification of flux density waveforms and data acquisition [2.74], [2.75]. Alternating and rotational core losses of various electrical steels can be measured successfully including measurement, modelling and application in rotating motor analysis [2.16], [2.23], [2.33], [2.76], [2.77], [2.78]. Both core losses are calculated by measuring magnetic field strength H , and magnetic flux density B .

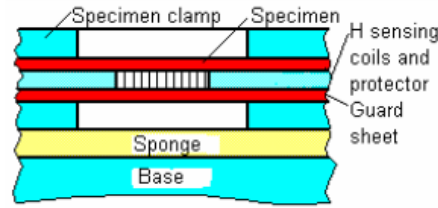


Fig. 2.29 Sandwich arrangement of H sensing coils [2.16], [2.33]

Zhu *et al.* (2005) used the 2-D magnetic property tester together with 50 x 50 x 1.25 mm sample of SMC material, SOMALOY 500. The sample has been tested by employing 2-D Rogowski-Chattock H coils in order to measure the surface field strength as illustrated in Fig. 2.30 (a). From Fig. 2.30 (b), it can be seen that H coils are closely attached with the sample surface to obtain the correct value of the surface field strength [2.22].

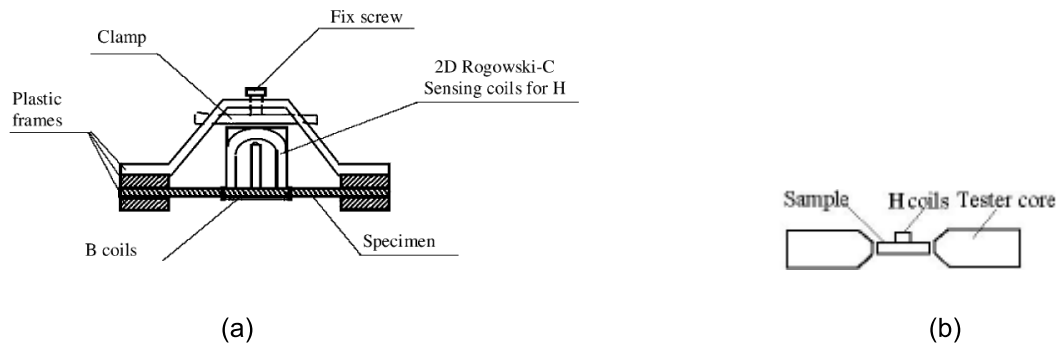


Fig. 2.30 (a) 2-D Rogowski-Chattock [2.79]. (b) Position of the sample between the magnetisation poles with attached conventional H coils [2.22]

By using the field metric methods, various shapes of sample were possible to be measured and this methods are able to imply great versatility [2.80]. The rotational core losses can be evaluated via Type I or Type II [2.74]. From Type I, the Poynting's theorem is able to compute the total specific core losses while type II uses the torque per unit volume in getting the core losses [2.74]. By using Poynting's theorem, the total core loss P_t in the sample can be expressed as [2.42], [2.44], [2.54], [2.55], [2.60], [2.76]

$$P_t = \frac{1}{T\rho_m} \int_0^T \left(H_x \frac{dB_x}{dt} + H_y \frac{dB_y}{dt} \right) dt \quad (2.28)$$

where T is the time period, ρ_m is the sample mass density, H_x , H_y , B_x and B_y are the x and y components of B and H .

There are some advantages of using the square samples in the measuring testing system. First, two components of magnetic fluxes are controlled by feedback. Thus, it can simulate the actual situation of electrical machine operation since the generation of magnetic field excitation can be controlled to be in various magnetic flux patterns. The distribution of magnetic field is more uniform when the measurement is carried out in the centre of the specimen. Besides that, the determination of B and H are able to obtain more information which contributes to the understanding of the mechanisms of rotational core losses. Furthermore, the specimen preparation is much simpler compared to the previous specimens. The major shortcoming of this system is the difficulty in controlling the excitation waveforms of B to be sinusoidal when the sample is close to saturation. As reported in [2.16] the highest flux density values are 1.6 T and 1.2 T for the non-oriented and grain oriented electrical sheet steels, respectively.

2.4.6 3-D Magnetic property testing system

Each magnetic material that is excited under an alternating or rotating magnetic flux density has been experienced on the rotation of magnetic domain which makes the 3-D vector flux excitation also needed to take into account [2.81].

The 3-D magnetic property testing system was successfully created by Zhu *et al.* in 2001 in order to magnetise cubic samples of soft magnetic materials [2.82], [2.83]. This system consists of a 3-D yoke to guide the magnetic fluxes in three axes, which is wound by three groups of excitation coils, a data acquisition system, three groups of coils to produce magnetic flux density B , along the orthogonal x-, y- and z-axes and they are able to produce different magnetic flux patterns such as alternating, rotating in a plane and rotating in a 3-D pattern with the loci of the flux density, thus various flux density loci like circularly and elliptically rotating flux density are able to be obtained by controlling the three components of the magnitude flux density B , vectors [2.40], [2.60], [2.84]. The 3-D tester also has been attached with a feedback control system which contains a control unit and three high power amplifiers [2.83], [2.85].

As shown in Fig. 2.31 (a), the voltage waveforms of magnetic flux density for the x, y and z components are generated by the software, and exported to a three-channel linear power amplifier, which feeds the excitation windings of the tester, through three isolated channels of the analog to digital (A/D) and digital to analog (D/A) board. The x, y and z components of B and H sensing coils generate voltage signals, which are collected by six independent input channels of the A/D and D/A board. The signals are used to

determine the relationship of B and H in order to calculate the core loss of the sample. The signals of B are also used for feedback control of the waveforms [2.81]. Fig. 2.31 (b) is the structure of the 3-D tester with cubic sample and search coils are located inside the tester [2.83].

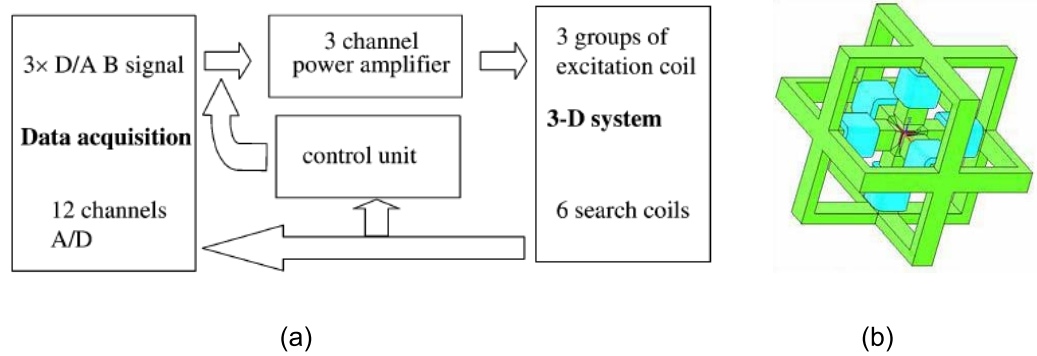


Fig. 2.31 (a) 3-D magnetic property testing system [2.86]. (b) Framework of 3-D Tester [2.82]

Three components of magnetic field vector is able to be detected by three search coils that are wound around the cubic sample while magnetic field strength can be measured by the calibrated H search coils which are located on the six surfaces of the sample as illustrated in Fig. 2.32 [2.82].

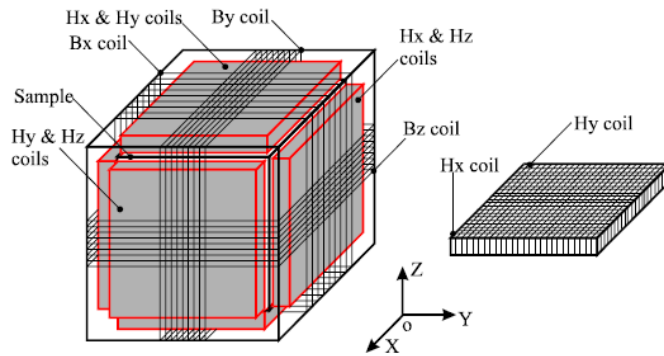


Fig. 2.32 A cubic sample and its B and H sensing coils [2.82]

Each surface of cubic sample has two H search coils such as (H_x and H_y) and one B search coil (B_z) which lead to twelve coils for H and six coils for B [2.82], [2.87]. Induced EMF of the search coils can be used in computing the components of magnetic field strength H , and magnetic flux density B , on each axis [2.82]. From both formulations, the value of coil coefficients K_H or K_B , would be determined to calculate the magnetic field at the sample surface [2.82]. The coil coefficients can be calculated by doing a calibration in a long solenoid as demonstrated in Fig. 2.33. Calibration of sensing coil was studied

by Guo *et al.* in 2006 considering the following equations. The calibration process is important in order to eliminate the system errors before being employed to measure the magnetic field components in the 3-D testing system [2.88].

$$B_i = \frac{1}{K_{B_i}} \int V_{B_i} dt \quad (2.29)$$

$$K_{B_i} = N_{B_i} A_{sp} \quad (2.30)$$

$$H_i = \frac{1}{\mu_0 K_{H_i}} \int V_{H_i} dt \quad (2.31)$$

$$K_{H_i} = \frac{V_H}{\sqrt{2} \pi f \mu_0 H_m} \quad (2.32)$$

($i=x, y, z$)

where V is the RMS value of the induced EMF, $\mu_0 H_m$ is the peak value of the flux density in the centre of the solenoid, f is the excitation frequency, and A_{sp} is the cross-sectional area of the sample.

During the calibration, excitation current which is supplied by AC power supply would enter the solenoid coils and the changing of current leads to the generation of varying magnetic flux density inside and outside the solenoid. The uniform and maximum magnetic flux density B_m , has been recorded at the centre of the long solenoid and it will be read by the gaussmeter. The H sensing coil inside the long solenoid is stationary and perpendicular to the magnetic flux density B .

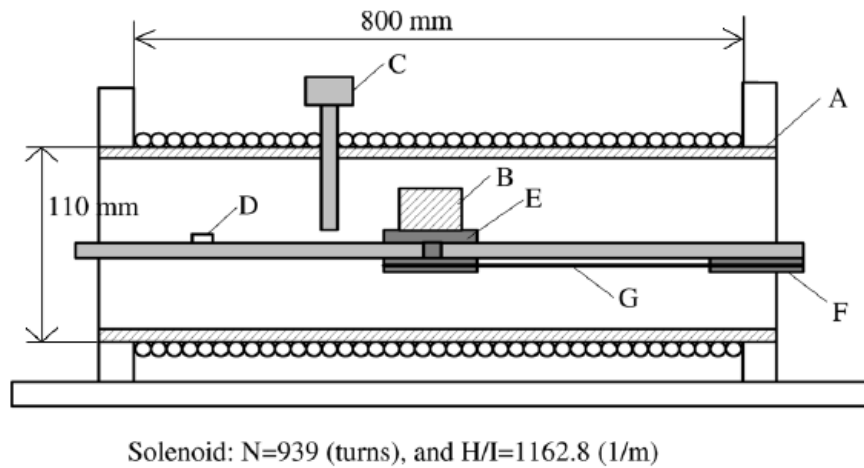


Fig. 2.33 Calibration of H sensing coils in the long solenoid [2.86]

In 2009, Li *et al.* improved the original structure of 3-D magnetic properties testing system by revising the size of the H coil which is approximately equal to the side of the cubic sample. The size of H sensing coil contributed to the non-uniform magnetic field at the measured area due to the demagnetisation factor [2.40]. H sensing coil was modified to be in minimum area (8.5×6) mm^2 in getting the accurate measurement. Two layers of coils with a small cross angle are able to induce signals with same magnitude but in different direction [2.87]. The improved structure also had been focused on sensing box part which combines six H coils and six B coils as shown in Fig. 2.34. The very thin and small circle of 60 turns B coil is embedded in the centre of the epoxy resin frame with 200 turns H coil is wound around a 0.5 mm thick epoxy resin and cover the B coil [2.40], [2.89]. The 0.05 mm enamelled copper wire is used for both B and H sensing coils to reduce the measurement error. Unwanted stray field will induce the additional EMF and adoption of cross bedded winding structure and twisted terminal are able to eliminate it [2.89]. Moreover, the twisted terminal of each coil would able to reduce the error induction [2.74]. In Fig. 2.35, six combination sets of H coils and B coils are attached at each surface of cubic sample and it will drive for coils on the opposite sides to be connected in series arrangement [2.40].

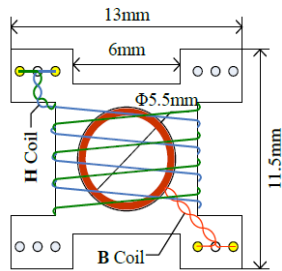


Fig. 2.34 Improved structure of H coils and B coils [2.40]

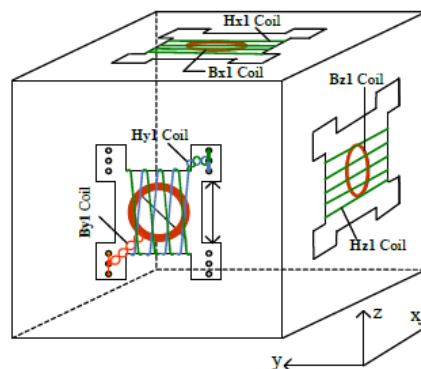


Fig. 2.35 Sample with sensing coils [2.40]

The measurements are accurate and precise with this new structure since there is a close attachment between H coils and sample. This condition is really demanded in getting the uniform magnetic field near the central area of the sample. The calibration of the improved H and B sensing coils also have been performed in a long solenoid due to the uniform magnetic flux density which is able to be obtained at the center of the solenoid [2.53]. The surface of the coil is set to be parallel to the generated magnetic field B [2.90] as shown in Fig. 2.36.

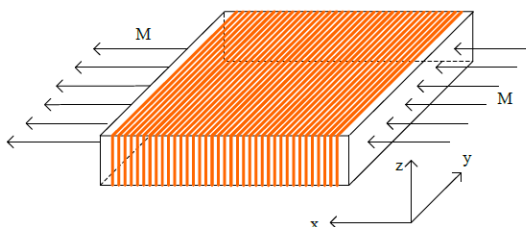


Fig. 2.36 Magnetic line of force through the coil [2.40]

The vectors of B and H in the 3-D magnetic properties measurement are detected by B-H sensing coils. In 3-D magnetic calculation, the coil coefficients should be in

3 x 3 matrix form with consideration of the diagonal and off-diagonal elements. From calibration of coils in a long solenoid, the diagonal elements which are the products of cross-sectional area and number of turns will be obtained. However, the non-cross sectional coefficients of the coils which are also known as the off-diagonal elements can be calibrated in the 3-D tester by using the calibrated diagonal elements of the coefficients [2.88].

The flux density in the center of the solenoid can be calculated by

$$B_0 = \mu_0 \frac{IN}{l} \frac{\frac{1}{2}}{\sqrt{r^2 + \frac{1}{2}^2}} \quad (2.33)$$

where l is the length of the solenoid, r is the radius of the solenoid, N is the number of two layers winding, μ_0 is the vacuum permeability, $4\pi \times 10^{-7}$ and I is the excitation current.

The induced EMF of the sensing coils under the alternating field is ruled by Faraday Induction Law and the coil coefficients K_{Bij} and K_{Hij} can be determined as per stated in equations (2.30) and (2.31).

As stated by Li *et al.* in 2014, once the cubic sensing box is getting well connected, the induction signal of each coil will be configured uniformly by following the sequence. The direction of the configured signal should be agreed with the excitation structures. Fig. 2.37 shows the value of E_B and E_H during the excitation of current along three axes. This figure describes that the EMF signals for H_x , H_y , H_z , B_x , B_y , and B_z are obtained from calibration in the long solenoid and it showed that the signals are good sinusoidal waveforms and have no phase difference [2.88]. Beside that, the phase angle is 90° between EMF signals and the excitation currents [2.88].

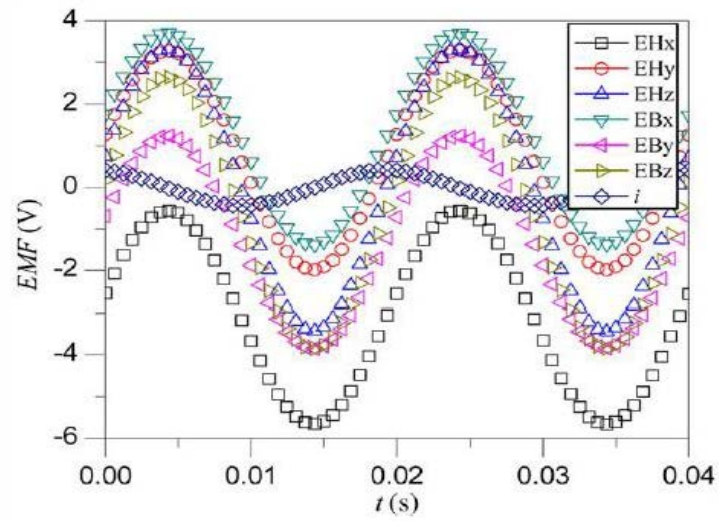


Fig. 2.37 The EMF signals of B and H sensing coils under three axes excitation current [2.88]

The alternating magnetisation in 3-D tester can be determined and the off-diagonal coefficients are also able to be calibrated by using the calibrated diagonal coefficients of the sensing coils as stated by Li *et al.* in 2014. Table 2-1 shows the diagonal coefficients of the B and H sensing coils. However, Table 2-2 exhibits the off-diagonal coefficients during the same calibration process. Both types of coefficients have been recorded from the sensing coil calibration inside the 3-D tester. K_{Hxy} and K_{Hxz} of H_x coil can be obtained by means of K_{Byy} and K_{Bzz} , respectively [2.88].

Table 2-1 Diagonal coefficients of the B and H sensing coils in unit of m^2 [2.88]

K_{Hxx}	K_{Hyy}	K_{Hzz}
2.346E-03	2.519E-03	2.462E-03
K_{Bxx}	K_{Byy}	K_{Bzz}
2.371E-03	2.359E-03	2.361E-03

Table 2-2 Off- diagonal coefficient of the B and H sensing coils in unit of m^2 [2.88]

K_{Hxy}	K_{Hxz}	K_{Hyx}
-8.591E-07	-1.933E-05	2.249E-05
K_{Hyz}	K_{Hzx}	K_{Hzx}
-6.996E-07	-4.820E-07	7.687E-06

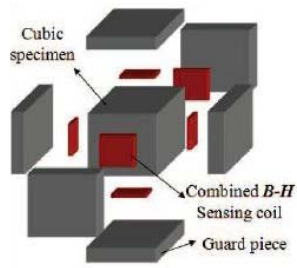
From Table 2-2, the positive values are expressed since the phase angle difference is 0° and the value will be negative when the phase angle difference is 180° [2.88].

The coefficients of the other two non-effective area direction are smaller and should be calibrated in the 3-D tester which can generate powerful field [2.91]. The off-diagonal coefficients of B coils are very small compared with the diagonal values and they can be ignored [2.92] while for H coils, the off-diagonal elements can not be ignored since the field perpendicular to the laminar H coil also induces large EMF due to irregularity of the H coil [2.93]. Hence, the induced voltages of the B and H coils can be expressed as

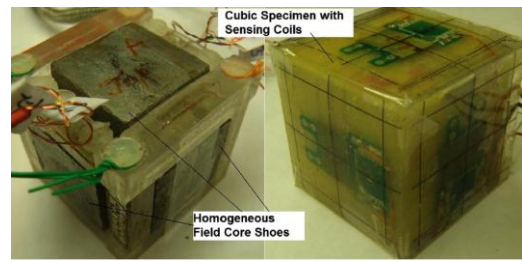
$$U_{Bi} = K_{Bi} \frac{dB}{dt} \quad (i = x, y \text{ and } z) \quad (2.34)$$

$$U_{Hx} = \mu_0 \left(K_{Hxx} \frac{dH_x}{dt} + K_{Hyy} \frac{dH_y}{dt} + \frac{K_{Hxz}}{\mu_0} \frac{dB_z}{dt} \right) \quad (2.35)$$

In measurement of magnetic material properties, the accuracy and precision during process of measurement are really demanded in preventing any errors from occurred. On top of that, many researchers are working on getting the best structure of 3-D tester in obtaining the high magnetic flux density production. Besides that, the uniformity of the magnetic flux density B , also has been focused during the magnetisation process. The guarding piece structure has been introduced by Li *et al.* [2.94] to improve uniformity of the magnetic field at the surface of the cubic specimen which leads to the measurement accuracy [2.79]. This guarding piece structure consists of six guard pieces that are made of same material with the test specimen [2.96] as shown in Fig. 2.38. Fig. 2.39 shows that the sensing coils are located inside the specimen [2.83]. This structure is able to hold the sensing coils to be at the center of each specimen surface and automatically will decrease the air gaps between core pole and specimen which leads to uniform magnetic flux density around that area [2.83].



(a)



(b)

Fig. 2.38 Structure of guarding pieces or field core shoes: (a) cubic sensing box with sample, sensing coils and guard pieces [2.83] (b) cubic specimen with homogeneous field core shoes [2.96]

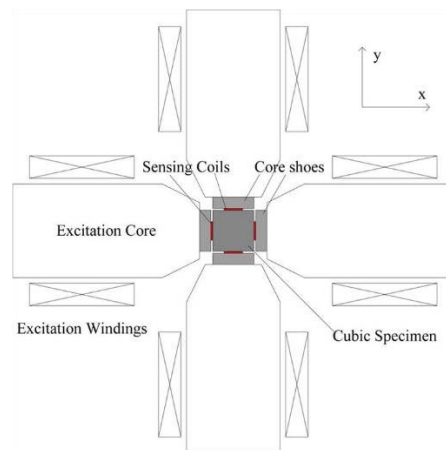


Fig. 2.39 Schematic diagram and cross section of the 3-D tester [2.88]

Fig. 2.40 shows the distribution of magnetic flux density inside the test specimen with and without guarding pieces enclosed around the sensing coils. Magnetic flux density is higher and more uniform with adoption of guarding pieces in the existence of homogeneous guarding pieces.

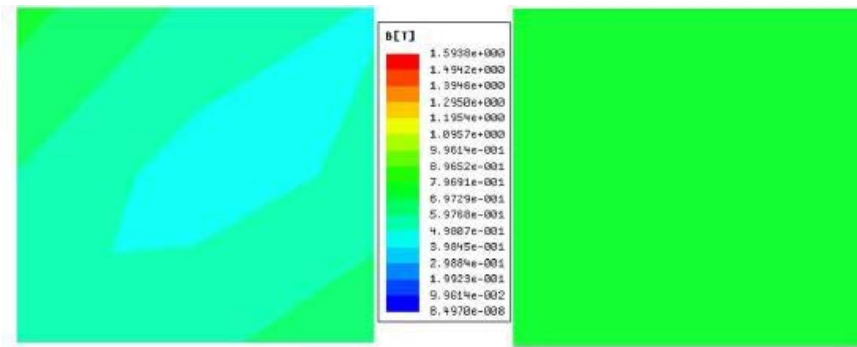


Fig. 2.40 Magnetic field distribution of the specimen without (left) and with (right) guarding pieces [2.96]

The structure of guarding pieces can significantly decrease the equivalent reluctance of the magnetic circuit and it is also able to reduce the required excitation current in magnetising the test specimen [2.83].

After some improvements done on the 3-D tester in getting the best results of measurement, Yang *et al.* realized that joints between cores and yoke of the original 3-D tester structure are not completely uniform. This non-uniformity would cause structural anisotropy and influence the results of measurement. The core-yoke structure has been improved by designing and modelling the “C-type” cores in the 3-D magnetisation structure. As shown in Fig. 2.41, this new model has three orthogonal “C-type” cores, six multilayer excitation windings, which are wound around the orthogonal core poles.

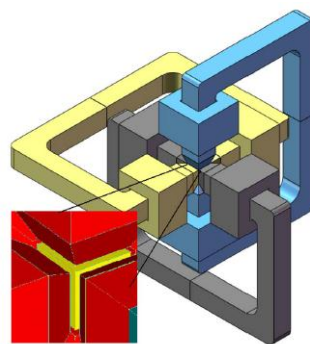


Fig. 2.41 Model of 3-D magnetisation structure with “C-types” cores [2.96]

This novel core is able to balance and smooth the path of the flux along the three axes. The “C-type” core is a laminated structure which is made of high grain-oriented silicon steel of HiB-27ZH95. From Fig. 2.42 (a) and Fig. 2.42 (b), it can be seen that the

terminals of the core poles are shaped to be in frustum of a square pyramid in order to concentrate the magnetic flux density B [2.96].

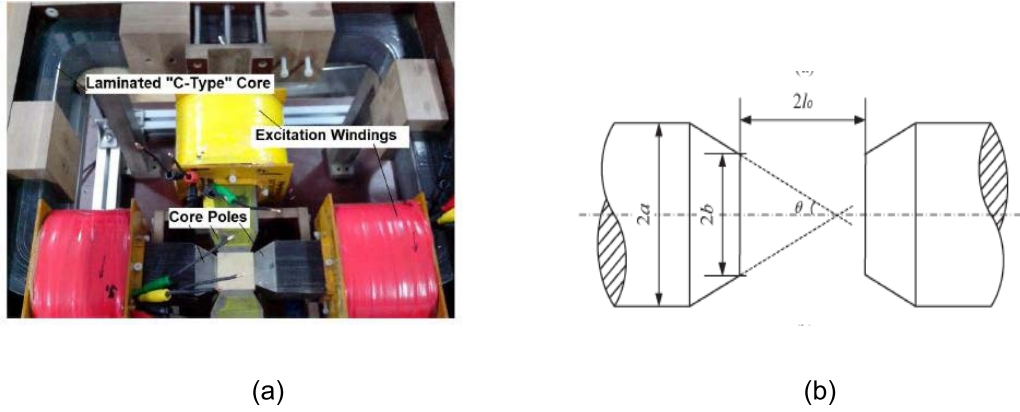


Fig. 2.42 (a) Prototype of laminated “C-type” core and excitation windings [2.96] (b) Schematic frustum structure of the core pole [2.96]

Since the very high magnetic flux density B , is claimed during the magnetisation of magnetic material specimen, the frustum core pole is proposed in generating a large gap magnetic flux density. More lines of magnetic force would be concentrated across the pole face, and the other fraction would pass through the conical surface which forms the concentrated magnetic field in the frustum of cone poles air gap [2.96]. The maximum magnetic flux density in the air gap can be formulated [2.97] as

$$B_o = \mu_o M \left(1 - \frac{l_0}{\sqrt{l_0^2 + b_r^2}} \right) + M \sin^2 \theta \cos \ln \frac{a_r}{b_r} \quad (2.36)$$

where a_r is the radius of the bottom circle, b_r is the radius of the upper circle, l_0 is the half length of the air gap, θ is the cone angle with the axis, and M is the magnetisation intensity.

As stated by Yang *et al.* [2.97] the maximum B_0 can be obtained when θ is 54.5° . Nevertheless, the uniformity of B_0 is not optimum at that angle. When cone angle with the axis is 39.5° , the relatively high and uniform magnetic flux density are obtained.

Fig. 2.43 displays the simulation of magnetic concentration in the core poles and cubic sample. It can be explained that magnetic fluxes are concentrated to the sample and being enhanced at the cone poles.

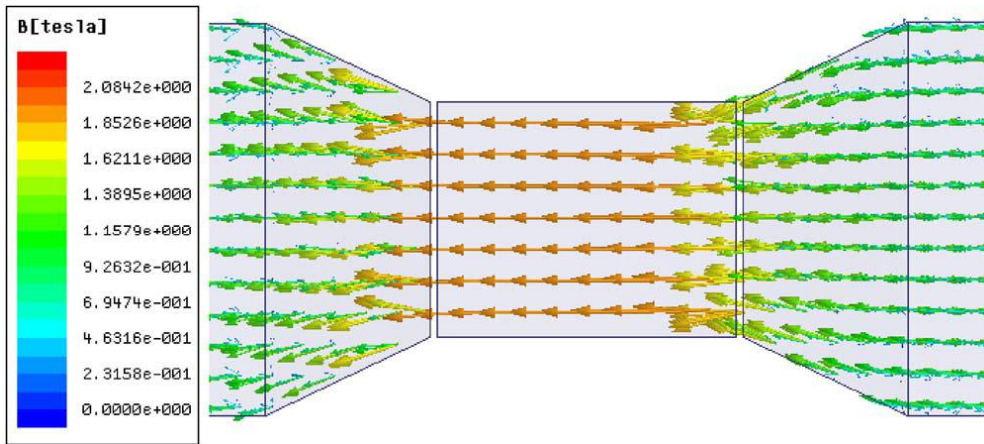
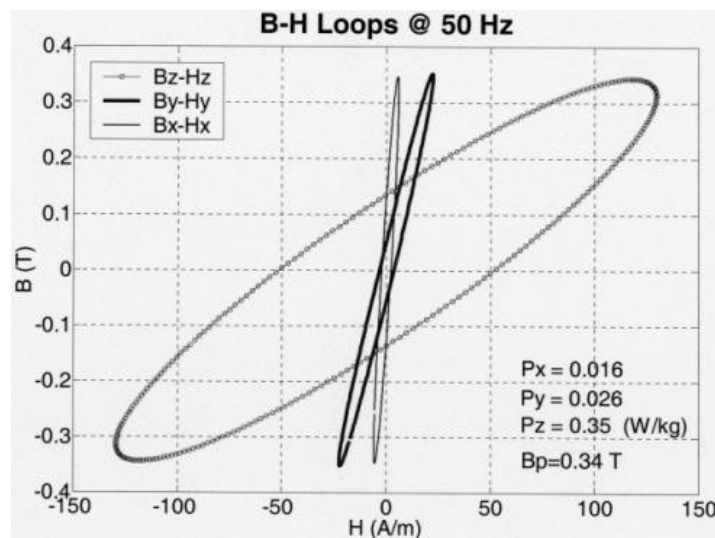


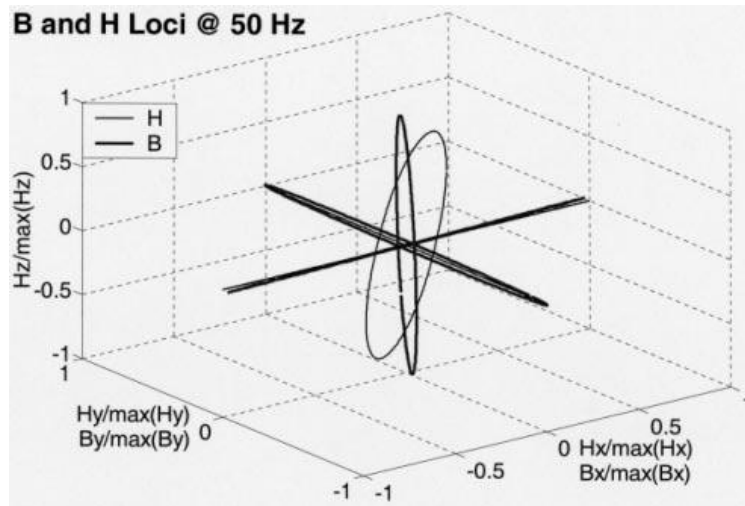
Fig. 2.43 Magnetic flux density distribution in the magnetic concentration model by finite element method [2.97]

2.5 Magnetic properties measurement of soft magnetic material by using 3-D magnetic properties system

In 2003, Zhu *et al.* used the 3-D magnetic property testing system to measure the characters of grain-oriented Hi-B M2-H 0.30 mm sheet steels. The measurement was done under alternating and rotating excitation fluxes to check the validity of the system and the results. The B and H loci are plotted by their maxima order in Fig. 2.44. Due to the strong eddy currents, the magnetic flux excitation in the z-axis is difficult to be maintained which made the corresponding B and H loci become ellipse.



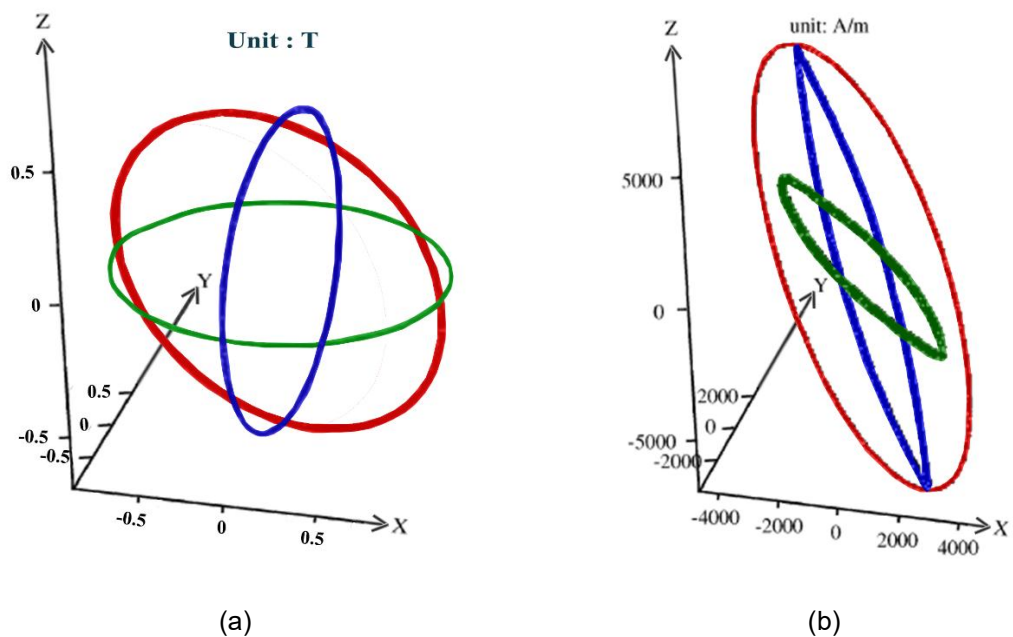
(a)



(b)

Fig. 2.44 (a) Hysteresis loop at 50 Hz along x-, y- and z-axes (b) B and H loci of grain oriented Hi-B in the XOY-plane [2.82]

The behaviour of SOMALOY 500 was investigated by using the 3-D magnetic property tester by Zhong *et al.* in 2005 [2.98]. Both 1-D and 2-D measurements are developed and Fig. 2.45 gives the B and H loci after being controlled to be circle at 0.7 T of diameter in the XOY-, YOZ-, and ZOZ-planes. The shapes are not completely matched and there is a small tilt due to the misalignment or imperfect winding of H sensing coils.



(a)

(b)

Fig. 2.45 (a) B loci when magnetic fluxes have been controlled to make B in circle shape (b) the corresponding of H loci [2.98]

Due to the misalignment of sensing coils with magnetic flux excitations, Guo *et al.* did some corrections by considering the rotational transformation of coordinates [2.86]. Fig. 2.46 shows the rotation of coordinates in three axes x , y and z . The prime axes x' , y' and z' are the misaligned axes of the 3-D sensor. θ_1 , ϕ_1 , and ψ_1 are the angles between x' and x , y and z respectively. Likewise, θ_2 , ϕ_2 , and ψ_2 and θ_3 , ϕ_3 , and ψ_3 respectively represent the angles between y' and x , y and z and z' and x , y and z .

θ_i , ϕ_i , and ψ_i ($i = 1, 2$ and 3) are able to be obtained when the excitation fields have been applied along the x -, y - and z -axes. The fields will generate field components of H_x' , H_y' and H_z' which are measured by H sensing coils. The projection angles θ_{x1} and θ_{x2} , both in the XOY- and XOZ-planes respectively can be calculated by considering method for 2-D measurement. Therefore, θ_1 , ϕ_1 , and ψ_1 can be determined by [2.98]

$$\theta_1 = \tan^{-1} \left(\sqrt{\tan^2 \theta_{x1} + \tan^2 \theta_{x2}} \right) \quad (2.37a)$$

$$\phi_1 = \tan^{-1} \left(\frac{1}{\cos \theta_{x2} \tan \theta_{x1}} \right) \quad (2.37b)$$

$$\psi_1 = \tan^{-1} \left(\frac{1}{\cos \theta_{x1} \tan \theta_{x2}} \right) \quad (2.37c)$$

The projection angles ϕ_{y1} and ϕ_{y2} which are denoted in the XOY- and YOZ-planes also can be evaluated and θ_2 , ϕ_2 , and ψ_2 can be calculated by [2.86]

$$\theta_2 = \tan^{-1} \left(\frac{1}{\cos \phi_{y2} \tan \phi_{y1}} \right) \quad (2.38a)$$

$$\phi_2 = \tan^{-1} \left(\sqrt{\tan^2 \phi_{y1} + \tan^2 \phi_{y2}} \right) \quad (2.38b)$$

$$\psi_2 = \tan^{-1} \left(\frac{1}{\cos \phi_{y1} \tan \phi_{y2}} \right) \quad (2.38c)$$

Similarly, the projection angle ψ_{z1} and ψ_{z2} , both in the XOZ- and YOZ-planes will give the formulation for θ_3 , ϕ_3 , and ψ_3 by considering these expressions.

$$\theta_3 = \tan^{-1} \left(\frac{1}{\cos \psi_{y2} \tan \psi_{y1}} \right) \quad (2.39a)$$

$$\phi_3 = \tan^{-1} \left(\frac{1}{\cos \psi_{y1} \tan \psi_{y2}} \right) \quad (2.39b)$$

$$\psi_3 = \tan^{-1} \left(\sqrt{\tan^2 \psi_{y1} + \tan^2 \psi_{y2}} \right) \quad (2.39c)$$

The actual value of the magnetic field strength H on the surfaces can be described from the measured values by [2.98]

$$\begin{bmatrix} H_x \\ H_y \\ H_z \end{bmatrix} = \begin{bmatrix} \cos \theta_1 & \cos \phi_1 & \cos \psi_1 \\ \cos \theta_2 & \cos \phi_2 & \cos \psi_2 \\ \cos \theta_3 & \cos \phi_3 & \cos \psi_3 \end{bmatrix}^{-1} \begin{bmatrix} H'_x \\ H'_y \\ H'_z \end{bmatrix} \quad (2.40)$$

where H'_x , H'_y and H'_z are the measured components of the magnetic field strength, and H_x , H_y and H_z are the true ones.

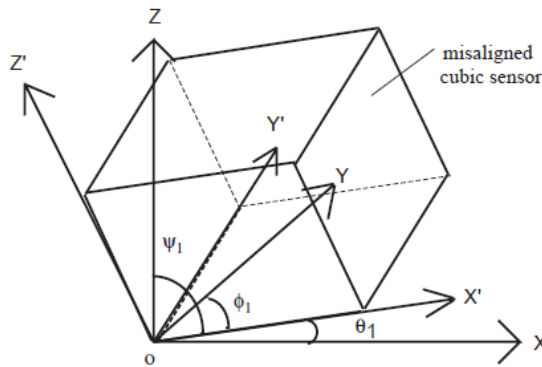


Fig. 2.46 Misalignment of sensors [2.98]

After some properties measurements of soft magnetic materials by using the 3-D tester had been successfully validated, Lin *et al.* (2005) characterized the magnetic properties of SOMALOY 500 in details by enhancing the accuracy factor such as sandwich arrangement comprising the sample, search coils and guard pieces. The 3-D measurements were developed by controlling the magnetic flux density. The magnetic flux densities are directed along three couples of yoke at 50 Hz of frequency after three components of magnetic fields B_x , B_y and B_z are controlled in sine waveforms with an amplitude of 1 T. Fig. 2.47 illustrates the B loci and the corresponding of H loci in 3-D space. Fig. 2.48 shows that the material is isotropic since the properties along x- and

y-axes look similar but the projection of plotted loop along z-axis gives slightly difference to x- and y-axes due to the pressure effect during the formation of the sample.

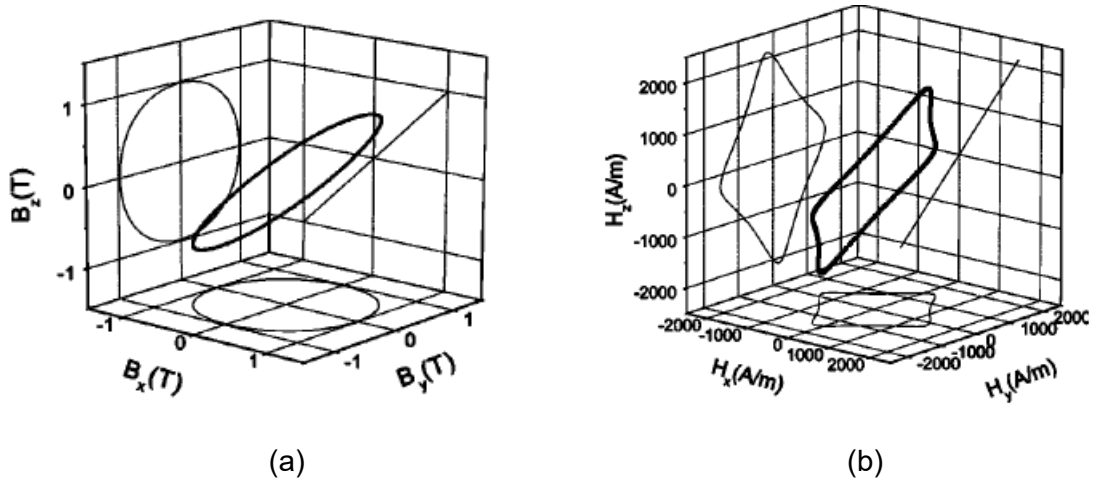


Fig. 2.47 (a) B loci and (b) the corresponding of H loci at operating frequency of 50 Hz [2.83]

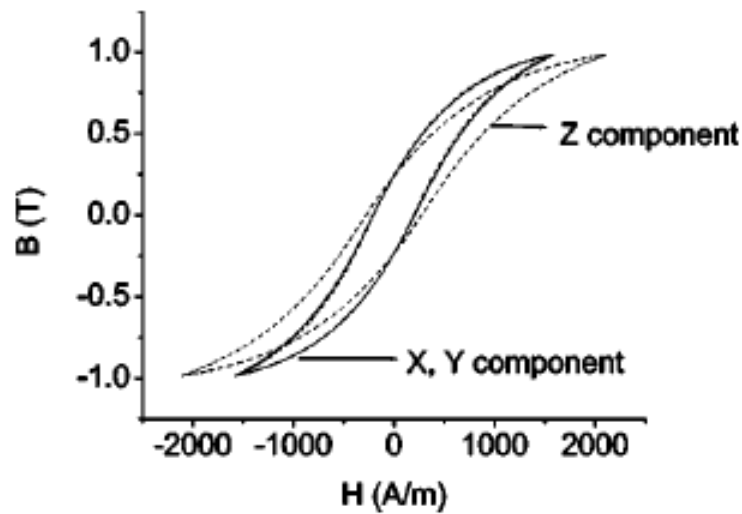


Fig. 2.48 The Hysteresis loop at 50 Hz along x-, y- and z-axes [2.83]

In 2005, Lin *et al.* designed and fabricated the sensing house for B and H coils. Fig. 2.49 shows the convenient sensing house has integrated six H coils with a planar correction coil which is embedded in each H coil before measuring the cubic sample under rotational flux densities. B loci are controlled to be circle and spherical shapes as shown in Fig. 2.50 and Fig. 2.51, respectively [2.85]. Both figures show that the calibration and calculation can well measure the B and H components.

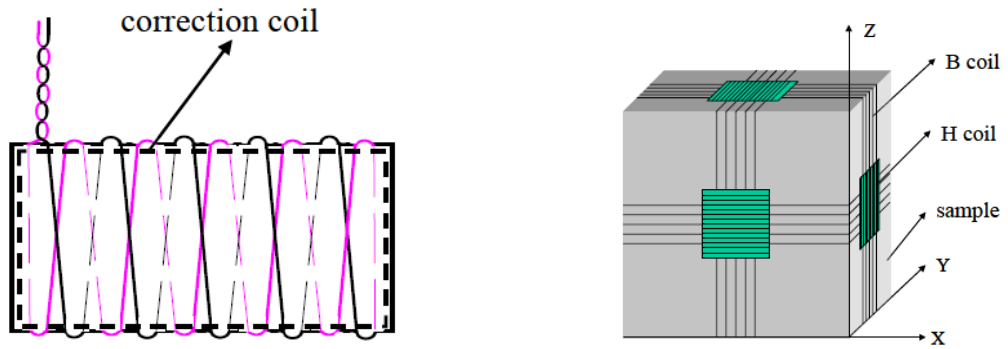


Fig. 2.49 Arrangement of B and H sensing coils (left) with consideration of planar structure for H coils (right) [2.85]

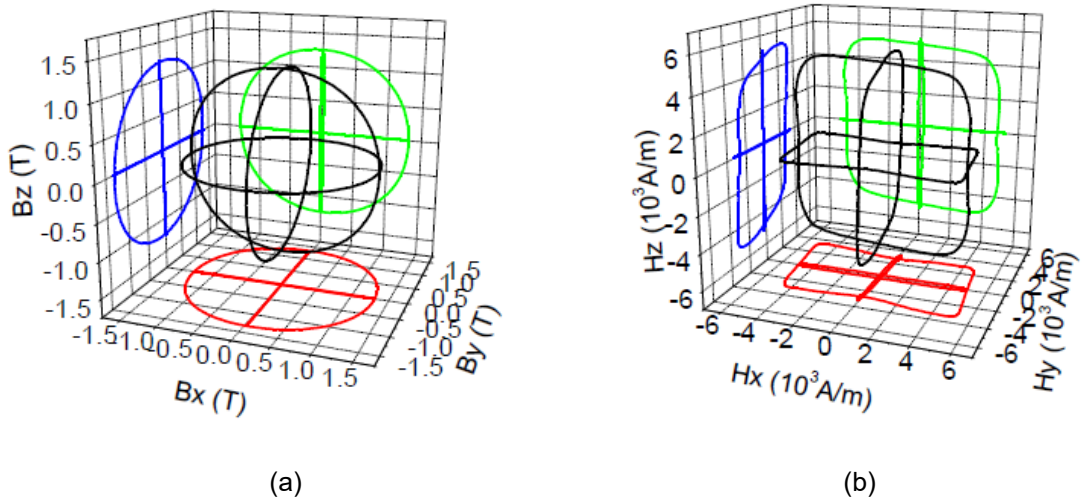


Fig. 2.50 (a) Circular B loci when the magnetic field has amplitude of 1.3 T at 50 Hz. (b) The corresponding of H loci in 3-D space [2.85]

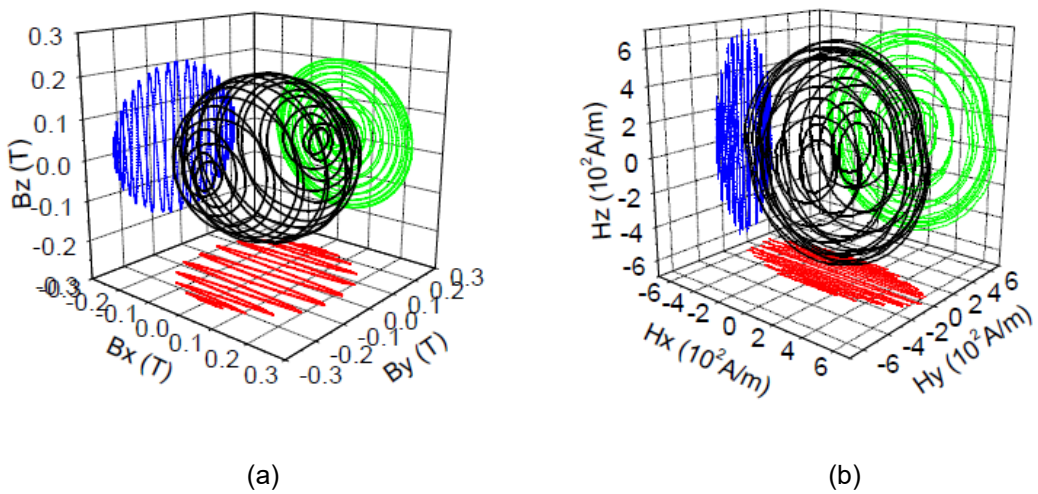
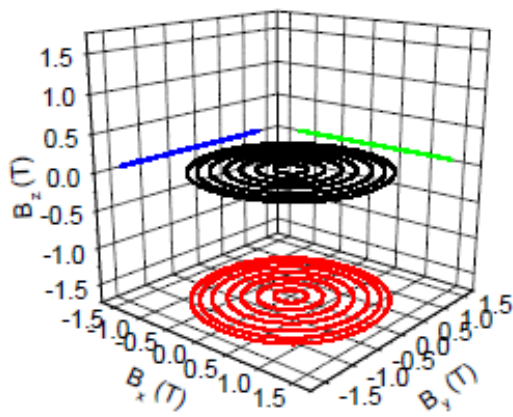
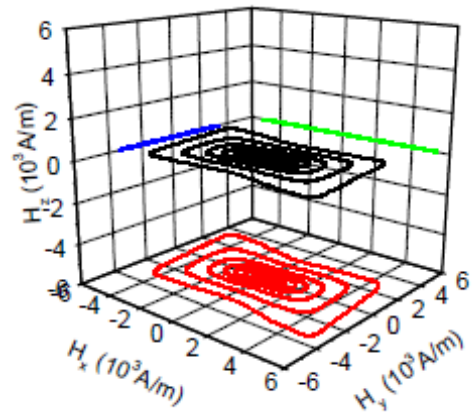


Fig. 2.51 (a) B loci in spherical shape at 50 Hz lying in three orthogonal planes. (b) The corresponding H loci [2.85]

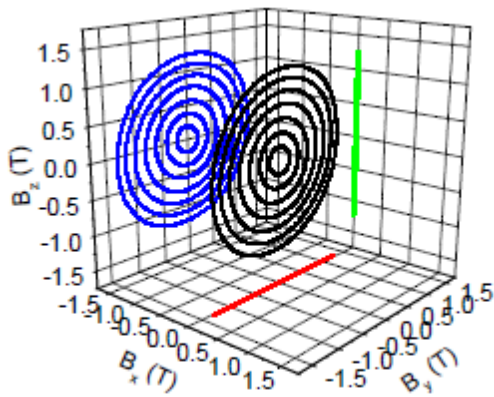
SOMALOY 500 was actively studied by Lin *et al.* in 2007 and the behaviour of this material has been continuously studied since. Special sensing devices are fabricated which consist of six H coils with embedded planar B coils to measure the properties of the sample under alternating and rotating magnetisations. Fig. 2.52 describes the shapes of B and H loci when magnetic flux densities are controlled to be circle with maximum amplitude of B is 1.3 T. It can be seen that H loci shape changes from circle to rectangle when there is an increment [2.99].



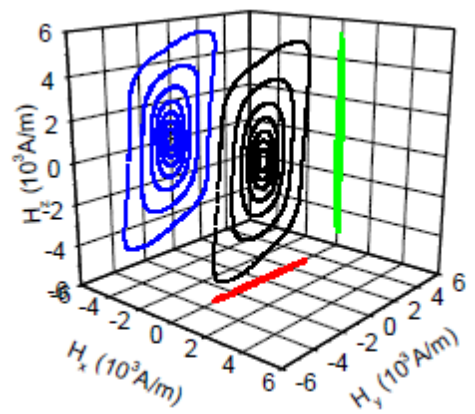
(a)



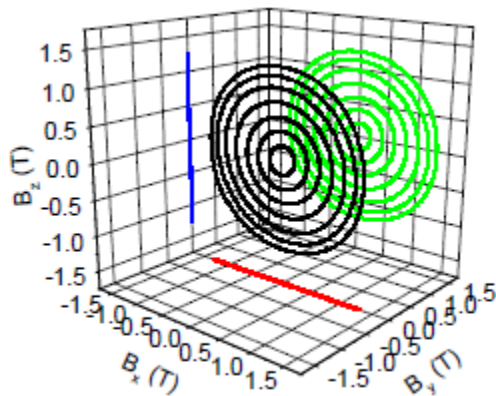
(d)



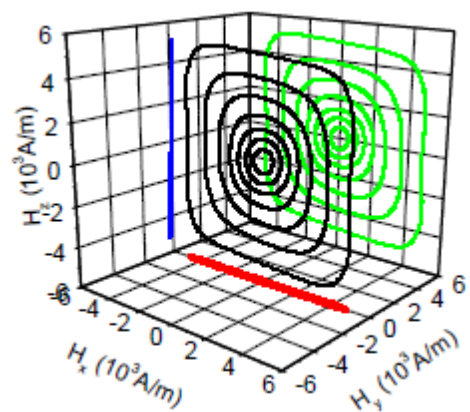
(b)



(e)



(c)



(f)

Fig. 2.52 Round B loci in (a) XOY-plane, (b) YOZ-plane, (c) ZOX-plane and the corresponding H loci in (d) XOY-plane, (e) YOZ-plane and (f) ZOX-plane at 50 Hz [2.99]

According to Fig. 2.53, the larger core losses are recorded when SOMALOY 500 sample is magnetised under rotational magnetic fluxes compared to the alternating magnetic fluxes and the magnetic properties under alternating fluxes are consistent with data given by manufacturer [2.99]. The magnetic properties of SOMALOY 500 material were studied in 2007 by controlling the magnetic fluxes to be in ellipse shape. This measurement was conducted at 50 Hz of operating frequency and it involves the series of shape changes of B loci by increasing the magnitude of B along the x-axis to evolve from a straight line into a perfectly round shape in the XOY-, YOZ- and ZOX-planes as indicates in Fig. 2.54. The corresponding of H loci are also described in the same figure. Similarly, Fig. 2.55 shows the evolvement of magnitude of B along the y-axis to make x-axis as a major axis [2.100].

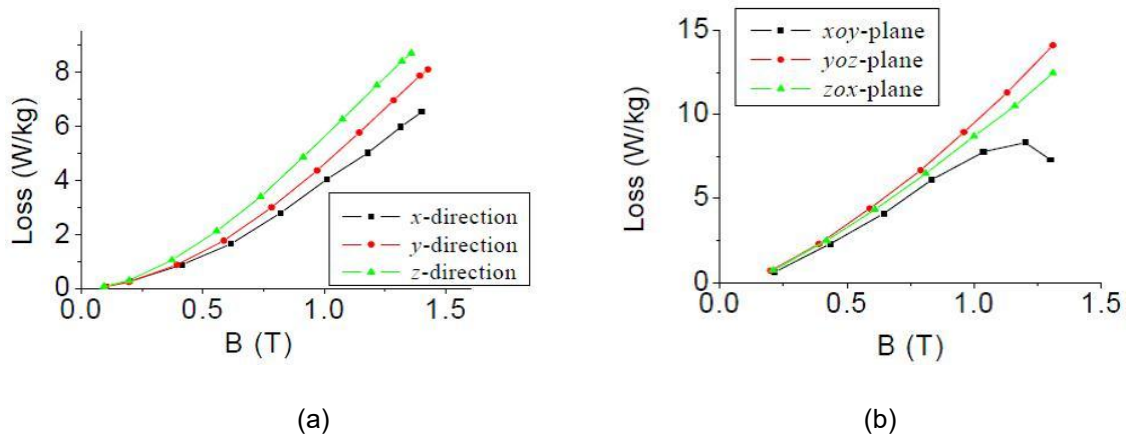
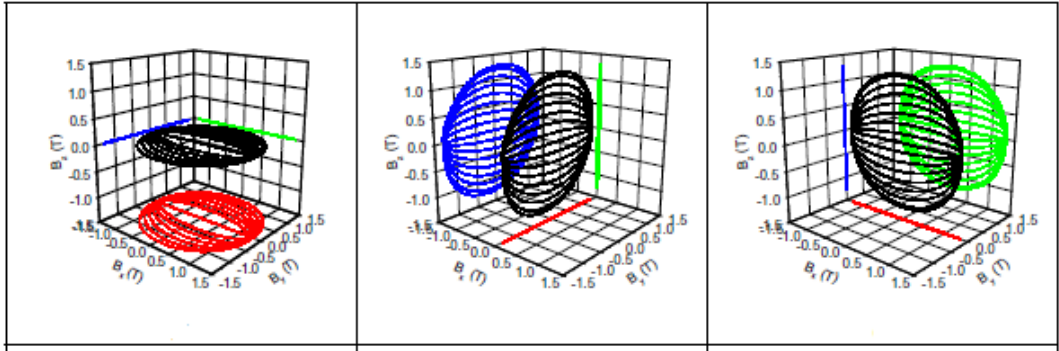


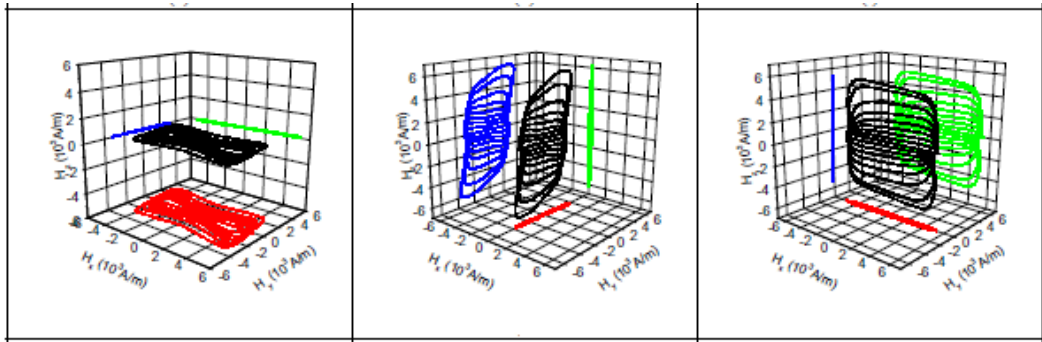
Fig. 2.53 Power core loss under (a) alternating magnetic fluxes along x-, y- and z-axes (b) rotational magnetic fluxes in three different planes at 50 Hz [2.99]



(a)

(b)

(c)



(d)

(e)

(f)

Fig. 2.54 Elliptical B loci with y as a major axis in (a) XOY- (b) YOZ- (c) ZOX-planes and their corresponding H loci in (d) XOY- (e) YOZ- (f) ZOX-planes [2.100]

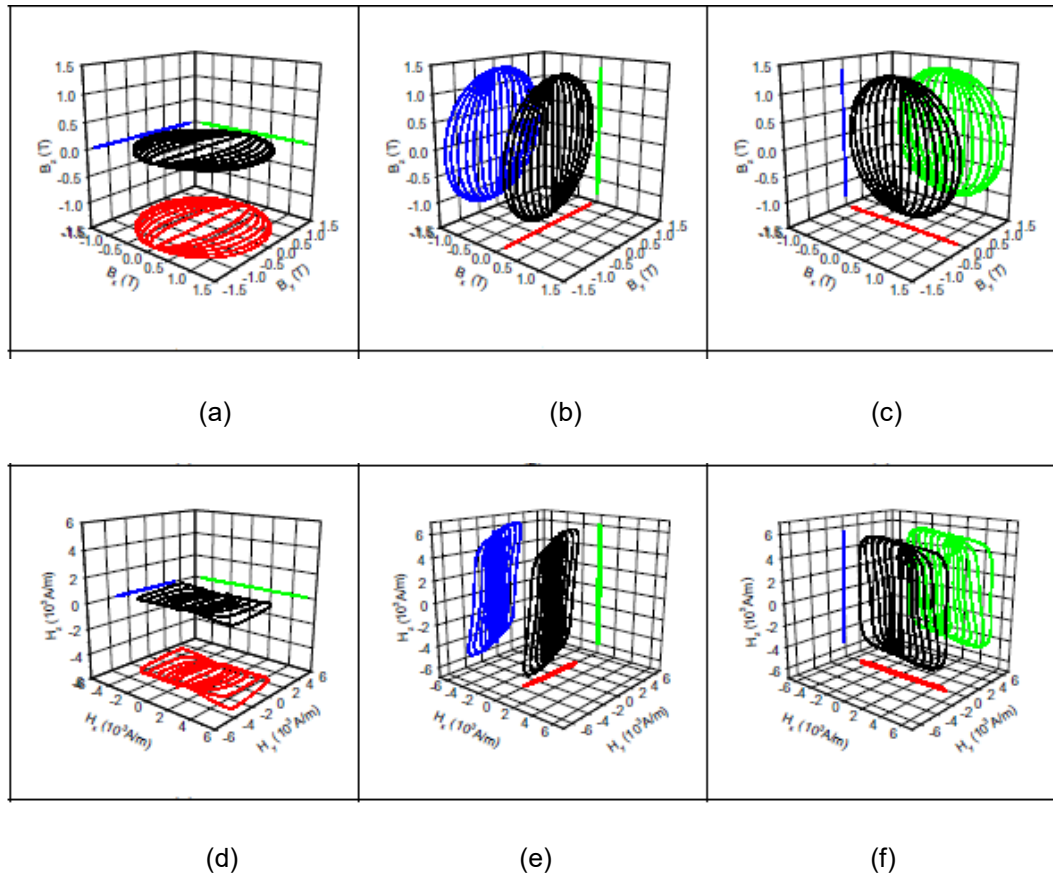


Fig. 2.55 Ellipse B loci with x as a major axis in the (a) XOY- (b) YOZ- (c) ZOX-planes and their corresponding H loci in (d) XOY- (e) YOZ- (f) ZOX-planes [2.100]

Nowadays, core loss is one of the main issues in getting the high performance of the electrical machines. To satisfy the demands of the human, the distribution of core losses should be studied and well understood. It is important to consider the magnetic reluctivity and permeability to get the relationship between magnetic flux density B , and magnetic field strength H , during magnetic field analysis. When B is parallel to H , the relationship of them can be formulated as

$$B = \mu_o H(1 + \chi_m) = \mu_o \mu_r H = \mu H \quad (2.41)$$

where μ_o is the vacuum permeability, μ_r is the relative permeability and χ_m is the susceptibility. B and H also can be related by the magnetic reluctivity ν .

$$H = \nu B \quad (2.42)$$

The conventional evaluations of the magnetic properties by the Epstein tester and single sheet tester are insufficient since there are restricted measurements under alternating

magnetisation field. It becomes a big issue since the rotating electrical machine will lead to the motion of the domain wall during the rotation of rotor [2.101].

For 2-D and 3-D excitation of magnetic flux, B and H are not in parallel due to the complex motion of wall domain during rotating process [2.92]. The magnetic property shows nonlinearity in magnitude and in the spatial phase angle between vector B and H [2.102]. The constitutive equation can be given as

$$H_i = \sum_j v_{ij} B_j \quad (2.43)$$

where v_{ij} is the reluctivity tensor and the magnetic properties with the existence of v_{ij} are known as vector magnetic properties.

In 2006, Urata *et al.* analysed the 2-D vector magnetic properties of the non-oriented electrical steel sheets which are applied in stator cores of a condensed motor [2.101]. Fig. 2.56 explains the condition during the alternating and rotating magnetic flux density.

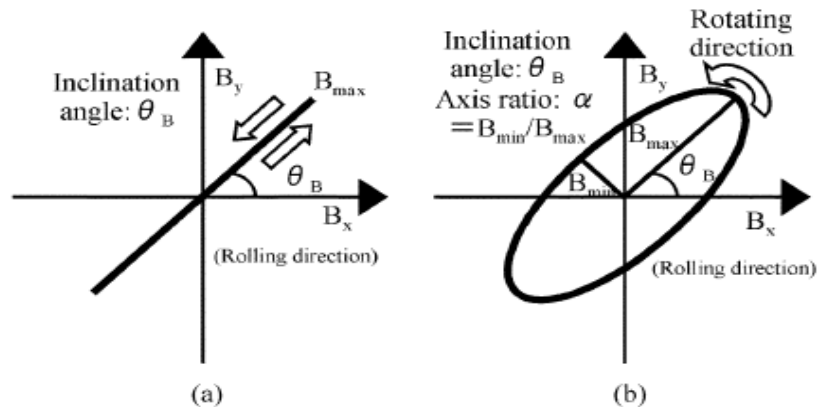


Fig. 2.56 (a) Alternating flux condition. (b) Rotating flux condition [2.101]

Finite element method is employed by considering the Enokizono, Soda and Shimoji (E&SS) model when using 2-D vector magnetic properties during numerical magnetic field analyses [2.101]. E&SS model is able to discuss the alternating and rotating magnetic field by considering the vector relationship of magnetic flux density B , and magnetic field strength H , during one period cycle [2.103]. The expression of H_x or H_y using E&SS model is stated as the following

$$H_x = v_{xr}(B_{max}, \alpha, \tau)B_x(\tau) + v_{xi}(B_{max}, \alpha, \tau) \int_0^\tau B_x(\tau) d\tau \quad (2.44)$$

where α is the axis ratio, τ is variable which is ranged from 0 to 2π , v_{xr} is the magnetic reluctivity coefficient, v_{xi} is the magnetic hysteresis coefficient and both of them are altered as a waveform in one period.

B_x has been approximated as a sinusoidal form and it was expressed to be like following

$$B_x = R_{B_x} \cos \tau - I_{B_x} \sin \tau \quad (2.45)$$

where R_{B_x} and I_{B_x} can be obtained by Fourier transform.

The end result of magnetic reluctivity coefficient v_{xr} , and the magnetic hysteresis coefficient v_{xi} , can be calculated by

$$v_{xr} = \frac{\sum_{n=1}^N R_{(n-1)H_x} \cos(2n-1)\tau}{\cos \tau} \left(\frac{R_{B_x}}{R_{B_x}^2 + I_{B_x}^2} \right) + \frac{\sum_{n=1}^N R_{(n-1)H_x} \sin(2n-1)\tau}{\sin \tau} \left(\frac{I_{B_x}}{R_{B_x}^2 + I_{B_x}^2} \right) \quad (2.46)$$

$$v_{xi} = \frac{\sum_{n=1}^N R_{(n-1)H_x} \cos(2n-1)\tau}{\cos \tau} \left(\frac{R_{B_x}}{R_{B_x}^2 + I_{B_x}^2} \right) + \frac{\sum_{n=1}^N R_{(n-1)H_x} \sin(2n-1)\tau}{\sin \tau} \left(\frac{I_{B_x}}{R_{B_x}^2 + I_{B_x}^2} \right) \quad (2.47)$$

From Fig. 2.57 shows that the loss difference between two materials, grain oriented electrical steel sheet (35GI55) and non-oriented electrical steel sheet (50A47) [2.101].

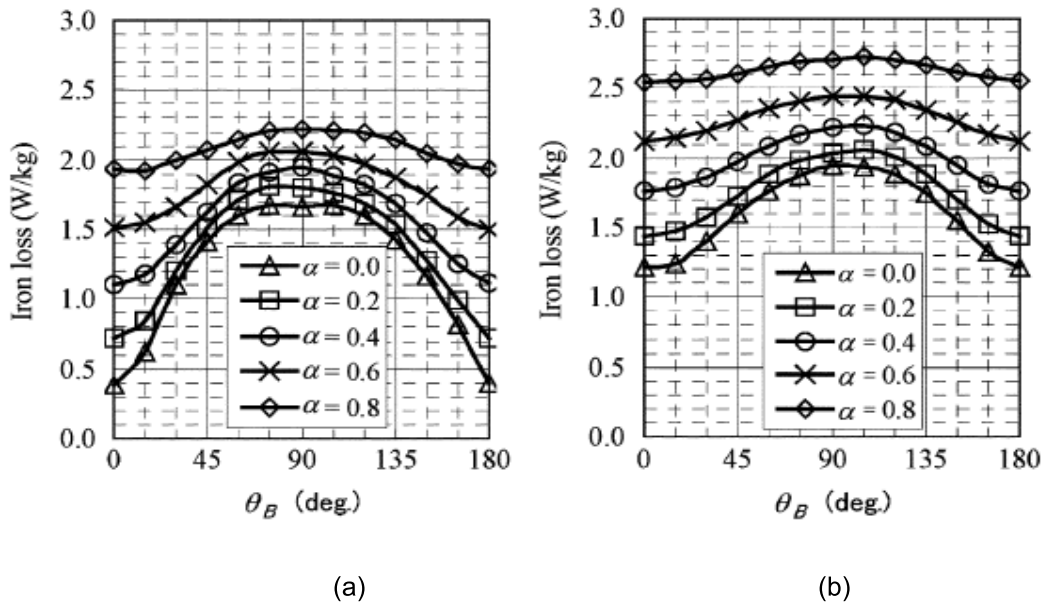


Fig. 2.57 Comparison of core losses depending of θ_B for (a) grain oriented and (b) non-oriented electrical steel sheets [2.101]

The core losses for both materials have increased when the axis ratio approaches 0.8 at 90° and it was recorded that core losses showed the minimum value when inclination angle is at 0° or 180° due to the parallel condition between magnetisation easy axis (rotating direction) and the direction of the maximum flux density vector. In order to get the high efficiency of the system motor, the parameter θ_B in the stator core should be kept at 0° and 180° [2.101].

However, calculation and application of 2-D magnetic reluctivity to 2-D finite element method (FEM) of rotating electrical machines is still unable to describe the actual magnetic properties of the certain materials since there is a 3-D magnetic flux path characteristic inside them such as SMC material.

The production of 3-D magnetic field by 3-D tester is able to detect the real 3-D effect of tensor magnetic properties. Hence, the vector of magnetic strength H , also can be expressed in the x, y and z components [2.87]

$$H_x = v_{xx}B_x + v_{xy}B_y + v_{xz}B_z$$

$$H_y = v_{yx}B_x + v_{yy}B_y + v_{yz}B_z \quad (2.48)$$

$$H_z = v_{zx}B_x + v_{zy}B_y + v_{zz}B_z$$

The magnetic reluctivity tensor v , can be expressed in a three-dimensional full rank matrix:

$$\begin{pmatrix} H_x \\ H_y \\ H_z \end{pmatrix} = \begin{bmatrix} v_{xx} & v_{xy} & v_{xz} \\ v_{yx} & v_{yy} & v_{yz} \\ v_{zx} & v_{zy} & v_{zz} \end{bmatrix} \begin{pmatrix} B_x \\ B_y \\ B_z \end{pmatrix} \quad (2.49)$$

$$v = \begin{bmatrix} v_{xx} & v_{xy} & v_{xz} \\ v_{yx} & v_{yy} & v_{yz} \\ v_{zx} & v_{zy} & v_{zz} \end{bmatrix} \quad (2.50)$$

During the rotor rotates under 3-D excitation of rotating flux, B and H loci at different positions in the core of rotating electrical machine exhibit different patterns. B or H locus can be transformed into a Fourier series and each of the harmonics basically forms a circular or elliptical locus [2.26]. The hysteresis loops and core losses of soft magnetic composite material are measured under a series of controlled B to be elliptical loci with different planes, orientations, peak flux densities, axis ratios and frequencies [2.87].

In fact, the vector magnetic properties are defined by the maximum magnetic flux density, axis ratio of the B ellipse and its orientation. The orientation is defined as the direction of major axis of the B ellipse which is given by the angles between the major axis and other three coordinate axes x, y and z as shown in the Fig. 2.58.

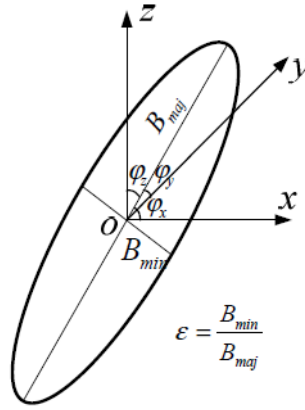


Fig. 2.58 Relationship among maximum magnetic flux density B_m , axis ratio ϵ , and inclination angles φ of the elliptical B locus [2.104]

Nine elements of reluctivity magnetic tensor would not be able to be solved even after the substitution of components B and H into the equation (2.49) because of the conditional variable. If B_{max} and axis ratio are fixed in one loop, a row of reluctivity tensor elements will be constant [2.105] and by considering three points of the loop, a condition-specified equation can be given as following

$$\begin{aligned}
 H_x(a) &= v_{xx}B_x(a) + v_{xy}B_y(a) + v_{xz}B_z(a) \\
 H_x(b) &= v_{xx}B_x(b) + v_{xy}B_y(b) + v_{xz}B_z(b) \\
 H_x(c) &= v_{xx}B_x(c) + v_{xy}B_y(c) + v_{xz}B_z(c)
 \end{aligned}
 \tag{2.51}$$

The first-row element of equation (2.49) can be solved by simultaneous equation and v_{xx} , v_{xy} and v_{xz} will be determined and followed by other elements v_{yx} , v_{yy} , v_{yz} , v_{zx} , v_{zy} and v_{zz} .

Fig. 2.59 illustrates a circle of magnetic reluctivity curves in the XOY-plane when B locus is controlled to be a circle with the axis ratio of 1. It shows that the change of v_{xx} and v_{xy} is smaller than that of v_{yy} and v_{yx} when the magnitude of circular B increases from 0.22 T to 1.32 T in the same plane. The v_{yy} and v_{yx} are different but symmetrical. It explains that x- and y-axes are the easy directions for magnetisation [2.104].

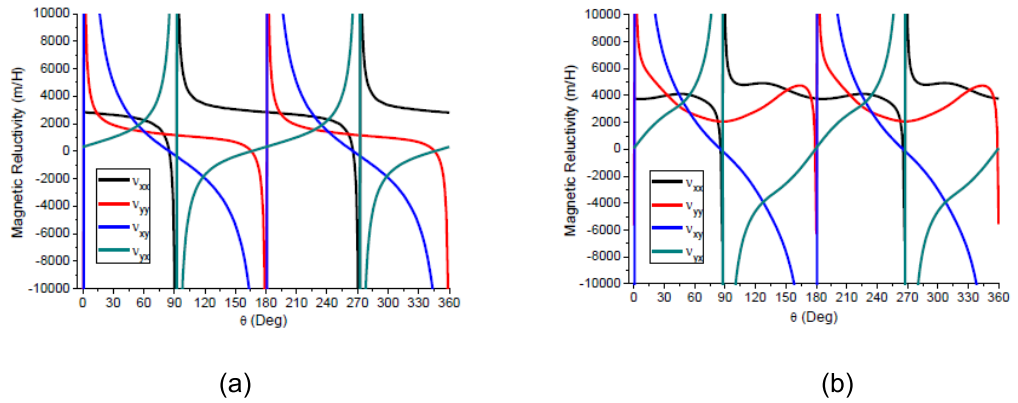
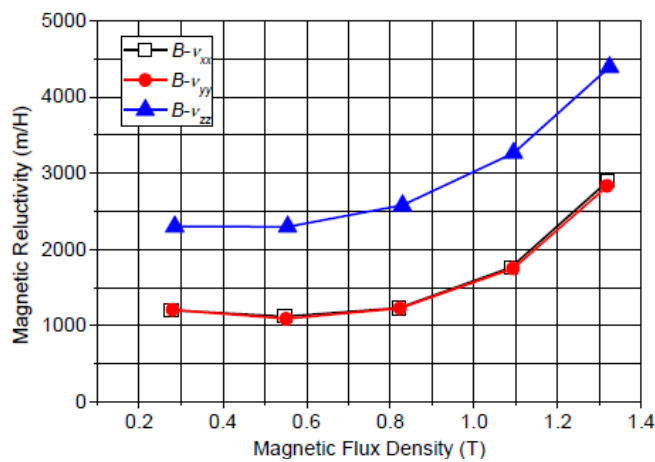
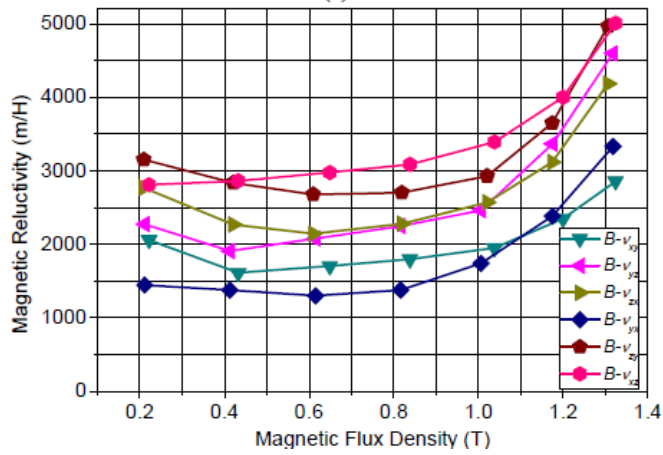


Fig. 2.59 Magnetic reluctivity tensor of one cycle in the XOY-plane when B is round rotating ($\epsilon = 1$), (a) $B_r = 0.22$ T (b) $B_r = 1.32$ T [2.104]

Fig. 2.60 displays the magnetic reluctivities at different magnitudes of magnetic flux density. The values of diagonal elements v_{xx} , v_{yy} and v_{zz} decreased with increase of B up to 0.6 T. After 0.6 T, they increased slowly. The curves of both v_{xx} and v_{yy} versus maximum magnetic flux density are coincidentally similar while their values are smaller than v_{zz} . It is consistent with the previous conclusion which described that the easy magnetised directions are lying in the x- or y-axis. With increase of magnetic flux density, the off-diagonal elements v_{xy} , v_{xz} , v_{yx} , v_{yz} , v_{zx} and v_{zy} decrease to a minimum value before dramatically increasing up to 1.4 T of B . The arbitrary values of the off-diagonal elements increase rapidly when the magnitude of B is close to the saturation [2.91]. It also can be seen that, v_{yx} and v_{yz} are the lowest compared to the others since the z direction is hard to be magnetised [2.104].



(a)



(b)

Fig. 2.60 Magnetic reluctivity tensor against the magnitude of the maximum B when the circle angle $\theta = 45^\circ$. (a) Diagonal elements and (b) Off-diagonal elements [2.104]

Then, Fig. 2.61 shows that the off-diagonal elements v_{xy} , v_{yz} and v_{zx} are obtained in the boundary condition of phase angle $\theta = 180^\circ$ and v_{yx} , v_{zy} and v_{xz} are obtained in the boundary condition of phase angle $\theta = 90^\circ$. Similar with the diagonal elements, the arbitrary values of the off-diagonal elements increase rapidly when the flux density approaches to the saturation value [2.104].

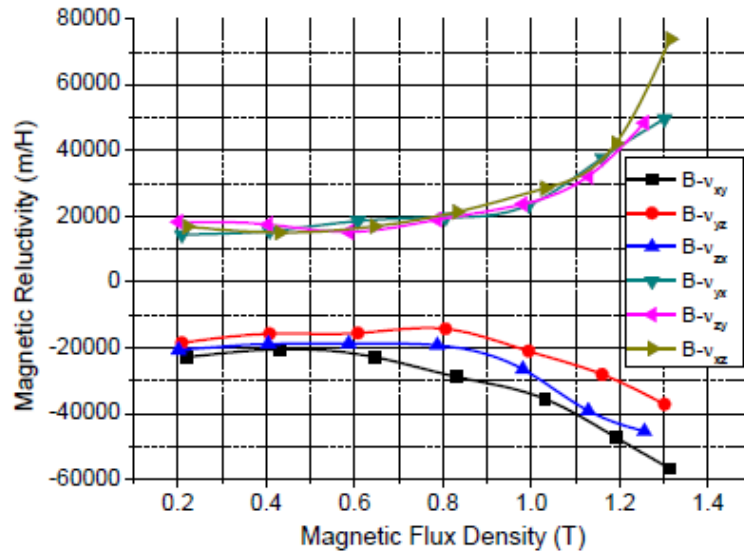


Fig. 2.61 Magnetic reluctivity tensor against the magnitude of the maximum round rotating B [2.104]

In 3-D vector magnetic properties, the off-diagonal elements are rising and dissolving with the increasing of magnetic flux density along the axis ratio increment from 0 to 1 in

the boundary condition of $\theta = 45^\circ$ as explained in Fig. 2.62. This situation explains the existence of anisotropic material in the SMC material due to imperfect preparation which leads to the asymmetry of iron powder particles. As described by Li, Zhao, *et al.* in 2012, there is lower reluctivity for local area which has higher content of pure iron and lower content of non-ferromagnetic material.

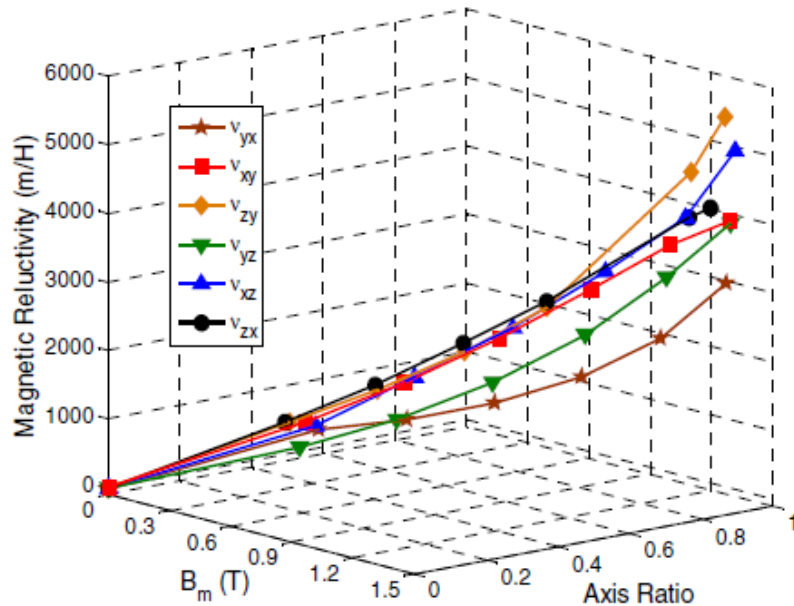


Fig. 2.62 Relation among the instant values of magnetic reluctivity of off-diagonal elements, axis ratio and phase angle $\theta = 45^\circ$ [2.104]

The manufacturing process has changed the isotropy property of SMC to be anisotropy which makes the abundance of particles be accumulated along certain axis and contribute to the high mass density at certain part. The axis will be known as the easy direction for magnetisation. From testing experiment, 3-D magnetic reluctivity tensor of the SMC material has been well investigated and nine tensor elements in given condition becomes a 3 x 3 full rank matrix when the vector is controlled to be ellipse. Besides, the off-diagonal elements of the tensor are obtained under controlling the series of round B due to the rotating magnetic flux [2.87]. Apparently, 3-D rotational magnetisation shows a complicated coupling interaction among different magnitude direction during demonstration of the tensor magnetic reluctivity which is not a simple combination of individual alternating magnetisation [2.91], [2.94], [2.104]. However, the complexity of this study will provide the significant knowledge to meet the demands in designing and optimizing the electrical machines these days.

In 2009, Li *et al.* actively enhanced the performance of the magnetic property testing system by improving the B and H sensing coils to be more sensitive in detecting the magnetic flux density and magnetic field strength of the magnetised SOMALOY 500 material. The improvement was continued in the following year, 2010 when Li *et al.* developed the multilayer of excitation winding coils in order to conduct the magnetic properties measurement of SMC material at wide range of frequency. This wide of range frequency is very important and is strongly demanded by electrical machine designers nowadays. As shown in Fig. 2.63, the hysteresis loops were plotted after considering the both improvements of the 3-D tester. The loops slowly change to ellipse when the excitation frequency is increased and this leads to the adding of core loss [2.93].

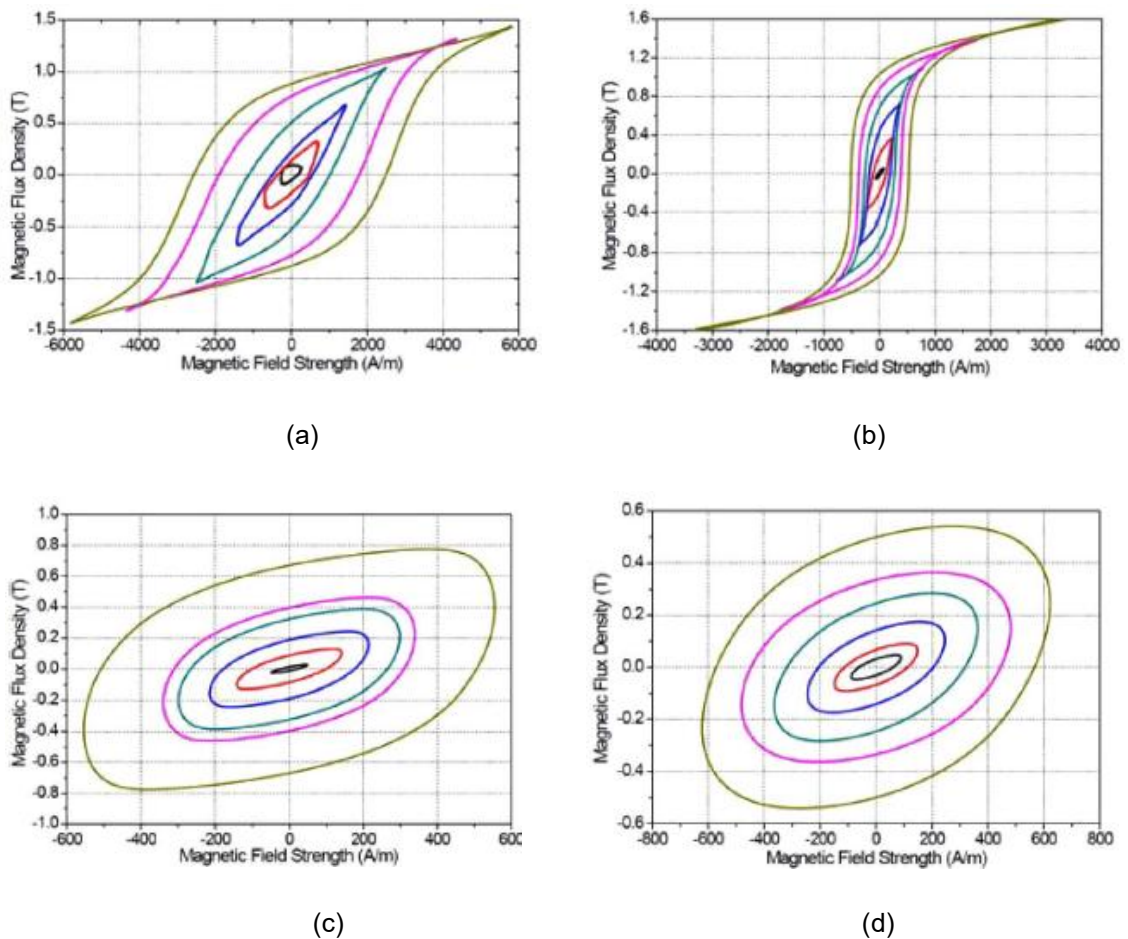


Fig. 2.63 The hysteresis loops of SOMALOY 500 at (a) 5 Hz (b) 20 Hz (c) 500 Hz and (d) 1000 Hz under alternating flux densities [2.93]

The magnetic properties measurement of SOMALOY 500 has been conducted along the x-, y- and z-axes as illustrated in Fig. 2.64. It can be described that y-axis is an easy axis due to the compaction effect during the manufacturing process. It is consistent with the

recorded B and H loci during the measurement under 2-D magnetic flux density as shown in Fig. 2.65. Both B and H loci are obtained when B is controlled to be in round shape with an amplitude of 1.3 T. The core loss curves are plotted in Fig. 2. 2.66. These curves explain the SOMALOY 500 core loss when there is 1-D alternating flux along an easy direction of y-axis at 5 Hz, 20 Hz, 50 Hz, 100 Hz, 200 Hz, 500 Hz and 1000 Hz. The core loss increased with the frequency due to that the loop area becomes bigger which is effect from the eddy current loss.

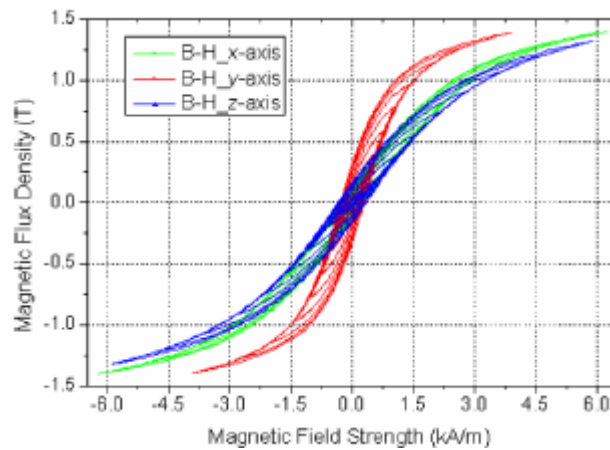


Fig. 2.64 Hysteresis loops along the x-, y- and z-axes at 50 Hz [2.93]

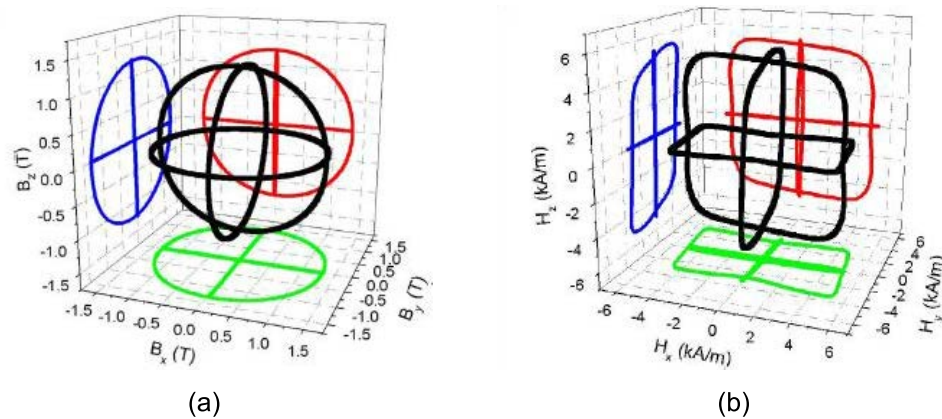


Fig. 2.65 (a) B loci and (b) the corresponding of H loci at 50 Hz of operating frequency [2.93]

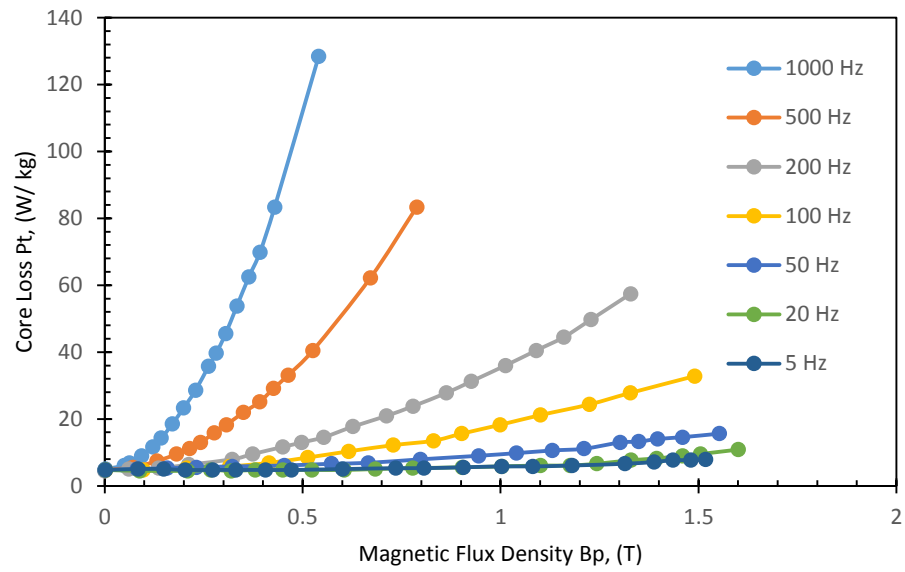
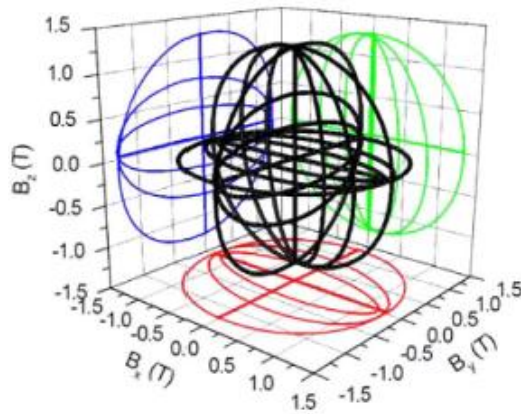
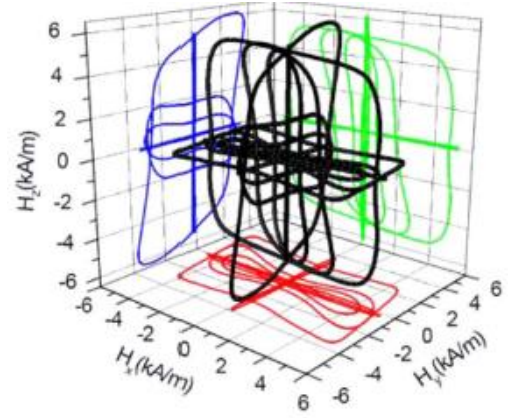


Fig. 2. 2.66 Loss curve along the y-axis at wide range of frequency up to 1000 Hz [2.93]

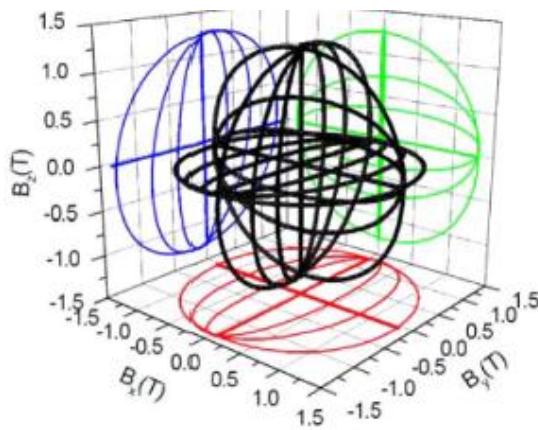
Fig. 2.67 describes the corresponding H loci for x and y major axis change from ellipse to rectangular shape where the axis ratio ϵ , is recorded from 0 to 1. Comparison can be made between H loci at 50 Hz in Fig. 2.67 (b) and H loci when ϵ is 1 at 200 Hz in Fig. 2.67 (d). It shows that the shape of H loci distorted with the increment of frequency due to the higher order of harmonics [2.93].



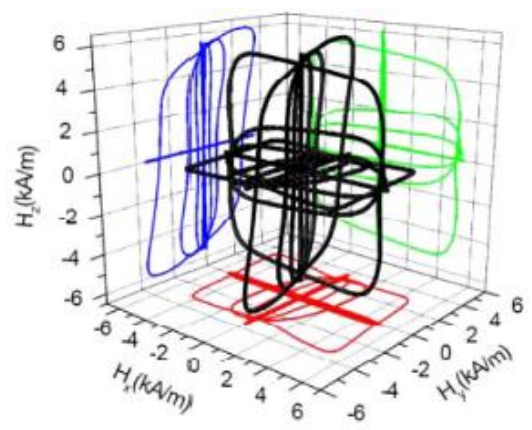
(a)



(b)



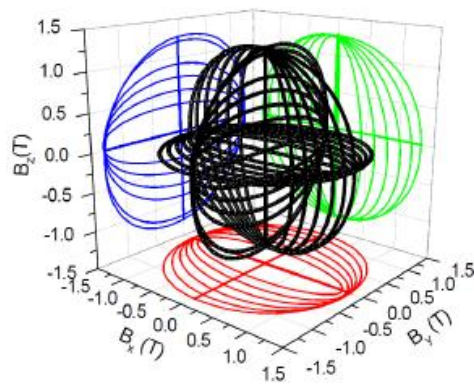
(c)



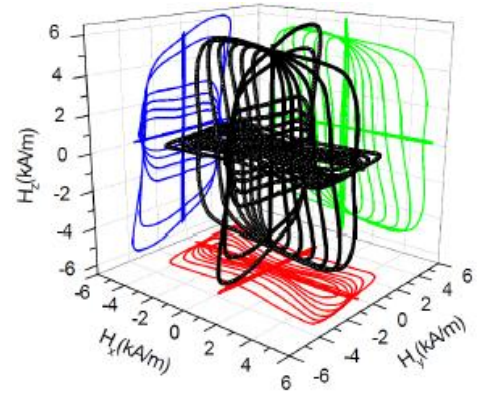
(d)

Fig. 2.67 3-D magnetic properties of SOMALOY 500 with elliptical rotating magnetic flux density at 200 Hz. (a) x, y and z as major axes for red, blue and green B loci, respectively. (b) The corresponding H loci for major axes x, y and z are represented by red, blue and green lines, respectively. (c) x, y and z as major axes for green, red and blue B loci, respectively and (d) the corresponding H loci for axes x, y and z are represented by green, red and blue lines, respectively [2.93]

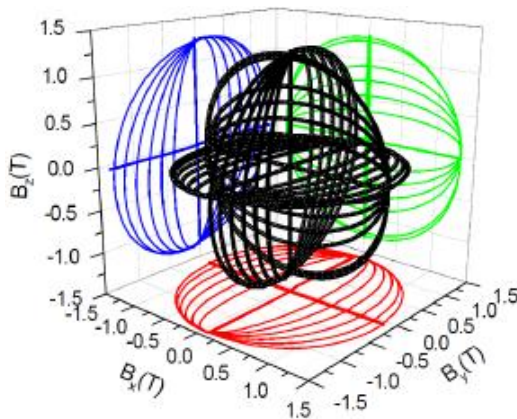
Li *et al.* has conducted a measurement under rotational magnetic flux at 50 Hz of operating frequency. During the experiment, magnetic flux densities are controlled to be in ellipse shape by increasing the magnitude of B along the x-axis to make y as a major axis and it is repeated by considering x as major axis. There are projections of B loci and H loci in Fig. 2.68 when B loci are ellipses with increasing magnitudes up to 1.4 T. H loci for both Fig. 2.68 (b) and Fig. 2.68 (d) are evolved from ellipse to rectangle when y is the major axis while they evolve from figure-of-eight to saddle like when x is the major axis.



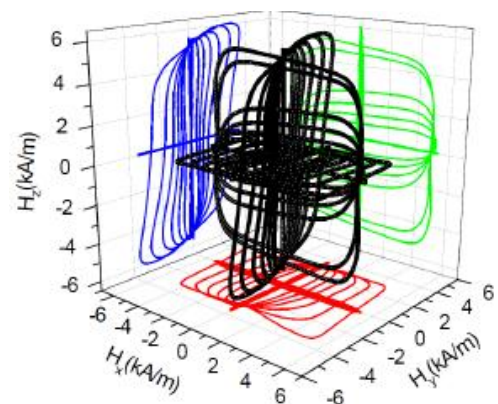
(a)



(b)



(c)



(d)

Fig. 2.68 The projection of (a) blue B loci with y as a major axis, (b) the corresponding blue H loci for y major axis (c) green B loci with x as a major axis and (d) the corresponding green H loci for x major axis [2.89]

These happened because of the different magnetisation process and the non-uniform distribution of particles in the sample material. Li *et al.* also expected this effect because of the anisotropy properties of the material in rotational magnetisation [2.89]. Fig. 2.69 describes the core losses of SOMALOY 500 after being magnetised at 50 Hz under rotating magnetic flux densities with B had been controlled to be in ellipse shapes. The core losses for all planes show the same pattern. It is known, that curves in the same plane, for instance YOZ-plane, the losses for ultimate circle which are developed along y- and z-axes give the same value and it is also agreed by other planes; XOY- and ZOX-planes. According to Li *et al.*, the losses strongly depend on the orientation of major axis and the ratio axis ϵ , when B loci are in elliptical shape.

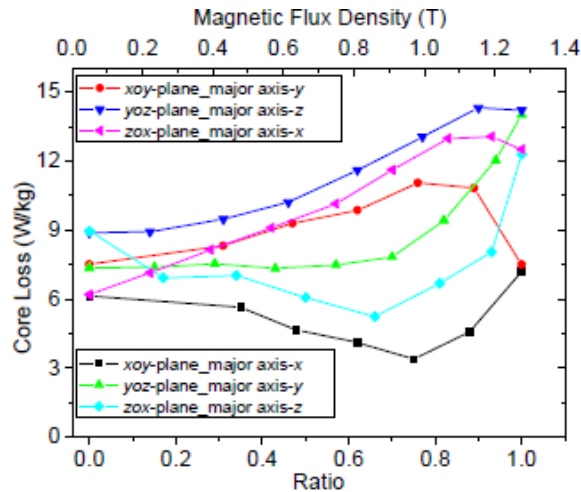


Fig. 2.69 The core losses versus ratio axis of elliptical B loci (0-1) and amplitudes of round B loci [2.89]

A spherical B loci and the corresponding H loci are plotted in Fig. 2.70. It is clearly explained that 3-D tester is really can measure the magnetic properties in 3-D space under rotating flux densities. B loci is controlled well to be in round in the XOZ-plane while the B loci looks like experienced some compression in plane which involved y-axis. This is caused by the easy axis along the y-axis and the effect is also can be seen in H loci projection which there is an oblate sphere lies in 3-D space.

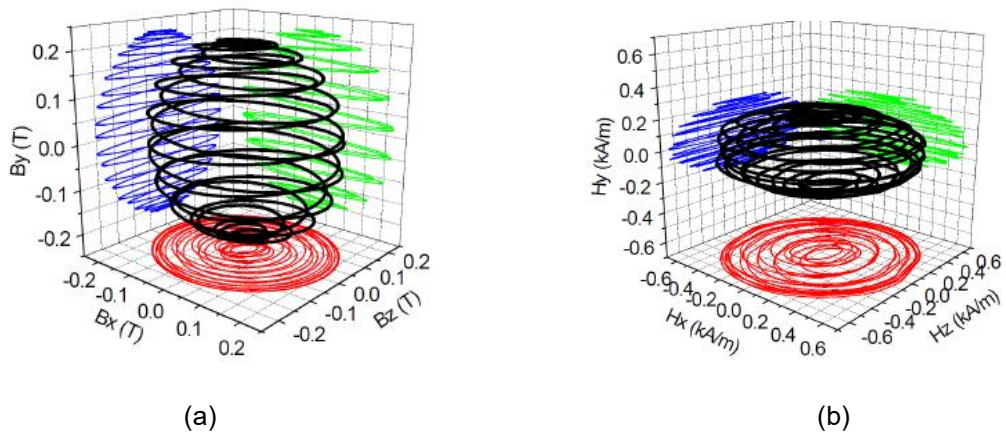


Fig. 2.70 (a) Sphere B loci are controlled in 3-D space at 50 Hz of operating frequency (b) the corresponding H loci in 3-D space [2.89]

In 2011, Li *et al.* had expanded the investigation of magnetic properties of SOMALOY 500 by measuring them at high frequency which is up to 1000 Hz. The sample has been magnetised by controlling the magnetic fluxes to be circle in the XOY-, YOZ- and

ZOX-planes as shown in Fig. 2.71. In this figure, H loci lie in the XOY-plane are deflected from the corresponding B loci. The projection of H loci in another two planes are also not straight lines. The deflection angle of H loci is increased with the frequency. Li *et al.* believed that the deflection angles are caused by the coupling effect from the core poles and the projection of H loci which is not in a straight line did not contribute to the core loss of the sample. Then, the alternating and rotational core losses are compared in Fig. 2.72. It explains the value of the rotational core loss is twice compared to the alternating core loss [2.106].

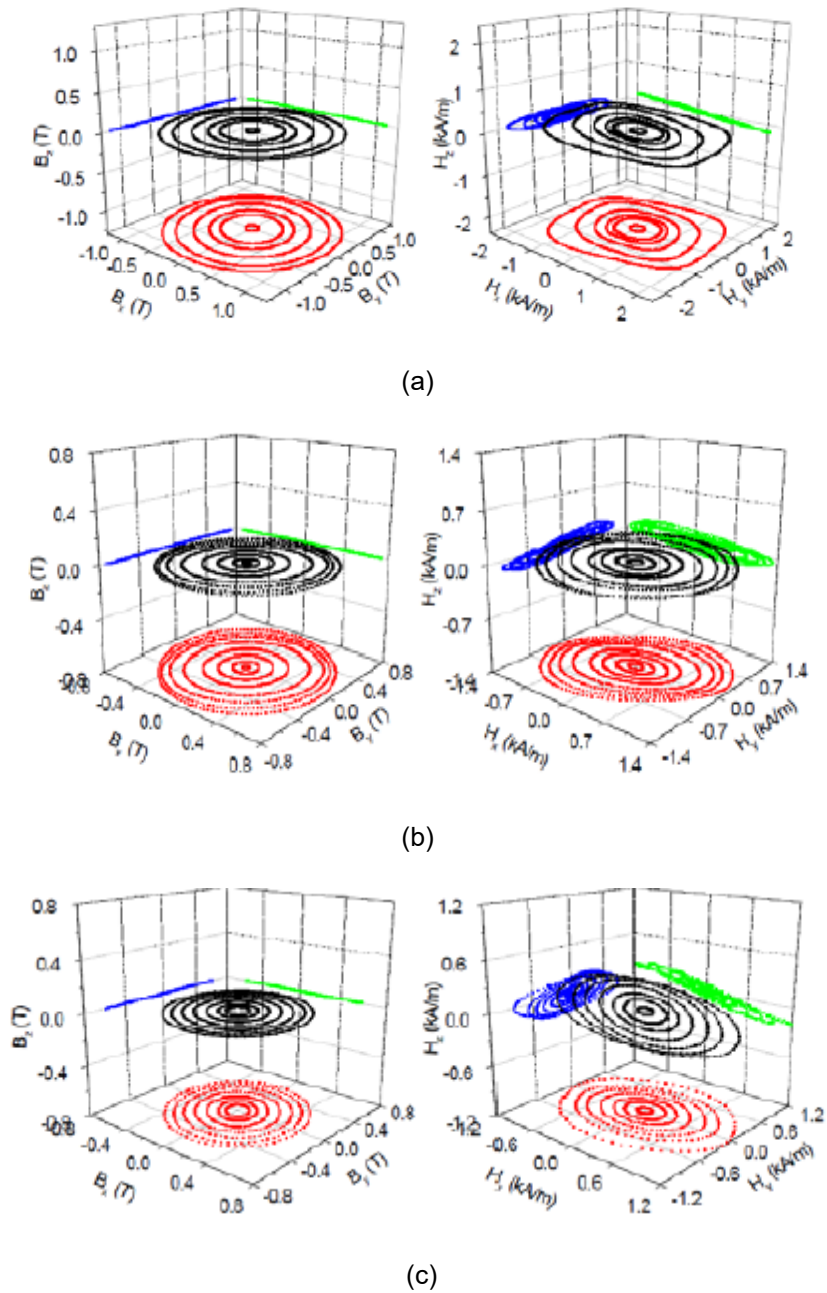
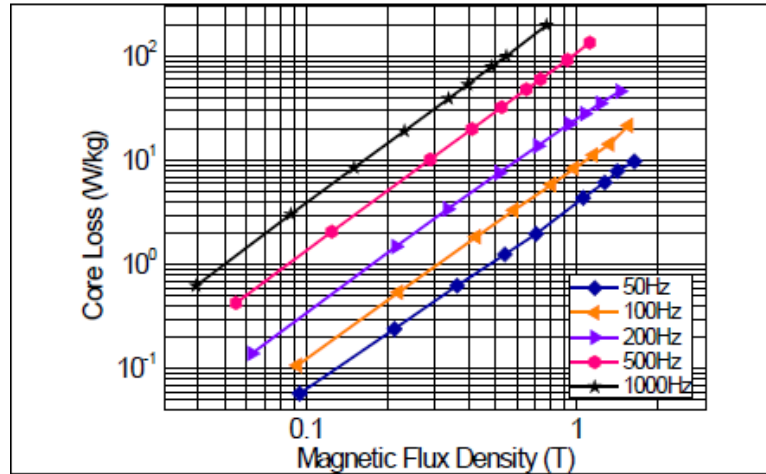
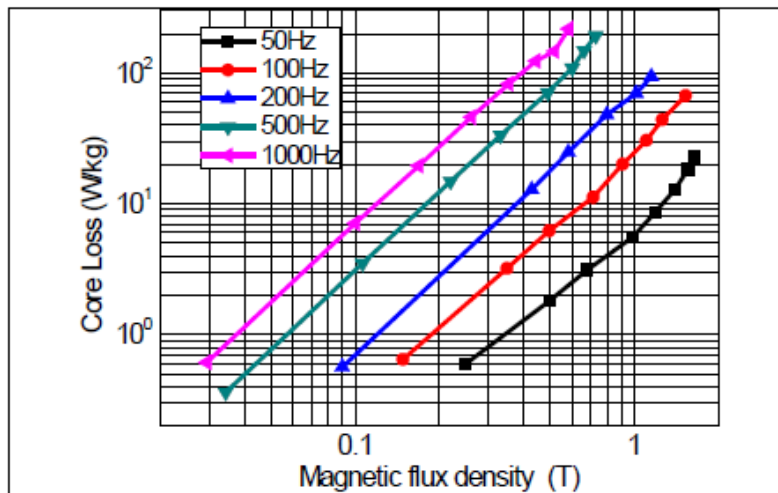


Fig. 2.71 The round B loci and H loci in the XOY-plane at (a) 200 Hz, (b) 500 Hz and (c) 1000 Hz [2.106]



(a)



(b)

Fig. 2.72 The core loss at 50 Hz, 100 Hz, 200 Hz, 500 Hz and 1000 Hz under (a) alternating magnetic fluxes (b) rotational magnetic fluxes [2.106]

This SMC material is ideal in developing devices with 3-D magnetic flux path and complex structure. Due to the different characteristics with the previous laminated steels, Guo *et al.* has studied about the core loss models based on the magnetic properties of SMC sample which had been measured under alternating and rotational core loss by using the 3-D magnetic property tester. The core loss in SMC machine with consideration of stator core part is calculated. The 3-D magnetic field time-stepping finite element analysis (FEA) is used to determine the B loci when the rotors are rotated by an electrical period. As shown in Fig. 2.73, there are B loci in the middle point of claw poles with no load, half load and full load during the motor operation [2.28].

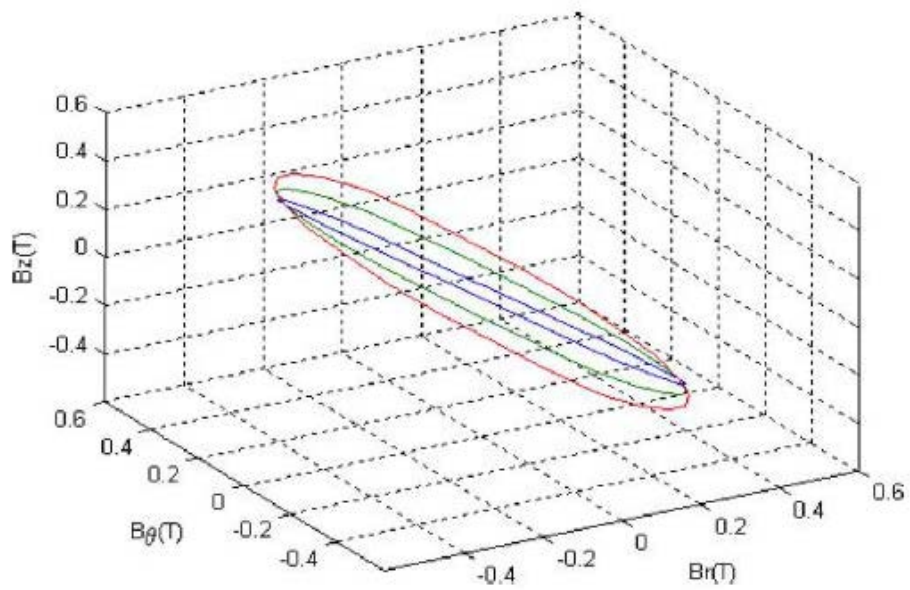


Fig. 2.73 B locus in the middle part of SMC stator core with the blue line shows the no load motor, the green line is the B locus for half load motor and the red line represents the full load motor [2.28]

The irregular loop of B locus is a function of time with a period of T_s which rotation of the rotor is 360° electrical. B locus can be divided into periodical function of time t ; B_r , B_θ and B_z along three axes. Fig. 2.74 illustrates the B locus waveform with respect to the rotor electrical angle in previous figure.

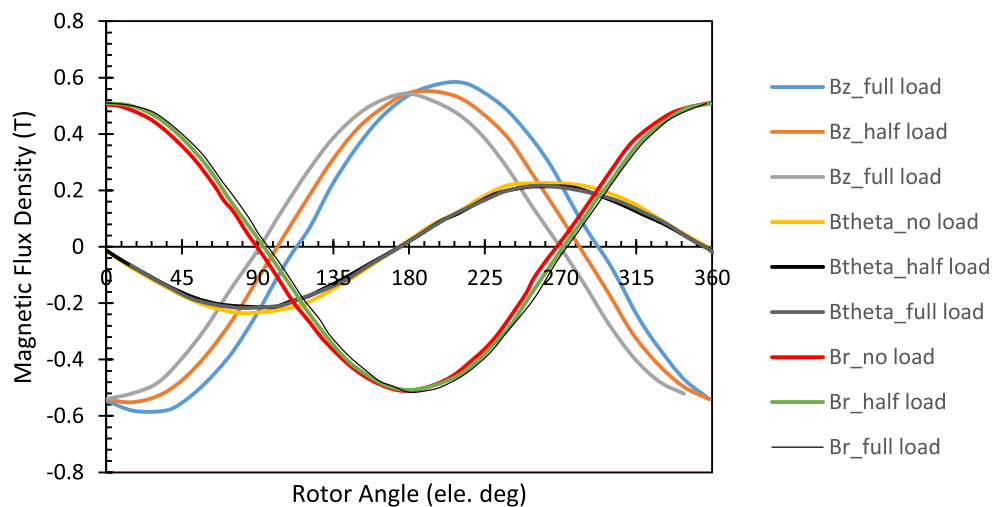


Fig. 2.74 Waveforms of B components from three different situations; no load, half load and full load [2.28]

In considering the Fourier series, the three components of B locus can be formulated as

$$\begin{aligned}
B_r(t) &= \sum_{k=0}^{\infty} [B_{rsk} \sin(2\pi k f_s t) + B_{rck} \cos(2\pi k f_s t)] \\
B_\theta(t) &= \sum_{k=0}^{\infty} [B_{\theta sk} \sin(2\pi k f_s t) + B_{\theta ck} \cos(2\pi k f_s t)] \\
B_z(t) &= \sum_{k=0}^{\infty} [B_{zsk} \sin(2\pi k f_s t) + B_{zck} \cos(2\pi k f_s t)]
\end{aligned} \tag{2.52}$$

where k is the order of harmonic and $f_s = 1/T_s$.

The harmonics can be divided into two parts

$$B_{sk} = n_{sk} \sqrt{B_{rsk}^2 + B_{\theta sk}^2 + B_{zsk}^2} \sin(2\pi k f_s t) \tag{2.53}$$

$$B_{ck} = n_{ck} \sqrt{B_{rck}^2 + B_{\theta ck}^2 + B_{zck}^2} \cos(2\pi k f_s t) \tag{2.54}$$

where n_{sk} and n_{ck} are two unit vectors and perpendicular to each other. Both can be obtained by

$$n_{sk} = \frac{B_{rsk}r + B_{\theta sk}\theta + B_{zsk}z}{\sqrt{B_{rsk}^2 + B_{\theta sk}^2 + B_{zsk}^2}} \tag{2.55}$$

$$n_{ck} = \frac{B_{rck}r + B_{\theta ck}\theta + B_{zck}z}{\sqrt{B_{rck}^2 + B_{\theta ck}^2 + B_{zck}^2}} \tag{2.56}$$

where r , θ and z are the unit vectors along the three axes, respectively.

Equations (2.53) and (2.54) form an ellipse with the larger of $|B_{sk}|$ and $|B_{ck}|$ as the major axis B_{kmaj} , and the smaller of them as the minor axis B_{kmin} . The core loss production by B elliptical can be obtained by

$$P_k = P_{rk} R_{BK} + (1 - R_{BK})^2 P_{ak} \tag{2.57}$$

where $R_{BK} = \frac{B_{kmin}}{B_{kmaj}}$ is the ratio of the k th harmonic ellipse. P_{ak} is the alternating core loss with magnitude of B_{kmaj} which can be computed by using (2.2) and coefficients derived for $f = kf_s$. P_{rk} is the circular rotating core loss obtained by using (2.6) - (2.8), $B_p = B_{kmaj}$ and $f = kf_s$ [2.28].

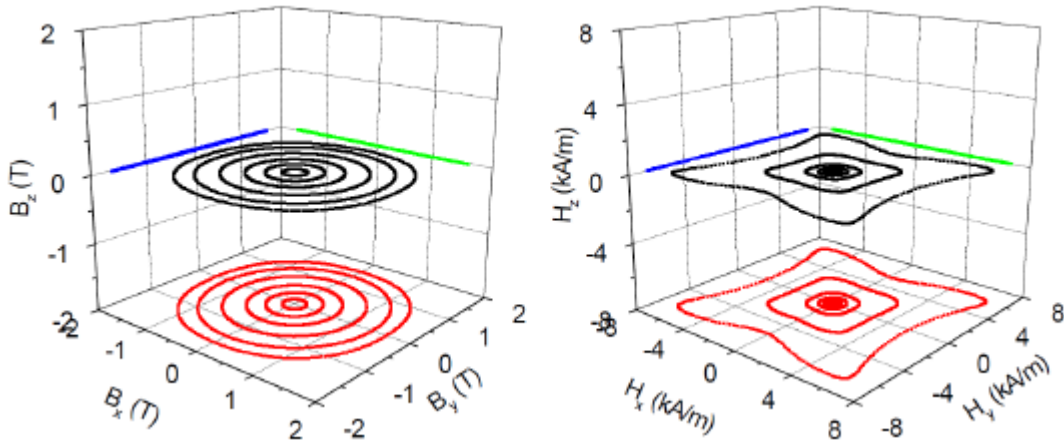
From (2.26), it can be derived that the core loss caused by an arbitrary B locus is the sum of all the harmonic losses. Therefore, the total core loss in the SMC core is

$$P_t = \sum_{e=1}^{N_e} \sum_{k=0}^{\infty} [P_{rk} R_{BK} + (1 - R_{BK})^2 P_{ak}] \quad (2.58)$$

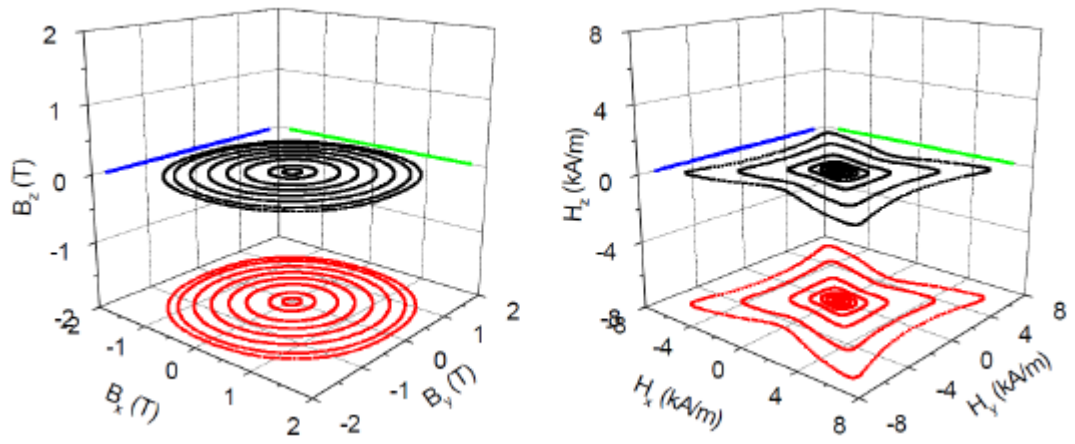
where N_e is the number of elements of the SMC core when performing the magnetic field FEA.

To validate the developed model, the dummy stator method had been used to measure the core loss of the motor prototype [2.26]. As stated by Guo *et al.*, the deficiency between the model and theory at no-load core losses is below than 10% when the speed rate is 1800 revolution per minute (rpm) [2.26]. This calculation was conducted on the three-phase three stack PM claw pole motor with SMC stator core in 2005 [2.26]. The measurement is extended up to 1000 Hz and it gave better results. The better fitting is achieved since the model coefficients are considered as frequency-dependent [2.28].

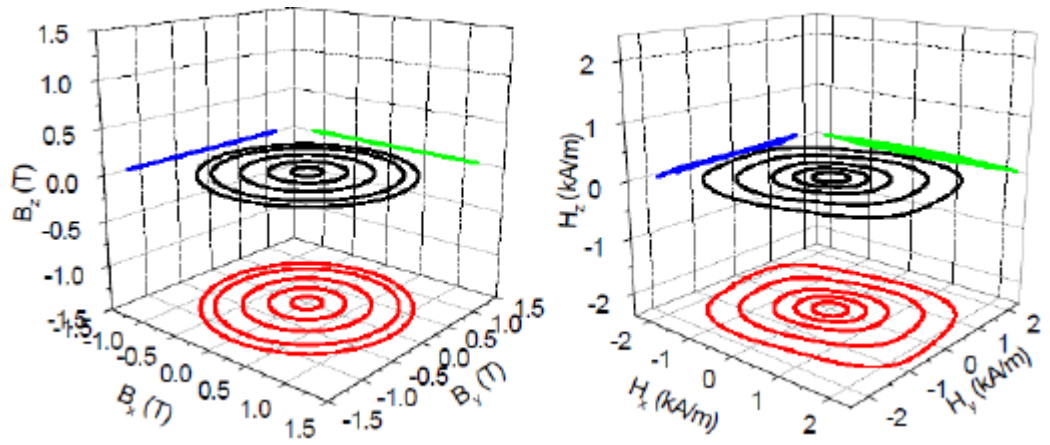
In 2013, Li *et al.* measured and discussed the magnetic properties of SOMALOY 500 under alternating and 3-D rotational magnetisation at 5 Hz to 1000 Hz by using the upgraded 3-D magnetic property tester which is able to conduct the measurement at a wide range of excitation frequency. Fig. 2.75 shows the round B loci and the corresponding H loci when there are rotational magnetic fluxes at 5 Hz, 20 Hz, 200 Hz and 500 Hz. At the lower frequency, such as 5 Hz, the shape of H loci changes from rectangular to saddle-like shapes. However, when the frequency becomes higher, the deflections are found and they clearly can be seen to lie in the YOZ- and XOZ-planes as shown in Fig. 2.75 (d) [2.107].



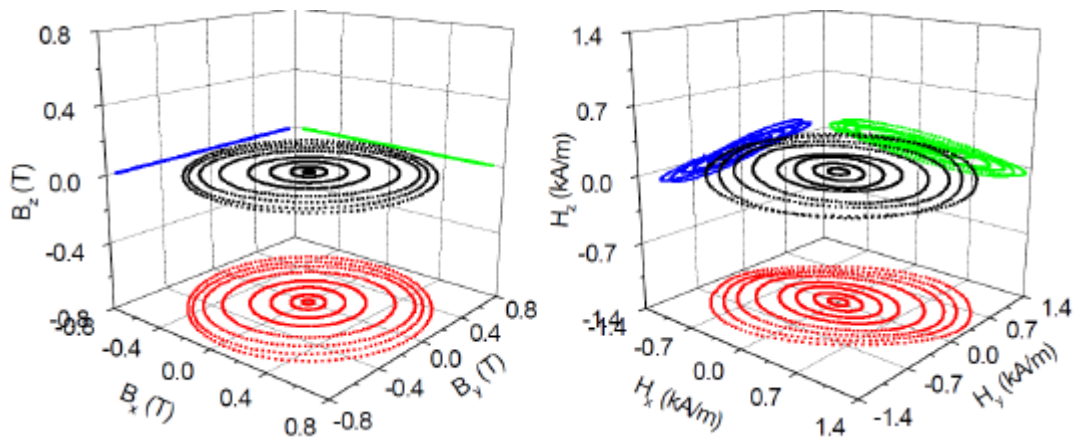
(a)



(b)



(c)



(d)

Fig. 2.75 Round B loci and the corresponding H loci at (a) 5 Hz, (b) 20 Hz, (c) 200 Hz and (d) 500 Hz [2.107]

Fig. 2.76 describes the core loss of the SOMALOY 500 material at 0.5 T of B when the sample is magnetised at certain range of frequency. It can be illustrated that the rotational core loss is twice the alternating core due to the rotating domain and domain wall motion which will produce the excessive loss to the sample [2.107].

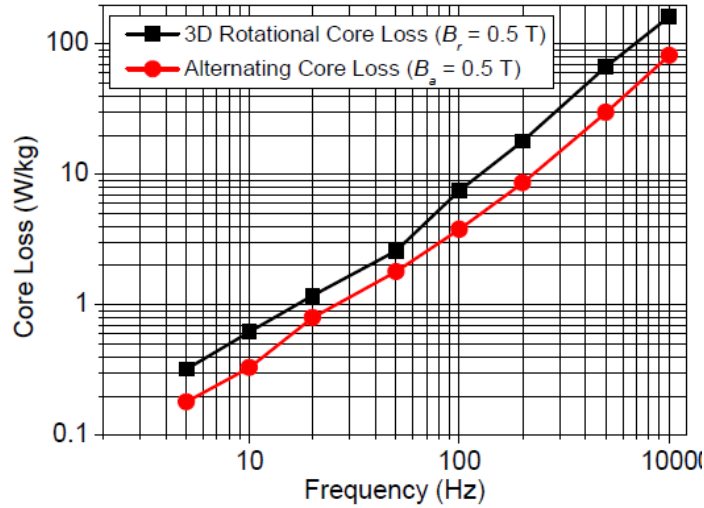


Fig. 2.76 Relationship between alternating and rotational excitations at 0.5 T of magnetic flux density [2.107]

Spherical loci are plotted in Fig. 2.77 when the B vector spiral spherical pattern is used during the measurement by using the improved C-type cores of 3-D magnetic property tester [2.97]. The associated trigonometric equations in three axes of directions are stated as

$$B_x(t) = A \cos 2\pi f_1 t \cos 2\pi f_2 t$$

$$B_y(t) = A \sin 2\pi f_1 t \cos 2\pi f_2 t \tag{2.59}$$

$$B_z(t) = A \sin 2\pi f_2 t$$

where A is the radius of the spherical B loci, f_1 is the excitation frequency of the B along the x- and y-axes, while f_2 is the excitation frequency of the B along the z-axis. f_1 can be square of f_2 to produce the waveform envelop frequency of B_x and B_y .

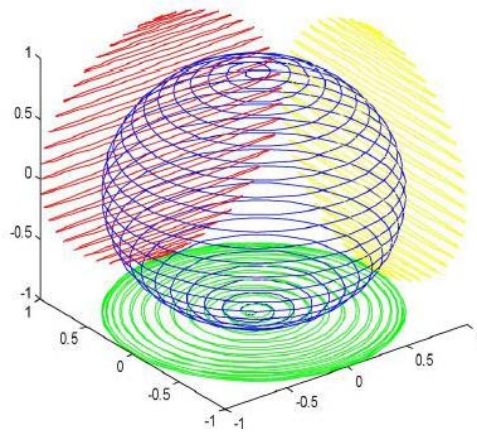


Fig. 2.77 Spherical B loci of magnetic material on three planes [2.96]

As shown in the figure above, the frequency of B_x and B_y is controlled to be 400 Hz, and the amplitudes vary for the B_z waveform. The similar 3-D magnetic properties measurement can be conducted in different excitation directions and different frequencies.

2.6 Summary

This chapter described the details of core loss by exploring the components that contribute to the total core loss. Core loss is able to be determined directly from the core material and also from the electrical machines. There are some models that are used to predict the core loss. SE and Statistical tool have been considered by the researchers in evaluating each components of core loss: hysteresis loss, eddy current loss and anomalous loss.

Besides that, the variation of techniques, methods and systems in measuring the magnetic properties of magnetic material are described. The embedded B coil method and 3-D magnetic testing system appear to be the best method and testing system in determining the core loss of SOMALOY 700 (5P) cubic sample under alternating and rotating magnetic flux density from low to high frequency. Many researchers use the field-metric method type I since it offers high accuracy and great versatility in measurement process by applying the Poynting's theorem during the core loss evaluation.

References

- [2.1] Y. Chen and P. Pillay, "An Improved Formula for Lamination Core Loss Calculations in Machines Operating with High Frequency and High Flux Density Excitation," *Conference Record - IAS Annual Meeting (IEEE Ind. Appl. Soc.*, vol. 2, pp. 759–766, 2002.
- [2.2] E. C. Snelling, *Soft Ferrites, Properties and Applications*, 2nd ed. London, UK: Butterworth, 1988.
- [2.3] C. P. STEINMETZ., "On the Law of Hysteresis," *Proceedings of the IEEE*, vol. 72, pp. 197–221, 1984.
- [2.4] J. Mühlethaler, J. Biela, J. W. Kolar, and A. Ecklebe, "Core Losses Under the DC Bias Condition Based on Steinmetz Parameters," *IEEE Transactions on Power Electronics*, vol. 27, no. 2, pp. 953–963, 2010.
- [2.5] Y. Sakaki and S. Imagi, "Relationship among Eddy Current Loss, Frequency, Maximum Flux Density and a New Parameter Polycrystalline and Amorphous Soft," *IEEE Transactions on Magnetics*, vol. 17, no. 4, pp. 1478–1480, 1981.
- [2.6] G. Bertotti and M. Pasquale, "Physical Interpretation of Induction and Frequency Dependence of Power Losses in Soft Magnetic Materials," 1992. *Digests of the Intermag Conference. International Magnetics Conference*, vol. 28, no. 5, pp. 5–7, 1992.
- [2.7] Y. Chen and P. Pillay, "An Improved Formula for Lamination Core Loss Calculations in Machines Operating with High Frequency and High Flux Density Excitation.," *IEEE Industrial Applications*, 37th Annual Meeting, Pittsburgh, PA, Oct. 13-18, 2002.
- [2.8] Christopher G. Oliver, *Measurement and Modeling of Core Loss in Powder Core Materials*. Micrometals, Inc. 2012. [Online]. Available: <http://ridleyengineering.com/images/phocadownload/new%20core%20loss%20model.pdf> [Accessed 20 February 2014]
- [2.9] J. Reinert, A. Brockmeyer, and R. W. A. A. De Doncker, "Calculation of Losses in Ferro- and Ferrimagnetic Materials Based on the Modified Steinmetz Equation," *IEEE Transactions on Industrial Applications*, vol. 37, no. 4, pp. 1055–1061, 2001.
- [2.10] J. L. J. Li, T. Abdallah, and C. R. Sullivan, "Improved Calculation of Core Loss with Nonsinusoidal Waveforms," *IEEE Industrial Application Conference*, vol. 4, pp.

2203–2210, 2001.

- [2.11] K. Venkatachalan, C. R. Sullivan, T. Abdallah, and Hemh Tacca, “Accurate Prediction of Ferrite Core Loss with Nonsinusoidal Waveforms Using Only Steinmetz Parameters,” *Proceedings of the IEEE Workshop on Computers Power Electron*, pp. 36–41, 2002.
- [2.12] M. Mu, F. Zheng, Q. Li, and F. C. Lee, “Finite Element Analysis of Inductor Core Loss Under DC Bias Conditions,” *IEEE Transactions on Power Electron.*, vol. 28, no. 9, pp. 4414–4421, 2012.
- [2.13] A. Krings, “Iron Losses in Electrical Machines - Influence of Material Properties , Manufacturing Processes , and Inverter Operation,” *Dr. Thesis, Stock. Sweden 2014*, 2014.
- [2.14] A. Krings, S. Nategh, and A. Stening, “Measurement and Modeling of Iron Losses in Electrical Machines,” *Proceedings of the 5th International Conference Magnetic Metal*, pp. 101-119, 2012.
- [2.15] F. Fiorillo and A. M. Rietto, “Rotational Versus Alternating Hysteresis Losses in Nonoriented Soft Magnetic Laminations,” *Journal of Applied Physics*, vol. 73, no. 10, pp. 6615–6617, 1993.
- [2.16] J. G. Zhu, “Numerical Modelling of Magnetic Materials for Computer Aided Design on Electromagnetic Devices,” *Ph.D. Thesis*, University of Technology Sydney, Australia, 1994.
- [2.17] F. Fiorillo and A. M. Rietto, “The measurement of rotational losses at I.E.N.: Use of the thermometric method,” in *First International Workshop on Magnetic Properties of Electrical Sheet Steel under Two-Dimensional Excitation, Proceedings of the 93. PTB-Seminar, Physikalisch-Technische Bundesanstalt (PTB), Braunschweig (Germany)*, pp. 162–172, 1991.
- [2.18] F. Fiorillo, “A phenomenological approach to rotational power losses in soft magnetic laminations,” *First International Workshop on Magnetic Properties Electrical Sheet Steel under Two-Dimensional Excit. Proc. 93. PTB-Seminar, Phys. Bundesanstalt (PTB), Braunschweig, Germany*, pp. 11–24, 1991.
- [2.19] J. G. Zhu, V. S. Ramsden, and P. A. Watterson, “Finite element calculation of core losses in motors with non-sinusoidal fields,” *Proceedings of the International Conference Electrical Machines (ICEM), Manchester, UK*, pp. 1182–1186, 1992.

- [2.20] J. G. Zhu and V. S. Ramsden, "Core Loss Modelling in Rotational Electrical Machines," *Proceedings of the International Conference on Electrical Machines in Australia (ICEMA), Adelaide, Australia*, pp. 52–57, 1993.
- [2.21] F. G. Baily, "The Hysteresis of Iron and Steel in a Rotating Magnetic Field," *Philosophical Transactions of the Royal Society*, London, vol. 60, no. 359–367, pp. 182–184, 1896.
- [2.22] J. Zhu, Y. Guo, Z. Lin, and J. Zhong, "Measurement and Modeling of SMC Materials under Vector Magnetizations," *Proceedings of the IEEE International Electric Machines and Drives Conference*, pp. 2354–2359, 2005.
- [2.23] J. G. Zhu and V. S. Ramsden, "Improved Formulations for Rotational Core Losses in Rotating Electrical Machines," *IEEE Transactions on Magnetics*, vol. 34, no. 4 PART 2, pp. 2234–2242, 1998.
- [2.24] Y. Guo, J. G. Zhu, J. J. Zhong, and W. Wu, "Core Losses in Claw Pole Permanent Magnet Machines with Soft Magnetic Composite Stators," *IEEE Transactions on Magnetics*, vol. 39, no. 5, pp. 3199–3201, 2003.
- [2.25] Y. Li, J. Zhu, Q. Yang, Z. W. Lin, Y. Guo, and C. Zhang, "Study on Rotational Hysteresis and Core Loss Under Three-Dimensional Magnetization," *IEEE Transactions on Magnetics*, vol. 47, no. 10, pp. 3520–3523, 2011.
- [2.26] Y. Guo, J. G. Zhu, Z. W. Lin, and J. J. Zhong, "Measurement and Modeling of Core Losses of Soft Magnetic Composites Under 3-D Magnetic Excitations in Rotating Motors," *IEEE Transactions on Magnetics*, vol. 41, no. 10, pp. 3925–3927, 2005.
- [2.27] Y. G. Guo, J. G. Zhu, and H. Y. Lu, "Effects of Armature Reaction on the Performance of a Claw Pole Motor with Soft Magnetic Composite Stator by Finite-Element Analysis," *IEEE Transactions on Magnetics*, vol. 43, no. 3, pp. 1072–1077, 2007.
- [2.28] Y. Guo, J. Zhu, H. Lu, Z. Lin, and Y. Li, "Core Loss Calculation for Soft Magnetic Composite Electrical Machines," *IEEE Transactions on Magnetics*, vol. 48, no. 11, pp. 3112–3115, 2012.
- [2.29] I. D. Mayergoyz and G. Friedman, "Generalized Preisach Model of Hysteresis.," *IEEE Transactions on Magnetics*, vol. 24, no. 1, pp. 212–217, 1988.
- [2.30] M. Enokizono and J.D. sievert, "Magnetic Field and Loss Analysis in an Apparatus

- for the Determination of Rotational Loss,” *Physica Scripta*, vol. 39, pp. 356–359, 1989.
- [2.31] M. Enokizono and J. D. Sievert, “Numerical Analysis of Accuracy of Rotational Measurement Apparatus,” *IEEE Translation Journal of Magnetism, Japan*, vol. 5, no. 9, pp. 742–748, 1990.
- [2.32] M. Enokizono, J. Sievert, and H. Ahlers, “Optimum Yoke Construction for Rotational Power Loss Measurements Apparatus,” *An. Fis.*, vol. 86, pp. 320–322, 1990.
- [2.33] J. G. and V. S. R. Zhu, “Two Dimensional Measurement of Magnetic Field and Core Loss Using a Square Specimen Tester Jian,” vol. 29, no. 6, pp. 2–4, 1993.
- [2.34] W. Salz and K. A. Hempel, “Which field sensors are suitable for a rotating flux apparatus,” *First International Workshop on Magnetic Properties Electrical Sheet Steel under Two-Dimensional Excit. Proc. 93. PTB-Seminar, Phys. Bundesanstalt (PTB), Braunschweig*, pp. 117–126, 1991.
- [2.35] T. Tanaka, S. Takada and T. Sasaki, “Measurement of rotational power loss and magnetization curves in a strip sample,” *First International Workshop on Magnetic Properties Electrical Sheet Steel under Two-Dimensional Excit. Proc. 93*, pp. 71–81, 1991.
- [2.36] T. Nakata, “Improvement of Measuring Accuracy of Magnetic Field Strength,” *IEEE Transactions on Magnetism*, vol. 23, no. 5, pp. 2596–2598, 1987.
- [2.37] F. J. Schulte, “A Two-Dimensional Measuring Device for Detecting the Magnetic Eigenschaften of Electrical Steel,” *Dissertation, RWTH Aachen, Fak. für Elektrotechnik*, 1989.
- [2.38] R. E. Tompkins, L. H. Stauffer, and A. Kaplan, “New Magnetic Core Loss Comparator,” *Journal Applied Physics*, vol. 29, no. 3, pp. 502–503, 1958.
- [2.39] Slawomir Tumanski, “Induction Coil Sensors—A Review,” *Measurement Science Technology*, vol. 18, no. 3, pp. 31–46, 2007.
- [2.40] Y. Li *et al.*, “Improved Measurement of Three-Dimensional Magnetic Properties of SMC material,” *International Conference on Applied Superconductivity and Electromagnetic Devices, ASEMD 2009*, 2009.
- [2.41] P. J. Flanders, “A Hall Sensing Magnetometer for Measuring Magnetisation, Anisotropy, Rotational Loss and Time Effects,” *IEEE Transactions on Magnetism*,

- vol. 21, no. 5, pp. 1584–1589, 1985.
- [2.42] Asa Kaplan, “Magnetic Core Losses Resulting from a Rotating Flux,” *Journal Applied Physics*, vol. 32, no. 3, pp. 370–371, 1961.
- [2.43] W. Brix, “Method for the Measurement of Rotational Power Loss and Related Properties in Electrical Steel Sheets,” *IEEE Transactions on Magnetics*, vol. MAG-18, no. 6, pp. 1469–1471, 1982.
- [2.44] J. Sievert, J. Xu, L. Rahf, M. Enokizono, and H. Ahlers, “Studies on the Rotational Power Loss Measurement Problem,” *An. Fis. Ser. B*, vol. 86, pp. 35–37, 1990.
- [2.45] W. Brix, “Loss and Anisotropy of Non-oriented Electrical Steel Rule Rotary Magnet in Fields,” *Approv. by Fac. Electr. Eng. RWTH degree a Dr. - Eng. Diss.*, 1983.
- [2.46] F. Brailsford, “Rotational Hysteresis Loss in Electrical Sheet Steels,” *Journal Institute. Electrical Engineering*, vol. 84, no. 507, pp. 399–407, 1939.
- [2.47] H. F. S. and J. E. T. W F Archenhold, “Rotational Hysteresis Loss in Grain-Oriented Silicon-Iron,” *British Journal of Applied Physics*, vol. 11, no. 1, 1960.
- [2.48] A. Cecchetti, G. Ferrari, F. Masoli, and G. P. Soardo, “Rotational Power Losses in 3% SiFe as a Function of Frequency,” *IEEE Transactions on Magnetics*, vol. 14, no. 5, pp. 356–358, 1978.
- [2.49] C. R. Boon, “Alternating and Rotational Power Loss at 50c/s in 3% Silicon-Iron Sheets,” vol. 112, no. 11, pp. 2147–2151, 1965.
- [2.50] E. Reisinger, “Measurement of Iron Losses Due to Alternating and Rotating Magnetization,” *Proceedings of the Electrical Energy Conference*, pp. 388–392, 1987.
- [2.51] A. J. Moses and B. Thomas, “Measurement of Rotating Flux in Silicon Iron Laminations,” *IEEE Transactions on Magnetics*, vol. 9, no. 4, pp. 651–654, 1973.
- [2.52] A. J. Moses and B. Thomas, “The Spatial Variation of Localized Power Loss in Two Practical Transformer T-Joints,” *IEEE Transactions on Magnetics*, vol. 9, no. 4, pp. 655–659, 1973.
- [2.53] M. Enokizono, G. Shirakawa, T. Suzuki, and J. Sievert, “Two-Dimensional Magnetic Properties of Silicon-Steel Sheet,” *Journal of the Magnetics Society of Japan*, vol. 15, no. 2, pp. 265-270, 1991.
- [2.54] J. Sievert, “On Measuring the Magnetic Properties of Electrical Sheet Steel under

- Rotational Magnetization,” *Journal of Magnetism and Magnetic Materials*, vol. 112, pp. 50–57, 1992.
- [2.55] Y. Alinejad-Beromi, A. J. Moses, and T. Meydan, “New Aspects of Rotational Field and Flux Measurement in Electrical Steel,” *Journal of Magnetism and Magnetic Materials*, vol. 112, no. 1–3, pp. 135–138, 1992.
- [2.56] A. D. K. S. Tan, “Rotational Loss in Thin Gage Soft Magnetic Materials,” *IEEE Transactions on Magnetics.*, vol. 5, pp. 1921–1923, 1985.
- [2.57] P. J. Flanders, “The Rotating-Sample Magnetometer,” *Journal of Applied Physics*, vol. 38, no. 3, pp. 1293–1294, 1967.
- [2.58] F. Fiorillo and A. M. Rietto, “Extended Induction Range Analysis of Rotational Losses in Soft Magnetic Materials.,” *IEEE Transactions on Magnetics*, vol. 24, no. 2, pp. 1960–1962, 1988.
- [2.59] A. Basak *et al.*, “Influence of Stress on Rotational Loss in Silicon Iron,” *Proceedings of the IEEE. Institute of Electrical and Electronics*, vol. 125, no. 2, pp. 165–168, 1978.
- [2.60] M. Tadashi Sasaki and S. T. and Y. S. Imamura, “Measurement of Rotational Power Losses in Silicon-Iron Sheets Using Wattmeter Method,” *IEEE Transactions on Magnetics*, vol. MAG-21, no. 5, pp. 1918–1920, 1985.
- [2.61] ASTM INTERNATIONAL, “ASTM International Products and Services.” [Online]. Available: https://www.astm.org/marketing_mail/index.html, [Accessed 2 January 2015]
- [2.62] L. T. Mthombeni and P. Pillay, “Core Losses in Motor Laminations Exposed to High-Frequency or Nonsinusoidal Excitation,” *IEEE Transactions on. Industrial Application*, vol. 40, no. 5, pp. 1325–1332, 2004.
- [2.63] James L. Kirtley, *Electromagnetic Forces, Electric Machines*. 2003. [Online]. Available: https://ocw.mit.edu/courses/electrical-engineering-and-computer-science/6-685-electric-machines-fall-2013/course-notes/MIT6_685F13_chapter1.pdf [Accessed 2 April 2014]
- [2.64] N. Mohan, T. M. Undeland, and W. P. Robbins, *Power Electronics: Converters, Applications and Design*, 2nd ed. John Wiley & Sons, Inc., 1991.
- [2.65] W. Brix, K. A. Hempel, F. J. Schulte, “Improved Method for the Investigation of the Rotational Magnetization Process in Electrical Steel Sheets,” *IEEE Transactions*

on *Magnetics*, vol. MAG-20, no. 5, pp. 1708–1710, 1984.

- [2.66] J. X. M. Enokizono, T. Suzuki, J. Sievert, “Rotational Power Loss of Silicon Steel Sheet,” *IEEE Transactions on Magnetics*, vol. 26, no. 5, pp. 42–45, 2000.
- [2.67] M. Enokizono, “Studies on two-dimensional magnetic measurement and properties of electrical steel sheets at Oita University,” *First International Workshop on Magnetic Properties of Electrical Sheet Steel under Two-Dimensional Excitation, Proc. 93. PTB-Seminar, Phys. Bundesanstalt (PTB), Braunschweig*, pp. 82–101, 1991.
- [2.68] J. Sievert, “Studies on the measurement of two dimensional magnetic phenomena in electrical sheet steel at PTB,” *First International Workshop on Magnetic Properties of Electrical Sheet Steel under Two-Dimensional Excitation, Proc. 93. PTB-Seminar, Phys. Bundesanstalt (PTB), Braunschweig*, pp. 102–116, 1991.
- [2.69] T. Tanaka, “Improvements of measuring equipment for rotational power loss,” *Improv. Meas. Equip. rotational power loss”, First International Workshop on Magnetic Properties of Electrical Sheet Steel under Two-Dimensional Excitation, Proc. 93. PTB-Seminar, Phys. Tech. Bundesanstalt (PTB)*, pp. 191–203, 1991.
- [2.70] T. Nakata, M. Nakano, and H. Fujii, “Magnetic Characteristics in Arbitrary Direction of Grain Oriented Silicon Steel,” *Pap. National Convention Magnetic Society Japan*, vol. 10, 1990.
- [2.71] A. M. Gumaidh, W. L. Mahadi, and T. M. Y. Alinejad-Beromi, A.J. Moses, “Measurement and analysis of rotational power loss in soft magnetic materials,” *First International Workshop on Magnetic Properties of Electrical Sheet Steel under Two-Dimensional Excitation, Proc. 93. PTB-Seminar, Phys. Bundesanstalt (PTB), Braunschweig*, pp. 173–190, 1991.
- [2.72] A. Kedous-Lebouc, S. Zouzou, and P. Brissonneau, “On the magnetization processes in electrical steel in unidirectional and rotational field,” *First International Workshop on Magnetic Properties of Electrical Sheet Steel under Two-Dimensional Excitation, Proc. 93. PTB-Seminar, Phys. Bundesanstalt (PTB), Braunschweig*, pp. 36–47, 1991.
- [2.73] S. Zouzou, A. Kedous-Lebous, and P. Brissonneau, “Magnetic Properties Under Unidirectional and Rotational Field,” *Journal of Magnetism and Magnetic Material*, vol. 112, no. 1–3, pp. 106–108, 1992.
- [2.74] J. J. Zhong, Y. G. Guo, J. G. Zhu, and Z. W. Lin, “Characteristics of Soft Magnetic

- Composite Material Under Rotating Magnetic Fluxes,” *Journal of Magnetism and Magnetic Material*, vol. 299, pp. 29–34, 2006.
- [2.75] J. J. Zhong, Y. G. Guo, J. G. Zhu, H. Y. Lu, J. X. Jin, “Techniques and Apparatus for Measuring Rotational Core Losses of Soft Magnetic Materials,” *Journal of Electronic Science and Technology, China*, vol. 5, no. 3, pp. 218-225, 2007.
- [2.76] J. J. Zhong, “Measurement and Modelling of Magnetic Properties of Materials with Rotating Fluxes,” *PhD Disertation*, University Technology of Sydney, Australia, 2002.
- [2.77] J. J. Zhong, J. G. Zhu, V. S. Ramsden, and Y. G. Guo, “Magnetic Properties of Composite Soft Magnetic Materials with 2-D fluxes,” *Proceedings of the Australasian Universities Power Engineering Conference, Hobart, Australia*, 1998, pp. 377–382.
- [2.78] Y. G. Guo, J. G. Zhu, and J. J. Zhong, “Measurement and Modelling of Magnetic Properties of Soft Magnetic Composite Material Under 2D Vector Magnetisations,” *Journal of Magnetism and Magnetic Material*, vol. 302, no. 1, pp. 14–19, 2006.
- [2.79] Y. Guo, J. G. Zhu, J. Zhong, H. Lu, and J. X. Jin, “Measurement and Modeling of Rotational Core Losses of Soft Magnetic Materials used in Electrical Machines: A Review,” *IEEE Transactions on Magnetics*, vol. 44, no. 2, pp. 279-291, 2008.
- [2.80] International Electrotechnical Commission publ. 404-3, “Methods of Measurement of the Magnetic Properties of Magnetic Sheet and Strip by Means of a Single Sheet Tester,” 1992.
- [2.81] J. J. Zhong and J. G. Zhu, “Electromagnetic Design of a 3D tester for Magnetic Properties of Soft Magnetic Materials,” *Proceedings of the 5th International Conference on Electrical Machines and Systems*, pp. 392-395, 2001.
- [2.82] J. G. Zhu, J. J. Zhong, Z. W. Lin, J. D. Sievert, “Measurement of Core Losses with 3-D Magnetic Fluxes”, *IEEE Transactions on Magnetics*, vol. 39, pp. 3429-3431, 2003.
- [2.83] Z. W. Lin, H. W. Lu, J. G. Zhu, J. J. Zhong, X. L. Wang, and S. Y. Ding, “Vector Characterization of Soft Magnetic Materials,” *Journal of Applied Physics*, vol. 97, no. 10, pp. 10R306-1-10R306-3, 2005.
- [2.84] Y. G. Guo, J. G. Zhu, Z. W. Lin, and J. J. Zhong, “3D Vector Magnetic Properties of Soft Magnetic Composite Material,” *Journal of Magnetism and Magnetic*

- Material*, vol. 302, no. 2, pp. 511–516, 2006.
- [2.85] Z. W. Lin, J. G. Zhu, G. Guo, J. J. Zhong, and H. W. Lu, “B and H Sensors for 3-D Magnetic Property Testing,” *International Journal of Applied Electromagnetics and Mechanics, Netherlands*, vol. 25, no. 1–4, pp. 517–520, 2007.
- [2.86] Y. Guo, J. Zhu, Z. Lin, J. Zhong, H. Lu, and S. Wang, “Calibration of Sensing Coils of a Three-Dimensional Magnetic Property Tester,” *IEEE Transactions on Magnetics*, vol. 42, pp. 3243-3245, 2006.
- [2.87] Y. Guo, J. G. Zhu, Z. W. Lin, J. J. Zhong, H. Y. Lu, and S. Wang, “Determination of 3D Magnetic Reluctivity Tensor of Soft Magnetic Composite Material,” *Journal of Magnetism and Magnetic Material*, vol. 312, no. 2, pp. 458–463, 2007.
- [2.88] Y. Li, Q. Yang, Y. Liu, Z. Zhao, C. Zhang, and D. Li, “A Novel Combined B–H Sensing Coil in Three-Dimensional Magnetic Properties Testing System,” *IEEE Transactions on Applied Superconductivity*, vol. 24, no. 3, pp. 1-4, 2014.
- [2.89] Y. Li, Q. Yang, J. Zhu, and Y. Guo, “Magnetic Properties Measurement of Soft Magnetic Composite Materials Over Wide Range of Excitation Frequency,” *IEEE Transactions on Industrial Applications*, vol. 48, no. 1, pp. 88-97, 2012.
- [2.90] J. Guo Zhu, J. Jiang Zhong, Z. Wei Lin, and J. D. Sievert, “Measurement of Magnetic Properties Under 3-D Magnetic Excitations,” *IEEE Transactions on Magnetics*, vol. 39, no. 5, pp. 3429-3431, 2003.
- [2.91] Y. Li, Q. Yang, J. Zhu, Z. Lin, Y. Guo, and J. Sun, “Research of Three-Dimensional Magnetic Reluctivity Tensor Based on Measurement of Magnetic Properties,” *IEEE Transactions on Applied Superconductivity*, vol. 20, no. 3, pp. 1932–1935, 2010.
- [2.92] V. Basso and G. Bertotti, “Hysteresis in Soft Magnetic Materials,” *Journal of Magnetism and Magnetic Material*, vol. 215, pp. 1–5, 2000.
- [2.93] Y. Li, J. Zhu, Q. Yang, Z. W. Lin, Y. Guo, and Y. Wang, “Measurement of Soft Magnetic Composite Material using an Improved 3-D tester with Flexible Excitation Coils and Novel Sensing Coils,” *IEEE Transactions on Magnetics*, vol. 46, no. 6, pp. 1971–1974, 2010.
- [2.94] Y. J. Li, J. G. Zhu, Q. X. Yang, J. F. Sun, Y. Wang, W. Xu “Analysis of the 3-D Magnetic Reluctivity Tensor Based on Magnetic Properties Measurement of SMC Materials,” *International Conferences on Electrical Machines and Systems*,

Incheon, Korea, pp. 1767–1772, 2010.

- [2.95] J. Mühlethaler and J. W. Kolar, “Core Loss Modeling of Inductive Components – Effects with Considerable Impact on Core Losses – Core Losses under DC Bias Condition Motivation,” 2012. [Online]. Available: <http://www.psma.com/sites/default/files/uploads/tech-forums-magnetics/presentations/2012-apec-134-core-loss-modeling-inductive-components-employed-power-electronic-systems.pdf> [Accessed 2 March 2014]
- [2.96] Q. Yang, Y. Li, Z. Zhao, L. Zhu, Y. Luo, and J. Zhu, “Design of a 3-D Rotational Magnetic Properties Measurement Structure for Soft Magnetic Materials,” *IEEE Transactions on Applied Superconductivity*, vol. 24, no. 3, pp. 1-4, 2014.
- [2.97] H. Zijlstra, *Experimental Methods in Magnetism*. Amsterdam, The Netherlands: Elsevier, 1967.
- [2.98] J. J. Zhong, J. G. Zhu, Z. W. Lin, Y. G. Guo, and J. D. Sievert, “Improved Measurement of Magnetic Properties with 3D Magnetic Fluxes,” *Journal of Magnetism and Magnetic Material*, vol. 290–291, no. 2005, pp. 1567–1570, 2005.
- [2.99] Z. Wei Lin, J. Guo Zhu, Y. Guang Guo, J. Jiang Zhong, and S. Wang, “Magnetic Properties of Soft Magnetic Composites Under Three-Dimensional Excitations,” *International Journal of Applied Electromagnetics and Mechanics*, vol. 25, no. 1–4, pp. 237–241, 2007.
- [2.100] Z. W. W. Ā. Lin and J. G. G. Zhu, “Three-Dimensional Magnetic Properties of Soft Magnetic Composite Materials,” *Journal of Magnetism and Magnetic Material*, vol. 312, no. 1, pp. 158–163, 2007.
- [2.101] S. Urata, M. Enokizono, T. Todaka, and H. Shimoji, “Magnetic Characteristic Analysis of the Motor Considering 2-D Vector Magnetic Property,” *IEEE Transactions on Magnetics*, vol. 42, no. 4, pp. 615-618, 2006.
- [2.102] M. Enokizono, H. Shimoji, A. Ikariga, S. Urata, and M. Ohoto, “Vector Magnetic Characteristic Analysis of Electrical Machines,” *IEEE Transactions on Magnetics*, vol. 41, no. 5, pp. 2032–2035, 2005.
- [2.103] M. Enokizono, H. Shimoji, and T. Horibe, “Loss Evaluation of Induction Motor by using Magnetic Hysteresis E&S² model,” *IEEE Transactions on Magnetics*, vol. 38, no. 5, pp. 2379–2381, 2002.
- [2.104] Y. Li, Z. Zhao, Q. Yang, Y. Wang, and J. Zhu, “Tensor Magnetic Reluctivity

Properties of Soft Magnetic Composite Materials,” *Electromagnetic Field Problems and Applications (ICEF), 2012 Sixth International Conference*, pp. 1–4, 2012.

- [2.105] M. Enokizono, T. Todaka, S. Kanao, and J. Sievert, “Two-Dimensional Magnetic Properties of Silicon Steel Sheet Subjected to a Rotating Field,” *IEEE Transactions on Magnetics*, vol. 29, no. 6, pp. 3550–3552, 1993.
- [2.106] Y. J. Li *et al.*, “Three-Dimensional Magnetic Properties of Soft Magnetic Composite Material at Different Frequencies,” *Journal of Applied Physics*, 2011.
- [2.107] Y. J. Li, Q. X. Yang, Y. H. Wang, J. G. Zhu, and Z. W. Lin, “Rotational Core Loss Features of Soft Magnetic Composite Materials Under Excitation Frequencies from 5 Hz to 1000 Hz,” *IEEE International Conference on Applied Superconductivity and Electromagnetic Devices*, 2013.

Chapter 3 : PREPARATION FOR MEASUREMENT TESTING SET UP

3.1 Introduction

Before the measurements are being conducted, there are some preparations that need to be considered. It started with the preparation of the sample and guarding pieces, formation of the B and H sensing coils, coating coils by epoxy glue, and formation of the plastic sensing box. The preparation continued by calibrating the sensing coils before setting up the equipment for the next magnetic properties measurement.

In 2005, SOMALOY 500 material was actively studied in University of Technology Sydney (UTS) [3.1]. This material was measured by using the magnetic property testing system that had been designed and developed by Zhu *et al.*, [3.2], [3.3]. In 2015, the studies of magnetic measurement by using the same tester are continued by considering the lowest loss material from the same manufacturer. The 20 x 20 x 20 mm of 7.5 kg/m³ SOMALOY 700 cubic samples were ordered from Hoganas. They came with six guarding pieces for each sample which is cut to be in 2 x 20 x 20 mm.

In order to measure the magnetic properties of that sample, the sensing coil is an important subject. Therefore, the structure of both B and H sensing coils should be well formed. By considering the uniform and high accuracy of magnetic flux density B , detection, the 0.05 mm diameter of enamelled copper wire is used for both sensing coils. The 200 turns of H sensing coil is wound around 0.6 mm thickness epoxy resin board. The round B sensing coil with 6 mm diameter has been embedded in the centre of the H coil. It has been wound for 60 turns as clearly described in chapter 2. It is important to ensure that the resistance for each sensing coil is the same since this will ease the measurement under 2-D and 3-D magnetic flux density excitations.

Fig. 3.1 shows the B and H sensing coils which are located on the surfaces of the cubic sample. The tiny sensing coils are protected by applying epoxy resin. Epoxy glue coats the coils to prevent the coils from damage.



Fig. 3.1 SOMALLOY 700 (5P) cubic sample with sensing coils

The sensing box was built to hold the guarding pieces, sensing coils, and sample together. Fig. 3.2 shows the sample of SOMALLOY 700 (5P) with its guarding pieces which have been held by sensing box. The box has been made from acrylic plastic in material testing lab.

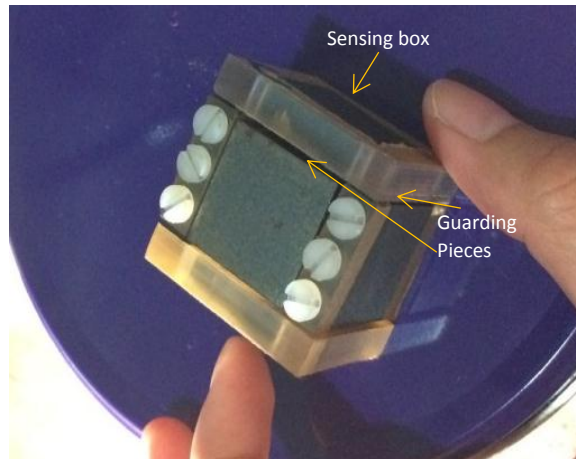


Fig. 3.2 An acrylic sensing box and guarding pieces hold the sensing coils to locate on the surfaces of the cubic sample

3.2 Calibration of sensing coils

To ensure the accuracy of magnetic properties measurement of SOMALLOY 700 (5P) material, the sensing coils used in detecting the magnetic flux density during the measurement, are gone through calibration process in the middle of a long solenoid. The calibration also offers the consistency with other and repetitive measurements.

The electromotive forces of the sensing coils are induced inside the solenoid after magnetic flux changed as stated in Faraday's Law. In this experiment, the maximum magnetic field created by the solenoid is measured. The magnetic flux density for a long solenoid of many turns is given as

$$B = \mu_0 \frac{N_s}{l} I \quad (3.1)$$

where B is the magnetic flux density within the solenoid, which is nearly uniform, N_s is the number of turns, l is the total length of the solenoid and I is the current passing through the solenoid. The magnetic flux over certain area A is,

$$\phi = B \cdot A \quad (3.2)$$

Faraday's Law relates the time rate of change of the flux, $d\phi/dt$, to the electromotive force (emf) voltage ε , as below

$$\varepsilon = N_s A_s \frac{dB}{dt} \quad (3.3)$$

In the equation above, the sensing coil is stationary and perpendicular to the penetration of B . If the AC current in the solenoid has a frequency f , $I = I_0 \sin(-\omega t)$ then, the magnetic flux density at the centre of the solenoid is $B = B_0 \sin(-\omega t)$. Thus, the sensing coil induces an emf voltage whose amplitude ε_0 is proportional to the angular frequency ω , and the amplitude B_0 of the magnetic flux density.

$$\varepsilon_0 = \omega N_p A_p B_0 \quad (3.4)$$

where N_p is the number of turns of the sensing coil and A_p is the area of sensing coil. If the sensing coil is located inside a solenoid, the induced emf of the coil is given by

$$\varepsilon_0 = 2\pi f N_p A_p \mu_0 n_s I_0 \quad (3.5)$$

where $2\pi f = \omega$, n_s is the number of turns per unit length of the solenoid. The emf of the sensing coil is proportional to both the frequency f , and the AC current I_0 , in the solenoid.

Fig. 3.3 illustrates the calibration process by the presence of equipment such as digital multimeter, solenoid, B and H sensing coils, AC supply, power supply, operational amplifier, 3-channel gaussmeter, National Instrument (NI) Data Acquisition Card (DAQ), and personal computer with installation of LabVIEW software.



Fig. 3.3 Calibration of B and H sensing coils

A circuit diagram of the experiment is shown in Fig. 3.4. The AC voltage supply produces a sine-wave voltage which drives an AC current through the solenoid. The solenoid with 0.8 m of length, 0.11 m of diameter, 939 turns and 13.3 mH of inductance can produce the magnetic flux density B . The change of magnetic fluxes induces in the B and H sensing coils. The operational amplifiers are needed to amplify the sensing voltages before being measured by the LabVIEW software.

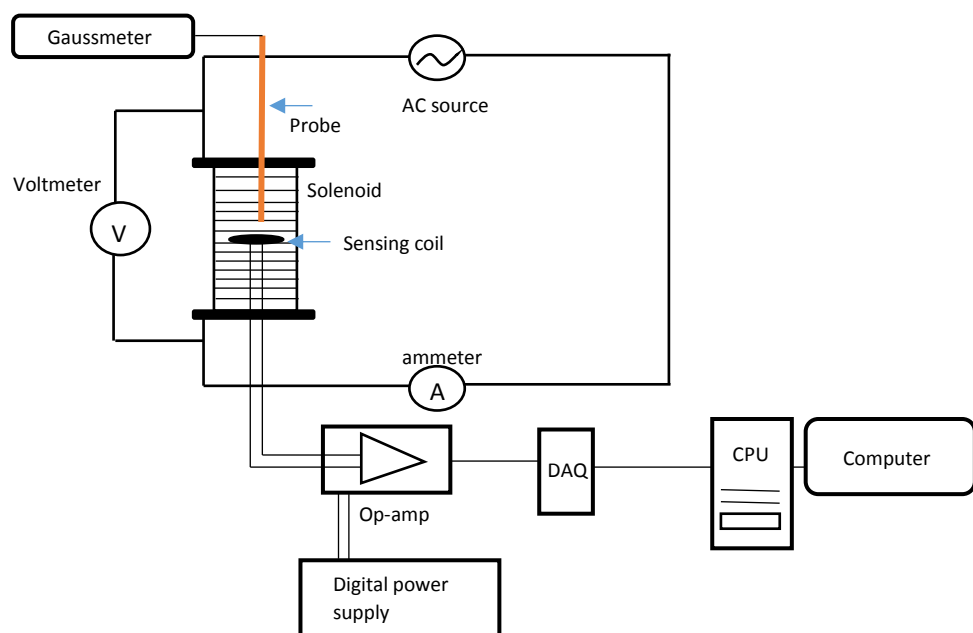


Fig. 3.4 Circuit diagram of calibration process

The magnetic flux density B , which is generated by solenoid, and induced emf of the sensing coil ε_0 , are used in obtaining the sensing box coefficients, K_H and K_B .

From Fig. 3.5, the slope of V versus I graph explains that the resistance of the long solenoid is 5.9 ohm. The consistency of recorded data shows that both measuring devices; ammeter and voltmeter are reliable besides the uncertainty of them are $\pm 1\%$ $\pm 0.7\%$, respectively. The emf produced in the sensing coil by the magnetic flux density, B from the solenoid is measured by the voltmeter and the magnetic field of solenoid is obtained by 3-D gaussmeter. The AC current, I_0 through solenoid is determined by monitoring the AC voltage V .

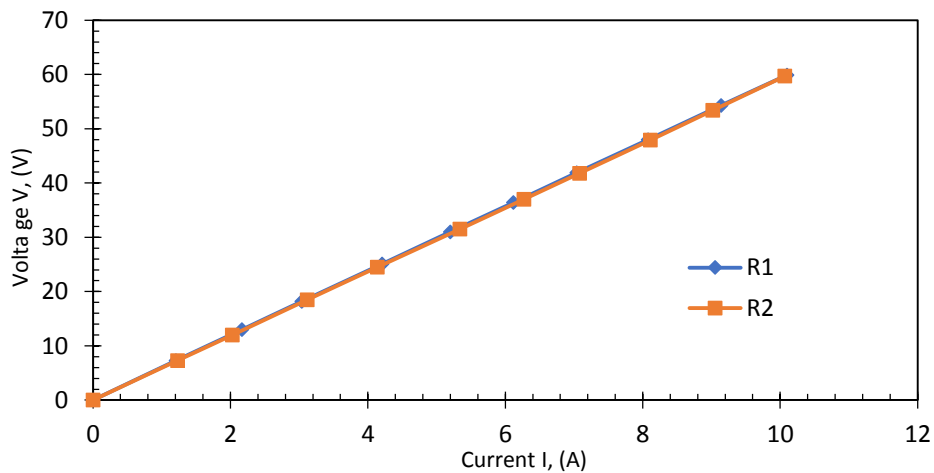


Fig. 3.5 Graph of V against I

The excitation of magnetic flux density is recorded before the calibration of sensing coil for three times for the accurate and precise measurements as exhibited in Fig 3.6. Three overlapping straight lines describes that the environment errors are insignificant in this situation.

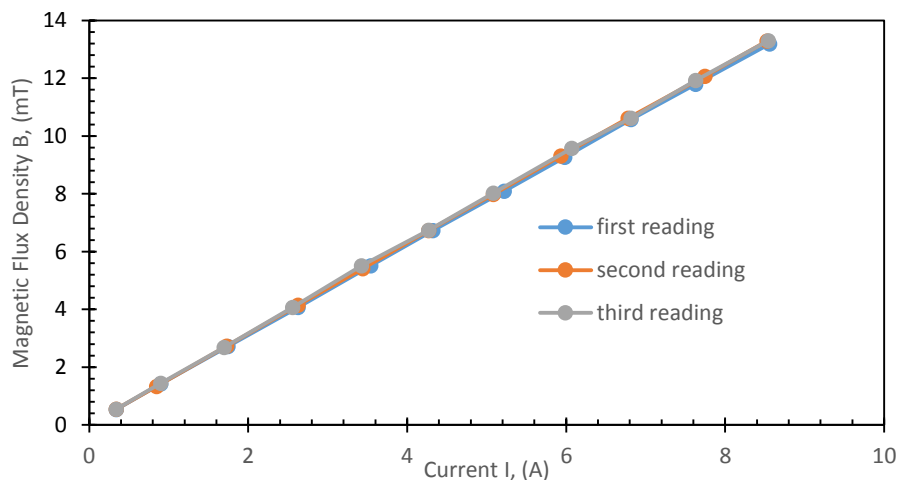


Fig. 3.6 Repeated measurement of magnetic flux density B .

Magnetic flux density produced inside the long solenoid is recorded before being compared to the excitation of B during the sensing coil calibration as shown in Fig. 3.6. From the figure, magnetic flux density is higher when the sample is located in the centre of the solenoid. This is due to the existence of core material that will increase the inductance of the solenoid. However, it did not affect the process of obtaining the box coefficients.

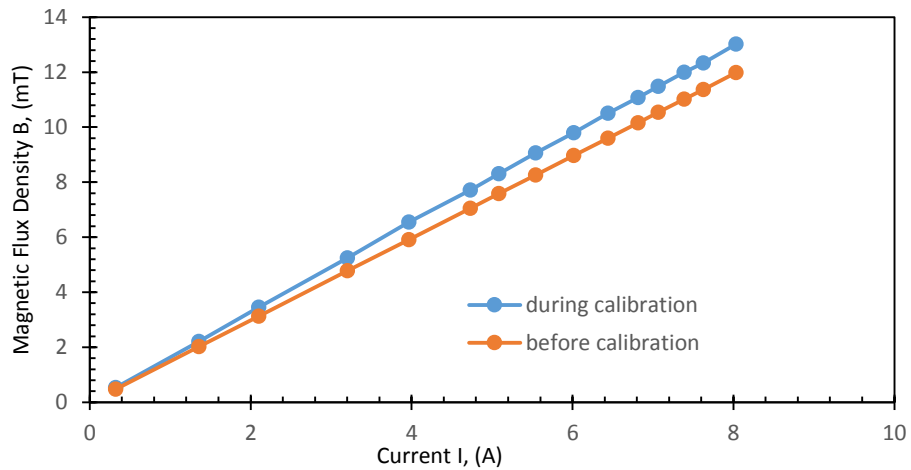


Fig. 3.6 Excitation of magnetic flux density before and during the calibration

The plotted sensing voltages V, along the x-, y- and z-axes versus alternating currents I, that passed through the solenoid are described in Fig. 3.7. It can be seen that the emf of the B and H sensing coils is directly proportional to amplitude of the AC current in the solenoid as stated in equation (3.5).

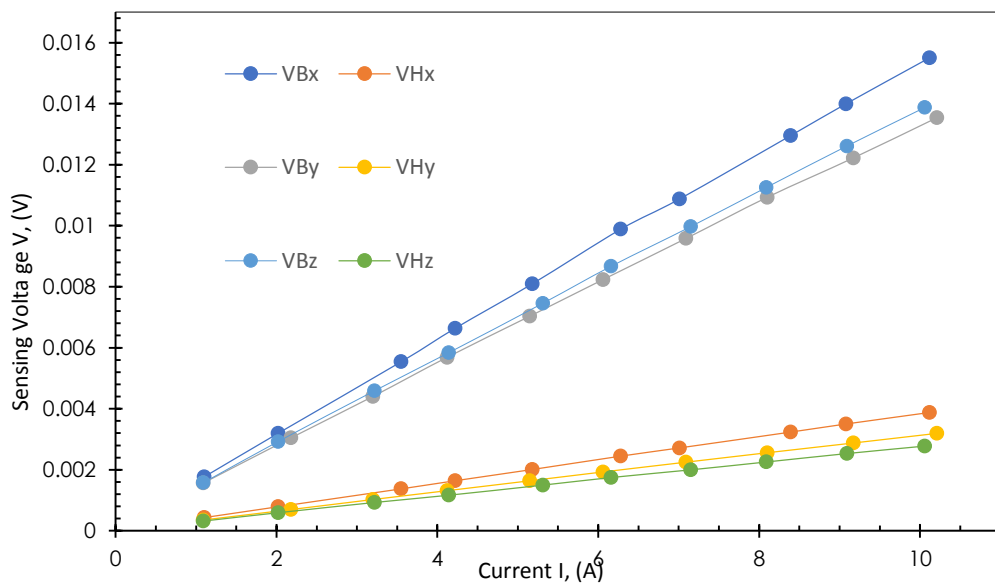


Fig. 3.7 The induced voltages of B and H coils during the calibration process

Box coefficients $K_{H(x,y,z)}$ and $K_{B(x,y,z)}$ are calculated by considering equation (2.29) – (2.32), and the box coefficients are directly proportional to the resistance of the sensing coils.

The results which are obtained by averaging over several measurements are $K_{Hx} = 0.0012$, $K_{Hy} = 0.0010$, $K_{Hz} = 0.0009$, $K_{Bx} = 0.0048$, $K_{By} = 0.0042$, and $K_{Bz} = 0.0043$.

Fig. 3.8 explains the relationship between coil resistance and the coil length by considering this equation,

$$R = \frac{\rho l}{A} \quad (3.6)$$

where R is the resistance of the sensing coil, l is the length of coil, A is the cross-sectional area of the copper wire, ρ is the resistivity of the copper wire that has been used to form the sensing coils and the $\rho_{copper} = 1.72 \times 10^{-8} \Omega^{-1}$

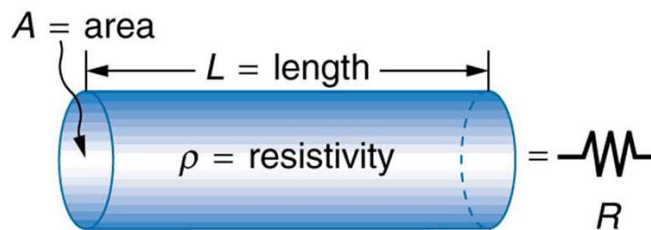


Fig. 3.8 A uniform wire of length L , and cross-sectional area A , [3.4]

By referring to the diameters of B and H sensing coils from the previous explanation, it shows that there is an inaccuracy in producing the coils since the resistance of H sensing coils should be higher than resistance of the B sensing coils as described in equation (3.6). This is due to the inconsistency during winding the coils which are supposed to have 60 turns for B coils and 200 turns for H coils. To face this issue, the proper device is needed to form the sensing coils as per desired since this would affect the value of coil coefficients K_B and K_H .

3.3 Software skills

In this study, data acquisition system is used in measuring the sensing voltages during the calibration process and magnetic properties measurement process. The complete data acquisition system consists of DAQ hardware, sensors and actuators, and a

computer with programmable software such as MATLAB and LabVIEW. In this study measurement, the LabVIEW software has been used by producing the block diagram to determine the sensing voltages as shown in Fig. 3.9 and Fig. 3.10.

3.3.1 LabVIEW software

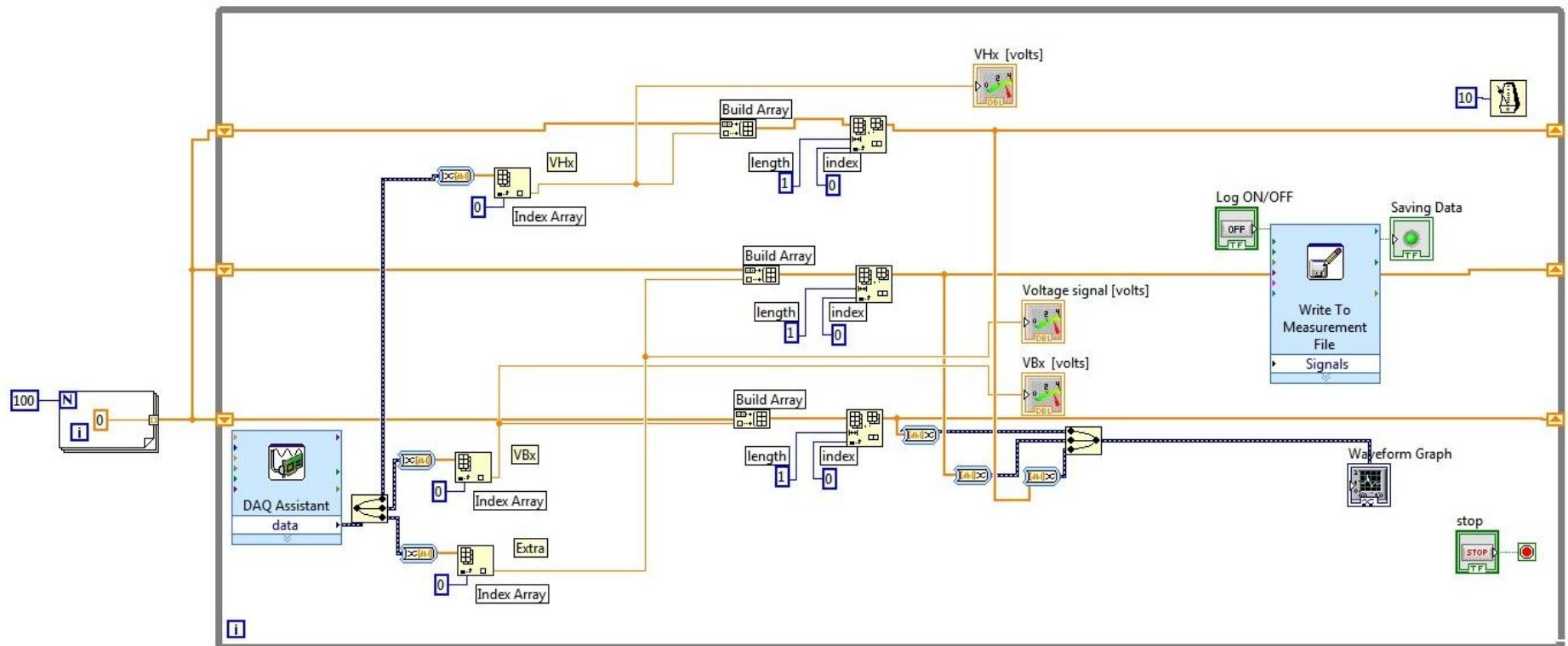


Fig. 3.9 Block diagram of LabVIEW in recording the induced sensing voltages during calibration process

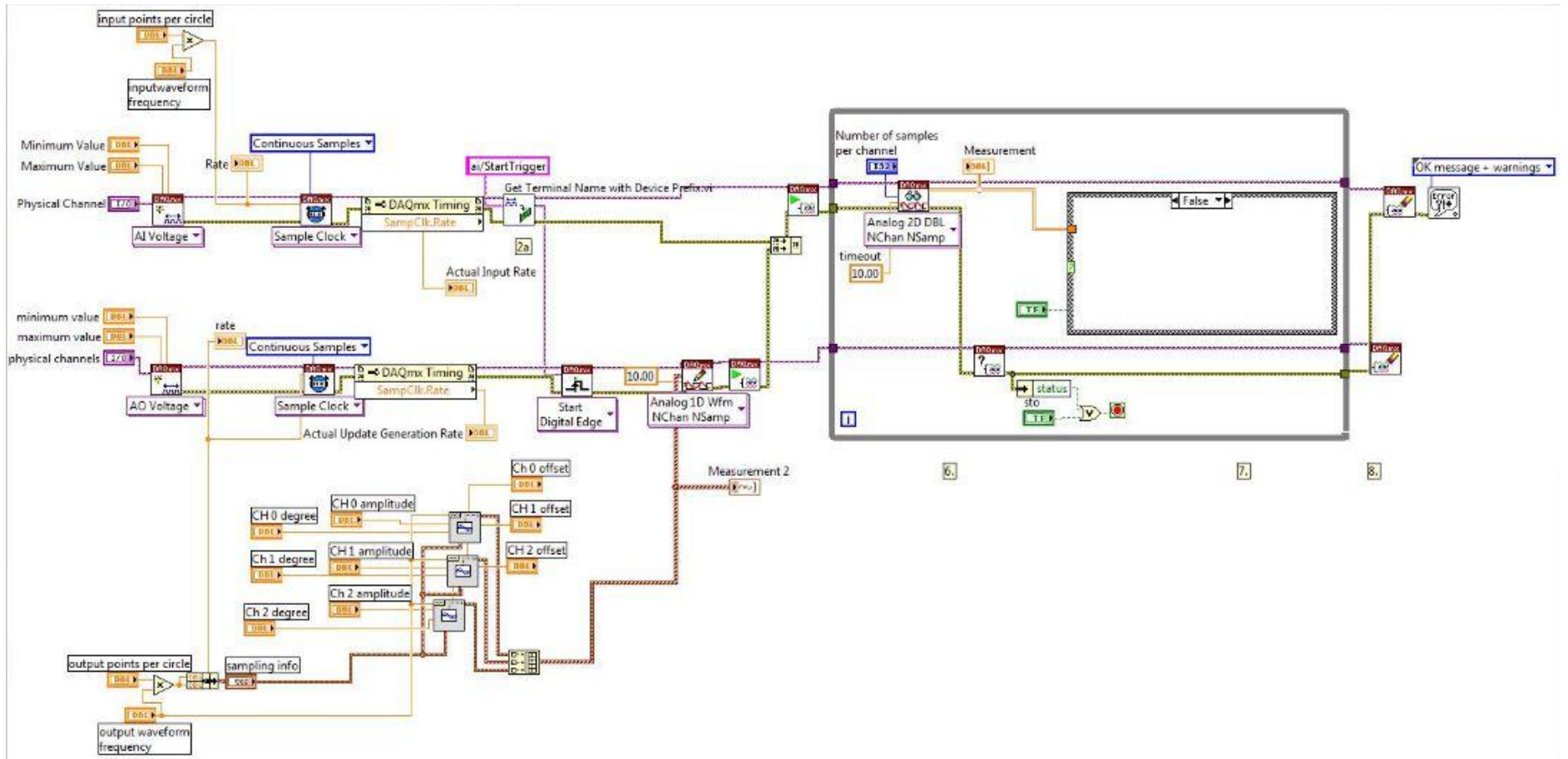


Fig. 3.10 Block diagram of LabVIEW in generating and controlling the magnetic flux density and determining the sensing voltages during magnetisation process

The sensing coils of B and H are calibrated in a long solenoid in the presence of magnetic field along x -axis. V_{Hx} and V_{Bx} can be accurately measured after being amplified and they are detected by DAQ measurement hardware. The sensing voltages for other axes, y and z are obtained by rotating the position of the coil by ensuring the normal of coil area is parallel to the direction of magnetic flux density.

3.3.2 Mathcad software

After determining the sensor voltages of B and H for x -, y - and z -axes during the measurement of magnetic properties, both V_B and V_H are integrated by using Mathcad software to obtain the total flux of magnetic field lines through a unit cross sectional area of the material, magnetic flux density B , and the field that is applied to the material H , as described in equations (2.29) and (2.31). Mathcad software is also used in determining the hysteresis loop and the core loss is obtained by calculating the area of the hysteresis loop by referring to Poynting's theorem in equation (2.26).

3.4 Experimental set up

As shown in Fig. 3.11, the waveforms of magnetic flux density are generated by controlling the magnetic flux densities through LabVIEW software, and they are exported to the channel of linear power amplifier which feeds the excitation winding coils of the tester. The operational amplifier amplifies the voltage signals of B and H before being sent to the A/D and D/A board for the data acquisition process. The voltage signals from the sensing coils are used to determine the relationship of B and H in order to calculate the core loss of the sample.

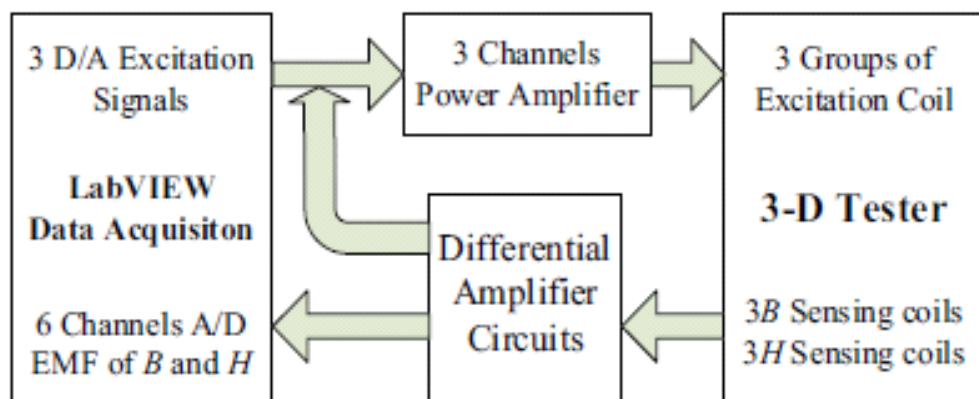


Fig. 3.11 Magnetic properties testing system [3.5]

Fig. 3.12 shows the operational amplifiers that have been used in voltage signal amplification. Due to the small magnitude of V_{Hx} , V_{Hy} and V_{Hz} , 1000x amplification gain is used while V_{Bx} , V_{By} and V_{Bz} use 10x during the amplification process.

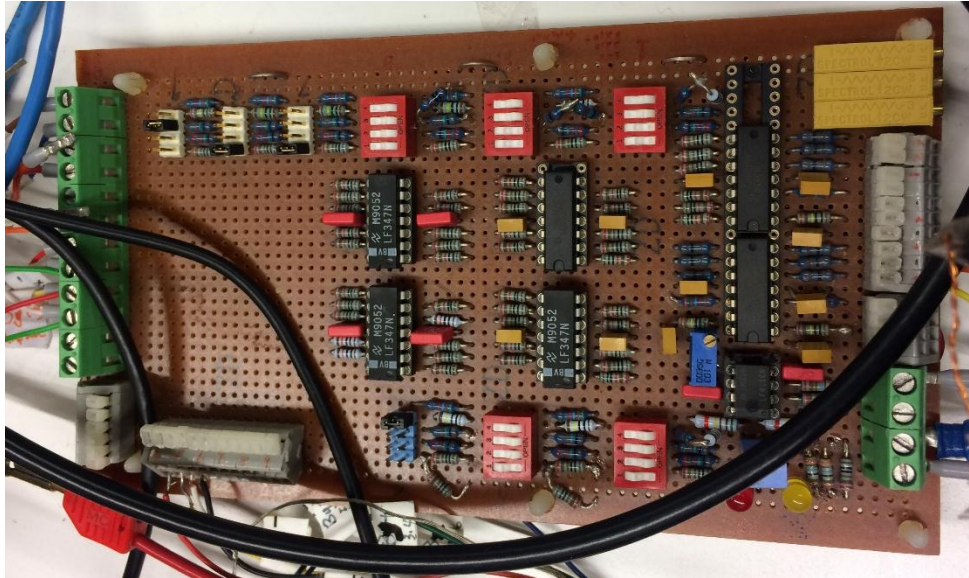


Fig. 3.12 Op-Amp module with 10x, 100x and 1000x amplification gain

In Fig. 3.13, the measurement of magnetic properties of SOMALOY 700 (5P) at 50 Hz, 100 Hz, 500 Hz and 1000 Hz has been carried out by using the 3-D tester under x-, y- and z-axes penetration of magnetic flux density, respectively.

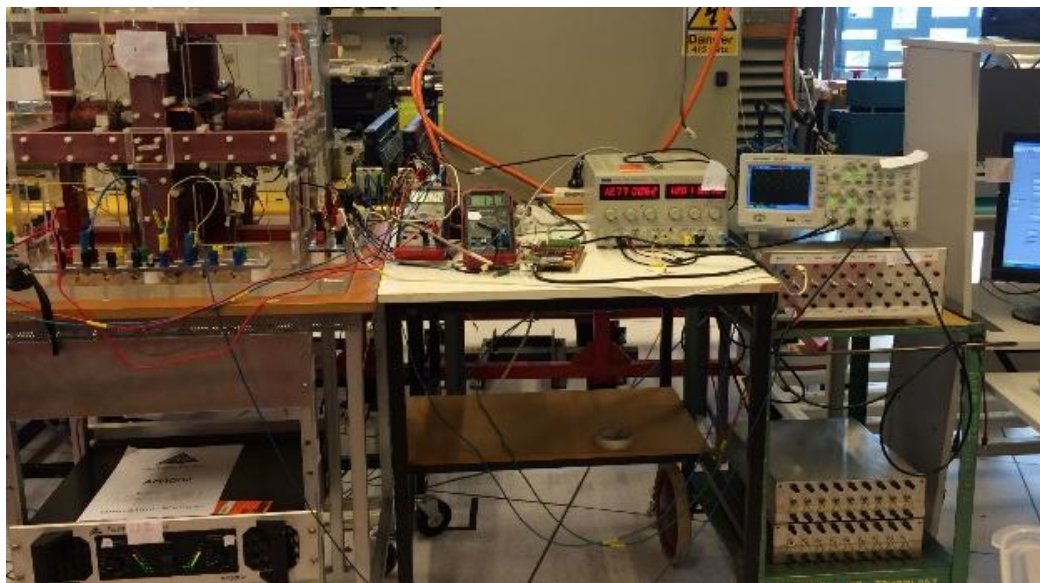


Fig. 3.13 Measurements of magnetic properties of SOMALOY 700 (5P) material

To acquire the maximum magnetic flux density, the resonance phenomenon is considered. Thus, the appropriate capacitance and resistance should be set since the inductance of the excitation winding coils is constantly fixed by adjusting the selection of winding coil number. The possible range of external resistance that has been used for three axes is 2~3 ohm. Table 3-1 displays the list of parameters in obtaining the maximum currents flowing through the tester.

Table 3-1 Parameters of the wide-range of frequency experiment

Frequency (Hz)	Capacitance (μC)	Number of coils
20	280	4
50	80	3
100	20	3
500	3.2	3
1000	7.238	2

The measurement results of V_B and V_H are used to determine B and H in the material. These B and H parameters are considered in plotting the hysteresis loop. The hysteresis loops for a number of increasing excitation voltages of the SOMALOY 700 (5P) material are used to calculate the core loss in that sample which will be explained in the following chapters.

3.5 Conclusion

Research project can only be successfully completed by well planning the whole work from the early stage to the last stage. Due to that it is important to do some preparation before conducting the experimental work. One year was spent to prepare all the basic stuff, skills and mastering in connecting the related equipment.

There are some limitations that have been triggered. It started with the existing sensing coils which are broken. Because of that, the new sensing coils were manually formed without using a proper device. The tiny sensing coils make the adhesive process becomes very hard in order to maintain the orientation of the whole turns of the coils. Besides that, the power amplifier used in measuring the magnetic property of the sample

is very sensitive. The wrong connection will damage the device and the cost of repairing the device is quite high.

In the future, proper device is needed to wind B and H sensing coils since these coils are the important elements in predicting the core loss. It would be good if the B and H sensing coils are being standardized by attaching them in a good way to avoid any broken issues in the future since formation of sensing coil is very complicated to be done.

References

- [3.1] J. J. Zhong, J. G. Zhu, Z. W. Lin, Y. G. Guo, and J. D. Sievert, "Improved Measurement of Magnetic Properties with 3D Magnetic Fluxes," *Journal of Magnetism and Magnetic Material*, vol. 290–291, no. 2005, pp. 1567–1570, 2005.
- [3.2] J. J. Zhong and J. G. Zhu, "Electromagnetic Design of a 3D Tester for Magnetic Properties of Soft Magnetic Materials," *Proceedings of the 5th International Conference on Electrical Machines and Systems*, pp. 392-395, 2001.
- [3.3] J. Guo Zhu, J. Jiang Zhong, Z. Wei Lin, and J. D. Sievert, "Measurement of Magnetic Properties Under 3-D Magnetic Excitations," *IEEE Transactions on Magnetics*, vol. 39, no. 5, pp. 3429-3431, 2003. 2003.
- [3.4] OpenStax. Resistance and Resistivity, [Online].
Available: <http://cnx.org/contents/pelFjTvw@6/Resistance-and-Resistivity>.
[Accessed 22 March 2017]
- [3.5] Y. J. Li, J. G. Zhu, Q. X. Yang, J. F. Sun, "Analysis of the 3-D Magnetic Reluctivity Tensor Based on Magnetic Properties Measurement of SMC Materials", *International Conference on Electrical Machines and Systems (ICEMS)*, pp. 1767-1772, 2010.

Chapter 4 : CORE LOSS MEASUREMENT UNDER ALTERNATING MAGNETIC FLUX DENSITY

4.1 Introduction

Magnetism is a phenomenon which has been exploited for many centuries. This non-contact force phenomenon is extremely used in real life including in the technological development currently. There are some magnetic materials which are employed in the distribution of electricity since these materials are able to generate energy by the movement of electrons. These materials are mostly applied in all electrical machines and they can act as a medium in shaping and directing magnetic flux densities for transferring and converting energy. Due to that, it is important to analyse, comprehend and describe the magnetic properties for better understanding of those devices.

The changing of magnetic flux density during the operation will contribute to the core loss of magnetic materials. Alternating core loss is produced by alternating magnetic flux densities which reverse twice per cycle with the current. The currents are alternated back and forth through a wire and lead to change the direction and magnitude of magnetic flux density. This situation is known as the production of alternating magnetic flux densities which cause the core loss to the magnetic materials.

It is very important to properly identify and model the magnetic properties of material under variation of magnetic flux densities in order to be employed in designing and simulation of electric devices as requested by engineers. With this valuable information, the performance of electrical machines can be well predicted.

This chapter describes the magnetic properties of SOMALOY 700 (5P) by conducting some measurements of alternating core loss. The magnitude of magnetic flux density is controlled in the x-, y- and z-axes. The measurements are conducted under wide range of frequency, 50 Hz, 100 Hz, 500 Hz and 1000 Hz to magnetise the cubic sample of SOMALOY 700 (5P) which is located inside the 3-D tester. These frequencies [4.1], [4.2], [4.3] are selected by referring to some published papers and this selection is reliable to be used during the whole measurement. The measured magnetic properties of SOMALOY 700 (5P) are compared to a previous material, SOMALOY 500.

In section 4.2, the principle of alternating core loss of magnetic material is described. The samples are penetrated by alternating magnetic flux density in transverse and

sinusoidal direction in different axes. The magnetic properties of the lowest loss material SOMALOY 700 (5P) are explained in section 4.3 by considering the core loss and the relationship between magnetic flux density B , and magnetic field strength H , i.e. hysteresis loop. The measured data are analysed and compared with the calculated data by considering the curve fitting technique. Each component of core loss is described in section 4.4.

4.2 Principle of alternating core loss

The cubic sample is penetrated by alternating magnetic flux density in transverse and sinusoidal direction in different axis. These magnetic flux densities are generated by the alternate currents from the winding coils of the 3-D tester. Because of that, there is a change of magnetic fluxes with time which lead to the heat dissipation. The dissipated heat during magnetisation can be represented as a core loss of the sample.

4.2.1 Hysteresis loop

The hysteresis loop is a magnetic characteristic which is able to describe the behaviour of magnetic material core by knowing the magnetic flux density and magnetic field strength during magnetisation process. This characteristic can describe the response of the magnetic material when an external magnetic flux has been applied. It is started by the increment of alternating current which raises the magnetic flux density and magnetic field strength that follow a non-linear magnetisation curve until the magnetic material is fully saturated by alignment of the domain. When current has been reduced to zero, the magnetic field strength is also reduced to zero. However, the magnetic flux density will not drop to zero since there is residual magnetism which presented within the magnetic material.

The negative reversing current will drive the magnetic flux density to be zero. In this phase, the magnetising force is needed to re-align the residual magnetic flux density and this force can be known as coercivity H_c . The magnetic material will be re-saturated by increasing the reverse current. The domains of the material are aligned in the opposite direction. If the reverse current is reduced to zero, the similar residual magnetism is presented as described earlier but in opposite direction. The positive current is increased and will reduce magnetic flux to zero before reaching the saturation condition by increasing the current in a positive direction. This completed cycle produces a hysteresis

loop that represents the total core loss of the magnetic material by calculating the area of the hysteresis loop [4.4].

4.2.2 Core loss curve

The total core loss can be explained by the core loss curve which describes the specific core loss in different peak magnetic flux density. For instance, Fig. 4.1 is the plotted graphs that explain the total core loss of SOMALOY 500 material in the x-, y- and z-axes.

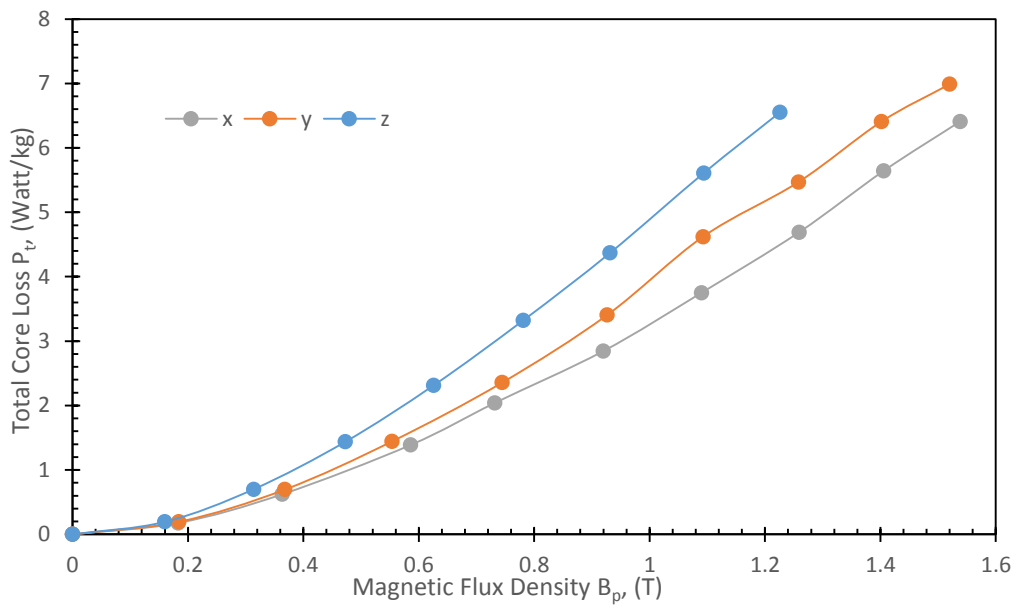


Fig. 4.1 The core loss curve of SOMALOY 500 at 50 Hz along the x-, y- and z-axes [4.5]

From the figure above, it clearly explained that the core losses in x and y directions are quite similar due to the range of core loss value. However, the recorded core loss which is generated by penetration of magnetic flux in z direction is slightly different and high compared to x- and y-axes. This is caused by the effect of the manufacturing process that makes the distribution of particle in z direction is not uniform [4.5].

4.3 Experimental results

The magnetic properties of the lowest loss material, SOMALOY 700 (5P), are investigated in this section by considering the core loss and the relationship between magnetic flux density B , and magnetic field strength H , i.e. the hysteresis loop.

The core loss of SOMALOY 700 (5P) has been measured under alternating magnetic flux density in three different axes; x, y and z, respectively. The hysteresis loop and the core loss curve are analysed by comparing the behaviour of measured SOMALOY 700 (5P) and SOMALOY 500. The performance of SOMALOY 500 is collected from other researchers [4.6]. Besides that, the performance of the measured SOMALOY 700 (5P) is compared to the data form the manufacturer, Hogan. The data verification is applied by considering the curve fitting technique in obtaining the calculated core loss.

4.3.1 Hysteresis loops of alternating core loss

The characteristics of the SOMALOY 700 (5P) material at 50 Hz is depicted in Fig. 4.2. The loops for both materials are resulted from the alternating magnetic flux densities up to 2.3 T. From the figure, it can be seen that SOMALOY 700 (5P) gives smaller loop compared to the SOMALOY 500. Theoretically, the area of the hysteresis loop represents the core loss which can be experienced by dissipating the heat when the field is reversed [4.7].

This describes that the SOMALOY 700 (5P) has offered the low loss due to the improved physical characteristic of the SOMALOY 700 (5P) particle during the manufacturing process. The larger grain of iron particles with ultra-thin insulation are produced by Hogan to provide low loss during the magnetisation process. These characteristics of SOMALOY 700 (5P) will also significantly reduce the eddy current loss as explained in this equation.

$$P_e = \frac{\pi^2 B_p^2 d^2 f^2}{6k\rho D} \quad (4.1)$$

where P_e is the eddy current loss, B_p is the peak magnetic field, d is the thickness of the sheet or diameter of wire, f is the frequency, k is the constant which is 1 for thin sheet and 2 for this wire, ρ is the resistivity of material and D is the density of the material.

Theoretically, the eddy current loss is produced if there are changes of magnetic flux density within the conducting magnetic material which will cause the currents being circulated by induced voltage of the material.

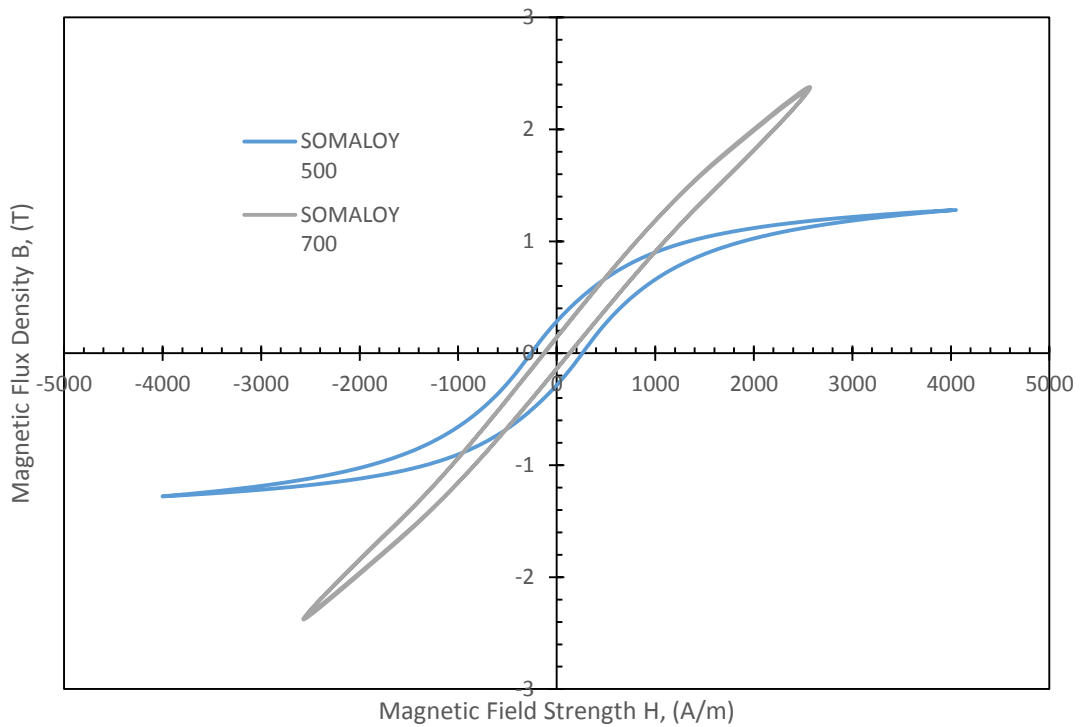
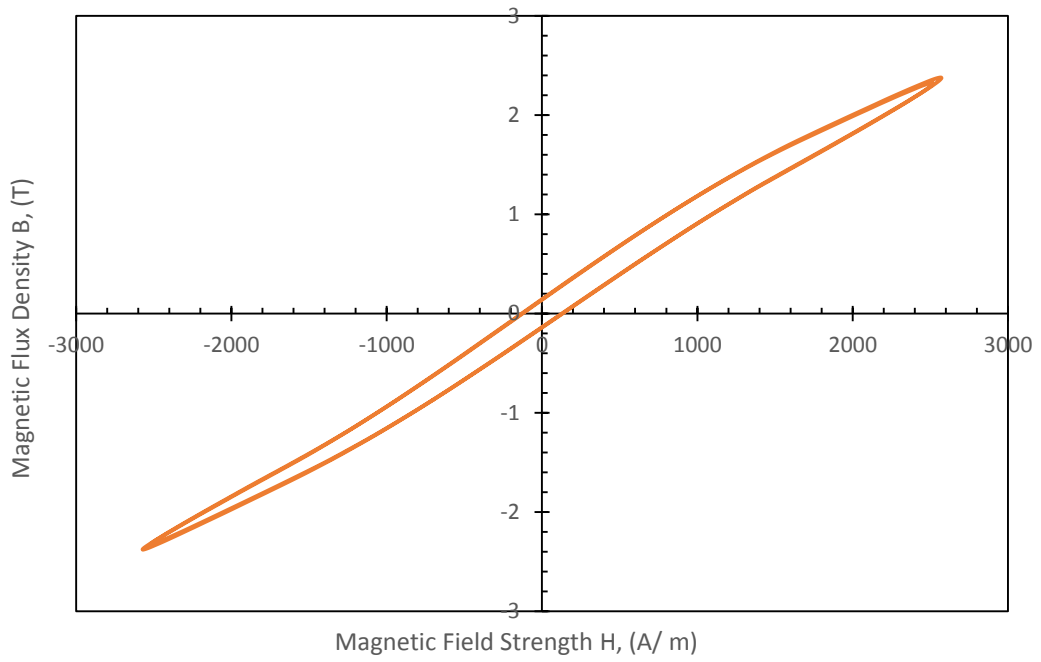


Fig. 4.2 The hysteresis loops of SOMALLOY 700 (5P) and SOMALLOY 500 at 50 Hz

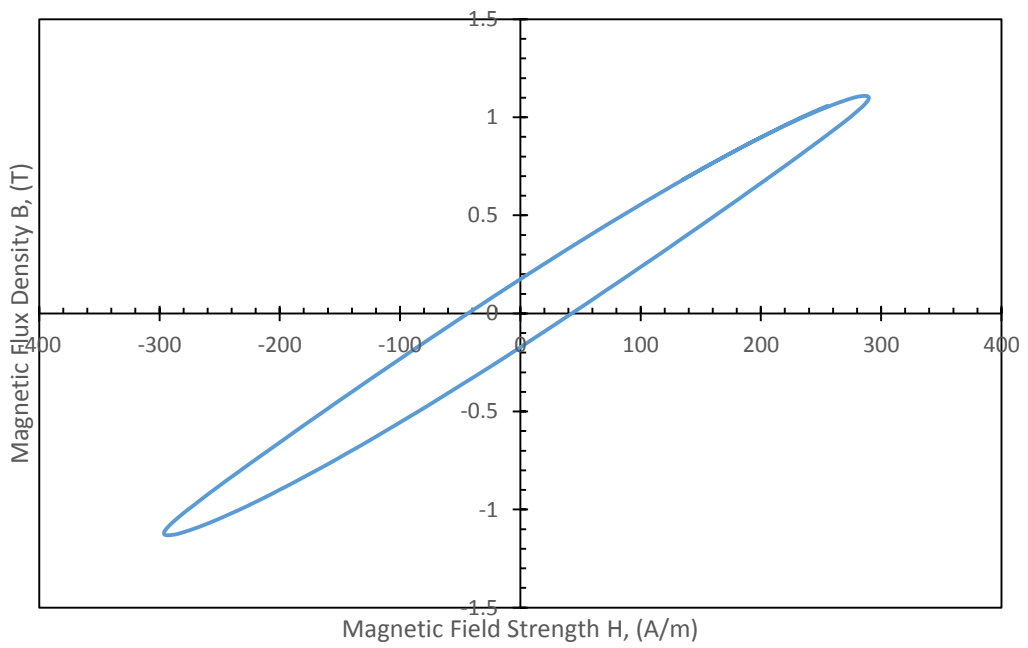
The remanence or residual magnetism of SOMALLOY 700 (5P) is low which defines the remaining magnetisation when magnetic field strength has been dropped to zero. The low remanence represents the low ability in memory and it explains that this material is not suitable for producing permanent magnets which demand a high remanence. From the figure, it is seen that the coercivity of SOMALLOY 700 (5P) is low compared to SOMALLOY 500 material. This defines the behaviour of this material which is magnetically soft due to the low coercivity. Low coercivity describes the needed applied field in reversing the magnetisation of the magnetic material is low.

Other than that, the figure above also describes that the SOMALLOY 700 (5P) is saturated at higher magnetic flux density which provides wide applications.

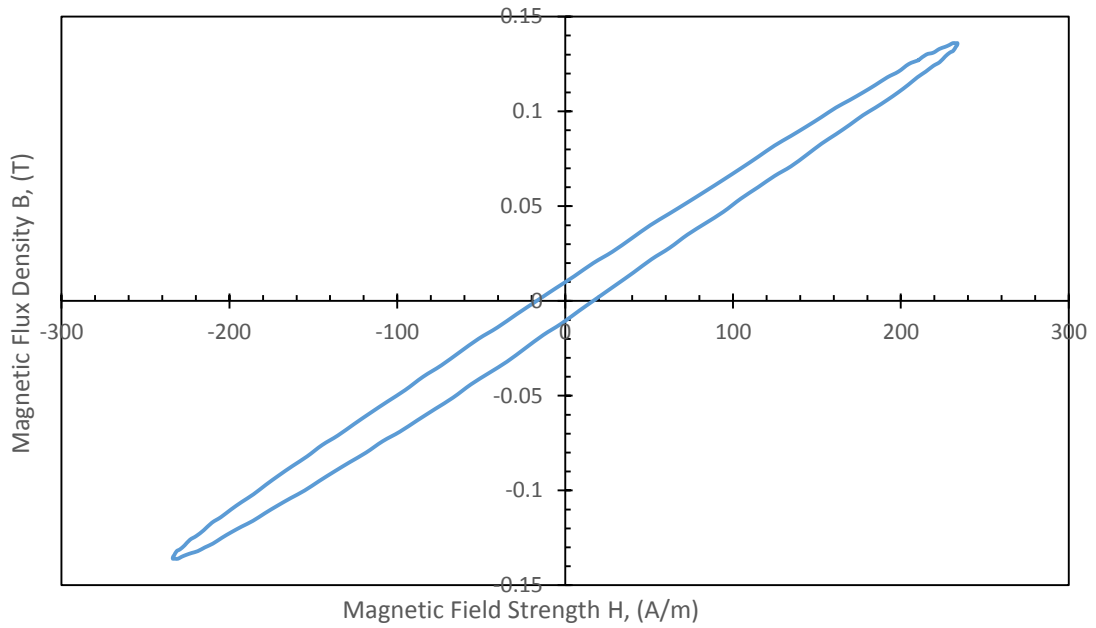
Fig. 4.3 exhibits the hysteresis loops at certain range of operating frequency. Hysteresis loops is able to provide the information related to the core loss since the total core loss of magnetic material is proportional to the area of hysteresis loops. The hysteresis loops of SOMALLOY 700 (5P) material at 50 Hz, 100 Hz, 500 Hz and 1000 Hz have been described in Figs.4.3 (a), (b), (c) and (d), respectively.



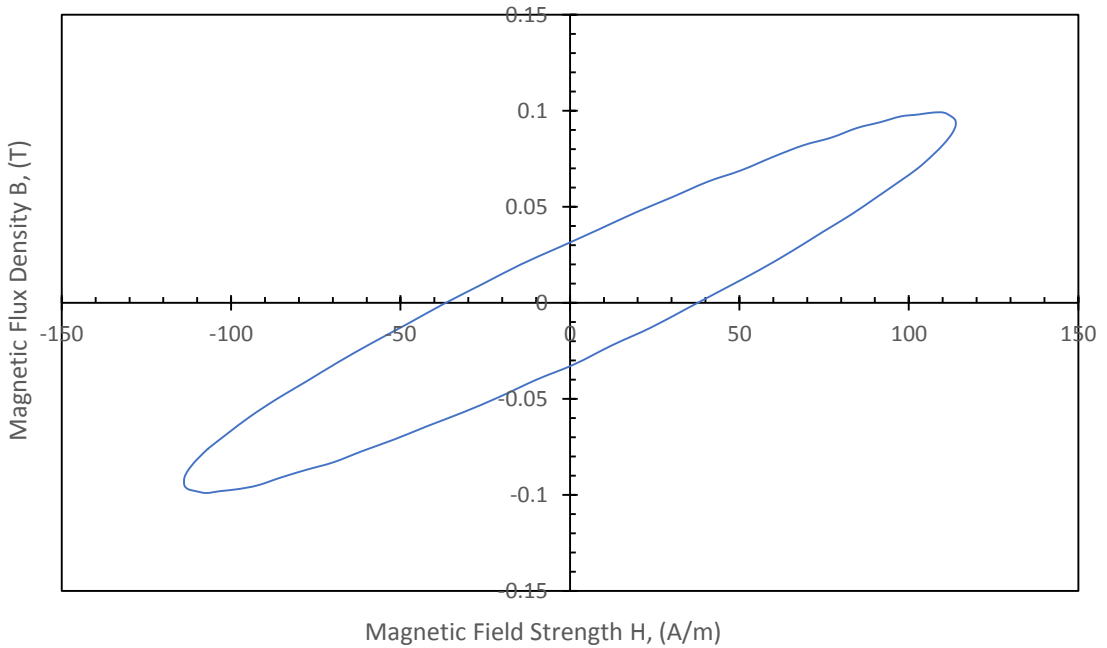
(a)



(b)



(c)



(d)

Fig. 4.3 The hysteresis loops of SOMALOY 700 (5P) in the x-axis at (a) 50 Hz (b) 100 Hz (c) 500 Hz and (d) 1000 Hz

Fig. 4.3 (a), (b), (c) and (d) show that the loop area is getting bigger with the frequency. This explains that the ability of the 3-D tester to magnetise the SOMALOY 700 (5P) material is decreased when the frequency is setting to be higher. Based on figure which

explains the measurement at 50 Hz, it shows that the recorded magnetic flux density is 2.3 T. However, the saturation magnetic flux density is around 2.45 T [4.8] that will cause the loop is flattened at both end in representing the saturation condition of magnetic material. The saturated magnetic flux density of SOMALOY 700 (5P) is higher than SOMALOY 500 which is saturated at 2.03 T as stated by Guo in 2006 [4.9]. The condition of the 3-D tester has affected the experimental work in measuring the magnetic properties of SOMALOY 700 (5P) material at very high saturation magnetic flux density.

At 100 Hz, the recorded magnetic flux density is 1.1 T as expressed in Fig. 4.3 (b). However there is 0.14 T recorded as the highest magnetic flux density when the measurement has been done at 500 Hz as shown in Fig. 4.3 (c), whereas the highest magnetic field strength at the same frequency is 231 A/m.

For core loss measurement at 1000 Hz, the peak magnetic flux density of the outer loop is 0.1 T and the corresponding magnetic field strength is 114 A/m. As stated in [4.10], the possible magnetic field can be generated at 1000 Hz by the original 3-D tester is only 0.1 T.

4.3.2 Core loss of alternating magnetic flux density

Three magnetic properties measurements have been conducted in the x-, y- and z-axes by performing the measurement for three times in obtaining the accurate results. Fig. 4.4 shows the three reading of core loss measurements at 50 Hz of frequency. The best curve is considered by calculating the standard deviation of the collected data. The curve that is covered in the error bars has been selected as the best curve. This method of finding the standard deviation and error bars are repeated for all the measurements in this study.

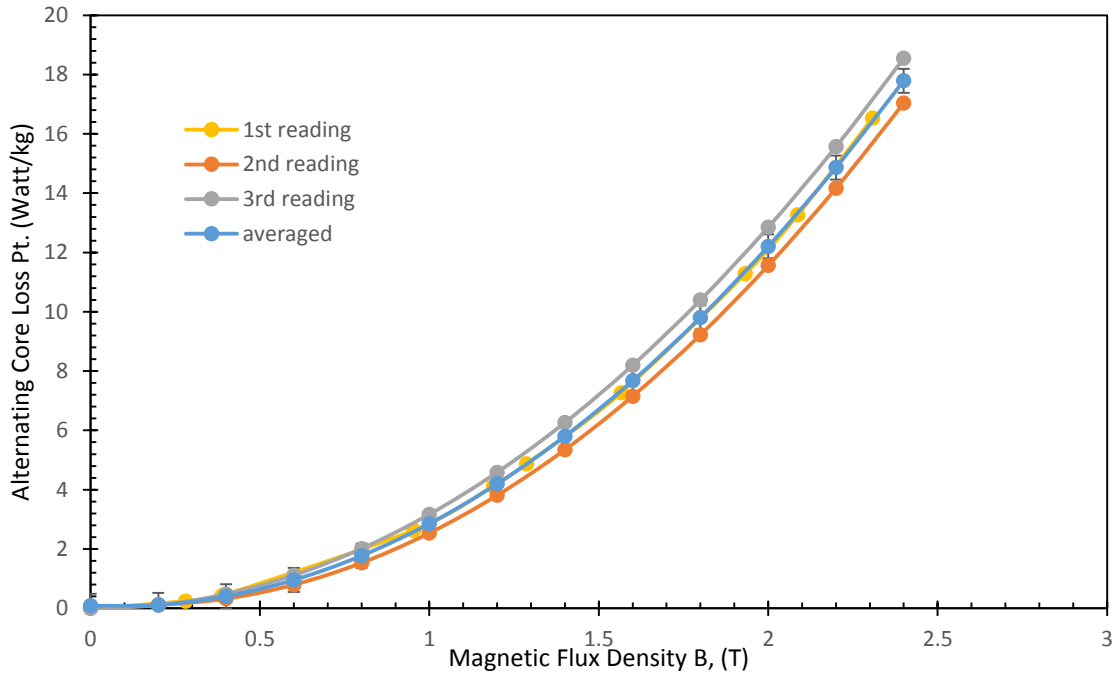


Fig. 4.4 Three reading of alternating core loss with 0.405 of standard deviation

Fig. 4.5 exhibits the plotted graphs which express the total core loss of SOMALLOY 700 (5P) material when there is a magnetic flux excitation in the x-, y- and z-axes and the core loss curve of SOMALLOY 500 material which has been provided by the manufacturer. It can be seen that the SOMALLOY 500 core loss is higher than SOMALLOY 700 (5P) core loss along all axes.

The figure visibly illustrates that the curve lines for all axes are quite similar and they have been plotted up to 2.3 T. The similarity is due to the isotropic characteristic that reflects the condition of the SOMALLOY 700 (5P) with the identical values of property in all directions.

However, the core loss along z-axes is slightly higher due to the stress induced during the manufacturing process [4.5]. As illustrated by the curve, the core loss of sample is proportional to the squared of magnetic flux density. There was a significant increase in the production of core loss from the low B to the high B due to the changes of magnetic flux passing through the magnetic material that makes the core loss getting larger when the magnetic flux density is increased to the right as shown in graph.

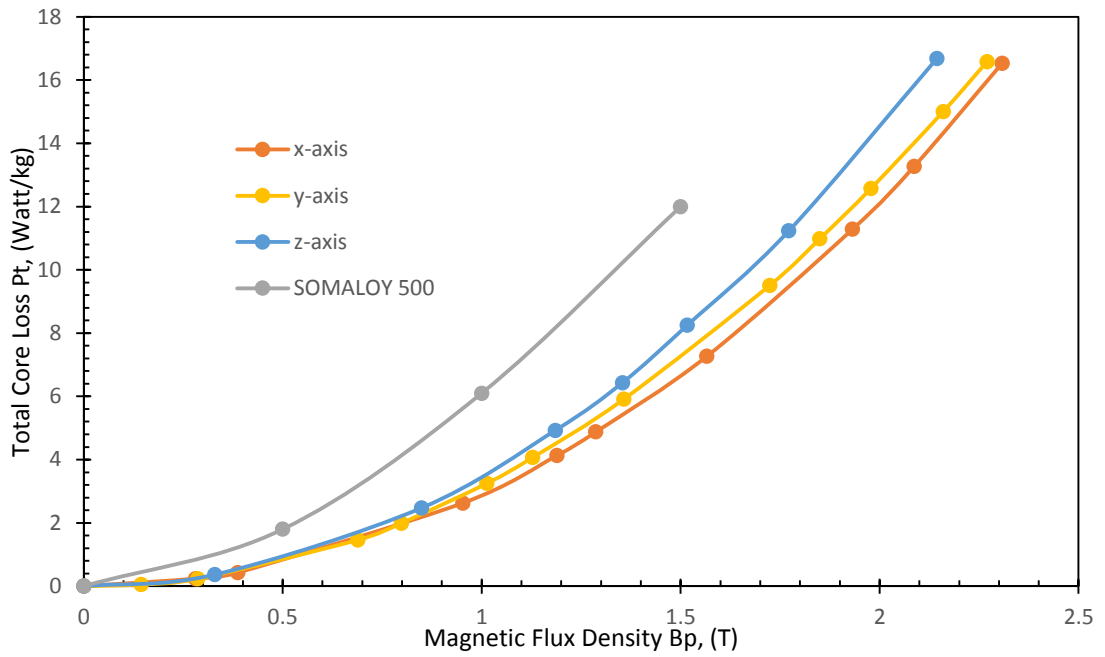


Fig. 4.5 Loss curve of SOMALLOY 700 (5P) at 50 Hz for three different axes

Fig. 4.6 explains the alternating core loss at 50 Hz when there is a variation of magnetic flux density which is up to 2.76 T. As illustrated by the figure, the curve is gradually risen from the start. However, it then becomes flat at 2.45 T and it shows that the SOMALLOY 700 (5P) saturated at this value.

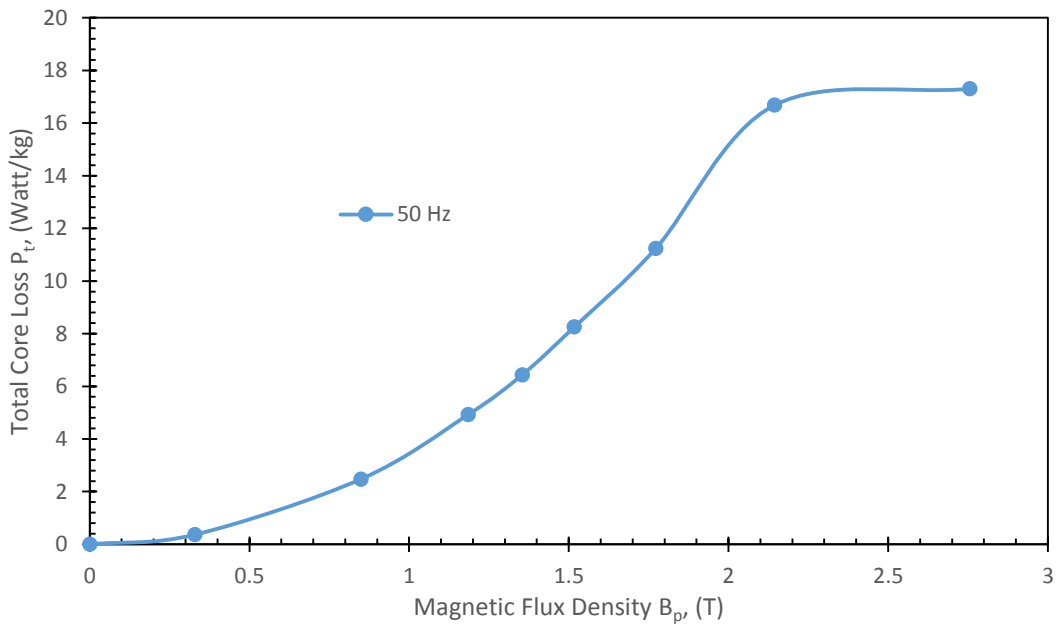


Fig. 4.6 The alternating core loss at 50 Hz

Fig. 4.7 illustrates the core loss of SOMALOY 700 (5P) material versus peak magnetic flux density. There are four graphs that represent the core loss curve at 50 Hz, 100 Hz, 500 Hz and 1000 Hz. As can be seen from the graph, all curves dramatically increased with the magnetic flux density at the end after the slowly risen in the beginning. The measurement at 1000 Hz is recorded as the highest in contributing the core loss and it has been followed by measurement under 500 Hz, 100 Hz and 50 Hz. As expressed in equation (2.1) in chapter 2, core loss is proportional to the operated frequency and it is proved in this study.

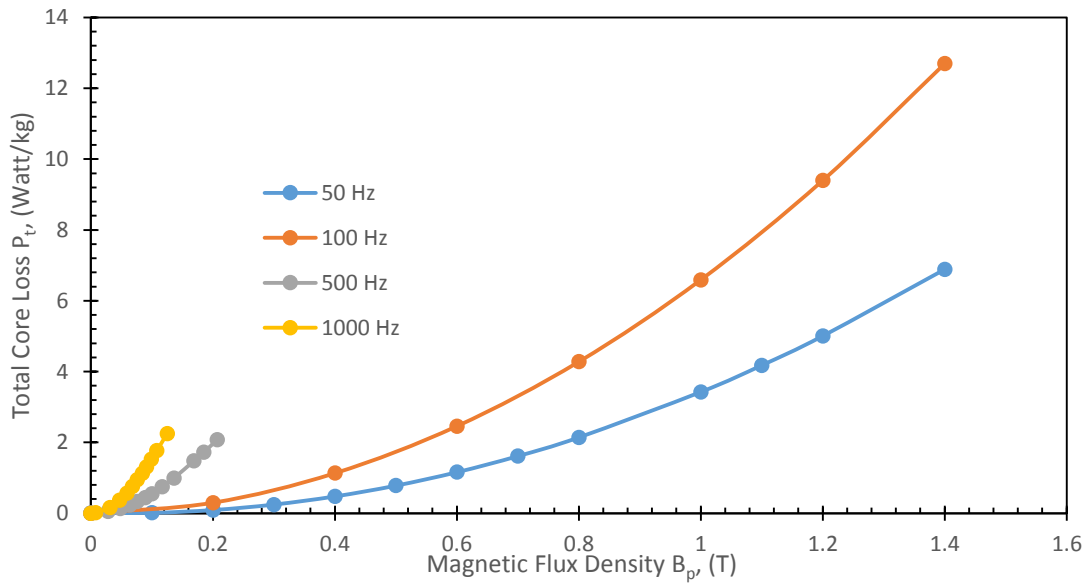


Fig. 4.7 Loss curve of SOMALOY 700 (5P) material at 50 Hz, 100 Hz, 500 Hz and 1000 Hz

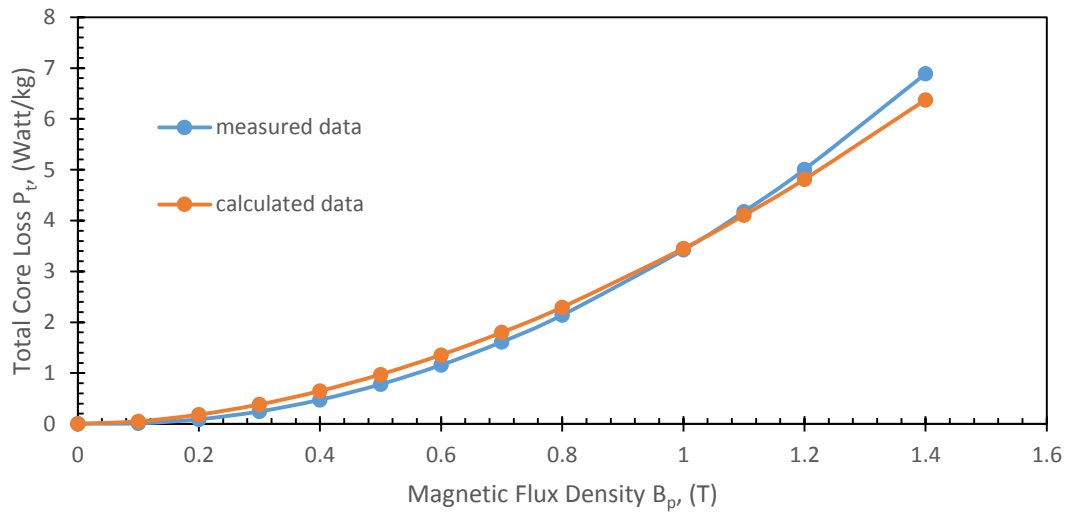
4.3.2.1 Loss coefficient

The curve fitting method is considered in obtaining the core loss coefficients. By fitting to the measured data, the coefficients C_h , C_e , C_a , and n are deduced as 0.063, 9×10^{-10} , 2.9×10^{-5} and 1.75, respectively. In this method, the determined coefficients are based on measurements at different frequencies with different magnetic flux densities. Squared error tool is used to fit both calculated and measured core losses in order to calculate the loss coefficients which will be used in determining each component of core loss in the next step.

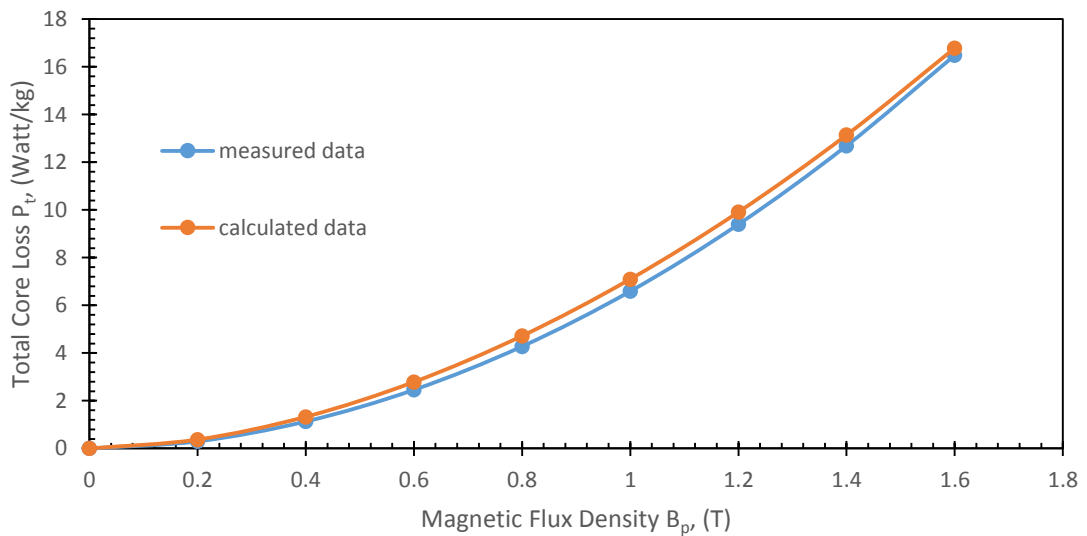
4.3.2.2 Core loss curve

The core loss of SOMALOY 700 (5P) material is measured under alternating magnetic flux density by focusing on x-axis only since this magnetic material is isotropic as proved in the section 4.3.2. Isotropic material can be defined as a material that has the identical values of mechanical and thermal properties in all directions.

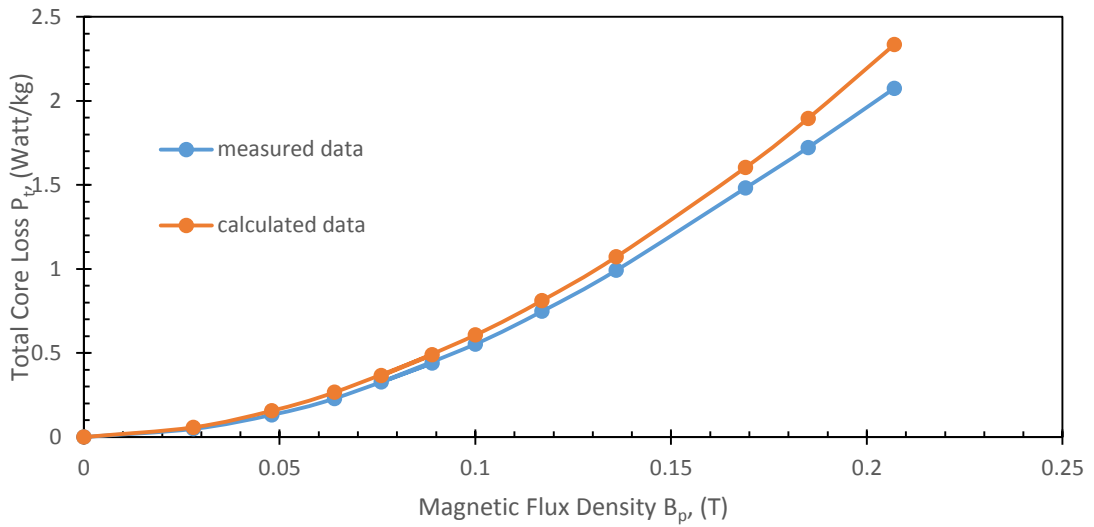
Fig. 4.8 (a), (b), (c) and (d) exhibit the core loss curve that involves the total core loss in Watt/kg versus peak magnetic flux density in T at 50 Hz, 100 Hz, 500 Hz and 1000 Hz, respectively. The experimental data from the measurement has been plotted before being compared to the calculated data.



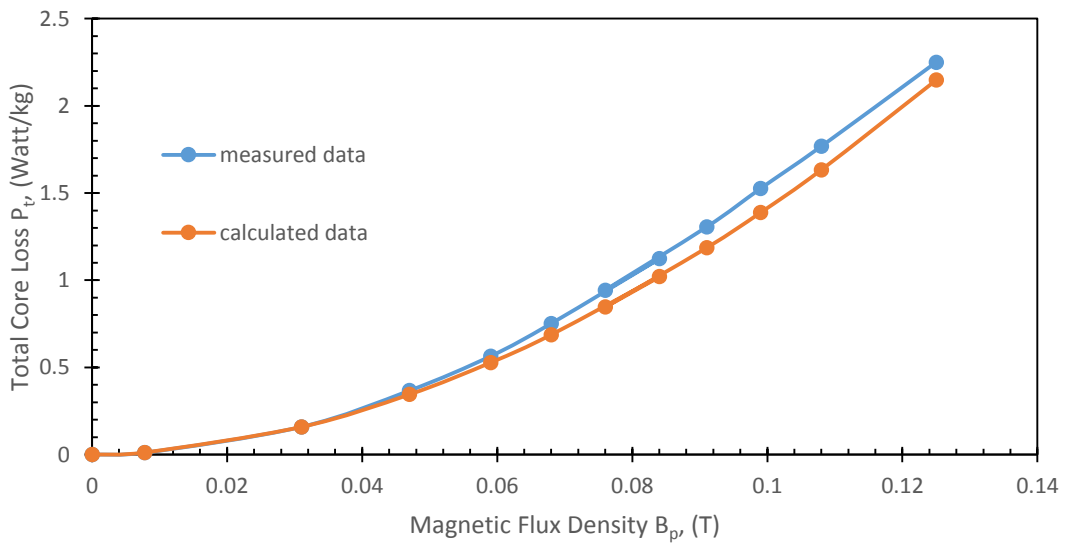
(a)



(b)



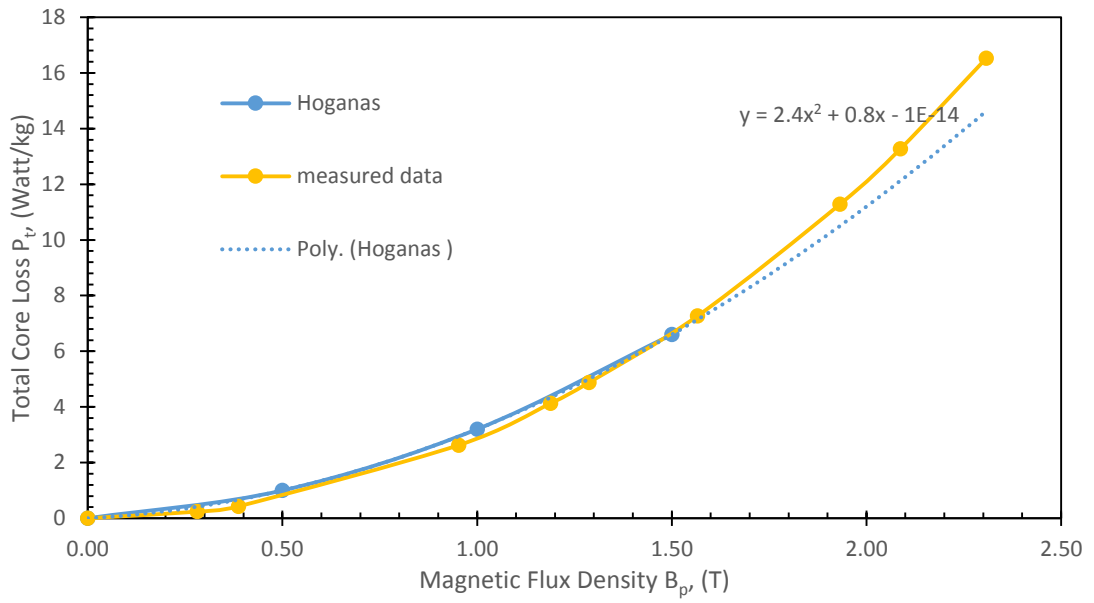
(c)



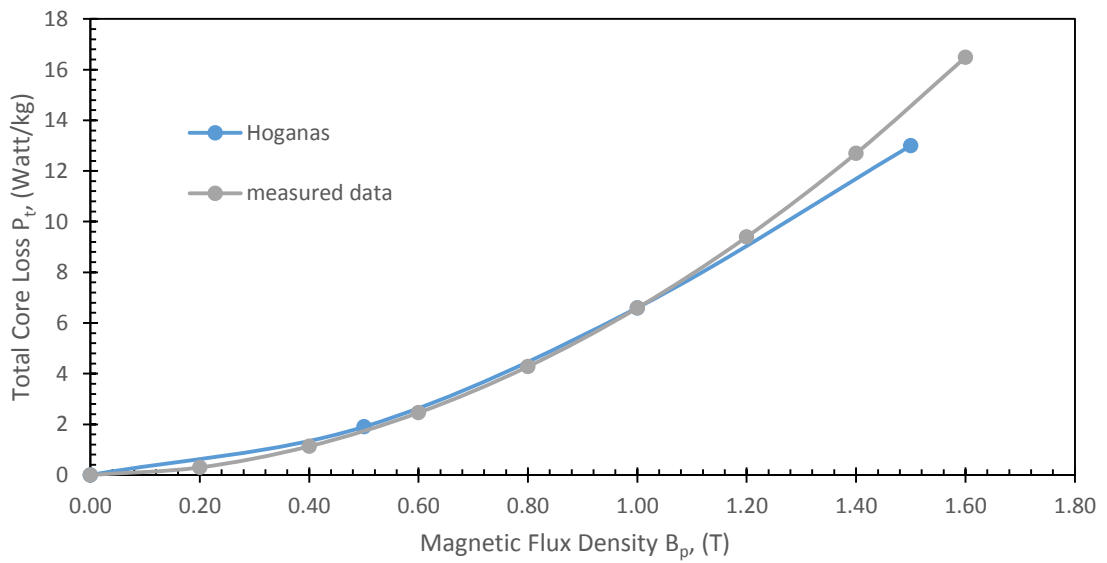
(d)

Fig. 4.8 Comparison between calculated and measured data at (a) 50 Hz (b) 100 Hz (c) 500 Hz and (d) 1000 Hz

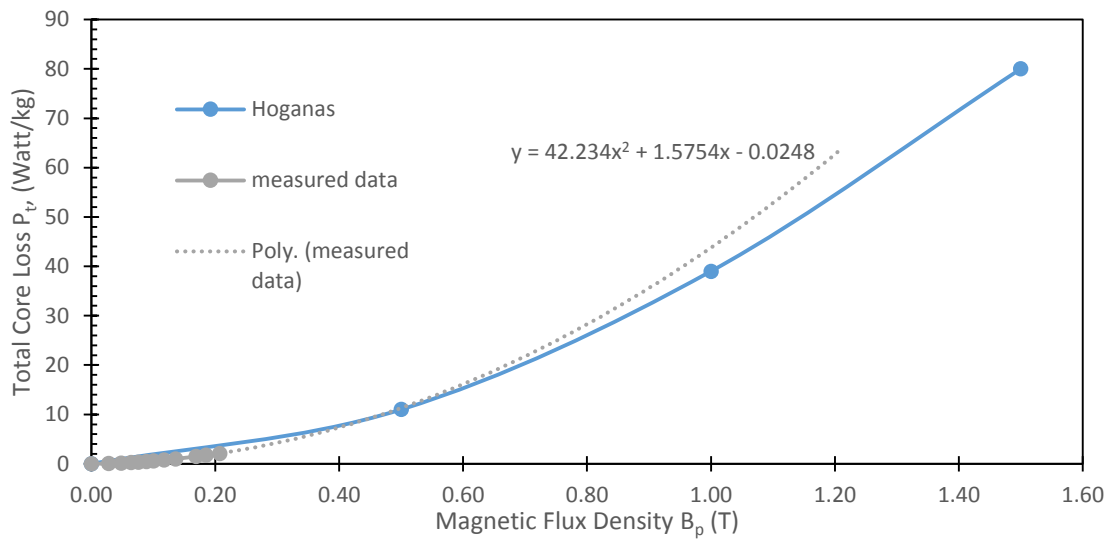
The performance of core loss measurement is validated by comparing the measured data to the manufacturing data. Set of core loss curves at 50 Hz, 100 Hz, 500 Hz and 1000 Hz are plotted as exhibited in Fig. 4.9 (a), (b), (c) and (d), respectively.



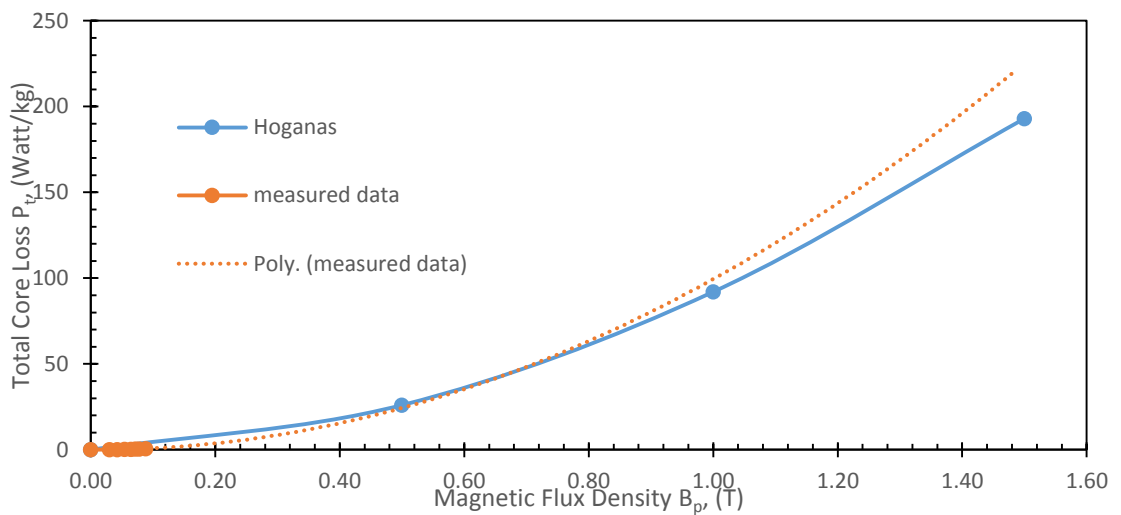
(a)



(b)



(c)



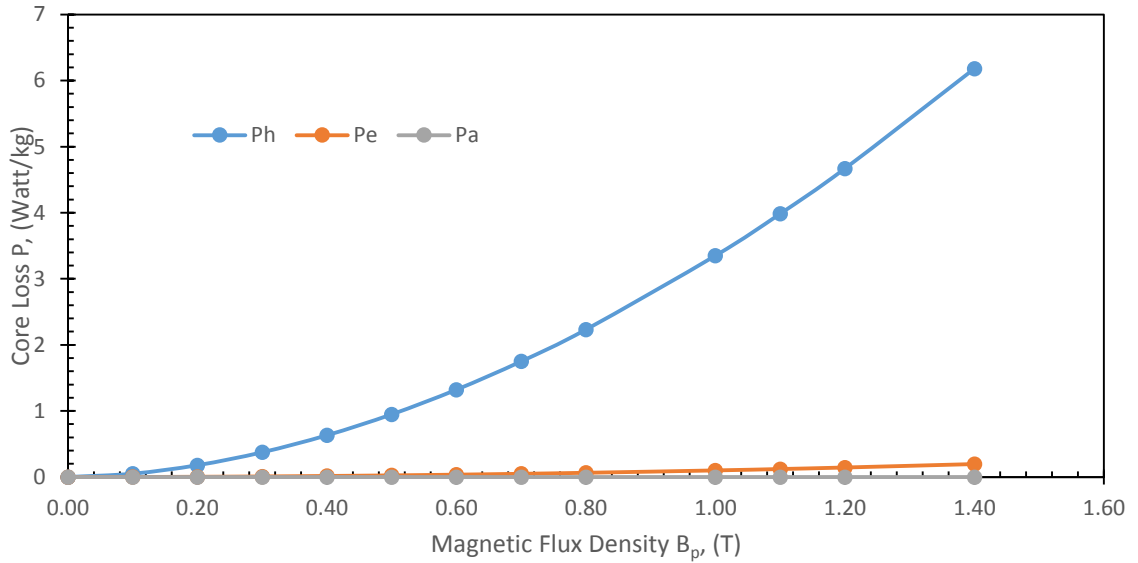
(d)

Fig. 4.9 The core loss curve of measured data and manufacturing data from Hogan at (a) 50 Hz (b) 100 Hz, (c) 500 Hz and (d) 1000 Hz

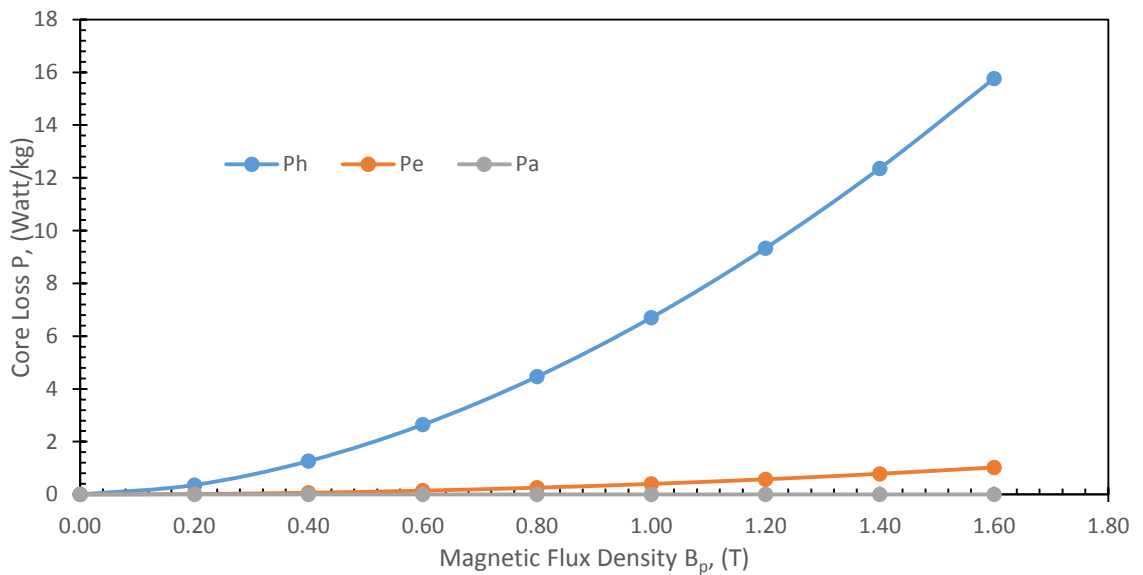
Based on the plotted core loss curves at all frequencies above, the theoretical calculation agrees with the core loss measurement by using 3-D tester. Nevertheless, the limitation of 3-D tester in measuring the core loss at high frequency forces the researcher to extrapolate the experimental data in order to be compared with the data given by Hogan.

4.4 Core loss separation

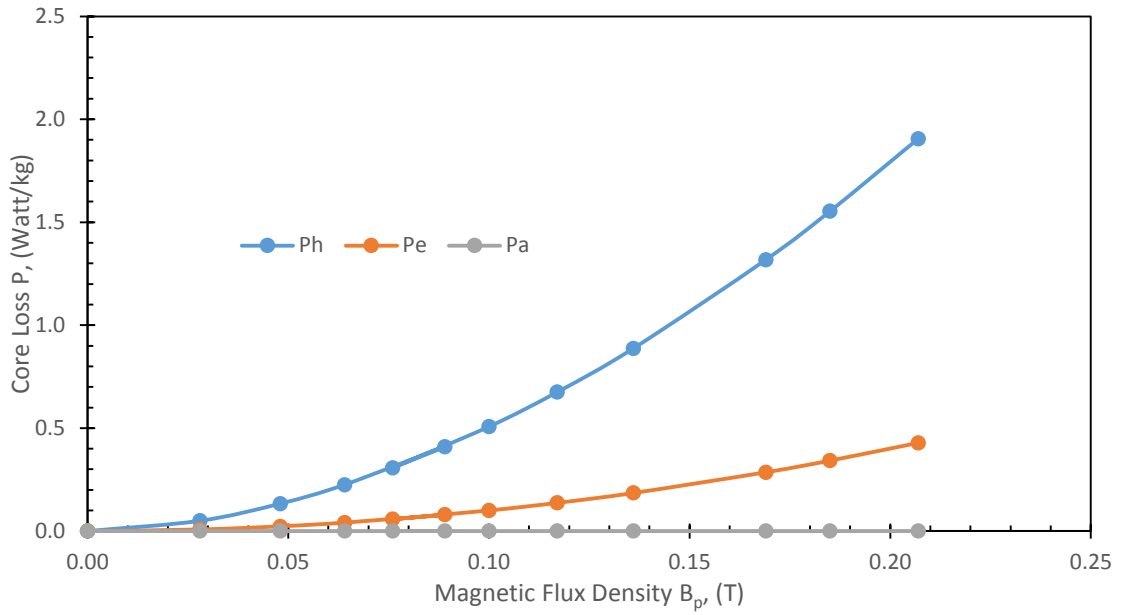
By knowing the loss coefficients C_e , C_α , C_h and n , each component of core loss can be described as illustrated in Fig. 4.10. Fig. 4.10 (a), (b), (c) and (d) show three components of core loss; hysteresis loss, eddy current loss and anomalous loss at 50 Hz, 100 Hz, 500 Hz and 1000 Hz, respectively.



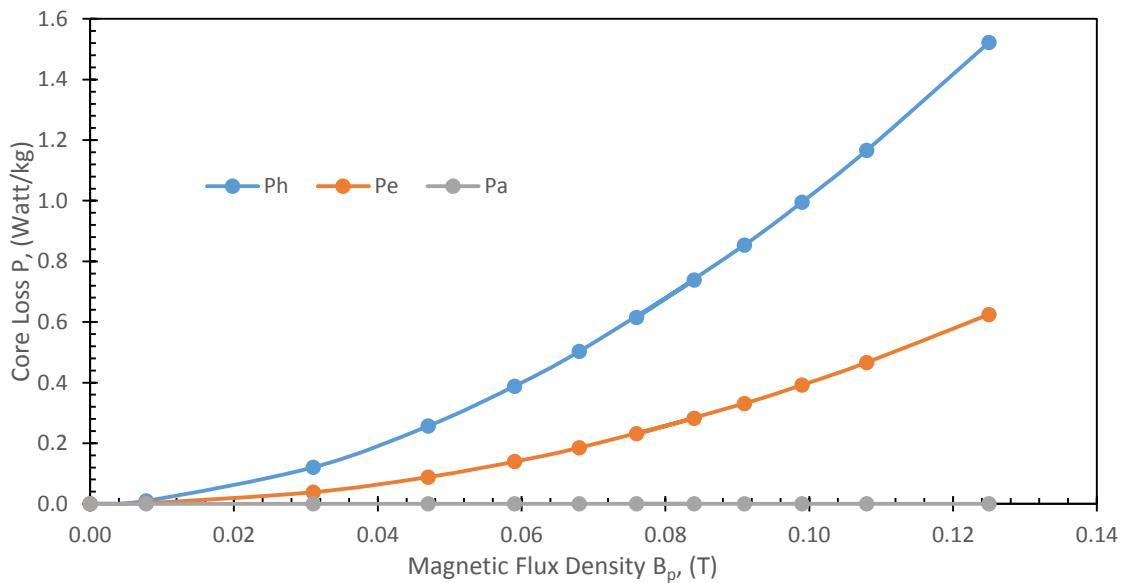
(a)



(b)



(c)



(d)

Fig. 4.10 Core loss components at (a) 50 Hz, (b) 100 Hz, (c) 500 Hz and (d)1000 Hz

By referring to Fig. 4.10, the total core loss is measured at 50 Hz, 100 Hz, 500 Hz and 1000 Hz has been separated into three components of losses which all the components are plotted in the core loss curve. Blue, brown and grey curves are represented hysteresis loss, eddy current loss, and anomalous loss, respectively. As can be seen from the graph, the total core loss is dominated by hysteresis loss and followed by eddy current loss and anomalous loss. In addition, the eddy current loss and anomalous loss

are negligible at low frequencies but the eddy current loss becomes more significant at high frequency.

From Table 4-1, the hysteresis losses at 50 Hz and 100 Hz slowly increased with the magnetic flux density and they are recorded as 6.18 Watt/kg and 12.36 Watt/kg, respectively when the magnetic flux density is 1.4 T. However, at the same magnetic flux density, both eddy current loss and anomalous loss are shown less than 0.20 Watt/kg and 1.02 Watt/kg when the measurement is conducted at 50 Hz and 100 Hz, individually. This explains that the hysteresis loss component dominates the total core loss at both frequencies.

At 500 Hz, the hysteresis loss of SOMALOY 700 (5P) is 1.91 Watt/kg when the magnetic flux density is 0.2 T. Though the hysteresis loss is dominated at this frequency, the eddy current loss seems to be drastically increased when compared to the eddy current loss at the lower frequencies 50 Hz and 100 Hz. At 0.2 T, the eddy current loss rises to 0.43 Watt/kg and the anomalous loss is still assumed to be negligible.

For core loss measurement at 1000 Hz, it clearly described that the hysteresis core loss is still dominated at very high frequency. This loss intensely increased with the magnetic flux density. At 0.13 T, the total hysteresis loss has been dissipated to surrounding is 1.52 Watt/kg. Nevertheless, the eddy current loss and anomalous loss have been recorded as 0.6 Watt/kg and 1.26×10^{-4} Watt/kg, respectively when the measurement is done at the same magnetic flux density.

The hysteresis core loss at all frequencies act as a main contributor in core loss production since this type of loss is considered when there is work done on wiping out the internal friction of magnetic material molecule which is in opposite direction with molecules of the magnetic material. Hence, the hysteresis loss is proportional to the number of magnetisation cycles during the magnetisation process. However, the eddy core loss is negligible at low frequency and started to be significant at high frequency due to high cycles per second.

Table 4-1 The components of alternating core losses at 50 Hz, 100 Hz, 500 Hz and 1000 Hz

f (Hz)	B_p (T)	P_h (Watt/kg)	P_e (Watt/kg)	P_a (Watt/kg)
50 Hz	0.1	0.0507	0.001	1.01E-06
	0.2	0.179	0.004	2.85E-06
	0.3	0.3745	0.009	5.23E-06
	0.4	0.6321	0.016	8.05E-06
	0.5	0.9488	0.025	1.13E-05
	0.6	1.3221	0.036	1.48E-05
	0.7	1.7503	0.049	1.86E-05
	0.8	2.2319	0.064	2.28E-05
	1	3.35	0.1	3.18E-05
	1.1	3.9846	0.121	3.67E-05
	1.2	4.6683	0.144	4.18E-05
	1.4	6.1801	0.196	5.27E-05
100 Hz	0.2	0.3581	0.016	8.05E-06
	0.4	1.2642	0.064	2.28E-05
	0.6	2.6443	0.144	4.18E-05
	0.8	4.4637	0.256	6.44E-05
	1	6.7	0.4	9.00E-05
	1.2	9.3365	0.576	1.18E-04
	1.4	12.3603	0.784	1.49E-04
	1.6	15.7606	1.024	1.82E-04
500 Hz	0.03	0.05	0.0078	4.71E-06
	0.05	0.1333	0.023	1.06E-05
	0.06	0.2251	0.041	1.63E-05
	0.08	0.3077	0.0578	2.11E-05
	0.1	0.507	0.1	3.18E-05
	0.12	0.6748	0.1369	4.03E-05
	0.14	0.8873	0.185	5.05E-05
	0.17	1.3176	0.2856	6.99E-05
	0.19	1.5535	0.3423	8.01E-05
	0.21	1.9059	0.4285	9.48E-05
1000 Hz	0.01	0.0098	0.0024	1.96E-06
	0.03	0.1203	0.0384	1.55E-05
	0.05	0.2566	0.0884	2.90E-05
	0.07	0.5026	0.185	5.05E-05
	0.08	0.6154	0.231	5.96E-05
	0.09	0.8541	0.3312	7.81E-05
	0.1	0.9957	0.392	8.87E-05
	0.11	1.1666	0.4666	1.01E-04
	0.13	1.5221	0.625	1.26E-04

4.5 Conclusion

The 3-D tester has measured the magnetic properties of the SOMALOY 700 (5P) material under alternating magnetic flux density at certain range of frequency. The characteristic of the SOMALOY 700 (5P) is compared to the SOMALOY 500, the magnetic material, which has been studied for over 15 years. Due to the new features that have been offered by the SOMALOY 700 (5P), the core loss dissipation is much lower. The magnetic properties have been further discussed by conducting core loss measurement at 50 Hz, 100 Hz, 500 Hz and 1000 Hz of operating frequency. The higher frequency will increase the vibration of the magnetic material during the magnetisation process which will cause extra heat dissipation. The current is flown in forward and reverse directions to complete the hysteresis cycle within the magnetic core which will increase the core loss of the material. The hysteresis loss is calculated to be main contributor of the core loss production followed by eddy current loss and anomalous loss when experimental works are conducted at 50 Hz, 100 Hz, 500 Hz and 1000 Hz. The poor condition of the 3-D tester caused the saturation magnetisation not be able to be reached at high frequency, 500 Hz and 1000 Hz. The tester became hot and vibrated when high AC current was provided. However, the magnetic properties of SOMALOY still can be measured by this tester. The core loss dissipation is also can be explained then will provide the details and information to the researchers and engineers for future simulation and designs.

References

- [4.1] Y. Li, Q. Yang, J. Zhu, and Y. Guo, "Magnetic Properties Measurement of Soft Magnetic Composite Materials Over Wide Range of Excitation Frequency," *IEEE Transactions on Industrial Applications*, vol. 48, no. 1, pp. 88-97, 2012.
- [4.2] Y. Li, J. Zhu, Q. Yang, Z. W. Lin, Y. Guo, and C. Zhang, "Study on Rotational Hysteresis and Core Loss Under Three-Dimensional Magnetization," *IEEE Transactions on Magnetics*, vol. 47, no. 10, pp. 3520-3523, 2011.
- [4.3] Y. Li, Z. Lin, H. Liu, Y. Wang, Y. Guo, J. Zhu, Q. Yang, "Three-Dimensional Magnetic Properties of Soft Magnetic Composite Material at Different Frequencies", *Journal of Applied Physics*, vol. 109, no. 7, 07B503, 2011.
- [4.4] Electronics Tutorials. Magnetic Hysteresis, [Online]. Available: <http://www.electronic-tutorials.ws/electromagnetism/magnetic-hysteresis.html>. [Accessed 2 April 2014].
- [4.5] Y. J. Li, J. G. Zhu, Q. X. Yang, J. F. Sun, Y. Wang, and W. Xu. "Analysis of the 3-D Magnetic Reluctivity Tensor Based on Magnetic Properties Measurement of SMC Materials," *International Conference on Electrical Machines and Systems*. pp. 1767-1772. 2010.
- [4.6] Y. J. Li, Q. X. Yang, J. G. Zhu, Z. W. Lin, Y.G. Guo, and J. T. Sun, "Research of Three-Dimensional Magnetic Reluctivity Tensor Based on Measurement of Magnetic Properties," *IEEE Transactions on Applied Superconductivity*, vol. 20, no. 10, pp. 1932-1935, June 2010.
- [4.7] University of Southampton. The Hysteresis Loop, [Online]. Available: <http://www.southampton.ac.uk/~rpb/thesis/node36.html>. [Accessed 2 April 2014].
- [4.8] Somaloy ® 700HR 5P. Hogan AB (publ.), February 2016.
- [4.9] Y. Guo and J. Zhu, "Application of Soft Magnetic Composite Materials in Electrical Machines," *Australian Journal of Electrical and Electronics Engineering*, vol. 3, no.1, pp. 37-46, 2006.
- [4.10] Y. Li, J. Zhu, Q. Yang, Z. W. Lin, Y. Guo, and Y. Wang, "Measurement of Soft Magnetic Composite Material Using an Improved 3-D Tester with Flexible

Excitation Coils and Novel Sensing Coils," *IEEE Transactions on Magnetics*, vol. 46, no. 6, pp. 1971–1974, 2010.

Chapter 5 : CORE LOSS MEASUREMENT UNDER CIRCULAR LOCI OF MAGNETIC FLUX DENSITY

5.1 Introduction

The study of rotating core loss gives big significance to the rotating electrical machines since in real situation, the magnetic flux densities in the electrical machines are rotated during the operation. Thus, the magnetic core loss under rotating magnetic field excitation is required to be examined before being applied in designing and performing simulation of the electrical machines.

It is very important to have good understanding of core loss in electrical machine. By identifying the actual core loss, the operating cost can be reduced after the determination of electrical machine efficiency. The heating of the machines also can be evaluated and the power output is able to be determined without excessive degradation of the insulation.

The flux densities are rotated in arbitrary shapes such as in circular and ellipse to resemble the actual core loss of rotating electrical machines. The presence of rotating magnetic flux density makes the magnetic domain rotated and the wall of domain started to move from the original position. Hence, it will increase the total core loss of the magnetic material due to the additional of eddy current loss which is affected by that domain wall motion.

In order to produce the circular shape of magnetic flux density, two sinusoidal waves of magnetic flux density are controlled to be in the same magnitude with 90° of phase angle. It will be resulting the circular B loci along a plane of 2 axes such as XOY, YOZ and ZOX.

In this chapter, core loss under rotating magnetic flux density is predicted and it can be realized by producing magnetic flux density to be circular as described in section 5.2. The core loss curves at some frequencies are explained in this section too.

Section 5.3 explains the experimental results of core loss measurement under rotating magnetic flux density in the XOY-plane after being controlled to be circular by adjusting the magnitudes and angles between B_x and B_y waveforms. Rotating core losses are examined by measuring them in clockwise and anti-clockwise direction. Each component of core loss is determined by considering curve fitting method.

5.2 Principle and production of rotating magnetic flux density

The basic key in alternating current (AC) motor operation is the rotating magnetic flux density which can be defined as a magnetic flux density that has constant angular rate which contain moving polarities and their opposite poles are rotating about a central axis. In AC machines, synchronous and induction motors are relying on this type of magnetic flux density in the stators part that makes the rotors to be turned [5.1].

Ideally, the magnetic flux density in the stator can be electrically rotated and it will be attracted or repelled by another magnetic flux density in rotor. Due to this concept, the rotating magnetic field is trying to be generated in this study as to obtain the accurate reading of core loss which is experienced by the stator and rotor parts during their operation [5.1]. Arbitrarily, the magnitude and direction of magnetic flux densities are circularly controlled and the plotted B loci are expressed in the XOY-, YOZ- or ZOX-plane.

To produce round magnetic flux density to be lied in the XOY-plane, the magnitudes of B_x and B_y should be in the same value with one of them is leading by 90° at certain desired frequencies. DAQ devices from National Instrumentation (NI) are used as an interface to generate and control the magnetic flux density waveforms by using LabVIEW software.

In details, the magnitude and phase angle between B_x and B_y are controlled in front panel of LabVIEW which is able to produce AC voltage waveforms in the x and y directions. Then, the waveforms are being amplified by using power amplifier (model: AM3002) which can amplify 63.5 times or 36 dB before generating the magnetic flux density by the existence of excitation winding coil in the 3-D tester [5.2].

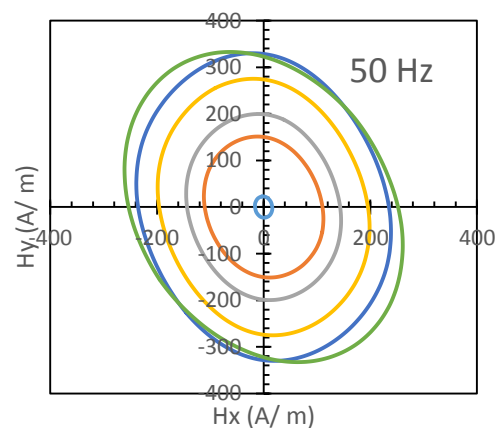
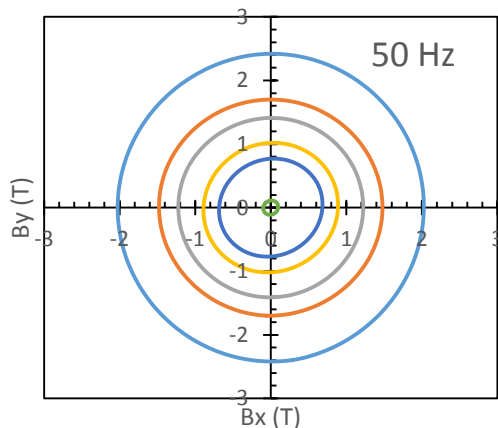
5.3 Experimental results

2-D measurement of SOMALOY 700 (5P) core losses is conducted by producing 2-D vector flux excitation on XOY-plane. In this chapter, the SOMALOY 700 (5P) cubic sample is magnetised at 50 Hz and up to 1000 Hz. The loci of B and H are plotted and core loss curves in clockwise and anti-clockwise are illustrated before is being averaged. Then, the average of rotating core loss is compared to the alternating core loss.

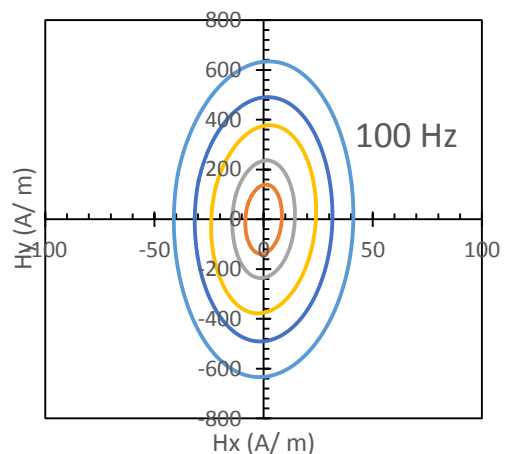
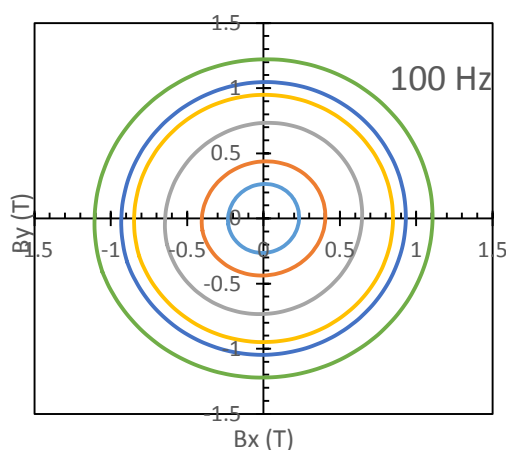
5.3.1 B-H loops of rotating core loss

The series magnetic properties of the SOMALOY 700 (5P) material are measured from low to high frequencies. All the recorded B loci and corresponding H loci are shown in Fig. 5.1, where Fig. 5.1 (a), (b), (c) and (d) show the B loci and the corresponding H loci under rotating magnetic flux densities at 50 Hz, 100 Hz, 500 Hz and 1000 Hz, respectively. The excitation of circular magnetic flux density is controlled to be increased up to 2.42 T and 1.22 T at 50 Hz and 100 Hz, respectively along the XOY-plane. Due to high vibration and high heat generation at high frequency, the magnetic flux excitation is only can be circularly controlled up to 0.37 T for 500 Hz and 0.09 T for 1000 Hz.

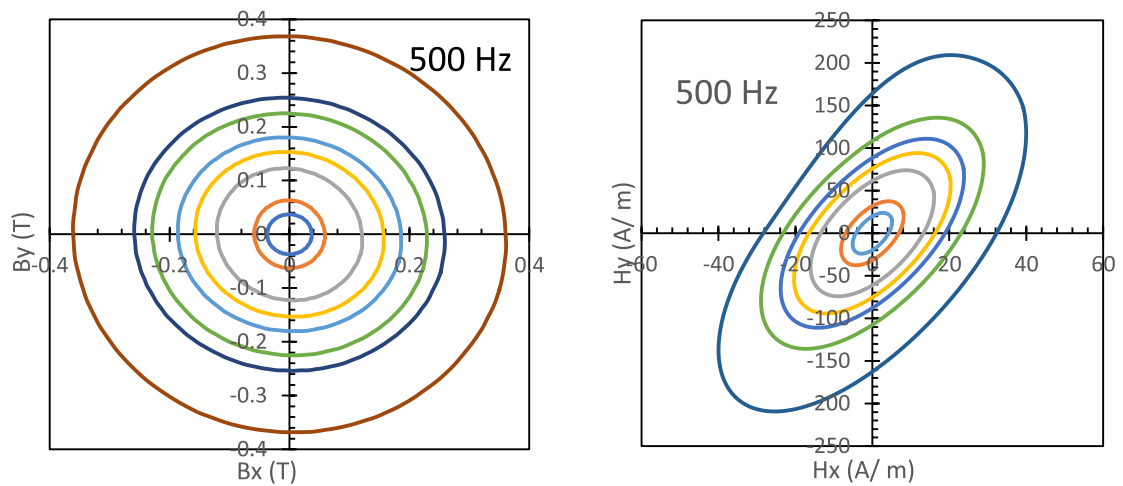
The figures explain that both B and H loci lie in the same magnetisation plane. However, the H loci are started with elliptical shape and become distorted in the end of the measurement. It is caused by the movement of rotating domain during the magnetisation which will portray the anisotropy property when there is involvement of high magnetic field in different direction [5.3], [5.4].



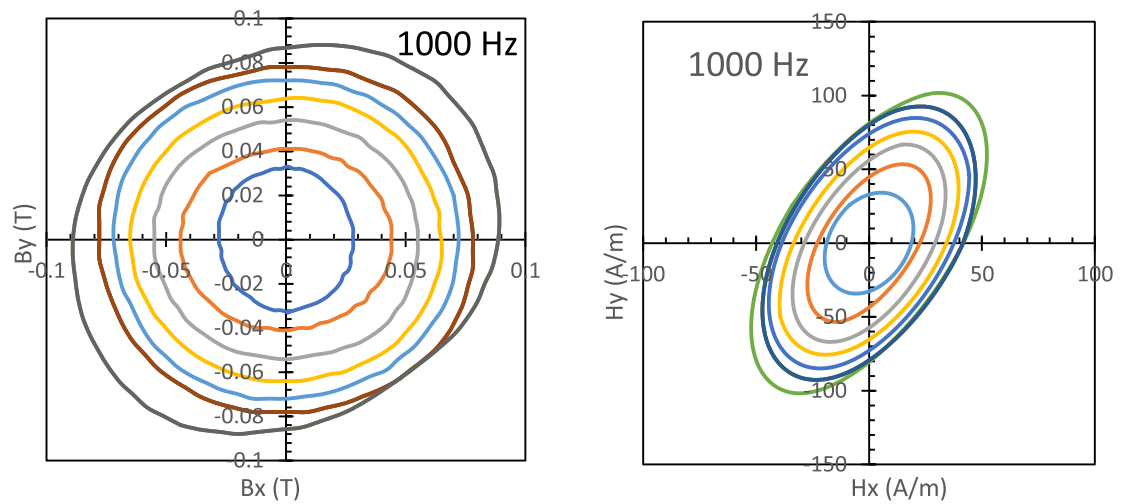
(a)



(b)



(c)



(d)

Fig. 5.1 Round B loci and corresponding H loci in the XOY-plane at (a) 50 Hz (b) 100 Hz (c) 500 Hz and (d) 1000 Hz

At 1000 Hz of magnetisation, it shows that the shape of circular B loci is quite shaky due to coupling between core poles which leads to the noise production. However, this does not contribute to the production of core losses [5.5].

5.3.2 Core loss of rotating magnetic flux density

The rotating core loss is contributed by two magnetic flux density from different axes, x and y. The measurements are started by repeating them for three times in order to ensure the collected data is accurate. Fig. 5.2 describes the data selection after three

times of measurements. From the figure, it can be shown that the first reading is considered because of the resemblance to the averaged data.

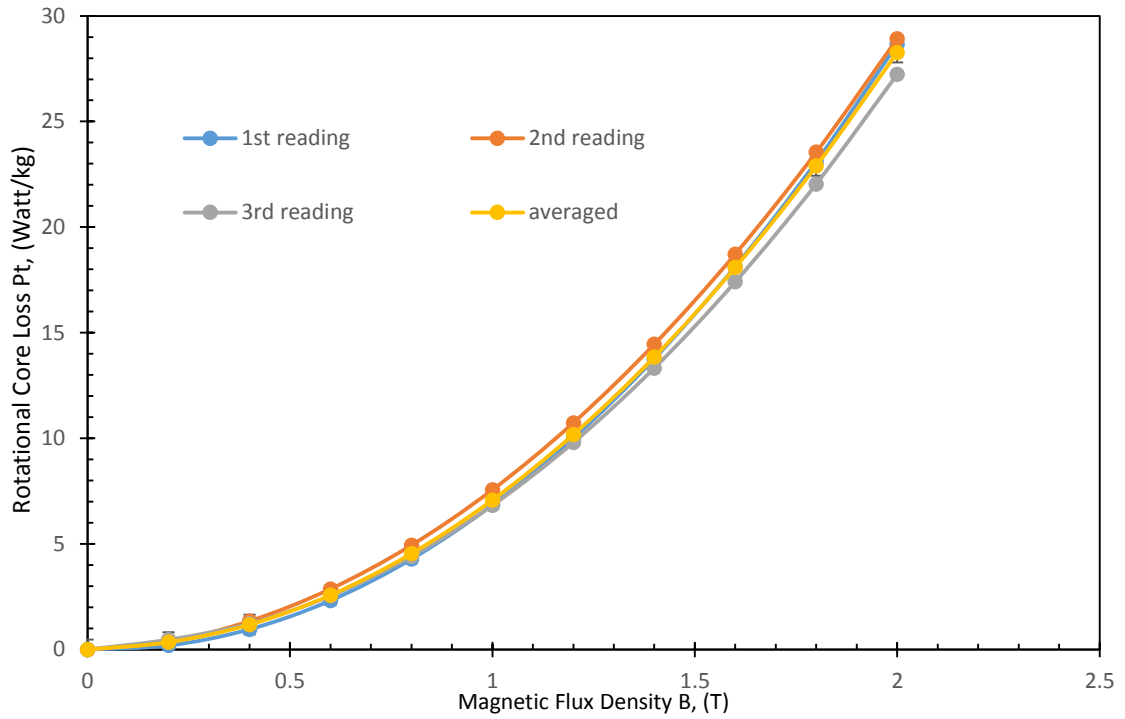
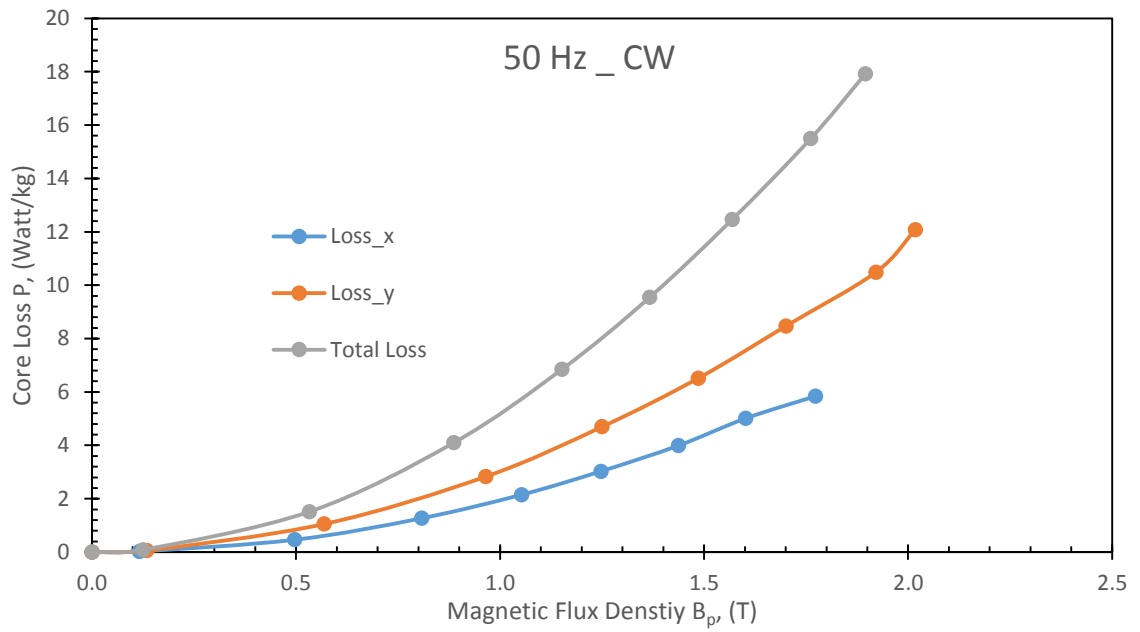
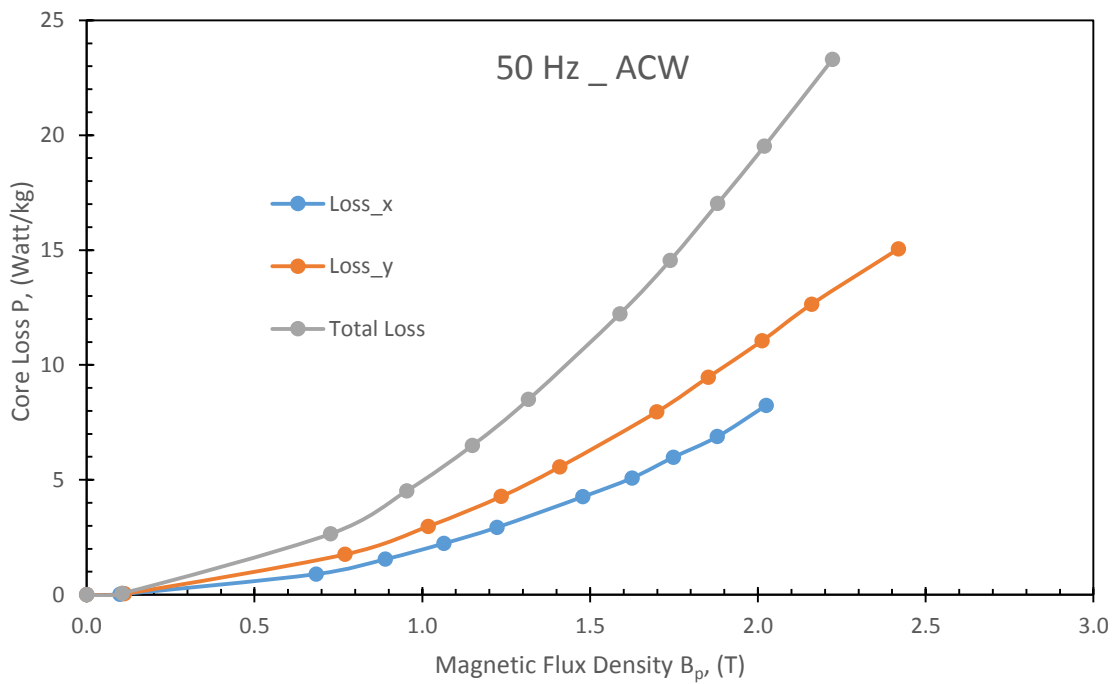


Fig. 5.2 Three times of rotational core loss measurements with 0.474 of standard deviation

Fig. 5.3 (a) and (b) explain the individual core loss in x- and y-axes in clockwise and anti-clockwise directions. The summation of these components will produce the actual rotating core loss of the material.



(a)



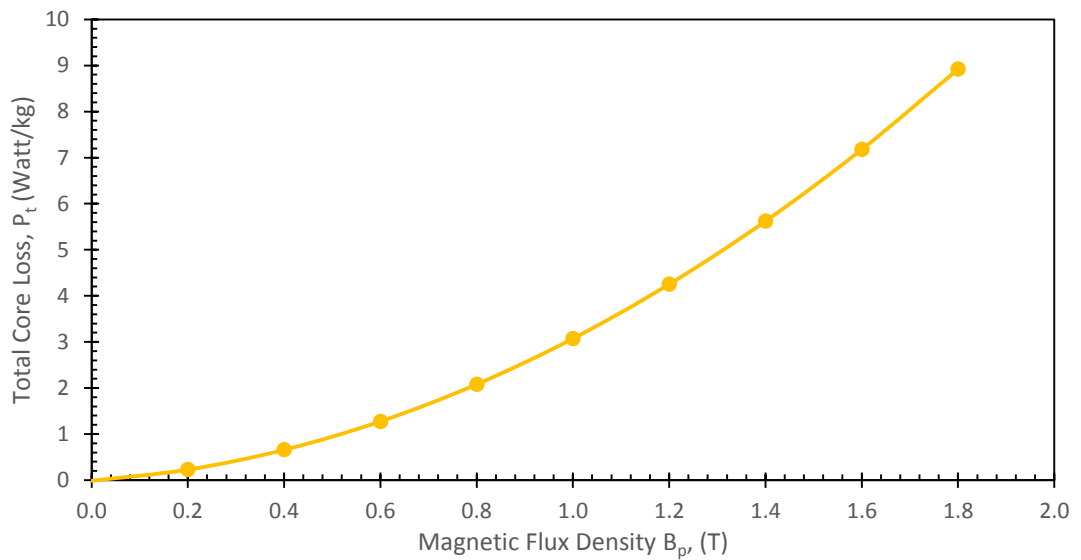
(b)

Fig. 5.3 The individual core losses and total core loss at 50 Hz in (a) clockwise and (b) anti-clockwise directions

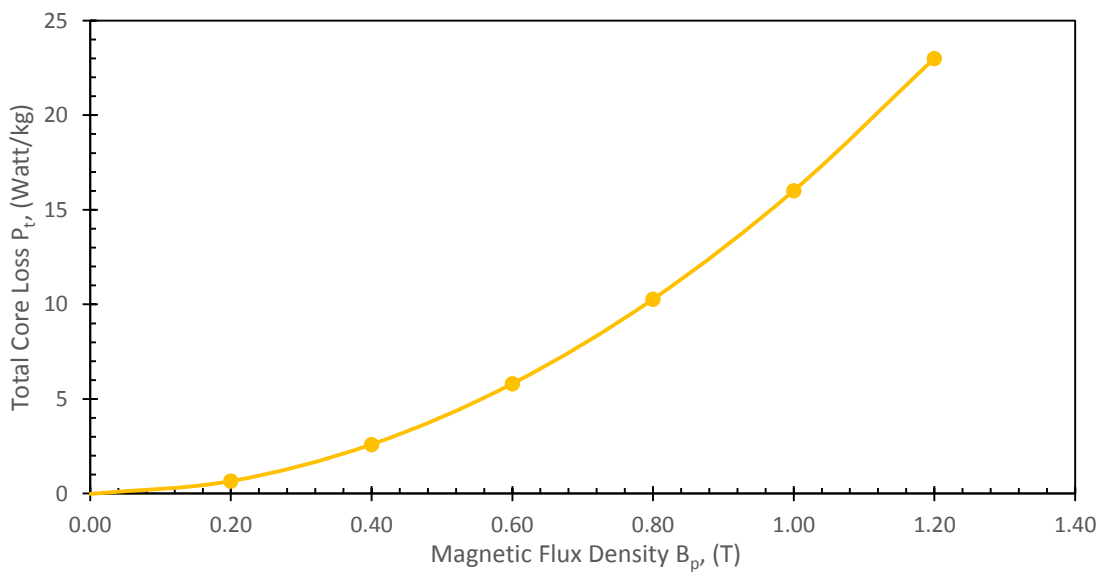
Fig. 5.4 (a), (b), (c) and (d) describe the total core loss of 2-D measurement for SOMALOY 700 (5P) material at 50 Hz, 100 Hz, 500 Hz and 1000 Hz, respectively. It is total summation of individual core loss from x and y magnetic flux density excitations.

These figures obviously show the total core loss is proportional to the squared of magnetic flux density. The changes of the magnetic domain during the sample magnetisation will make the domain wall to be moved. Thus, in the presence of high magnetic flux excitation, the possibility of domain walls to be snagged to crystal structure of material is high and this situation contributes to the high core loss.

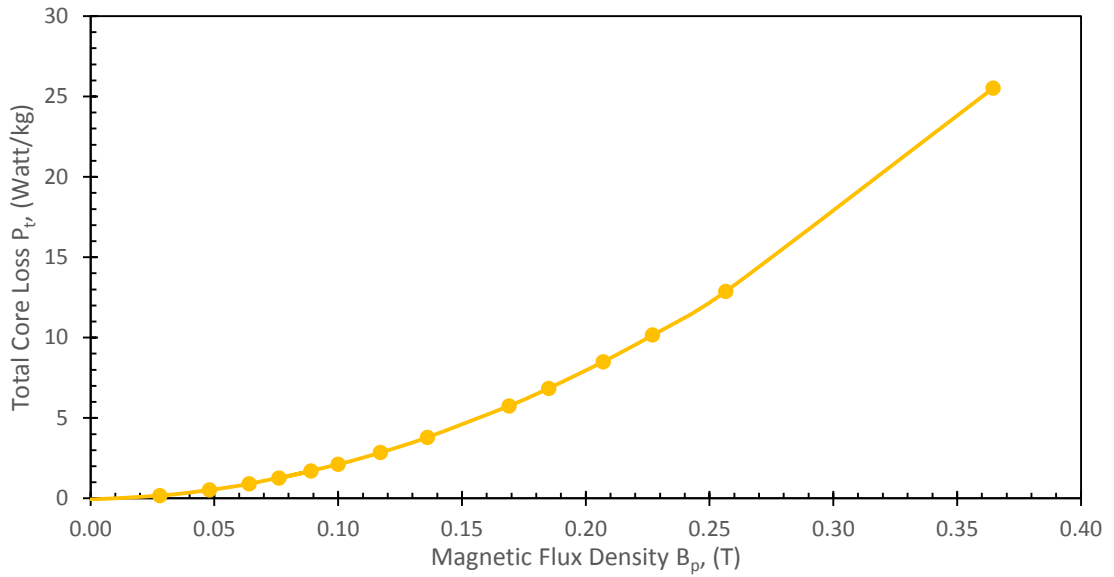
At 1.8 T of magnetic flux density, the recorded total core loss at 50 Hz is about 8.92 Watt/kg whereas at 1.2 T, the rotating core loss is 23.01 Watt/kg when the measurement is conducted at 100 Hz. However, the rotating core loss at 500 Hz and 1000 Hz is 25.51 Watt/kg and 2.14 Watt/kg when B is at 0.36 T and 0.085 T, respectively.



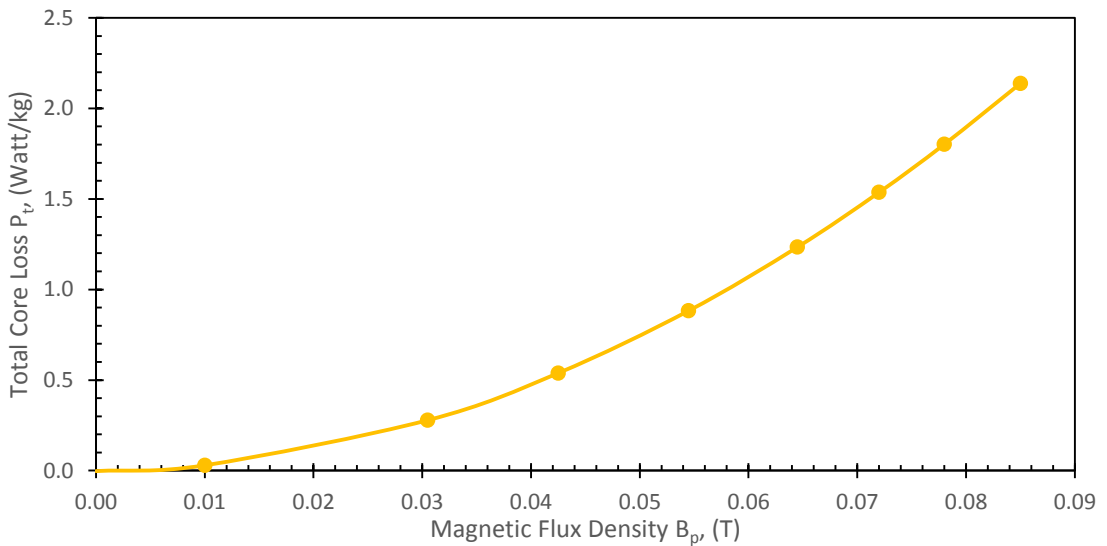
(a)



(b)



(c)



(d)

Fig. 5.4 Loss curve of SOMALOY 700 (5P) material in the XOY-plane when flux densities are controlled to in round shape at (a) 50 Hz (b) 100 Hz, (c) 500 Hz and (d) 1000 Hz

By referring all plotted curves in Fig. 5.5, it shows that the core loss steadily increased with the magnetic flux density and frequency. This is caused by the magnetic material vibrations at high magnetic flux density and frequency lead to the extra heat dissipation upon core loss measurement. Other than magnetic core loss, there are another effects that can be contributed in high frequency of magnetisation such as thermal effects on hysteresis, skin effects in winding coils and cores, and the effect of leakage inductance and stray capacitance [5.6], [5.7].

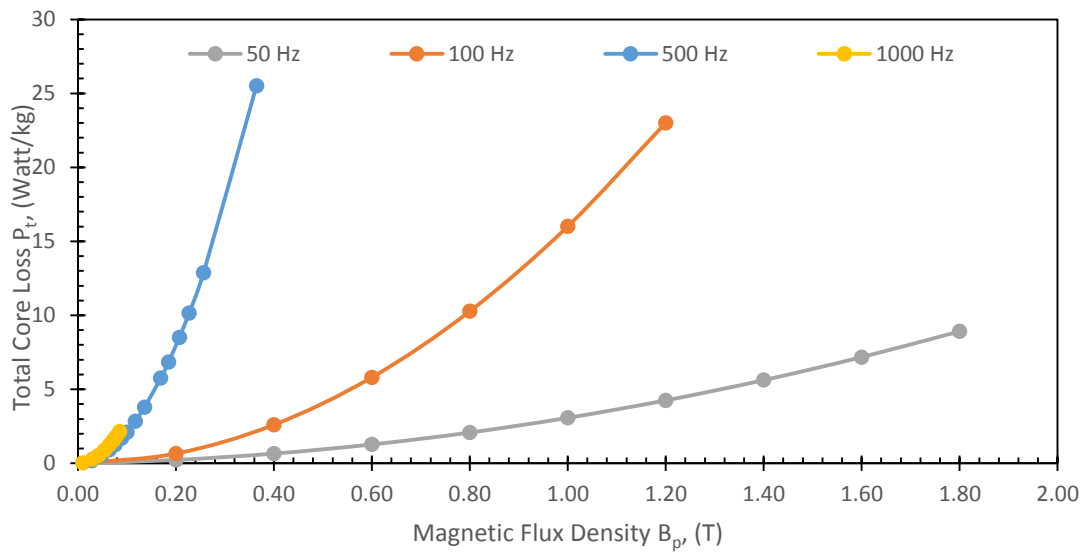
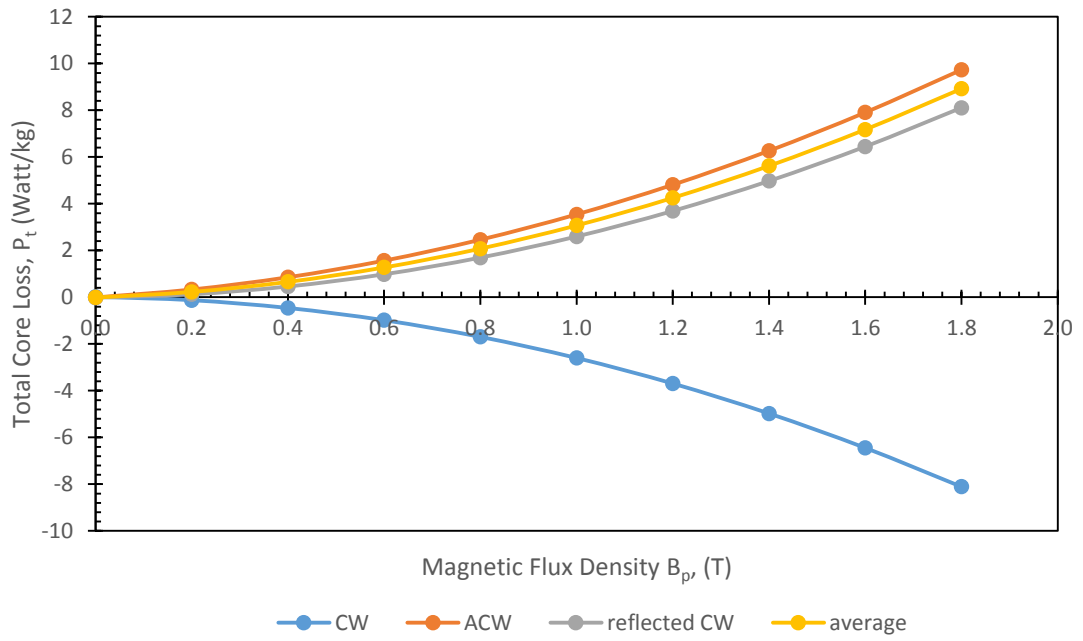


Fig. 5.5 The rotating core losses at low to high frequencies

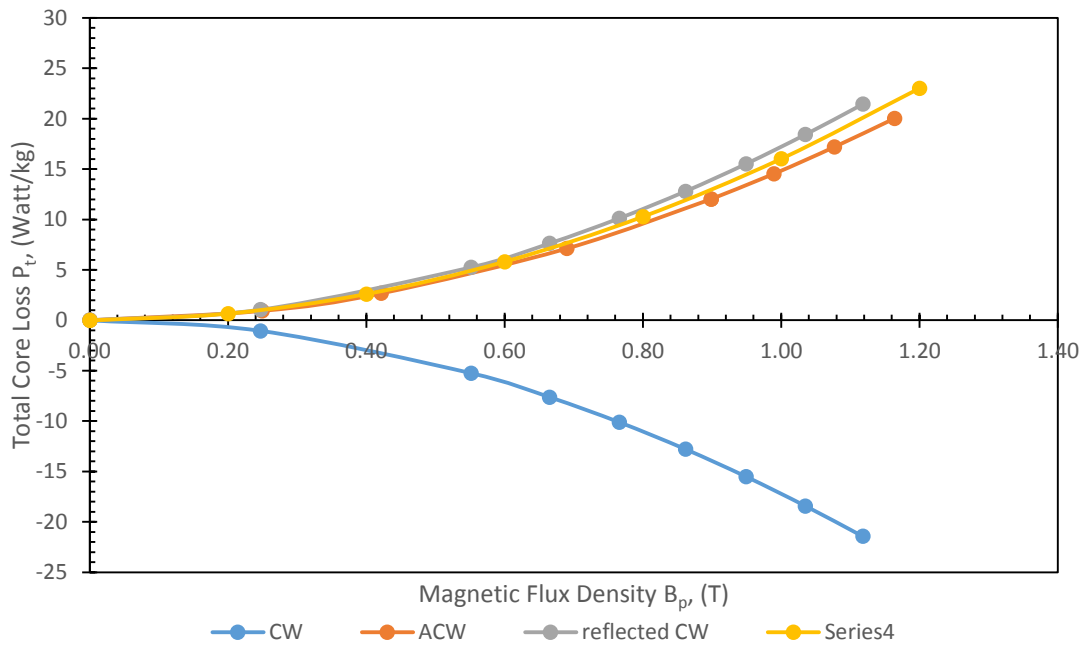
5.3.3 Clockwise and anti-clockwise 2-D measurements

2-D measurements of SOMALOY 700 (5P) are conducted in clockwise and anti-clockwise directions at 50 Hz, 100 Hz, 500 Hz and 1000 Hz of operating frequencies. Fig. 5.6 (a), (b), (c) and (d) are the set of plotted graphs that explain the total core loss of each frequency in clockwise, anti-clockwise directions and the reflected of clockwise core loss at 50 Hz, 100 Hz, 500 Hz and 1000 Hz, respectively. There are four different colours of curve line that describe modes of rotation during the magnetisation process. The blue line represents the clockwise rotation and the brown line represent the magnetic flux rotation in anti-clockwise direction, the grey line is the reflected curves of clockwise rotation and the yellow line represents the average of rotating core loss.

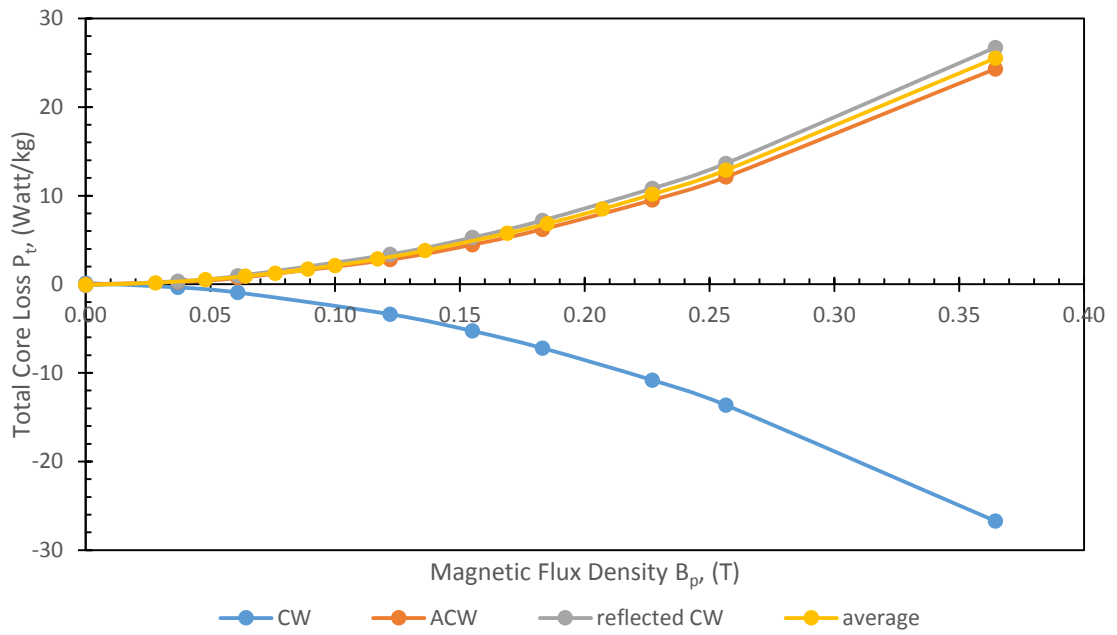
It can be seen that, there is a mirror-image which describes the total core loss for both directions; clockwise and anti-clockwise has same magnitude that has been reflected on the x-axis due to opposite pole of magnetic flux density during the magnetisation process. This proved that the core loss production for both directions is the same and can be determined by averaging the core losses of both directions.



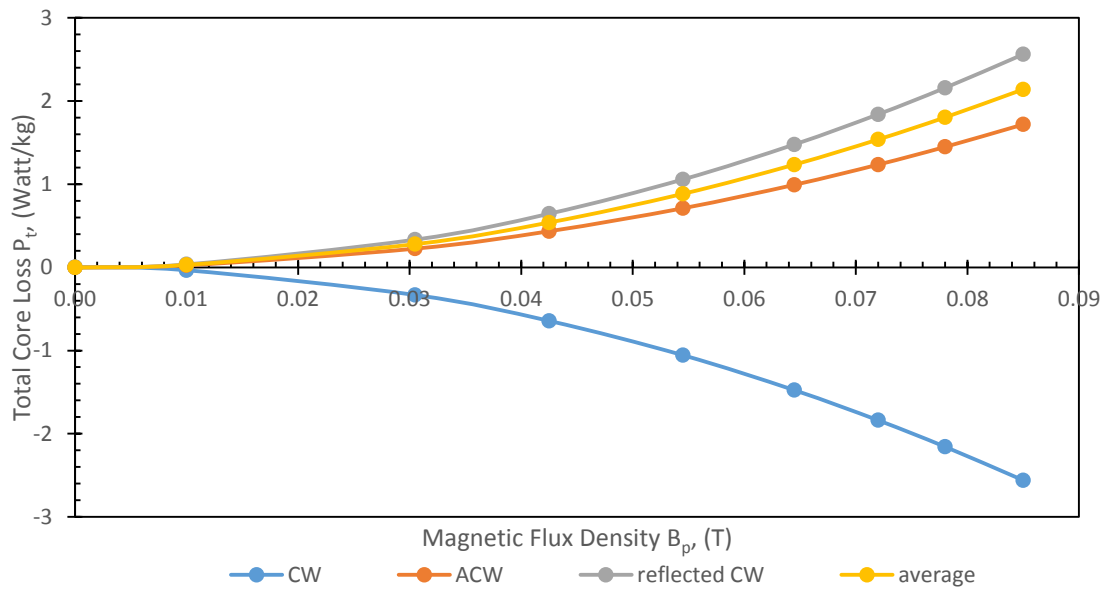
(a)



(b)



(c)



(d)

Fig. 5.6 The loss curve of SOMALOY 700 (5P) material in clockwise and anti-clockwise 2-D measurements at (a) 50 Hz (b) 100 Hz (c) 500 Hz and (d) 1000 Hz

5.3.4 Core loss under alternating and rotating magnetic flux densities

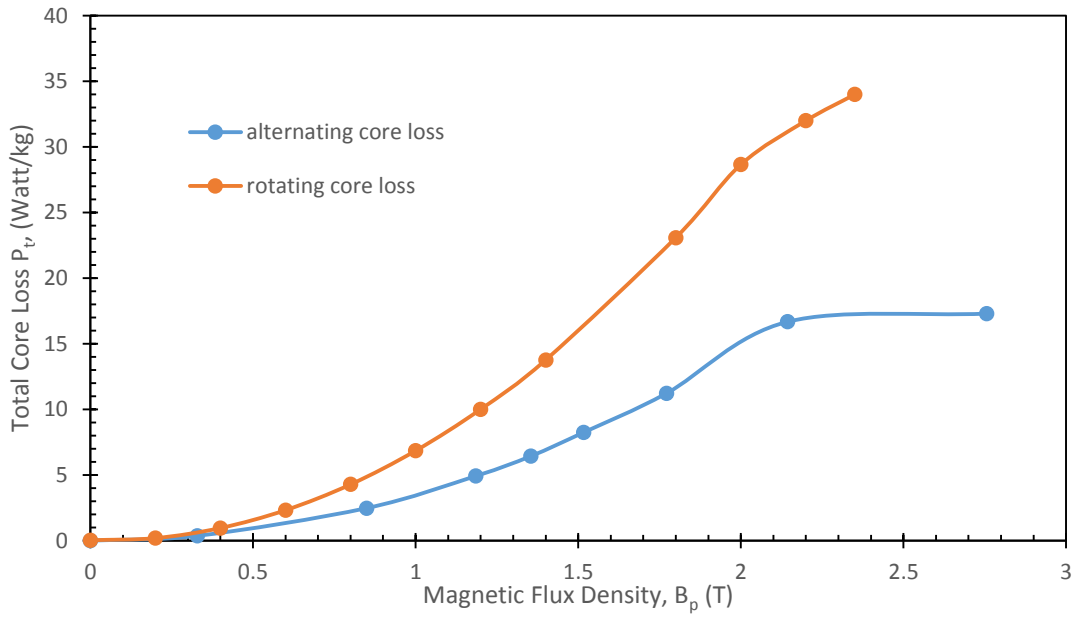
The magnetic flux densities are controlled to be in circular shape along XOY-plane during the 2-D measurement. This is resemblance of rotating electrical machine which is operated in the presence of rotating magnetic flux density. Due to that, the core loss under rotating magnetic flux density is important to be studied in order to predict the total core loss of the magnetic material which will be used in designing the real electrical machines in the future.

In this section, the production of rotating core loss is compared to the alternating core loss which is described in previous chapter. Both types of core losses are plotted in the same graph to estimate the ratio between them.

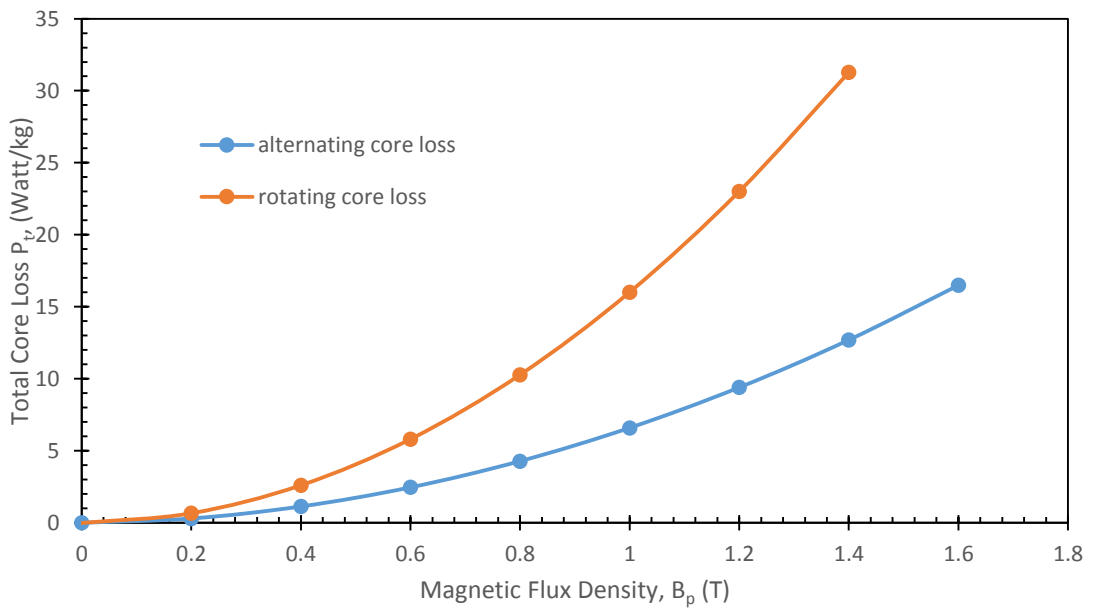
Fig. 5.7 (a), (b), (c) and (d) illustrate the core losses of SOMALOY 700 (5P) under alternating and rotating magnetic flux density at 50 Hz, 100 Hz, 500 Hz and 1000 Hz, respectively. The alternating core loss is measured in the presence of sinusoidal B and the rotating core loss is measured by considering circular B vector with different magnitude of magnetic flux densities.

The figures below explain that the ratio of rotating core loss to alternating core loss at 50 Hz, 100 Hz, 500 Hz and 1000 Hz are approximately 2. These show the strong agreement with a conclusion by other researchers that the rotational core loss of SMC is larger than alternating core loss due to the extra heat dissipation upon the magnetisation process [5.8]. In 2006, Guo *et al.* stated that the rotational core loss is nearly twice compared to the alternating core loss with the same peak value at the mid-range of magnetic flux density as showed in Fig. 5.7 [5.9].

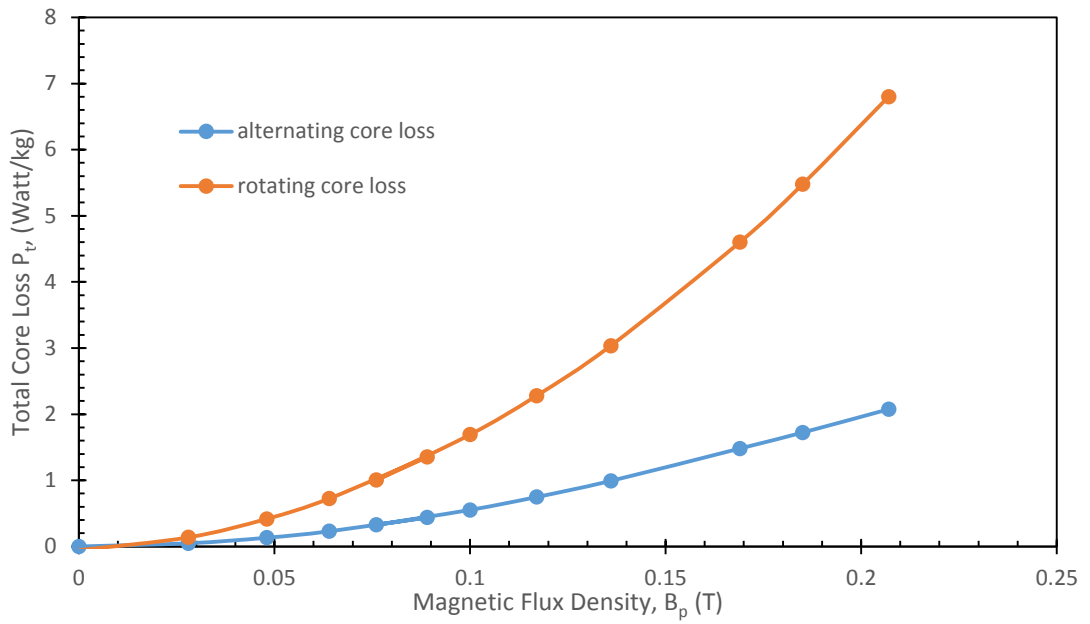
Based on the core loss measurement at 50 Hz in Fig. 5.7 (a), the core losses slowly decreased when approaching 2.4 T for both types of core losses due to the saturation condition of SOMALOY 700 (5P) material.



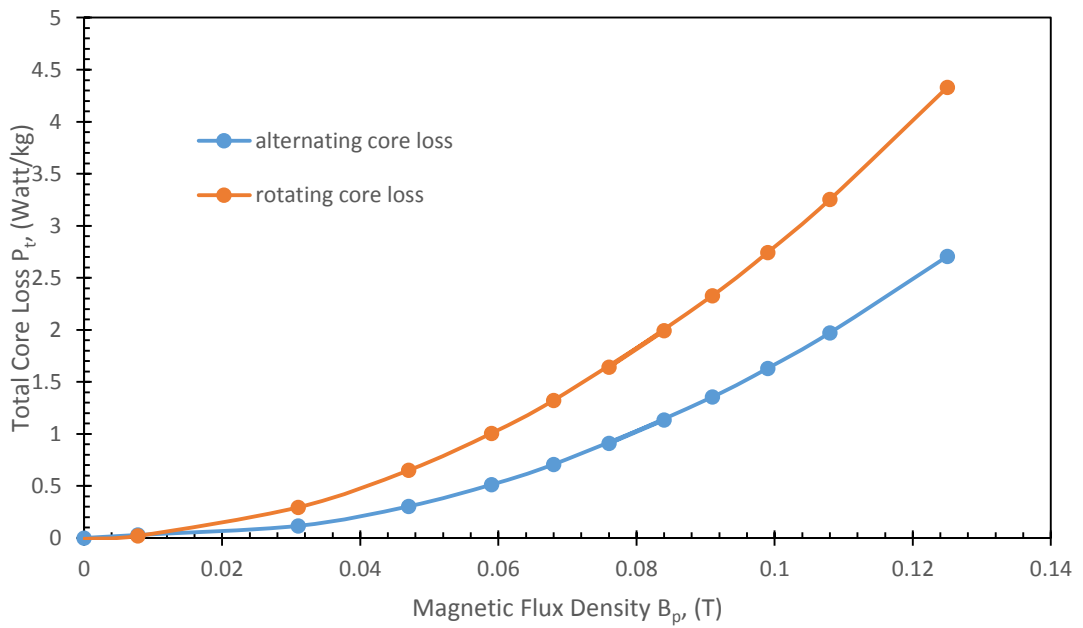
(a)



(b)



(c)



(d)

Fig. 5.7 The alternating core loss and rotational core loss of SOMALOY 700 (5P) at (a) 50 Hz, (b) 100 Hz, (c) 500 Hz and (d) 1000 Hz

Based on previous chapter, SOMALOY 700 (5P) material shows lower alternating core loss as compared to SOMALOY 500 material. However, the alternating core loss of SOMALOY 500 is halved from the rotational core loss of same material. Therefore, it can be concluded that the rotational core loss of SOMALOY 700 (5P) is also lower than the rotational core loss of SOMALOY 500 material.

5.4 Core loss separation

In a soft magnetic material, total core loss P_t can be divided into three components. There are hysteresis loss P_h , eddy current loss P_e , and anomalous loss P_a . All these three can be expressed as follow

$$P_t = P_h + P_e + P_a \quad (5.1)$$

In terms of magnetic flux density and frequency, the equation (5.1) is expanded to be as

$$P_t = C_h f B^n + C_e (fB)^2 + C_a (fB)^{1.5} \quad (5.2)$$

where C_h , C_e , C_a and n are the core loss coefficients which are obtained by fitting the equation (5.2) to the experimental data by using Microsoft Excel. 0.015178, 1.907, 0.000055 and 9×10^{-7} are the core loss coefficients C_h , n , C_e and C_a , respectively.

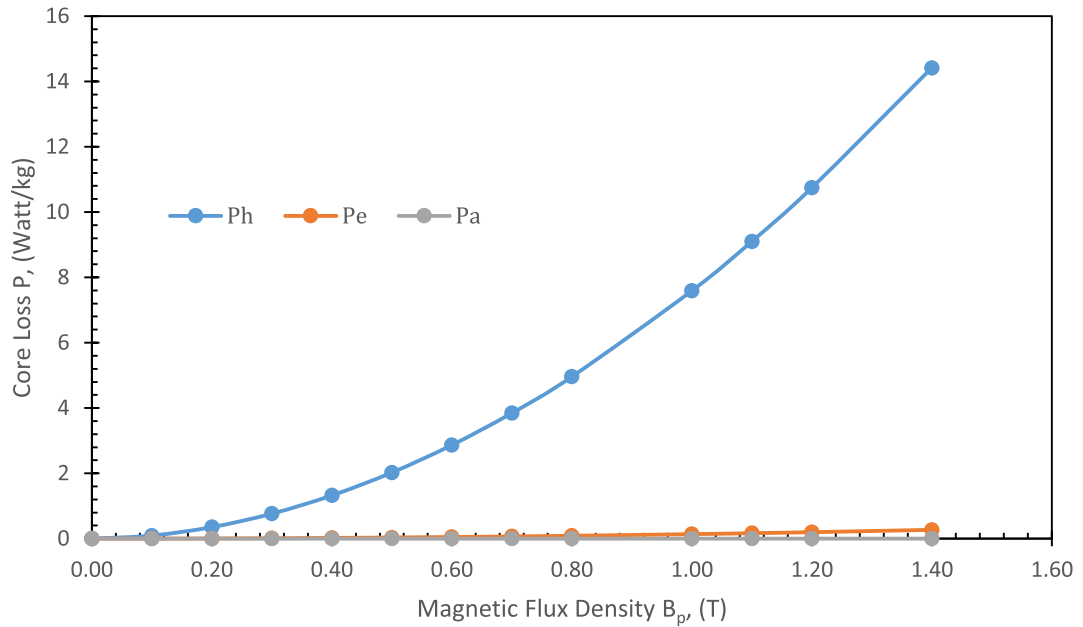
5.4.1 Hysteresis loss, eddy current loss and anomalous loss

Table 5-1 shows three components of core loss at 50 Hz, 100 Hz, 500 Hz and 1000 Hz. At 1.4 T, the hysteresis losses at 50 Hz and 100 Hz are recorded as 14.4 Watt/kg and 28.83 Watt/kg, correspondingly. The measurements at 500 Hz and 1000 Hz when B is 0.1 T contribute to 0.94 Watt/kg and 1.84 Watt/kg of hysteresis losses. By comparing the measurements at 1.4 T and 0.1 T, it explains that hysteresis loss increased with the frequency due to the high vibration in the magnetic material as described in section 5.3.2.

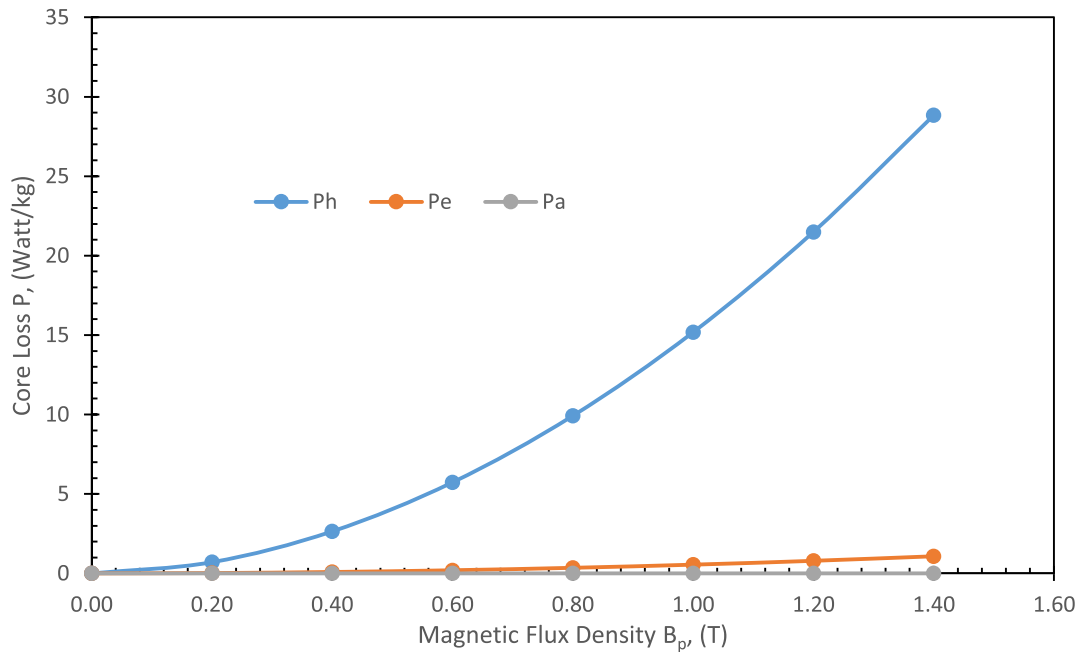
Table 5-1 The components of rotating core losses at 50 Hz, 100 Hz, 500 Hz and 1000 Hz

f (Hz)	B_p (T)	P_h (Watt/kg)	P_e (Watt/kg)	P_a (Watt/kg)
50 Hz	0.1	0.094	0.0014	0.0000
	0.2	0.3526	0.0055	0.0000
	0.3	0.7639	0.0124	0.0001
	0.4	1.3222	0.022	0.0001
	0.5	2.0236	0.0344	0.0001
	0.7	3.844	0.0674	0.0002
	0.8	4.9588	0.088	0.0002
	1	7.589	0.1375	0.0003
	1.1	9.1017	0.1664	0.0004
	1.2	10.7444	0.198	0.0004
	1.4	14.4162	0.2695	0.0005
100 Hz	0.2	0.7051	0.022	0.0001
	0.4	2.6445	0.088	0.0002
	0.6	5.7299	0.198	0.0004
	0.8	9.9176	0.352	0.0006
	1	15.178	0.55	0.0009
	1.2	21.4889	0.792	0.0012
	1.4	28.8324	1.078	0.0015
500 Hz	0.03	0.083	0.0108	0
	0.05	0.2319	0.0317	0.0001
	0.06	0.4014	0.0563	0.0002
	0.08	0.5571	0.0794	0.0002
	0.1	0.9401	0.1375	0.0003
	0.12	1.2683	0.1882	0.0004
	0.14	1.6898	0.2543	0.0005
	0.19	3.0387	0.4706	0.0008
	0.21	3.7648	0.5892	0.0009
1000 Hz	0.01	0.0145	0.0033	0
	0.03	0.2015	0.0529	0.0002
	0.05	0.4456	0.1215	0.0003
	0.06	0.6874	0.1915	0.0004
	0.08	1.1141	0.3177	0.0006
	0.09	1.5707	0.4555	0.0008
	0.1	1.8446	0.5391	0.0009
	0.11	2.1775	0.6415	0.001
	0.13	2.8775	0.8594	0.0013

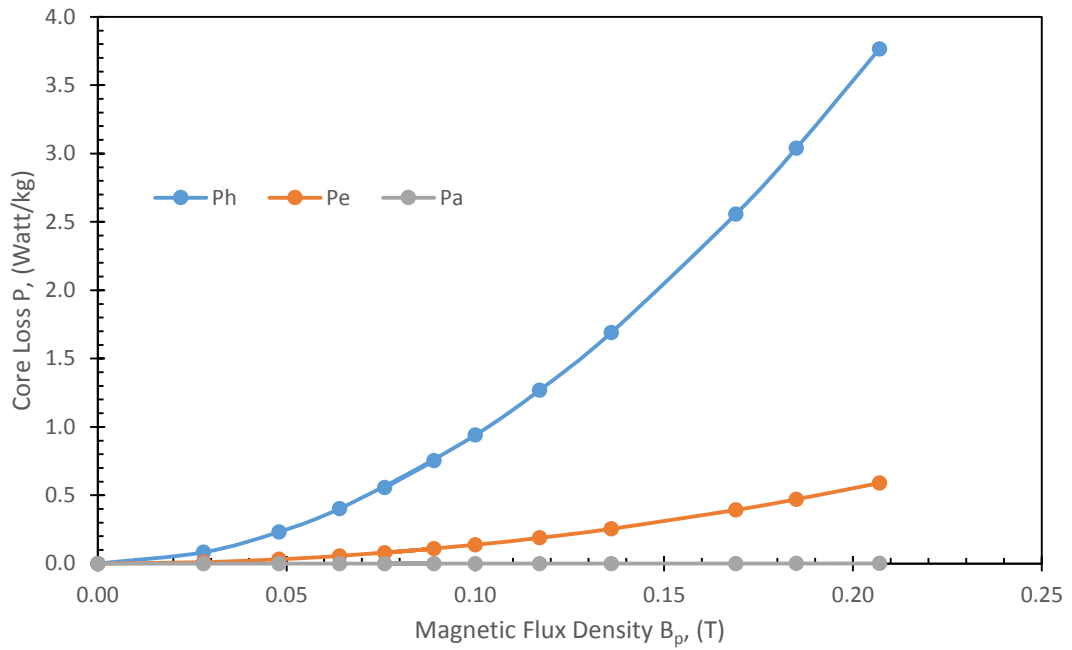
The core loss components, P_h , P_e and P_a at 50 Hz, 100 Hz, 500 Hz and 1000 Hz are plotted in Fig. 5.8 (a), (b), (c) and (d), respectively. The hysteresis loss P_h , is dominated at all frequencies but the eddy current loss P_e , become more significant with the growth of frequency. The anomalous loss P_a , is still the lowest among others.



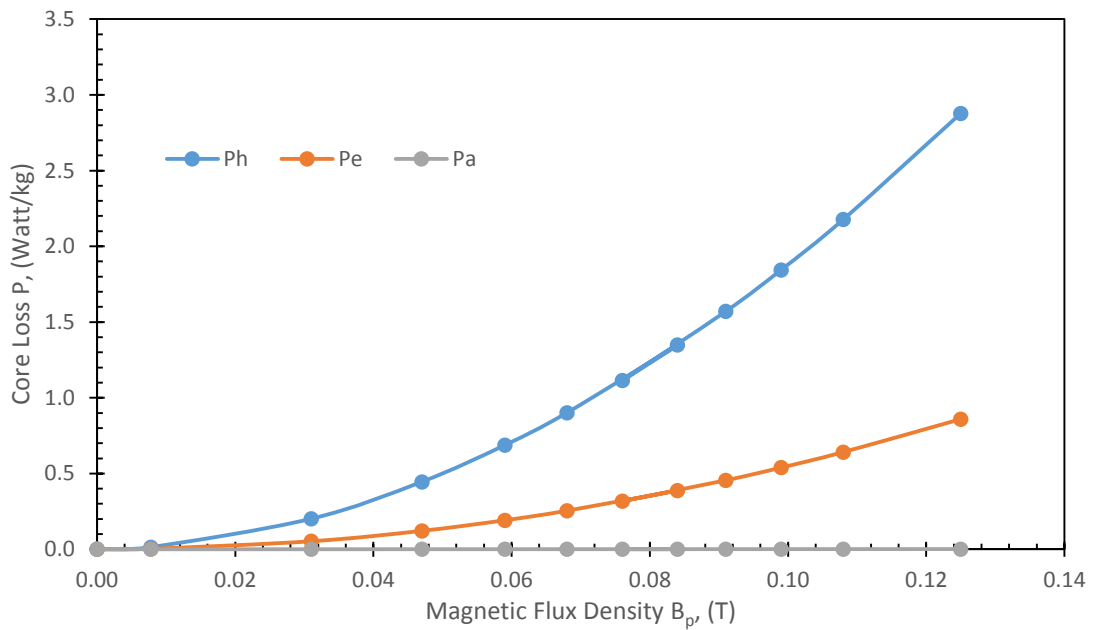
(a)



(b)



(c)



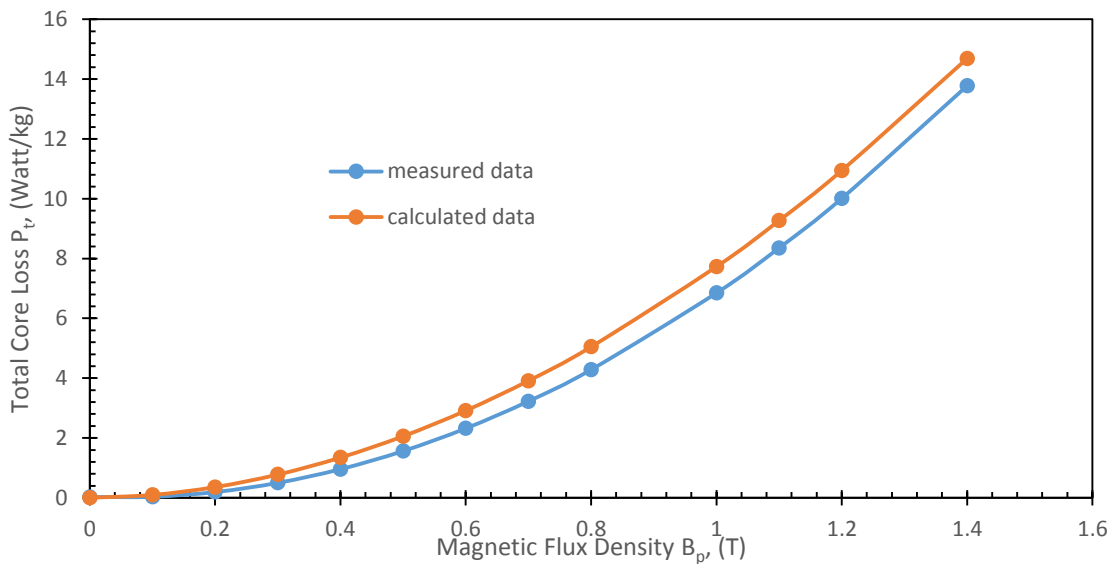
(d)

Fig. 5.8 Separation of total core loss which contains P_h , P_e and P_a when B is controlled to be in round shape at (a) 50 Hz, (b) 500 Hz and (c) 1000 Hz

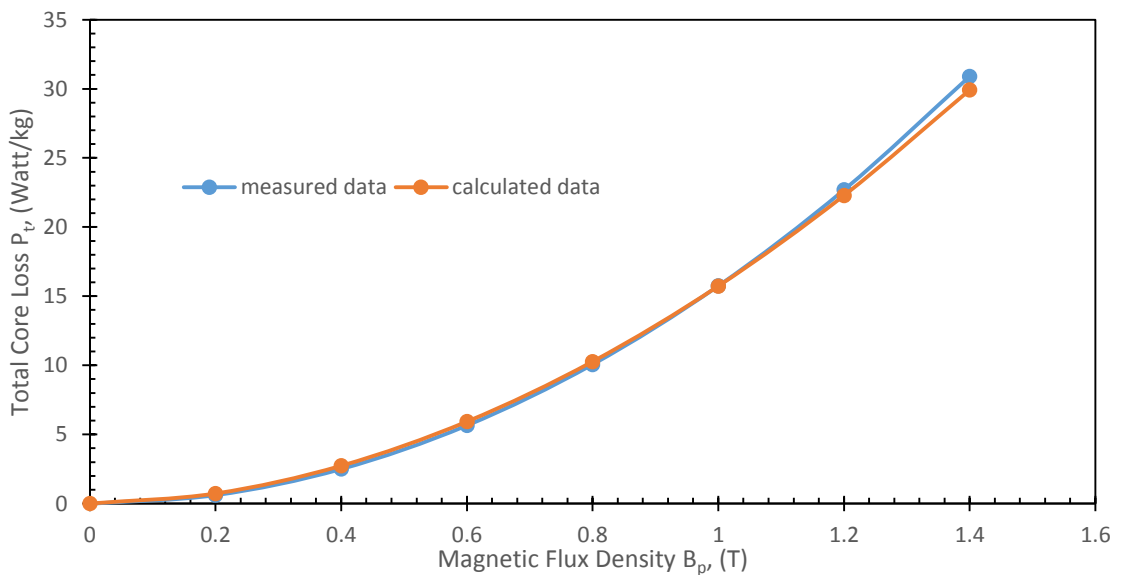
Theoretically, more magnetisation cycle will increase the hysteresis loss. This is caused by the increased works needed in diminishing the internal friction of magnetic material

that is in opposite direction with magnetic material molecules which will lead to the significantly growth of hysteresis loss.

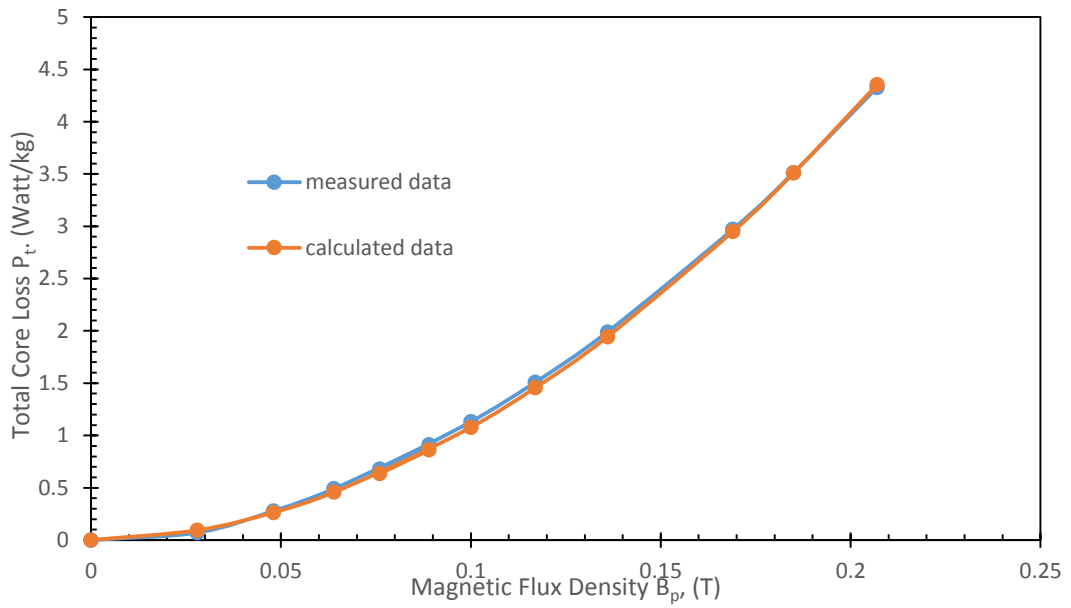
Fig. 5.9 (a), (b), (c) and (d) plot the measured and calculated core loss curves of rotational core loss at frequencies 50 Hz, 100 Hz, 500 Hz and 1000 Hz, respectively. From the curves shown in figures below, it can be seen that the agreement between measured and calculated rotational core loss for SOMALOY 700 (5P) is excellent especially at 100 Hz and 500 Hz. The agreement between measured and calculated data at 1000 Hz is started to distance away due to the worst condition of the 3-D tester at high frequency that makes the measured data is slightly higher than calculated data.



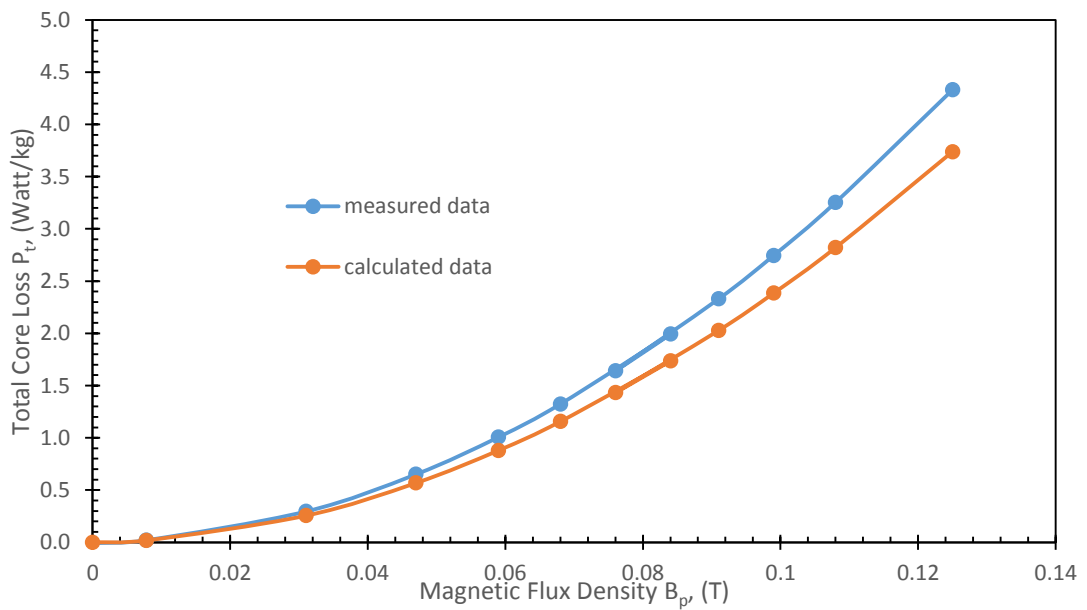
(a)



(b)



(c)



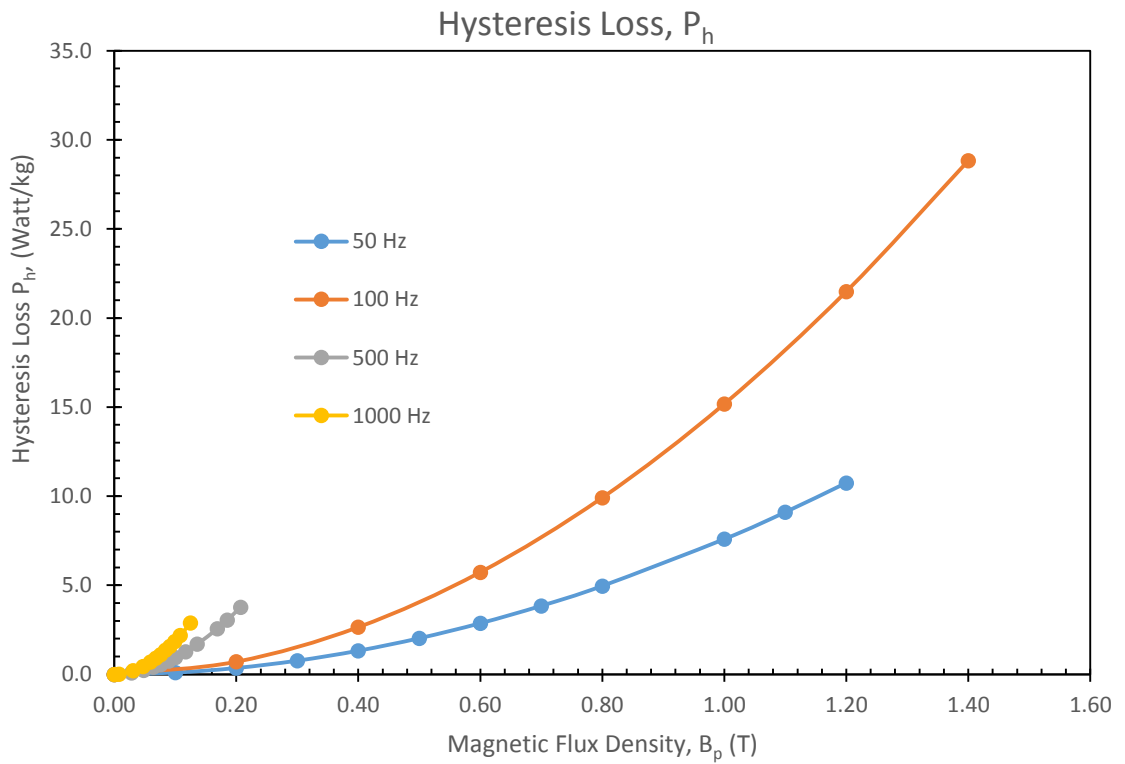
(d)

Fig. 5.9 The measured and calculated rotational core loss at 50 Hz, 100 Hz, 500 Hz and 1000 Hz

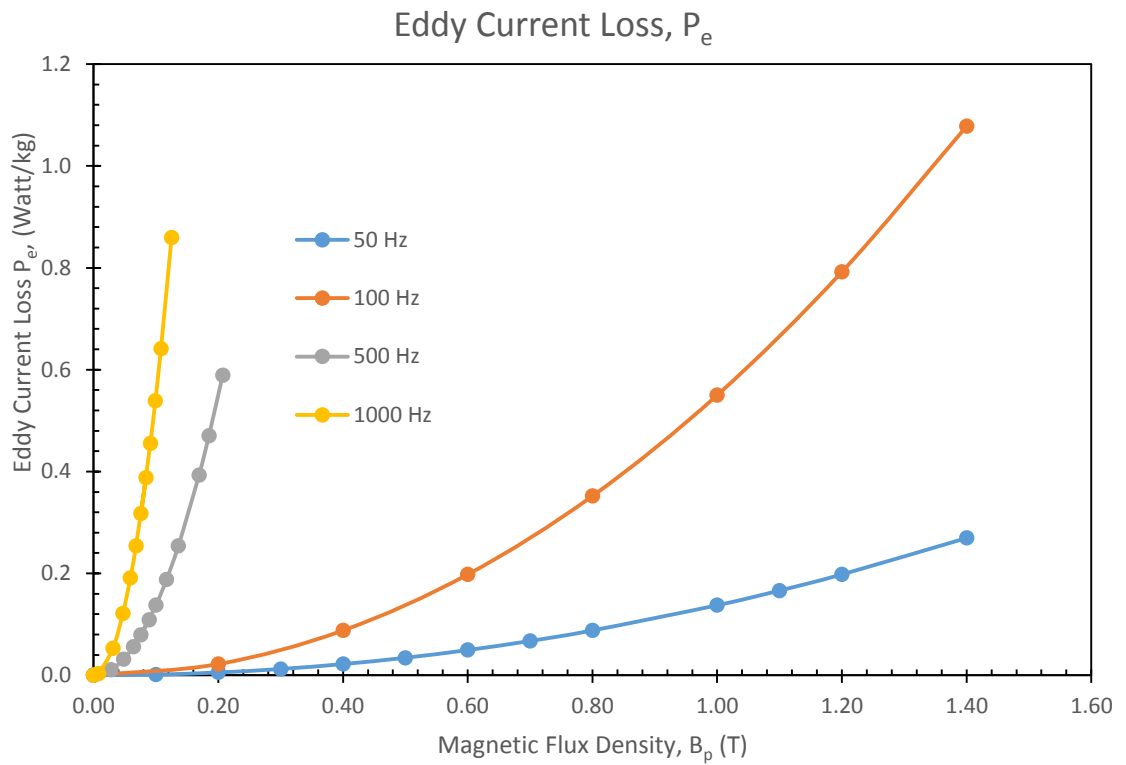
5.4.2 Rotational hysteresis loss

After some repeating measurements, hysteresis loss is still dominated in total core loss contribution compared to other losses, eddy current loss and anomalous loss. Fig. 5.10 (a), (b) and (c) plot the hysteresis losses, eddy current core losses and anomalous losses

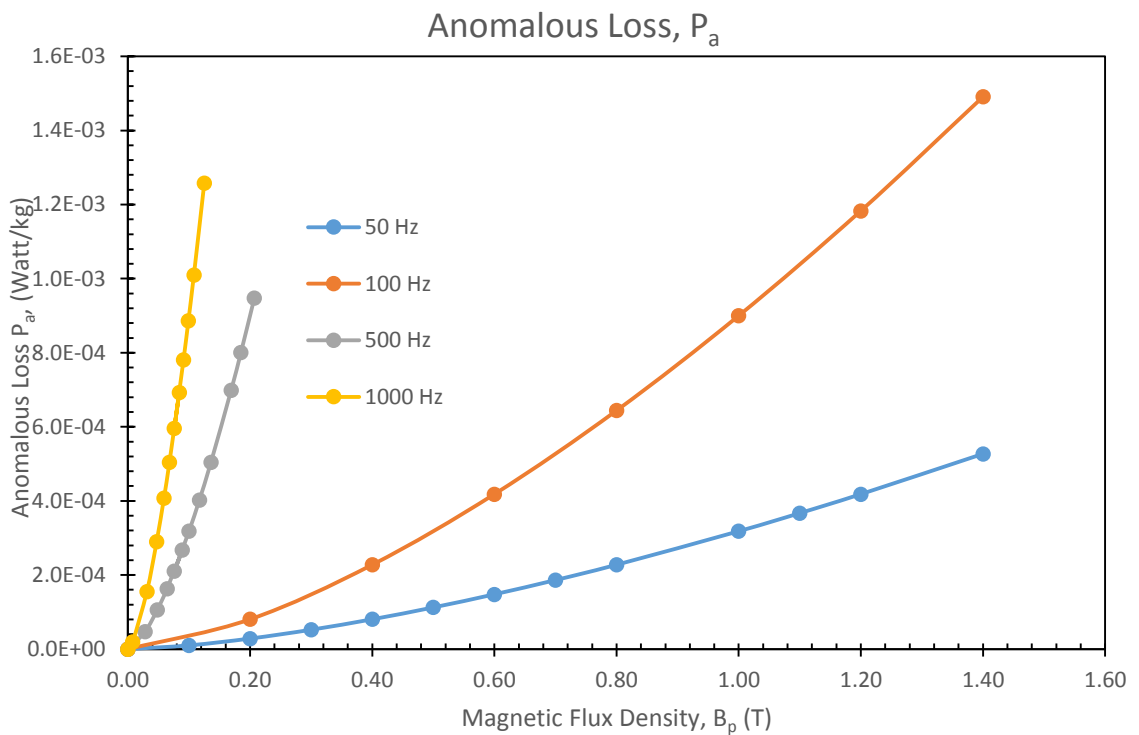
at four different frequencies when there is rotating magnetic field magnetising the SOMALOY 700 (5P) material. All components of losses show their highest at 1000 Hz of operating frequency because of the frequent currents which are flown in forward and reverse directions in order to complete the hysteresis cycle within the magnetic core which will increase the core loss of the material. Theoretically, more magnetisation cycle will increase the hysteresis loss. This is caused by the increased works needed in diminishing the internal friction of magnetic material that is in opposite direction with magnetic material molecules.



(a)



(b)



(c)

Fig. 5.10 The components of rotational core loss of SOMALLOY 700 (5P) material in the XOY-plane (a) hysteresis core loss (b) eddy current core loss (c) anomalous loss

Eddy current loss arises because of the core material itself which is made of conducting material. This loss depends on the rate of flux change and the path resistance. The variation of magnetic flux density and frequency will lead to the eddy current loss as stated in Steinmetz equation in chapter 2. This describes the plotted curves in Fig. 5.10 (b) which shows eddy current loss increased with the magnetic flux density and frequency.

Since the hysteresis loss is a main contributor in rotating magnetisation, a formulation of the rotational hysteresis loss per cycle in an electrical steel sheet and SMC sample has been modelled in 1998 by Zhu *et al.* as below [5.10]

$$\frac{P_{hr}}{f} = \alpha_1 \left[\frac{1/s}{\left(\alpha_2 + \frac{1}{s}\right)^2 + a_3^2} - \frac{1/(2-s)}{\left(a_2 + \frac{1}{2-s}\right)^2 + a_3^2} \right] \quad (5.6)$$

This equation can be expressed in terms of four parameters, α_1 (in J/kg), α_2 (non-dimensional), α_3 (non-dimensional) and B_s (in T) is the saturation magnetic flux density and s can be defined as

$$s = 1 - \frac{B}{B_s} \sqrt{1 - \frac{1}{a_2^2 + a_3^2}} \quad (5.7)$$

The curve fitting method was performed to minimise the error between the measured and calculated hysteresis losses in order to obtain the coefficients of the tested SOMALOY 700 (5P) material.

The value of core loss coefficients $\alpha_1 = 10.8$, $\alpha_2 = 0.44$ and $\alpha_3 = 7$ are obtained where SOMALOY 700 (5P) material is saturated at 2.47 T [5.11].

The measured and calculated rotational hysteresis loss per cycle in SOMALOY 700 (5P) at 50 Hz up to 2.2 T is plotted in Fig. 5.11. Good agreement between measured and calculated rotational hysteresis loss per cycle is described. The rotational hysteresis loss per cycle gradually increased at the beginning stage and started to slow down the growth at 2.2 T. Based on the theory, the curve line is dramatically dropped when the magnetic material is saturated.

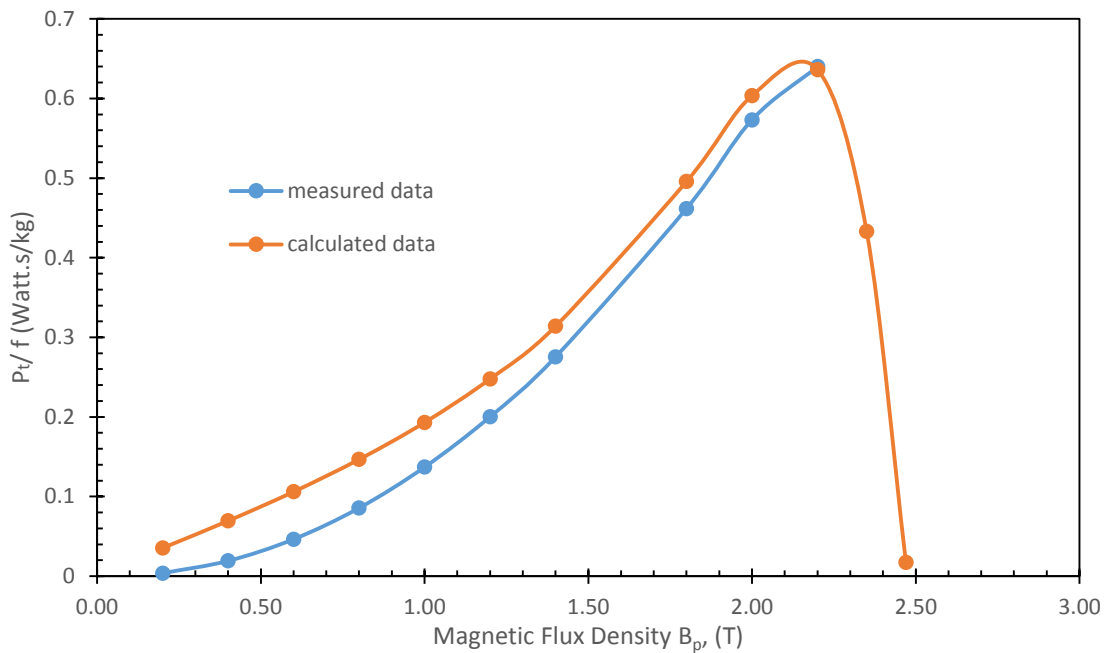


Fig. 5.11 The measured and calculated hysteresis losses per cycle at 50 Hz

5.5 Conclusion

The measurements that involved the circular magnetic fluxes have been conducted by using the 3-D tester. The results of experiment at certain range of frequency such as B loci, corresponding H loci, loss curve, and the components of the core loss and core loss coefficients are described in details. From the graphs and explanations, it can be concluded that the hysteresis loss is a significant contributor in core loss production when the material has been magnetised by rotating magnetic fluxes. Due to that, details of rotational hysteresis loss are described by comparing the results with the mathematical model which has been developed by Zhu *et al.* in 1998 [5.10]. The measurement of SOMALOY 700 (5P) magnetic properties are proceed by considering both directions clockwise and anti-clockwise rotating magnetic fluxes as proposed by Sievert [5.12], [5.13], [5.14], [5.15].

The rotational core loss which is twice as big as alternating core loss, increased with the frequency and magnetic flux density. From the recorded data, the SOMALOY 700 (5P) has lower core loss as compared to SOMALOY 500 which made SOMALOY 700 (5P) is more suitable to be considered in rotating electrical machines.

References

[5.1] Integrated Publishing Inc., Series AC Motor, [Online].

Available: <http://electriciantraining.tpub.com/14177/css/Rotating-Magnetic-Fields-87.htm>. [Accessed 15 June 2017]

[5.2] Australian Motor. Operation Manual AM3002, [Online].

Available:<http://www.australianmonitor.com.au/assets/Uploads/Products/Australian-Monitor/Discontinued-Products/Australian-Monitor-Pre-2005---Manuals/AM3002-Manual.pdf>. [Accessed 1 April 2014]

[5.3] Y. Li, Q. Yang, J. Zhu, and Y. Guo, "Magnetic Properties Measurement of Soft Magnetic Composite Materials Over Wide Range of Excitation Frequency," *IEEE Transactions on Industrial Applications*, vol. 48, no. 1, pp. 88-97, 2012.

[5.4] V. Basso and G. Bertotti, "Hysteresis in Soft Magnetic Materials," *Journal of Magnetism and Magnetic Material*, vol. 215, pp. 1-5, 2000.

[5.5] Y. J. Li, Q. X. Yang, Y. H. Wang, J. G. Zhu, and Z. W. Lin, "Rotational Core Loss Features of Soft Magnetic Composite Materials Under Excitation Frequencies from 5 Hz to 1000 Hz," *IEEE International Conference on Applied Superconductivity and Electromagnetic Devices*, 2013.

[5.6] H. Lu, Y. Guo, J. Zhu, J. Zhong, and J. Jin, "Soft Magnetic Materials for High Frequency High Power Density Transformers in Power Electronic Systems," *Academic Magazine*, vol. 11, no. 1, 2007.

[5.7] H. Y. Lu, "Numerical Simulation of High Frequency Transformers in Power Electronic Systems," *Ph.D. Thesis*, University of Technology Sydney, Australia, Aug. 2001.

[5.8] Y. J. Li *et al.*, "Three-Dimensional Magnetic Properties of Soft Magnetic Composite Material at Different Frequencies," *Journal of Applied Physics*, vol. 109, no. 7, 2011.

[5.9] Y. Chen and P. Pillay, "An Improved Formula for Lamination Core Loss Calculations in Machines Operating with High Frequency and High Flux Density Excitation," *Conference Record - IAS Annual Meeting IEEE Industrial Applications Society*, vol. 2, pp. 759–766, 2002.

[5.10] J. G. Zhu and V. S. Ramsden, "Improved Formulations for Rotational Core Losses in Rotating Electrical Machines," *IEEE Transactions on Magnetics*, vol. 34, no. 4, pp. 2234–2242, 1998.

- [5.11] Somaloy ® 700HR 5P. Hoganas AB (publ.), February 2016.
- [5.12] J. Sievert, J. Xu, L. Rahf, M. Enokizono, and H. Ahlers, "Studies on the Rotational Power Loss Measurement Problem", *Anales de Fisica Serie B*, vol. 86, pp. 35- 37, 1990.
- [5.13] J. Sievert, "Studies on the Measurement of Two Dimensional Magnetic Phenomena in Electrical Sheet Steel at PTB", First International Workshop on Magnetic Properties of Electrical Sheet Steel under Two-Dimensional Excitation, *Proceedings of the 93. PTB-Seminar, Physikalisch-Technische Bundesanstalt (PTB), Braunschweig (Germany)*, pp. 102-116, 16 and 17, Sept., 1991.
- [5.14] J. Sievert, H. Ahlers, M. Enokizono, S. Kauke, L. Rahf, and J. Xu, "The Measurement of Rotational Power Loss in Electrical Sheet Steel using a Vertical Yoke System", *Journal of Magnetism and Magnetic Materials*, vol 112, no. 1-3, pp. 91-94, 1992.
- [5.15] J. G. Zhu, "Numerical Modelling of Magnetic Materials for Computer Aided Design on Electromagnetic Devices," *Ph.D. Thesis*, University of Technology Sydney, Australia, 1994.

Chapter 6 : CORE LOSS MEASUREMENT UNDER ELLIPTICAL LOCI OF MAGNETIC FLUX DENSITY

6.1 Introduction

The invention of electric motor was started in the 19th century. All electric motors apply working principle of electromagnetic fields during the operation. There are many kinds of electrical machines in this era but they still have some similar components such as stator and rotor due to the similar physical principle that governing their behaviour.

In rotating electrical machines, the analytical techniques are varied and quite different depending on the type and the objective of the machine. An induction motor is one of the electric motors that is operated by electromagnetic induction from the magnetic flux density. Generally, the induction motor has three important components in operating the machines such as stator, winding coils and rotor as shown in Fig. 6.1. It can be seen that the winding coils are passing through slots of the stator where this stator acts as a stationary part, whereby rotor is the rotating component in this electromagnetic system.

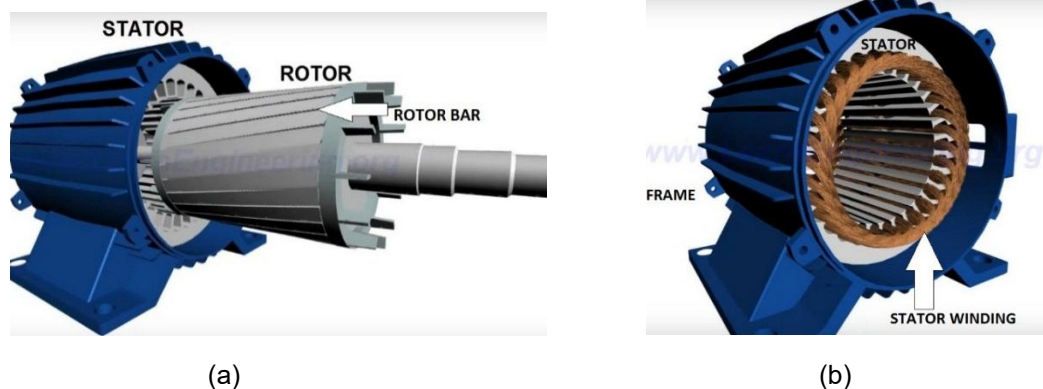


Fig. 6.1 The induction machine (a) The stator and rotor parts (b) the inner part of stator [6.1]

The stator and rotor are made of magnetic material to aid the production of magnetic flux density. The rotating magnetic flux densities are generated after three phase AC currents flow through the winding coils since each wire carrying current is able to produce magnetic flux density around it. In order to predict the actual core loss which has been produced by the actual electrical motor, the magnetic properties of material are investigated under similar mode of magnetic flux density propagation which is rotating.

Due to that, the flux densities are produced to be ellipse by controlling the magnitude, direction, and phase angle of individual magnetic flux density in the XOY-, YOZ- and ZOX-planes.

The elliptical B loci are examined by producing major and minor axis during the measurement. Thus, the rotating core loss with elliptical B loci can be predicted by considering equation (2.9) in chapter 2.

In this chapter, elliptical magnetic flux densities are generated in the XOY-plane at 50 Hz, 100 Hz and 1000 Hz of operating frequency. Section 6.2 describes the previous study of elliptical B loci and their corresponding H loci. Their corresponding core loss curves are also discussed in this section.

Experimental results for rotating core loss under elliptical B loci are explained in section 6.3. The measurement has been conducted under elliptical magnetic flux density on 2-D plane. The B and H loci are plotted together with the core loss curve in understanding the properties of the SOMALOY 700 (5P) material. The measured core loss under penetration of elliptical B loci is verified by comparing them with the alternating and purely circular formulation as given in equation (2.9).

6.2 Rotating elliptical magnetic flux density

Historically, the rotating magnetic flux density has been used to describe the field or flux that has moving polarities in which its opposite pole rotated about a central axis. This rotating magnetic flux density is set up in two-phase or three-phase machines. In three-phase machines, a symmetric three-phase AC sine current system is considered [6.2].

The rotating magnetic flux density is generated by a symmetrical three-phase winding that is being fed with three-phase AC sine current system. This generated magnetic flux density is called circular magnetic flux density since the circle locus of the resultant rotating magnetic flux density phasor is formed. The elliptical magnetic flux density is produced if three-phase AC sine current is unbalanced and / or the winding is asymmetrical. This situation will form an elliptical locus of the resultant rotating magnetic flux density [6.3].

In this study the elliptical B loci are generated by producing major and minor axis during the core loss measurement. Thus, $P_t = R_B P_r + (1 - R_B)^2 P_a$ is used to calculate the

rotating core loss under the elliptical B loci. As explained in chapter 2, P_α is the core loss under alternating B , P_r is the core loss with a circular B and R_B is the axis ratio that can be determined by dividing B_{min} to B_{maj} . In this case, B_{min} and B_{maj} are the minor axis and major axis of the elliptical B locus, respectively.

6.3 Experimental results

Measurement of core loss has been conducted by producing 2-D vector flux excitation. Elliptical magnetic flux densities are controlled to be lied in the XOY-plane at 50 Hz, 100 Hz and 1000 Hz of operating frequencies. Each measurement at certain frequencies is performed twice for representing x and y major axes. The core loss curves of each frequency are plotted for both measurements.

However, each measurement is conducted for three times for the best and accurate results by performing the same methods that have been explained in chapter 4 and chapter 5.

6.3.1 B-H Loci under elliptical magnetic flux density

Fig. 6.2 (a) and (b) show both B loci for major axes B_x and B_y that lie in the same magnetisation plane. It can be seen that, the B loci are distorted at high frequency, 1000 Hz. It caused by the movement of rotating domain that increased during the magnetisation which portrays the anisotropy property when there is involvement of high magnetic flux density in different directions [6.4], [6.5].

At 1000 Hz of magnetisation, the shape of elliptical B loci becomes shaky due to the coupling between core poles. This also leads to the noise production but it does not contribute to the core losses [6.6].

The corresponding H loci are plotted in Fig. 6.3, where Fig. 6.3 (a) illustrates the H loci when B_x acts as the major axis while Fig. 6.3 (b) describes the H loci when B_y is the major axis.

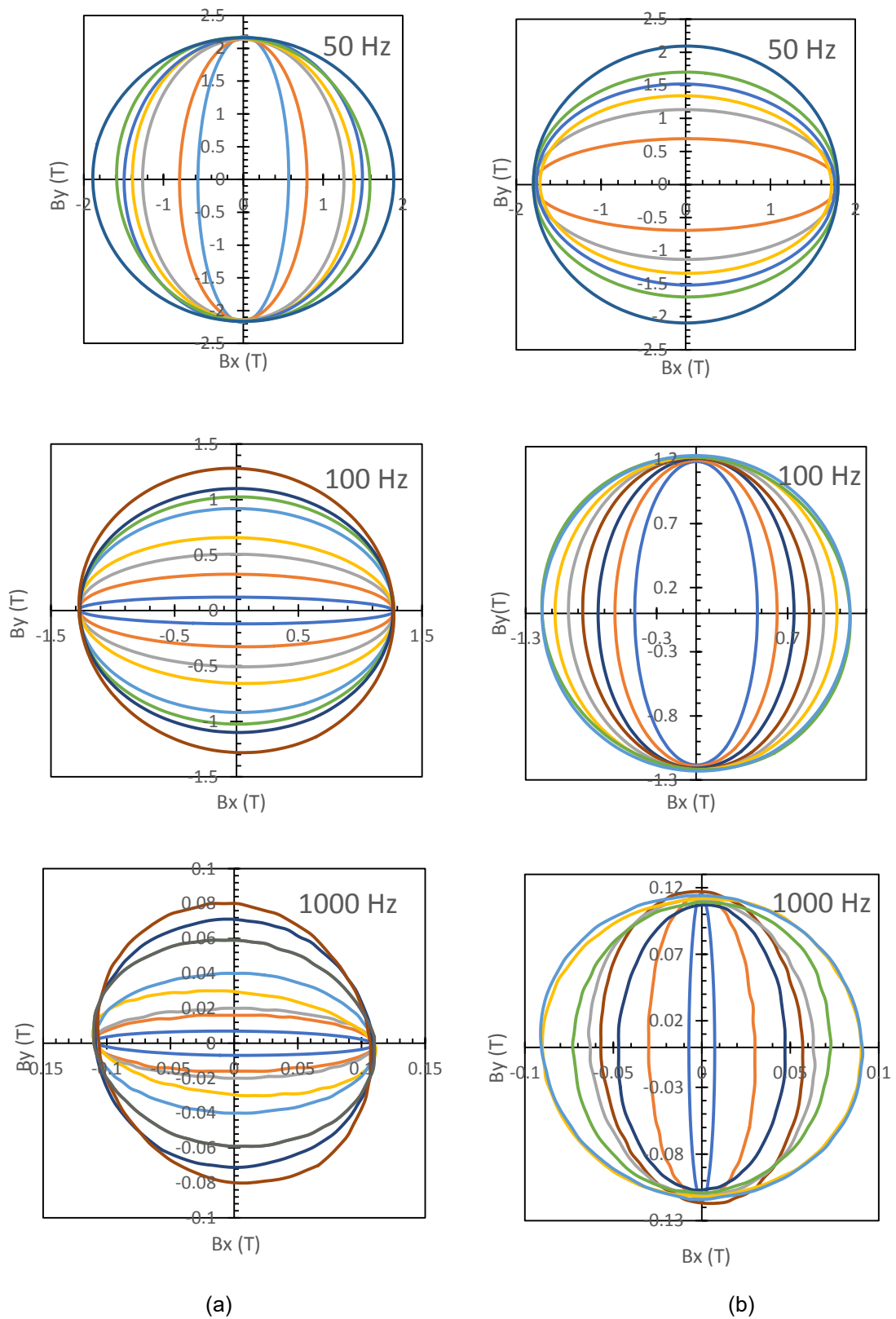


Fig. 6.2 B loci at 50 Hz, 100 Hz and 1000 Hz of operating frequency: (a) x- and (b) y-major axes

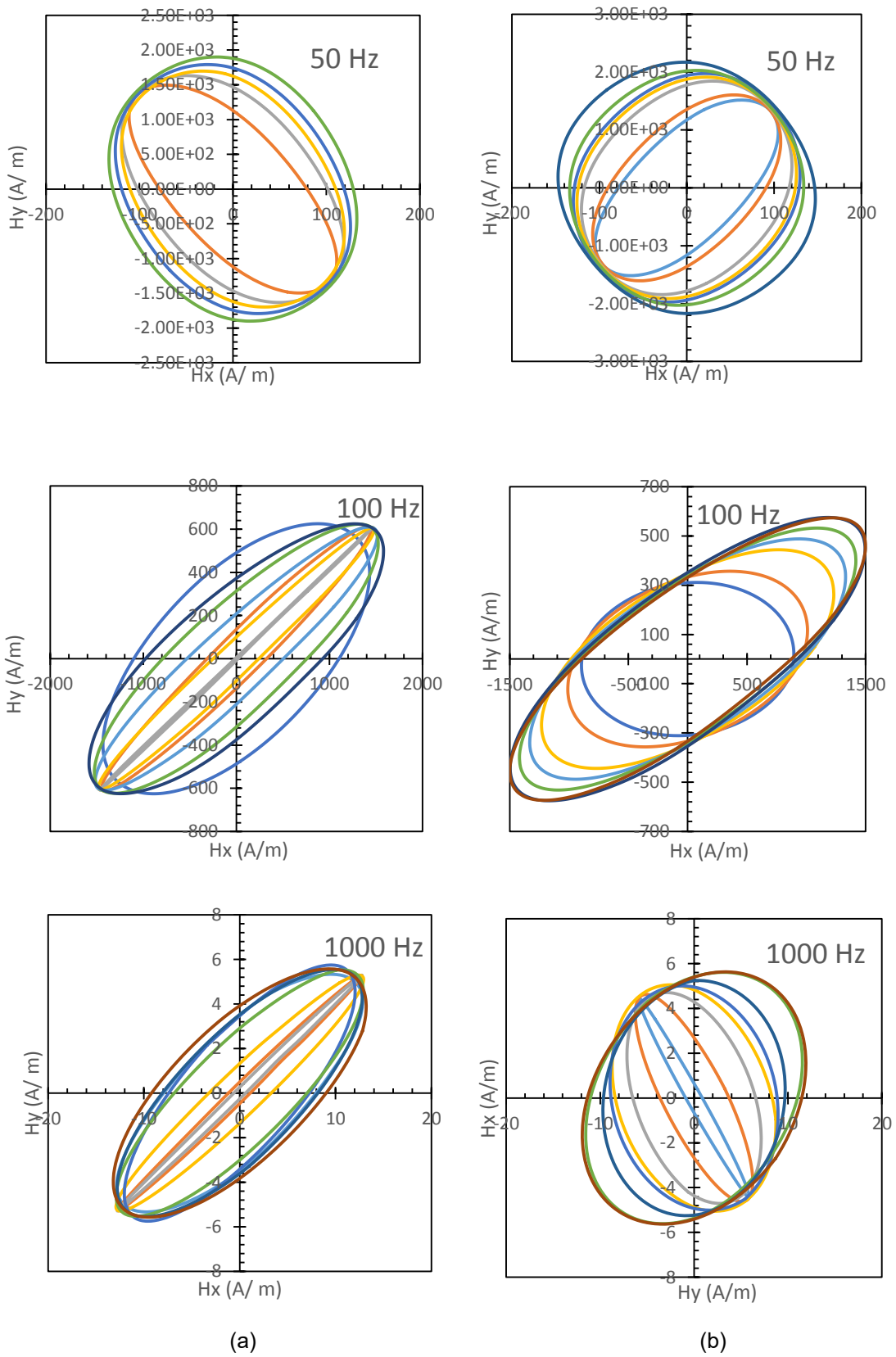
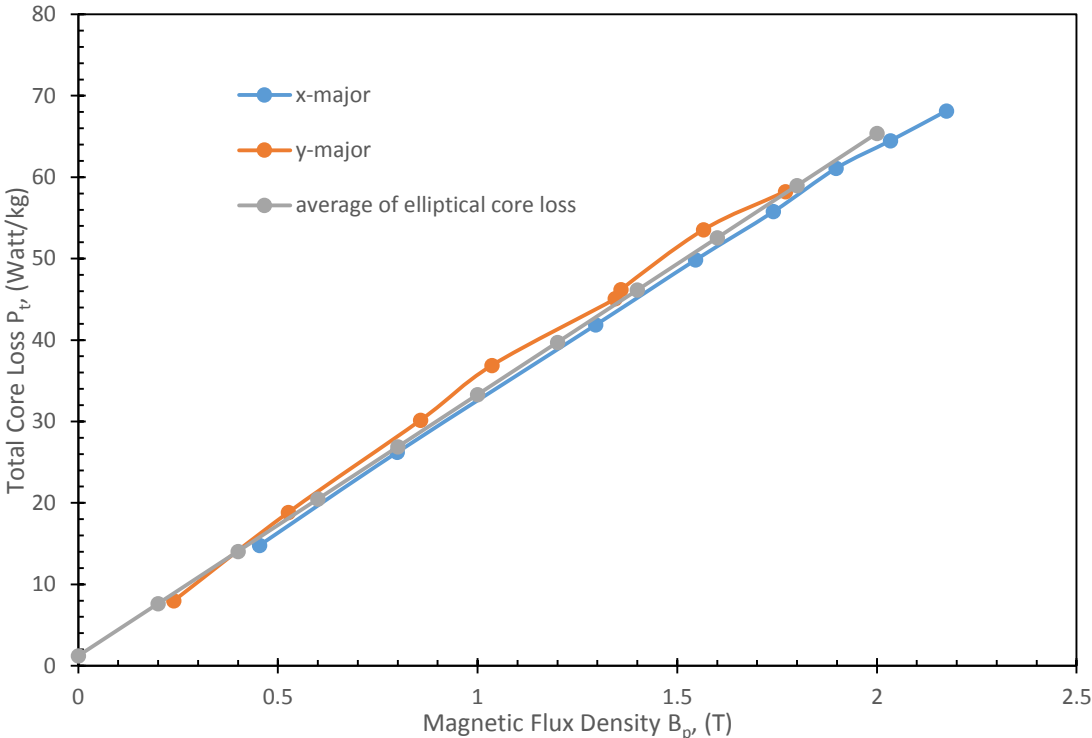


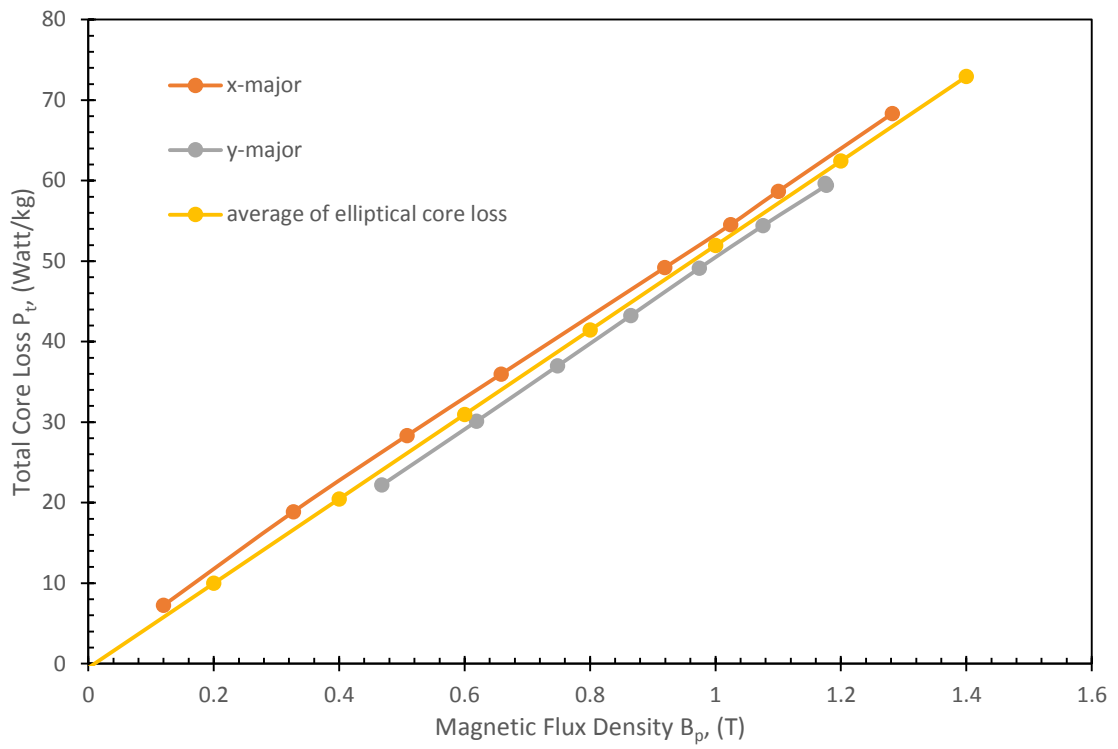
Fig. 6.3 H loci at 50 Hz, 100 Hz and 1000 Hz of operating frequency: (a) x- and (b) y-major axes

6.3.2 Core loss curve under rotating magnetic flux density

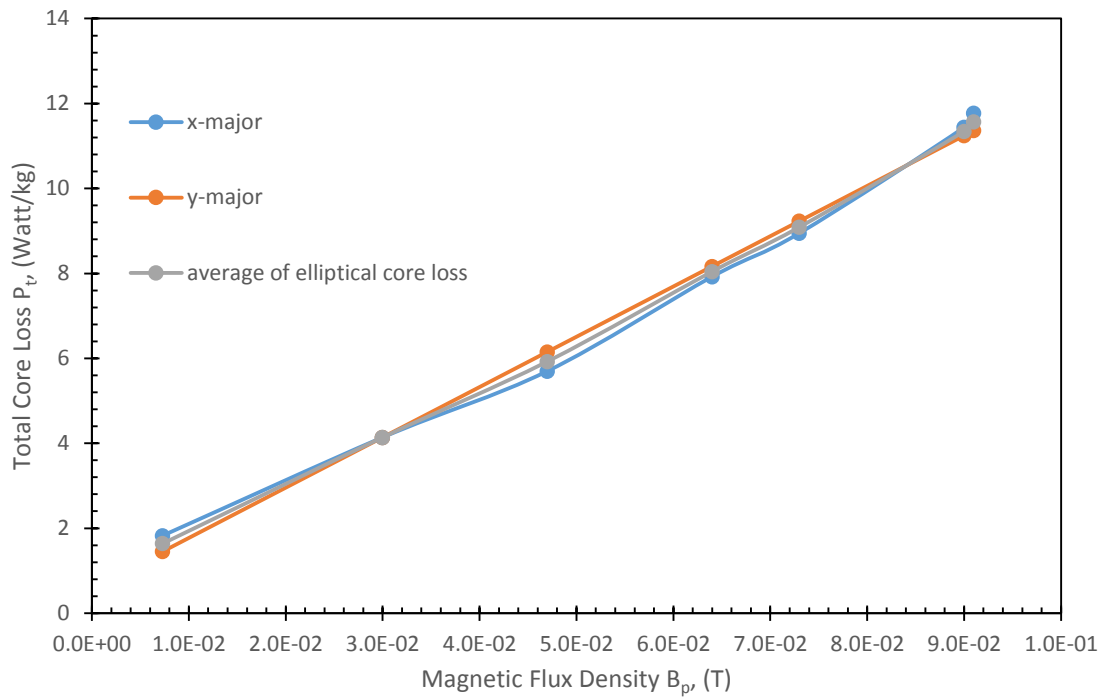
The SOMALOY 700 (5P) cubic sample is magnetised at three different frequencies, 50 Hz, 100 Hz and 1000 Hz by using 3-D tester. The core loss curves of each frequency are plotted twice which represent two different major axes, x and y. Fig. 6.4 (a), (b) and (c) explain the elliptical core losses that have been produced versus peak of magnetic flux densities at 50Hz, 100 Hz and 1000 Hz, respectively.



(a)



(b)



(c)

Fig. 6.4 Elliptical core loss curve of SOMALOY 700 (5P) material when B loci are elliptical at (a) 50 Hz, (b) 100 Hz and (c) 1000 Hz

All three figures show that the core losses increased with the magnetic flux density when the magnetic flux is rotating in elliptical shape. The performance of SOMALOY 700 (5P) core loss at 50 Hz, 100 Hz and 1000 Hz for both major axis, x and y are obeyed the theory which increased with the magnetic flux density. The total core losses at x- and y-major axes at all frequencies are similar along the XOY-plane and both recorded core losses are averaged in order to be considered in the future analysis.

Table 6-1 explains the average value of both elliptical core losses which are measured at two different major axes, x and y. The average value of this elliptical core loss is used during the comparison between the actual and measured core loss in the next section.

Table 6-1 The elliptical core loss for x- and y-major axes and their average at 50 Hz, 100 Hz and 1000 Hz.

f (Hz)	B_p (T)	Elliptical Core Loss (Watt/kg)		
		x-major	y-major	average
50 Hz	0.200	7.372	7.908	7.640
	0.400	13.622	14.491	14.057
	0.600	19.873	21.074	20.473
	0.800	26.124	27.656	26.890
	1.000	32.375	34.239	33.307
	1.200	38.626	40.822	39.724
	1.400	44.876	47.405	46.141
	1.600	51.127	53.988	52.557
	1.800	57.378	60.570	58.974
	2.000	63.629	67.153	65.391
	2.200	69.880	73.736	71.808
100 Hz	0.200	8.022	11.926	9.974
	0.400	18.598	22.332	20.465
	0.600	29.173	32.739	30.956
	0.800	39.749	43.145	41.447
	1.000	50.325	53.552	51.938
	1.200	60.900	63.959	62.429
	1.400	71.476	74.365	72.921
1000 Hz	0.007	1.826	1.452	1.639
	0.030	4.140	4.140	4.140
	0.047	5.700	6.153	5.926
	0.064	7.924	8.166	8.045
	0.073	8.948	9.231	9.090
	0.090	11.438	11.244	11.341
	0.091	11.772	11.363	11.567

In Fig. 6.5, the elliptical core loss curves of SOMALOY 700 (5P) at 50 Hz, 100 Hz and 1000 Hz are plotted in the same graph. It clearly shows that the core loss under elliptical B loci at 1000 Hz is the highest followed by the core losses at 100 Hz and 50 Hz. Based on the SE as described in chapter 2, the core loss is depending upon the frequency of magnetic reversal and the magnitude of the magnetic flux density.

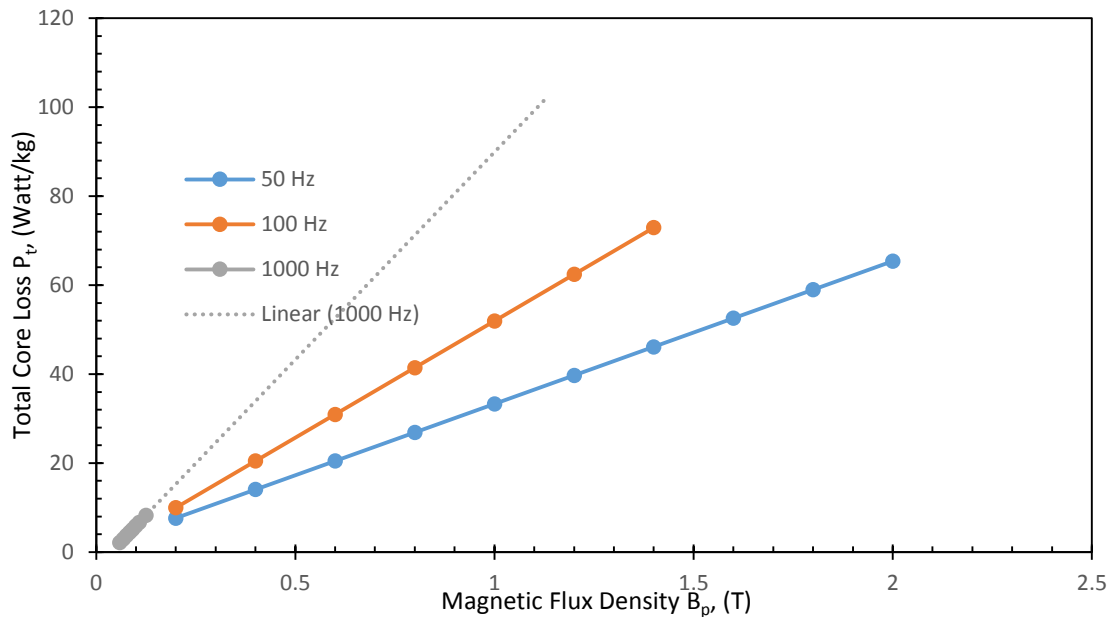
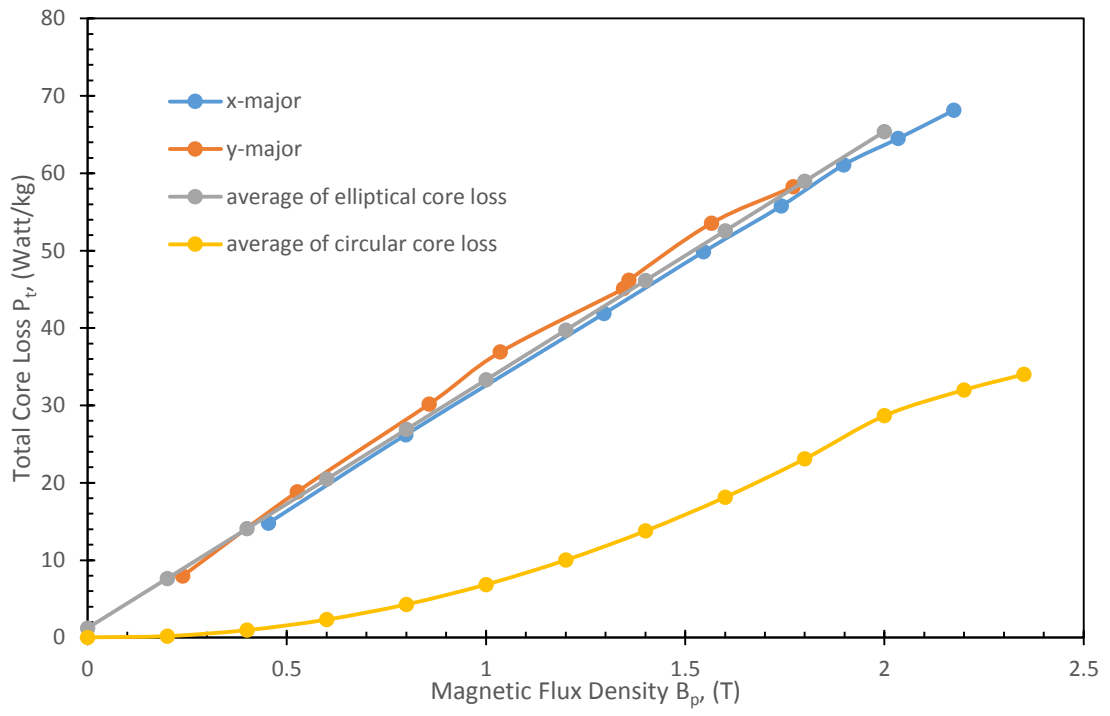


Fig. 6.5 Elliptical core loss curves of SOMALOY 700 (5P) material when B loci are elliptical at 50 Hz, 100 Hz and 1000 Hz.

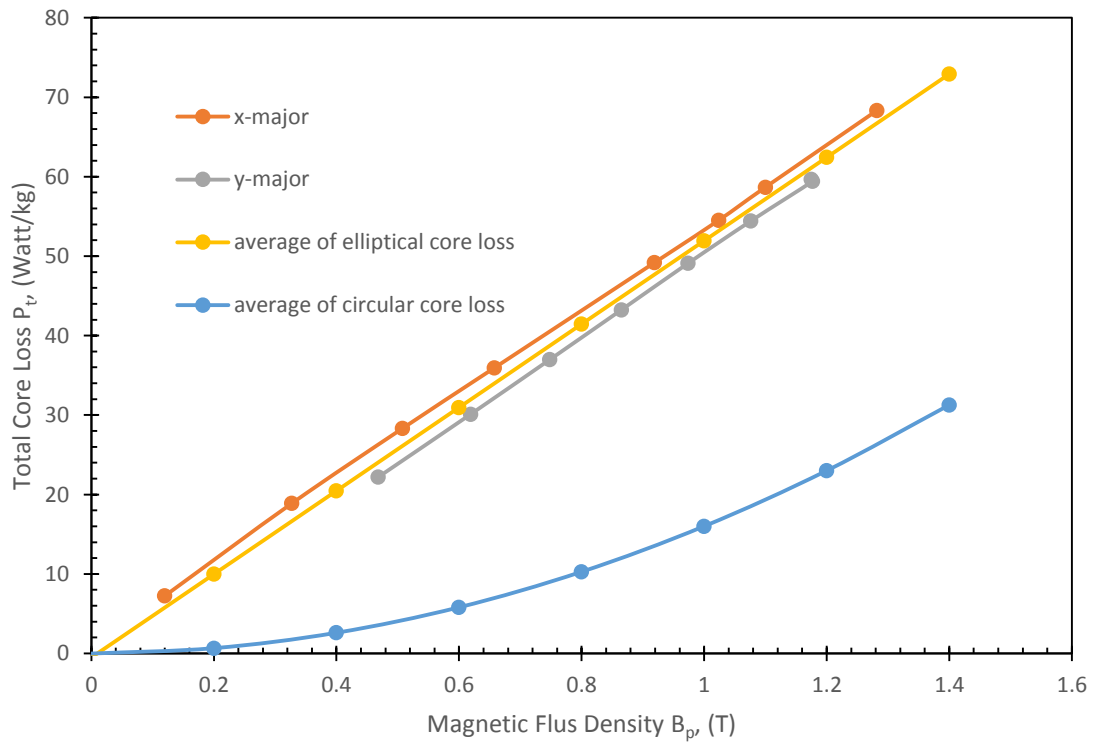
6.3.2.1 Circular and elliptical core loss

There are two shapes of B loci that have been generated under rotating magnetic flux density during the core loss measurement. After completing the measurement under alternating magnetic flux density, the magnetic flux is controlled to be in circle and ellipse shapes by adjusting the magnitude of magnetic flux density and the phase angle of the waveform voltage.

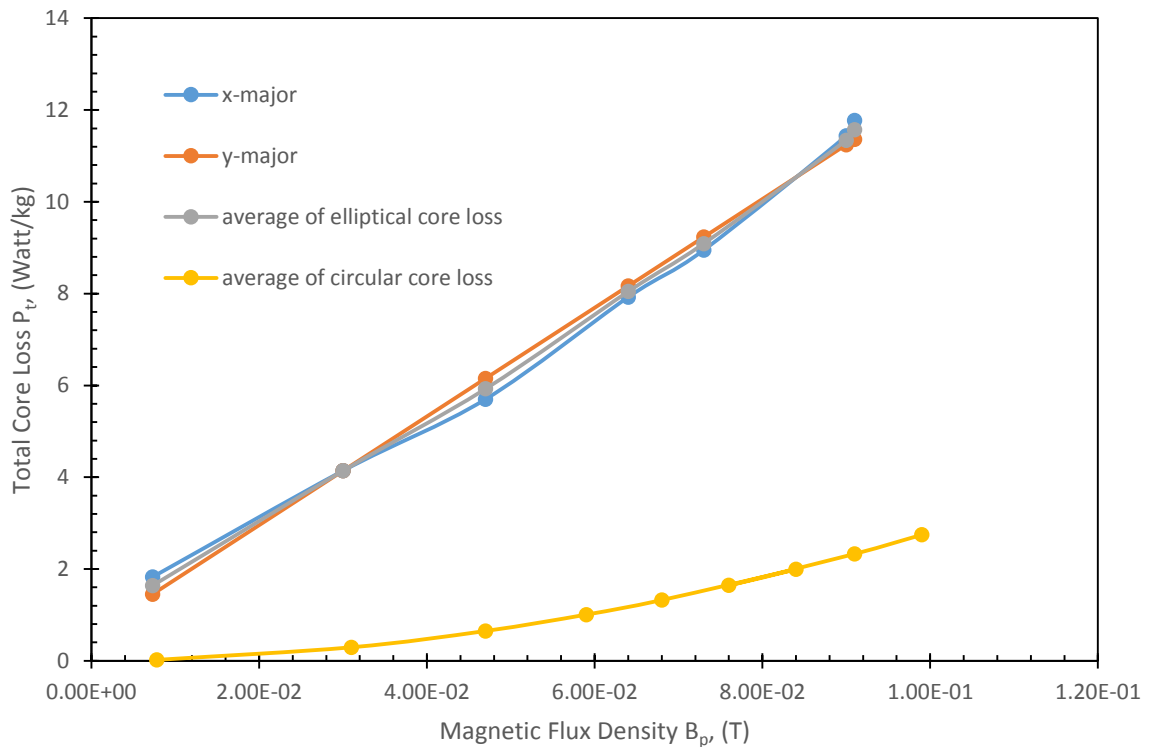
The core loss when subjected to external sinusoidal magnetic flux density in circular and elliptical B loci at three different frequencies, 50 Hz, 100 Hz and 1000 Hz are compared by plotting their core loss curves in a same graph as illustrated in Fig. 6.6 (a), (b) and (c), correspondingly. As shown in the figures, they show similar patterns which the graphs are linearly plotted for elliptical core losses and quadratics for circular core losses at 50 Hz, 100 Hz and 1000 Hz. It is reflected the calculation theory that is explained in equations (2.6) and (2.9).



(a)



(b)



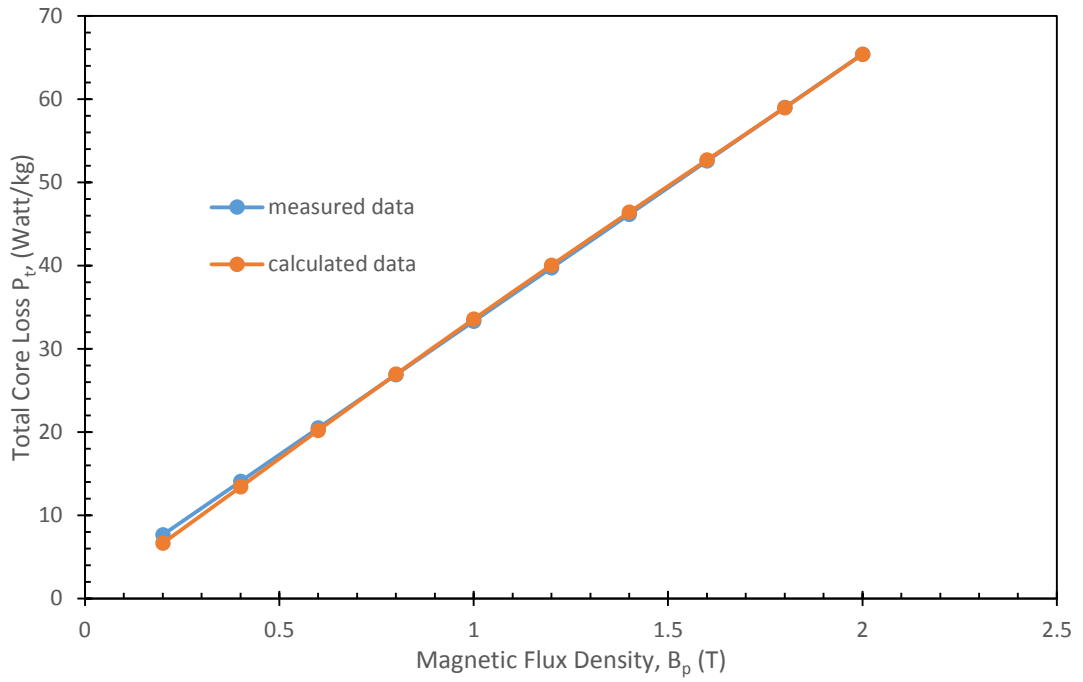
(c)

Fig. 6.6 Comparison between elliptical and circular core losses of SOMALOY 700 (5P) material when B loci are elliptical at (a) 50 Hz, (b) 100 Hz and (c) 1000 Hz

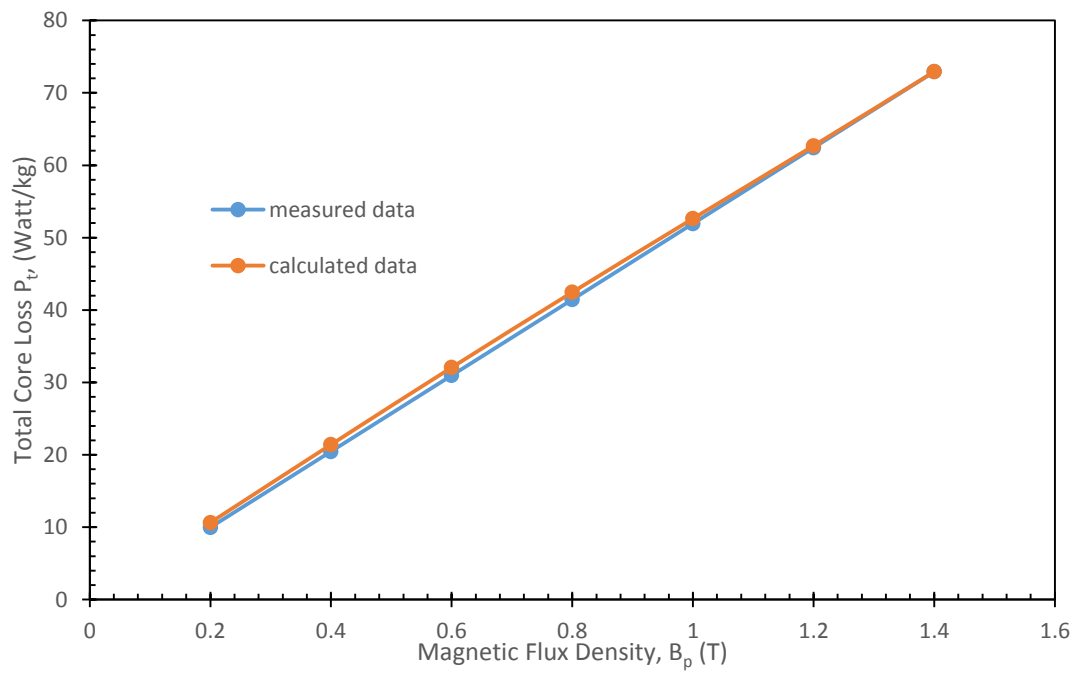
It can be seen that the core losses are higher when the cubic sample is magnetised under elliptical magnetic flux densities when compared to circular magnetic flux densities. This is caused by constant magnetic flux density which acts as a major axis in generating the elliptical loci during the measurements.

6.3.2.2 Accuracy of core loss measurement

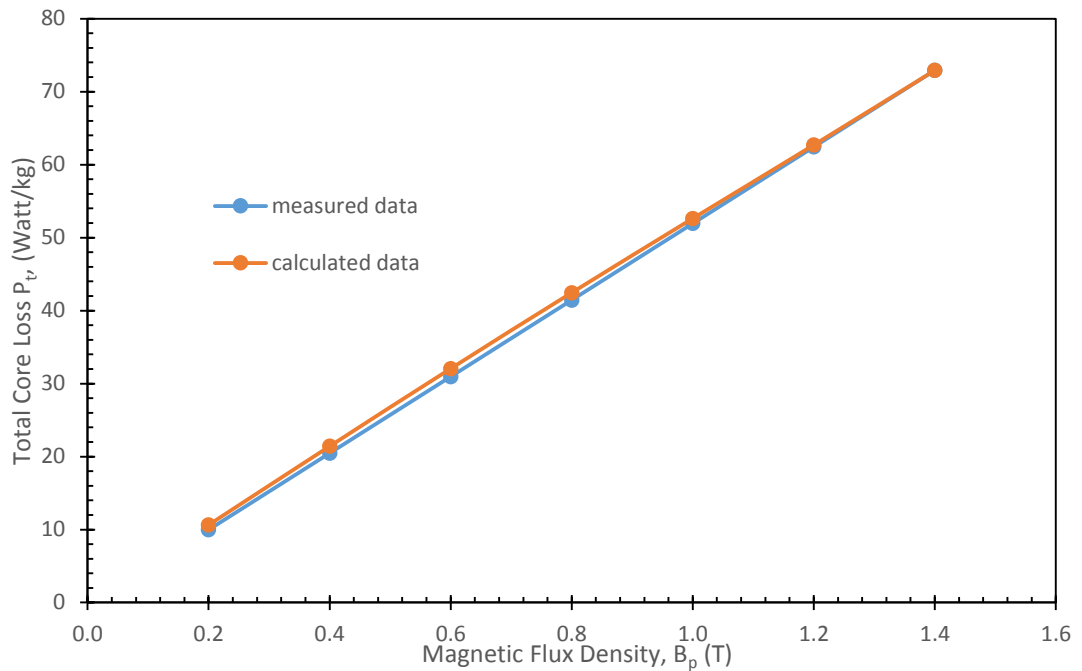
Accuracy in measurement is very crucial to check the degree of measurement trueness. In order to analyse the accuracy of the recorded data, both calculated and measured core losses versus magnetic flux density are plotted in the same graph. Based on Fig. 6.7, the measured and calculated elliptical core losses are described at three different operating frequencies, 50 Hz, 100 Hz and 1000 Hz. This can explain the strong agreement of measured and calculated elliptical core loss for all frequencies.



(a)



(b)



(c)

Fig. 6.7 Comparison between measured and calculated core losses of SOMALOY 700 (5P) material when B loci are elliptical at (a) 50 Hz, (b) 100 Hz and (c) 1000 Hz

To validate the accuracy of plotted results, the Mean Absolute Percentage Error (MAPE) is obtained by considering the equation below

$$MAPE = \left(\frac{1}{n} \sum \frac{|Actual - Forecast|}{Actual} \right) \times 100 \quad (6.1)$$

The calculated value is the actual value which is determined by the elliptical core loss formulation as described in previous section. Table 6-2 shows the absolute percent errors of elliptical core losses. It exhibits that the error in the core loss measurement under elliptical B loci at 50 Hz, 100 Hz and 1000 Hz are 2.18%, 2.71% and 5.13% respectively.

Table 6-2 The absolute percent errors of elliptical core loss measurement at (a) 50 Hz, (b) 100 Hz and (c) 1000 Hz

f (Hz)	B _p (T)	P _a (Watt/kg)	P _e (Watt/kg)		accuracy	
			measured	calculated	Absolute Square Error	MAPE (%)
50	0.200	0.112	7.640	6.630	1.021	2.18
	0.400	0.496	14.057	13.395	0.437	
	0.600	1.182	20.473	20.197	0.077	
	0.800	2.171	26.890	26.938	0.002	
	1.000	3.462	33.307	33.561	0.064	
	1.200	5.055	39.724	40.043	0.102	
	1.400	6.950	46.141	46.399	0.067	
	1.600	9.148	52.557	52.679	0.015	
	1.800	11.648	58.974	58.968	0.000	
	2.000	14.451	65.391	65.391	0.000	
100	0.200	0.298	9.974	10.636	0.439	2.71
	0.400	1.132	20.465	21.412	0.897	
	0.600	2.458	30.956	32.054	1.206	
	0.800	4.278	41.447	42.455	1.015	
	1.000	6.591	51.938	52.624	0.470	
	1.200	9.396	62.429	62.695	0.071	
	1.400	12.695	72.921	72.921	0.000	
1000	0.008	0.011	1.539	0.972	0.322	5.13
	0.031	0.159	4.286	3.913	0.139	
	0.047	0.367	6.180	5.939	0.058	
	0.059	0.564	7.601	7.433	0.028	
	0.068	0.752	8.666	8.542	0.015	
	0.084	1.123	10.560	10.479	0.007	
	0.076	0.943	9.613	9.517	0.009	
	0.091	1.305	11.389	11.318	0.005	
	0.099	1.526	12.336	12.274	0.004	
	0.108	1.768	13.402	13.351	0.003	
	0.125	2.250	15.414	15.415	0.000	

Criteria of MAPE are explained Table 6-3. Based on Lewis, the percentage error below 10% is excellent which reflects the elliptical core loss measurements at all frequencies [6.7]. 2.18%, 2.71% and 5.13% of error are recorded by the elliptical core loss measurement at 50 Hz, 100 Hz and 1000 Hz, respectively.

Table 6-3 Criteria of MAPE [6.7]

MAPE (%)	Forecasting power
< 10	Excellent
10 - 20	Good
20 - 50	Reasonable
> 50	Incorrect

6.4 Conclusion

The elliptical core loss of SOMALOY 700 (5P) material is measured by controlling the individual magnetic fluxes B_x and B_y to be in ellipse shape at 50 Hz, 100 Hz and 1000 Hz. However, the elliptical B loci become shaky at 1000 Hz and at this frequency, the core loss recorded is higher compared to the elliptical core loss at 100 Hz and 50 Hz due to the rotating domain particles during the magnetisation process. The elliptical loci is determined by averaging the elliptical core loss when B_x and B_y as the major axis. Besides that, the SOMALOY 700 (5P) gives the lowest loss compared to the SOMALOY 500 material. The performance of both elliptical and circular core loss is compared before the accuracy of the elliptical core loss measurement is determined by considering the percentage error of the measured data. The measurement of elliptical core loss at 50 Hz, 100 Hz and 1000 Hz show the excellent results since all the percentage errors are lower than 10%.

References

- [6.1] Learn Engineering, 'How does an Induction Motor Work?,' 2013.
[Online]. Available: <http://www.learnengineering.org/2013/08/three-phase-induction-motor-working-squirrel-cage.html>. [Accessed 2 July 2017].
- [6.2] D. P. Kothari and I. J. Nagrath, *Electrical Machines*. Tata McGraw- Hill, 1995.
- [6.3] Jacek F. Gieras, *Electrical Machines: Fundamental of Electromechanical Energy Conversion*. Boca Raton, Florida: CRC Press, 14 October 2016.
- [6.4] Y. Li, Q. Yang, J. Zhu, and Y. Guo, "Magnetic Properties Measurement of Soft Magnetic Composite Materials Over Wide Range of Excitation Frequency," *IEEE Transactions on Industrial Applications*, vol. 48, no. 1, pp. 88-97, 2012.
- [6.5] V. Basso and G. Bertotti, "Hysteresis in Soft Magnetic Materials," *Journal of Magnetism and Magnetic Material*, vol. 215, pp. 1-5, 2000.
- [6.6] Y. J. Li, Q. X. Yang, Y. H. Wang, J. G. Zhu, and Z. W. Lin, "Rotational Core Loss Features of Soft Magnetic Composite Materials under Excitation Frequencies from 5 Hz to 1000 Hz," *Proceedings of the IEEE International Conference on Applied Superconductivity and Electromagnetic Devices*, 2013.
- [6.7] C. D. Lewis, "Industrial and Business Forecasting Methods," *Journal of Forecasting*, vol. 2, no, 2, pp. 194-196, Apr 1983.

Chapter 7 : CONCLUSIONS AND RECOMMENDATIONS

7.1 Conclusions

In this chapter, the contribution of this thesis and the possible impact to the community are described. In prior to that, the limitation in collecting the valuable data is explained since this impacted and influenced the interpretation of the research findings. The important directions of future works are portrayed in the last part of this chapter.

The main purpose of this study is to determine the magnetic properties of the new material that has been produced by Hoganas. This lowest loss material is known as SOMALOY 700 (5P) material. The low-to-high frequency electromagnetic devices such as power transformers, rotating electrical machines, fast switching actuators and sensors can consider this material to increase their efficiency during the operation. To date, no large-scale studies have been performed to investigate the prevalence of studying magnetic properties of SOMALOY 700 (5P) material under 2-D flux excitation by using the 3-D tester. The data given by the Hoganas are always under 1-D magnetic flux excitation which is not compatible with electrical machines application. Due to that, the core loss measurement of SOMALOY 700 (5P) material is investigated to be a reference or benchmark for the future electrical machines.

To accomplish that purpose, there are some prerequisite goals that need to be reached. The suitable model, method and tester are used together with the proper and detail preparation especially the sensing coils part. In order to sense the accurate voltage sensor, the turn numbers of B and H sensing coils must be similar for each cubic sample surfaces. The orientation and position of both coils should be in the centre of the cubic sample which will detect high penetration of magnetic flux density during the magnetisation process. Besides that, the excitation winding coils of three axes are very important to produce the uniform flux excitation which is used to magnetise the cubic sample inside the 3-D tester. Both sensing coils and excitation winding coils are very crucial in this study since the experiments are conducted up to 2-D measurement which demands high and uniform vector flux excitation. Furthermore, high accuracy in simultaneously recording the voltage sensors, V_B (s) and V_H (s) is mandated specifically when B is controlled circularly and elliptically.

Dissimilarity surface contact size between guarding pieces and yokes contributed the air gaps which reduced the penetration of magnetic flux density. This limited the experiment

to be conducted at high B due to high noise and high vibration of the tester. The small different values of K_B (s) and K_H (s) among surfaces give an effect in forming the perfect shape of circle and ellipse in 2-D core loss measurement. Besides that, the condition of 3D tester is quite bad. The cylindrical pole of laminated core caused the connection disagreement between the laminated cores and yokes which will be reducing the magnetic flux density distribution through the sample. The research aims and objectives were achieved through the completed core loss measurements of SOMALOY 700 (5P) material and data verification for every measurement from chapter 4 until chapter 6. These are achieved by:

- Assortment of suitable measuring method, tester and model in predicting SOMALOY 700 (5P) core losses.

Embedded B coil method is used by allocating circular B coil in the middle of cubic sample with H coil is wound and covered the circular B coil. Both coils are closely attached to the cubic sample which gives high impact in detecting magnetic flux density. 3-D magnetic property testing system or 3-D tester that is able to provide up to 3-D magnetic flux excitation is used to magnetise the SOMALOY 700 (5P) material. In order to calculate core loss of the material, Steinmetz Equation (SE) and curve fitting method have been considered.

- Measurement of alternating core loss of SOMALOY 700 (5P) along the x-, y- and z-axes.

The magnetic properties of SOMALOY 700 (5P) are discussed by conducting core loss measurement at 50 Hz, 100 Hz, 500 Hz and 1000 Hz under 1-D magnetic flux density along the x-, y- and z-axes. The higher frequency contributes to the higher loss due to the vibration of magnetic material which causes extra heat dissipation. Besides that, the forward and reverse directions of flew current during the hysteresis cycle completion also contribute to the higher core loss at high frequency. The core loss along the three axes shows a small discrepancy for z-axis. This is caused by the effect of the manufacturing process that makes the distribution of particle in the z direction is not uniform. The measured core loss data are analysed by using curve fitting method to obtain each component of core losses that shows hysteresis loss is dominated at 50 Hz, 100 Hz, 500 Hz and 1000 Hz. It has been followed by the eddy current loss and anomalous loss.

- Determination of the magnetic properties of SOMALOY 700 (5P) material under circular loci in clockwise and anti-clockwise directions.

The measurements that involve the circular magnetic fluxes have been conducted at 50 Hz, 100 Hz, 500 Hz and 1000 Hz in clockwise and anti-clockwise directions by using the 3-D tester. Both directions have the same magnitude of core loss but the plotted graphs showed the mirror image that has been reflected on the x-axis due to the opposite pole of magnetic flux densities during the magnetisation process. Core loss parameters that are used in obtaining each component of core loss are determined by fitting the calculated circular core loss to the measured circular core loss. The hysteresis loss is a significant contributor in core loss production when the material has been magnetised by rotating magnetic fluxes. High hysteresis loss is recorded at 1000 Hz followed by 500 Hz, 100 Hz and 50 Hz. The core loss measurements under circular magnetic flux density and alternating magnetic flux density are compared. The verification concludes that core loss under circular loci of B is higher than core loss under 1-D magnetic flux excitation. However, the tester has a restriction in measuring the core loss at high frequencies which limits the magnetic material to be magnetised at high magnetic flux density.

- Determination of the magnetic properties of SOMALOY 700 (5P) material under elliptical loci at B_x and B_y major axis.

By controlling the loci of B_x and B_y to be elliptical, the elliptical core loss of SOMALOY 700 (5P) material is measured at 50 Hz, 100 Hz and 1000 Hz. The elliptical core loss is highest at 1000 Hz compared to the elliptical core loss at 100 Hz and 50 Hz due to the rotating domain particles during the magnetisation process. The elliptical loci is determined by averaging the elliptical core loss when B_x and B_y as the major axis. Besides that, the performance of both elliptical and circular core loss is compared before the accuracy of the elliptical core loss measurement is determined by calculating the percentage error of the measured data. The measurement of elliptical core loss at 50 Hz, 100 Hz and 1000 Hz is excellent since the percentage errors for all measurements are below 10%. It explains that the elliptical core loss measurement is a good agreement with the calculation theory.

- Comparison the characteristics of SOMALOY 700 (5P) material with the SOMALOY 500 material.

The characteristic of the new material, SOMALOY 700 (5P) is compared to the SOMALOY 500, the magnetic material, which has been studied for over 15 years. The core losses of SOMALOY 500 under alternating magnetic flux density at 50 Hz along the x-, y- and z-axes is verified by considering core losses of SOMALOY 500

at the same frequency and axis. The hysteresis loops of SOMALLOY 700 (5P) along x-, y- and z-axes give the smallest loop compared to the SOMALLOY 500 material. The coercivity of SOMALLOY 700 (5P) is low that defines the behaviour of this material is magnetically soft. Low coercivity describes the needed applied field in reversing the magnetisation of the magnetic material is low. This larger grain of iron particles with ultra-thin insulation has offered the lowest loss due to the improved physical characteristic of the magnetic material particles during the manufacturing process. These characteristics of SOMALLOY 700 (5P) material significantly reduce the eddy current loss.

7.2 Recommendations for future research

Although the core loss measurement under alternating and rotating magnetic flux density is able to describe the magnetic properties of SOMALLOY 700 (5P) material, there are still some critical areas that have not been addressed through this research. Hence, future research towards this area is suggested to widen the efficiency of the electrical machines. These include:

- Comparing the 2-D core loss measurement of SOMALLOY 700 (5P) material to the real electromagnetic devices.
By using the same model and measured magnetic properties data of SOMALLOY 700 (5P) material, the comparison between measured data and real data from rotating devices is needed. The discrepancy between them will explain the accuracy and efficiency of 2-D core loss measurement. In this work, the measurement data at circular B loci and elliptical B loci are pondered by taking into account the possible factors that contribute to the core loss. The anomalous loss is also demanded to be clarified in details.
- Core loss measurement and modelling of SOMALLOY 700 (5P) material under 3-D magnetic flux excitation.
In dealing with the rapid technology, core loss measurements of SOMALLOY 700 (5P) material under 3-D vector flux excitation and 3-D core loss model are required since the rotating magnetic flux density in electrical machine becomes complex in order to produce a powerful machine. Sphere B loci and ellipsoidal loci can be considered in resembling the actual magnetic flux density that rotates in the machine.
- Development of small and simple 3-D tester.

Despite success in measuring the core loss of SOMALOY 700 (5P) material, the crucial and hardness moment in collecting the data also should be considered. The excitation coils should be improved in order to provide more measurement works at high frequencies. The small and simple 3-D tester is always good to be used. Besides that, the user-friendly 3-D tester also can lead to the effective measurement. The magnetic property measurements would be more accurate if the 3-D tester can be used for any size of cubic sample in order to prevent from fabricating the new sensing coils which are attached to the plastic sensing box of the cubic sample. It is important to avoid the sensing coils from being disassembled and assembled frequently which will damage the coils.

- Consideration of “C-type” cores in core loss measurement

The ability in predicting the magnetic properties of SOMALOY 700 (5P) can be increased by considering the symmetrical ‘C type’ cores of 3-D tester. This type of laminated core provides the frustum of cone pole that is able to balance the magnetic flux path in three axes smoothly for the higher field homogeneity inside the sample. Thus, the sensing voltages of B and H can be induced easily and efficiently.

APPENDIX A: List of publications

Conference Proceedings

1. A.R. Asari, Y. Guo, J. Zhu, and F.S. Ismail, "A Review on 3-D Magnetic Property Testing System for Measuring Rotational Core Loss of Soft Magnetic Materials", *10th Asian Control Conference*, Kota Kinabalu, Malaysia, pp.294-299, 2015
2. A. Asari, Y. Guo, and J. Zhu, "2-D Magnetic Measurement of SOMALOY 700 (5P) Material", *14th International Workshop on 1 & 2-Dimensional Magnetic Measurement and Testing*, Tianjin, China, 2016
3. A. Asari, Y. Guo, and J. Zhu, "Magnetic Properties Measurement of Soft Magnetic Composite (SOMALOY 700) Material by using 3-D Tester", *2nd International Conference on Applied Physics and Engineering*, Batu Feringhi Penang, Malaysia, vol. 1875, no. 1, pp. 030015-1 – 030015-9, 2017
4. A. Asari, Y. Guo, J. Zhu, "Measurement of Magnetic Properties of SMC Material (SOMALOY 700) by using 3-D Magnetic Tester", *International Conferences on Electrical Machines and Systems*, Tokyo, Japan, 2016
5. A. Asari, Y. Guo, and J. Zhu, "Core Loss Measurement under Elliptical Loci of Magnetic Flux Density", *20th International Conferences on Electrical Machines and Systems*, Sydney, Australia, 2017

Journal

6. A. Asari, Y. Guo, J. Zhu, "Core Loss Measurement of SOMALOY 700 Material under Round Loci of Magnetic Flux Density", *ADVANCED SCIENCE LETTERS (ASL)*, American Scientific Publishers, ISSN: 1936-6612 (Print): E-ISSN: 1936-7317 (Online), April- May 2018.

APPENDIX B: Procedures applied in Software used

LabVIEW (generating the magnetic flux densities)

1. Create an
 - a. analog input voltage (analog input converts a voltage level into a digital value that can be stored and processed in a computer) channel.
 - b. analog output voltage (*analog outputs* convert digital values from a computer into a variable voltage level presented on an *output* terminal) channel.
2. Set the rate of sample clock. Define the sample mode to be continuous. Also set the sample clock rate for the signal generation.
 - a. Call the Get Terminal name with Device Prefix VI. This will take a Task and a terminal and create a properly formatted device + terminal name to use as the source of the Trigger.
3. Define the parameters for a Digital Edge Start Trigger. Set the analog output to trigger off the AI Start Trigger. This is an internal trigger signal.
4. Use the Basic Function Generator VI to create the signal to be generated.
5. Call the Start VI to arm the two functions. Make sure the analog output is armed before the analog input. This will ensure both will start at the same time.
6. Read the waveform data in a loop until the user hits the stop button or an error occurs. Is the Task done? VI is used to check for errors in the Analog Output Task.
7. Call the Clear VI to Clear the Task.
8. Use the popup dialog how to display an error if any

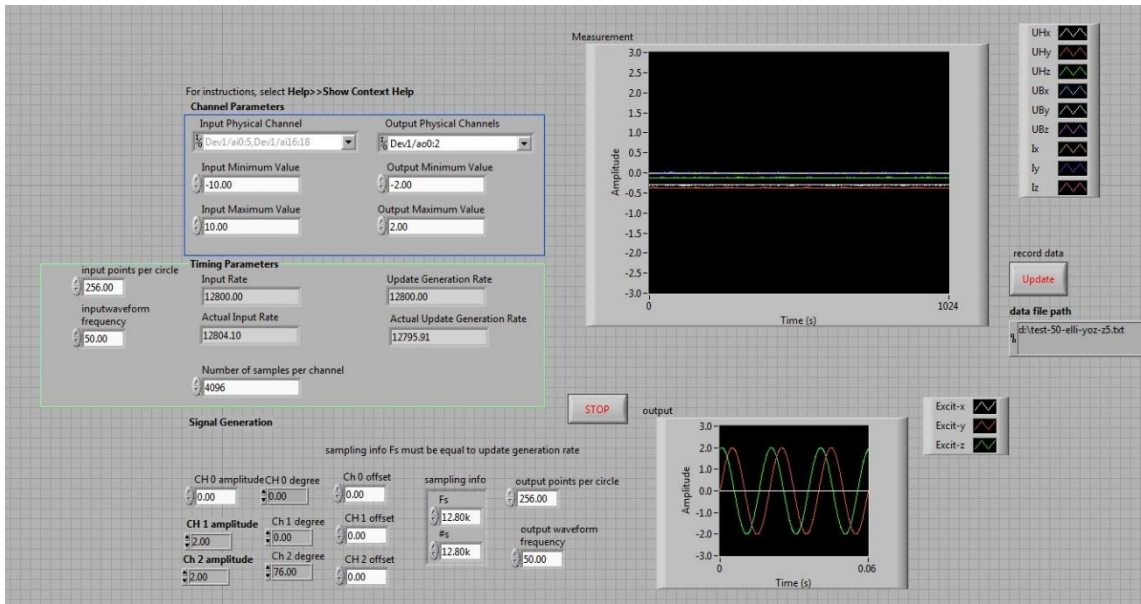


Fig. B1 LabVIEW front panel of 3D magnetic properties measurement

MathCAD (analysing the collected data)



Fig. B2 Identification of measured data by confirming the columns involved

Circle parameter

Res := 0.1 f := 1000 $\omega := 2 \cdot \pi \cdot f$ scale of differential probe Ah := 1000 PT := 64 points per circle $\mu := 4 \cdot \pi \cdot 10^{-7}$
 $\mu = 1.257 \times 10^{-6}$

Input data

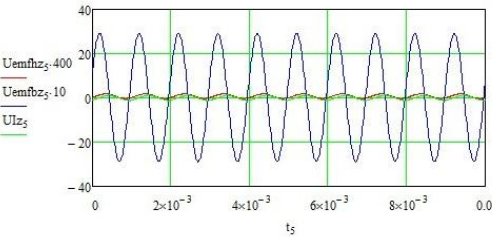
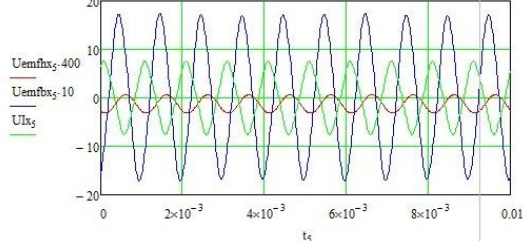
$\frac{1}{\omega} := \frac{f}{PT}$

k := 0..1023 $TI_k := \delta \cdot k$

rawdata₁ := C:\PH...\1.txt rawdata₆ := C:\PH...\6.txt
rawdata₂ := C:\PH...\2.txt rawdata₈ := C:\PH...\8.txt
rawdata₄ := C:\PH...\4.txt rawdata₇ := C:\PH...\7.txt
rawdata₃ := C:\PH...\3.txt rawdata₅ := C:\PH...\5.txt

```
loczero(v) :=
j ← 0
n ← rows(v) - 1
for k ∈ 0..n - 1
if vk ≤ 0 ∧ vk+1 > 0
  mj ←  $\begin{pmatrix} k \\ v_k \end{pmatrix}$ 
  j ← j + 1
end for
return m
```

Fig. B3 Data calling process from txt file to MathCAD

Smooth and balance the signal

$smuUemfz_1 := \text{supsmooth}(t_1, Uemfz_1)$ $smuUemfbz_1 := \text{supsmooth}(t_1, Uemfbz_1)$
 $smuUemfbz_2 := \text{supsmooth}(t_1, Uemfbz_2)$ $smuUemfbz_3 := \text{supsmooth}(t_1, Uemfbz_3)$
 $smuUIz_1 := \text{supsmooth}(t_1, UIz_1)$ $smuUIx_1 := \text{supsmooth}(t_1, UIx_1)$

n := 7

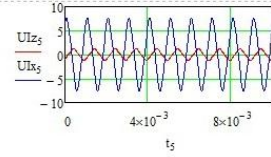


Fig. B4 Smoothing the measured data

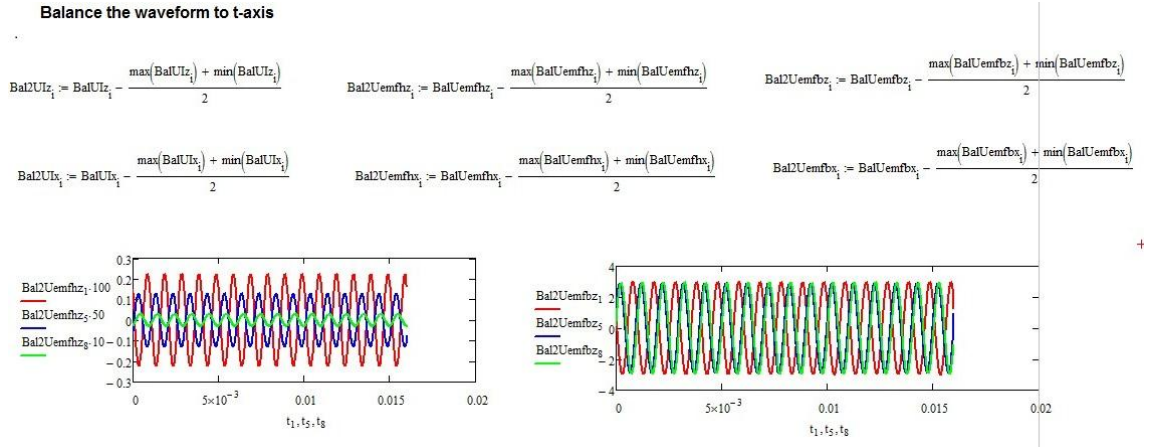


Fig. B5 Balancing the measured data

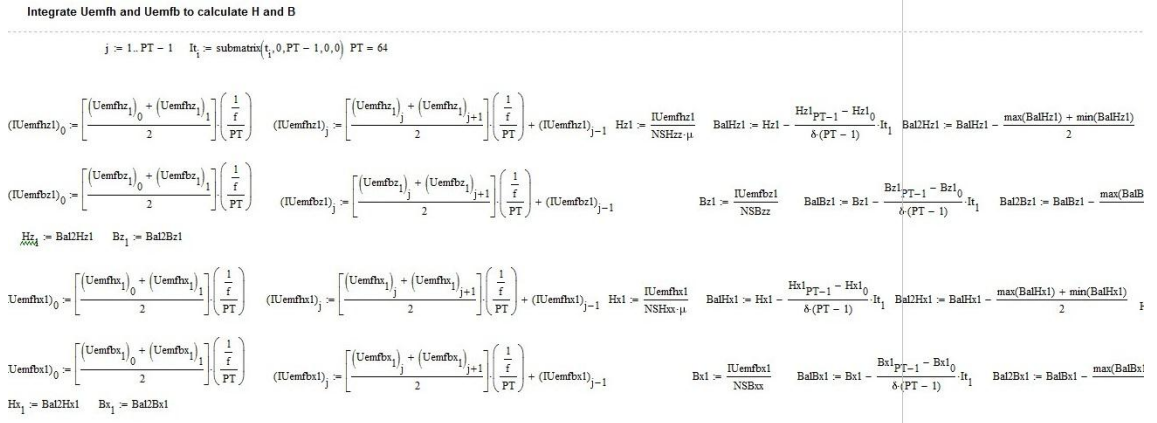


Fig. B6 B and H determination before plotting the hysteresis loop.

APPENDIX C: Figures and apparatus of experiment

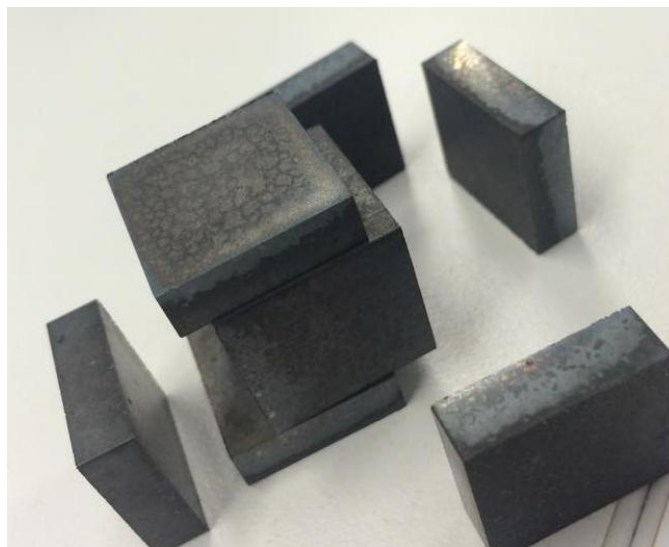


Fig. C1 SOMALOY 700 (5P) cubic sample with six guarding pieces.

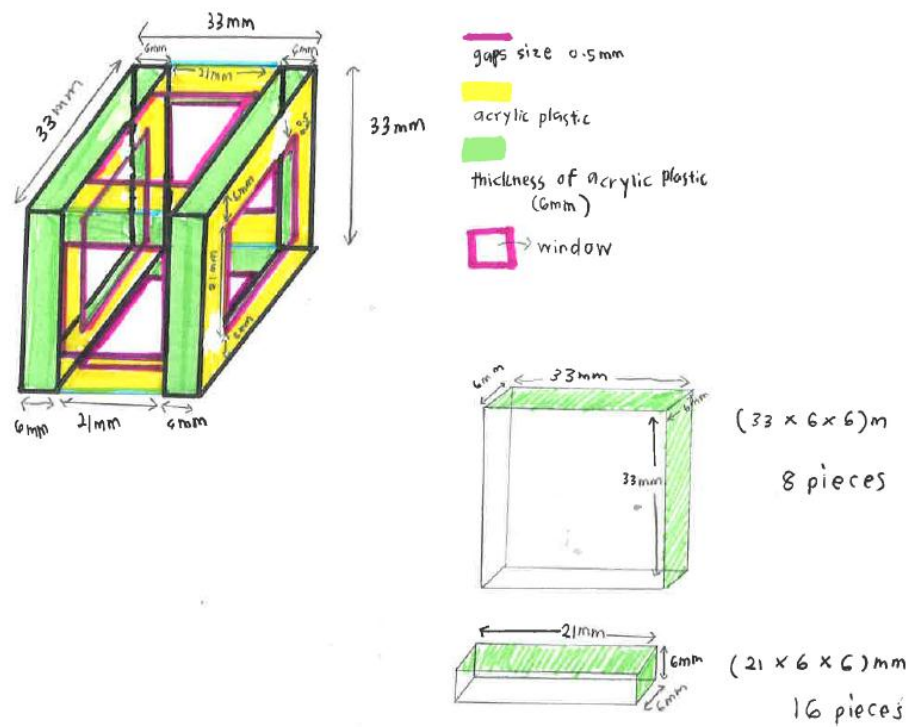


Fig. C2 Acrylic box fabrication.

a. Apparatus for calibration process

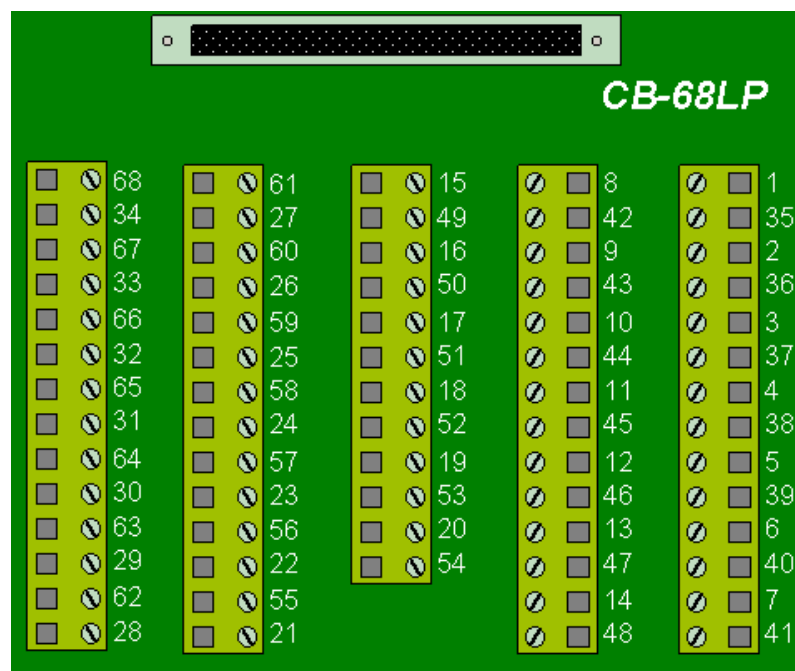
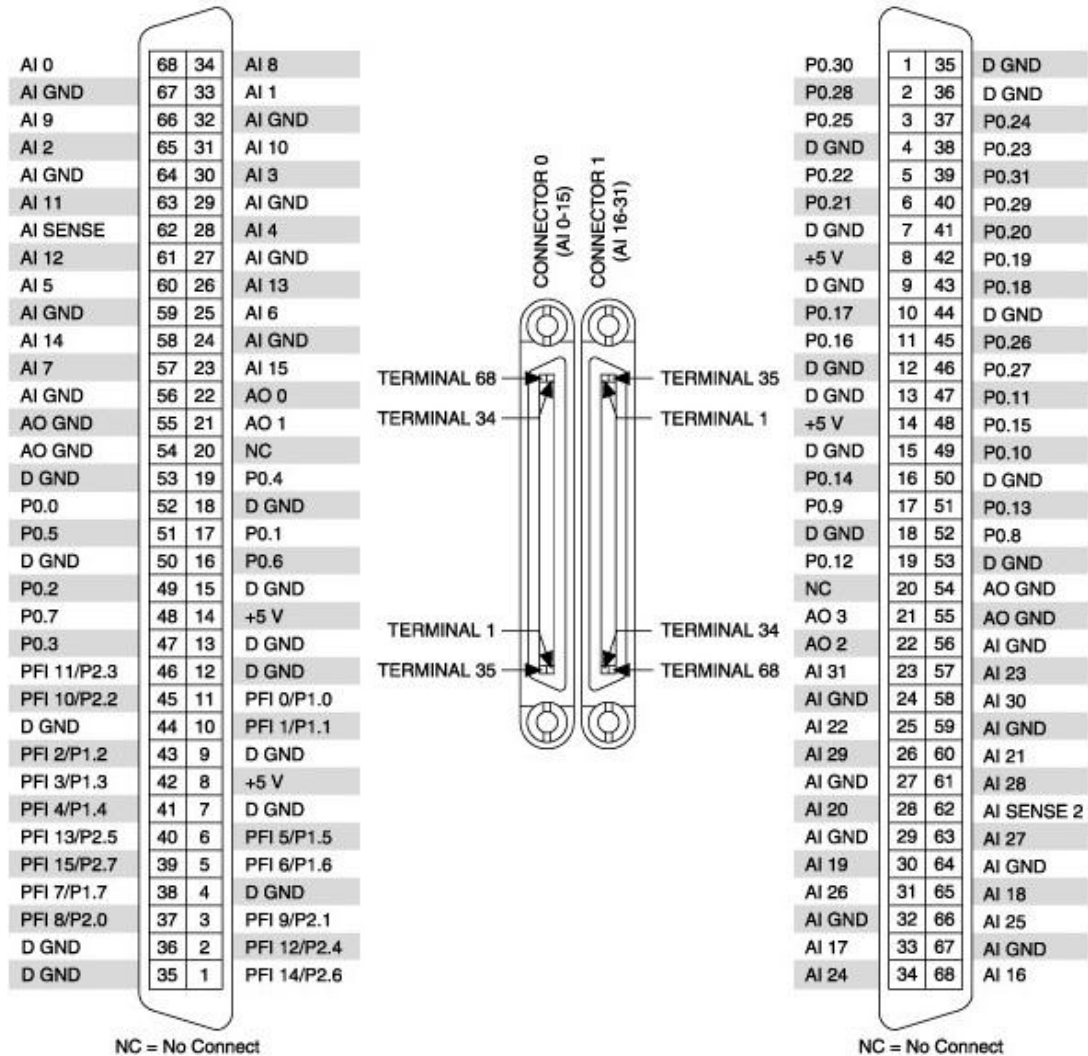


Fig. C3 NI CB-68LP Unshielded 68-Pin I/O Connector Block.

NI 6229



Default NI-DAQmx Counter Terminals (Connector 0)

Terminal	Signal
37	CTR 0 SRC
3	CTR 0 GATE
45	CTR 0 AUX
2	CTR 0 OUT
42	CTR 1 SRC
41	CTR 1 GATE
46	CTR 1 AUX
40	CTR 1 OUT

Fig. C4 DAQ NI PCI-6229 where Ground Referenced Single-Ended Mode is used.

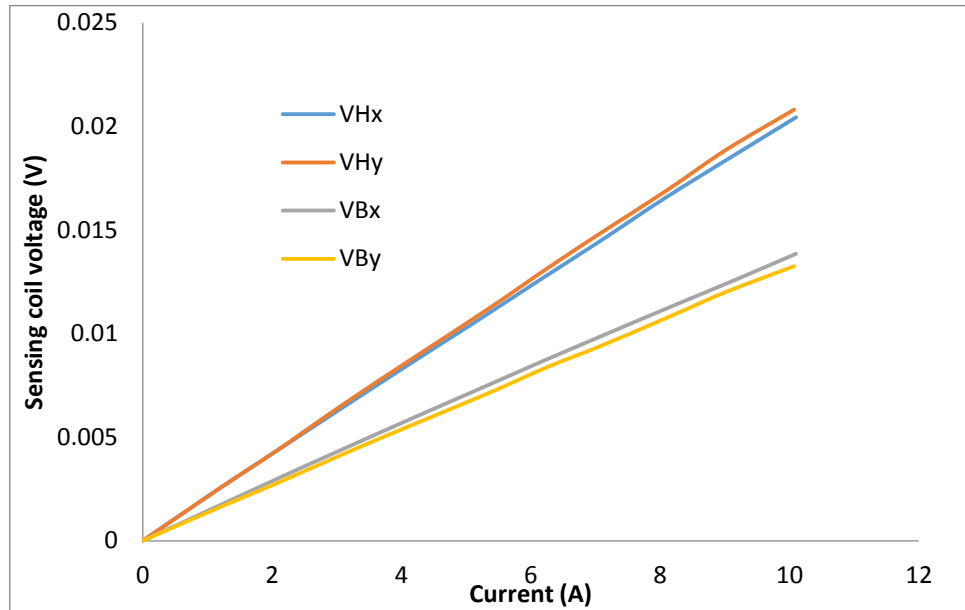


Fig. C5 Sensor voltages V_H and V_B for both axes x and y.

b. Apparatus for generating B and measuring sensor voltages (V_B and V_H).

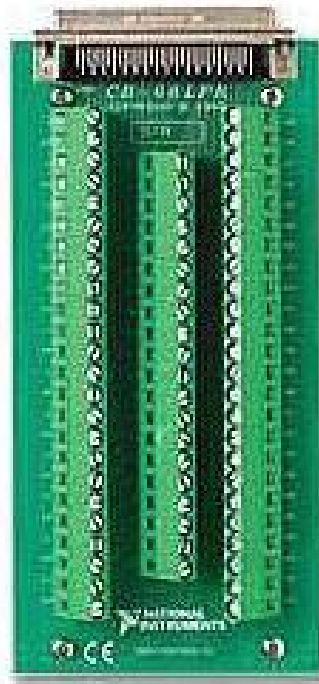


Fig. C6 NI CB-68LPR Unshielded 68-pin I/O Connector Block.